



HAL
open science

Evaluation of glyco-saccharides in a theranostic approach

Mattia Mazza

► **To cite this version:**

Mattia Mazza. Evaluation of glyco-saccharides in a theranostic approach. Radiochemistry. Ecole nationale supérieure Mines-Télécom Atlantique, 2021. English. NNT: 2021IMTA0237. tel-03917488v2

HAL Id: tel-03917488

<https://theses.hal.science/tel-03917488v2>

Submitted on 2 Jan 2023

HAL is a multi-disciplinary open access archive for the deposit and dissemination of scientific research documents, whether they are published or not. The documents may come from teaching and research institutions in France or abroad, or from public or private research centers.

L'archive ouverte pluridisciplinaire **HAL**, est destinée au dépôt et à la diffusion de documents scientifiques de niveau recherche, publiés ou non, émanant des établissements d'enseignement et de recherche français ou étrangers, des laboratoires publics ou privés.

THESE DE DOCTORAT DE

L'ÉCOLE NATIONALE SUPERIEURE MINES-TELECOM ATLANTIQUE
BRETAGNE PAYS DE LA LOIRE - IMT ATLANTIQUE

ÉCOLE DOCTORALE N° 596
Matière, Molécules, Matériaux
Spécialité : Chimie Analytique et Radiochimie

Par

Mattia MAZZA

Evaluation de glyco-saccharides dans une approche théranostique

Thèse présentée et soutenue à Nantes, le 26 Mars 2021
Unité de recherche : SUBATECH UMR 6457
Thèse N°: 2021IMTA0237

Rapporteurs avant soutenance :

Philippe Barthelemy
Serge Battu

Professeur, Université de Bordeaux
Professeur, Université de Limoges

Composition du Jury :

Président : Yves Andres
Examineurs : Philippe Barthelemy
Serge Battu
Vincent Ferrieres
Dominique Heymann
Dir. de thèse : Sandrine Huclier-Markai
Co-dir. de thèse : Pascal Reiller

Professeur, IMT Atlantique, Nantes
Professeur, Université de Bordeaux
Professeur, Université de Limoges
Professeur, Université de Rennes
Professeur, Université de Nantes
Maître de Conférences, Université de Nantes
Directeur de recherche, Université Paris-Saclay, CEA, Gif-sur-Yvette
Ingénieur de recherche, GIP ARRONAX, Saint Herblain

Encadrant scientifique : Cyrille Alliot

Invité(s)

Sylvia Colliec-Jouault Directeur de recherche, IFREMER, Nantes
Corinne Sinquin Ingénieur de recherche, IFREMER, Nantes

Acknowledgements

Acknowledgements

The thesis work here present is the result of contribution, collaboration and implication of many people who I really want to say thank you. Their help, support and advices have been precious in realizing the entire thesis.

This PhD thesis work was supported by SUBATECH laboratory (UMR 6457) and the experimental work was performed at GIP ARRONAX. This work was also realized in collaboration with several other teams:

- the LEMMBB laboratory of IFREMER (Institut français de recherche pour l'exploitation de la mer);
- the LANIE laboratory of CEA Saclay (Commissariat à l'Energie Atomique et aux énergies alternatives);
- the laboratory "Hétérogénéité Tumorale and Médecine de Précision" of ICO (Institut de Cancérologie de l'Ouest).

I would like to thank the two reviewers of this final work, Pr. Serge Battu (University of Limoges) and Pr Philippe Barthelemy (University of Bordeaux) for having accepted to evaluate this manuscript.

I also would like to thank Pr. Yves Andres (IMT Atlantique) for having accepted to be part of my defense jury, and especially to be the president of the jury.

I would also thank my two members of "Comité de suivi de these" Pr Vincent Ferrieres (University of Rennes) and Pr. Dominique Heymann for evaluating my progresses year by year and who both serve as examiners for my defense .

I warmly thank Dr. Pascal Reiller, research director of CEA Saclay, my co-director who has followed my work despite the geographic distance. He helped me developing an important part of my thesis in his laboratory, notably doing TRLFS experiments, and understanding some challenging parts of this work. I thank him for the precious work in revising this manuscript.

I would like to express my sincere thanks to my thesis director Dr. Sandrine Huclier-Markai and to my scientific supervisor Dr. Cyrille Alliot. I am grateful to them for daily supervising my work with big patience and interest despite their full schedules. Every lesson learned from them helped to clarify and organize my work and their suggestions and revisions have been really precious for the redaction of this manuscript. They both help me growing in the profession of researcher through their priceless teachings and advices.

Then, I would like to thank Mrs Corinne Siquin and Dr. Sylvia Collic-Jouault, respectively research engineer and research director of IFREMER Nantes who have hosted me so many times in their laboratory and for providing me the raw materials of this work. Their advices have helped me a lot in the way of better exploiting their biomaterials.

Acknowledgements

Finally I acknowledge Pr Dominique Heymann and Dr. Javier Munoz-Garcia, from Institut de Cancérologie de l'Ouest (ICO) who hosted me for running the cell experiments, and for teaching me many different things on that matter, revealing to me a different side of science that before today was unexplored to me.

I am grateful to Pr Abdesselam Abdelouas (head of the radiochemistry group in SUBATECH) and Pr. Ferid Haddad (Director of GIP ARRONAX) who both provide me the opportunity to work in their facilities.

I would like to thank my co-workers from GIP ARRONAX, making coming to work every day with pleasure and for their support and smiles.

A big thank you goes to some people beyond professional. I would like to thank Dr. Claire Charbonnet and Dr. Myriam De Summa for the medical and psychological support over this last year. Last but not least, an enormous thank you goes undoubtedly to Kevin, my sister, my parents and my friends who have constantly accompanied me in this rollercoaster of thoughts and emotions.

Table of contents

Acknowledgements	3
Table of contents	6
List of Figures	8
List of Tables.....	10
Glossary.....	11
Résumé long en français.....	14
General introduction.....	20
References.....	24
Chapter 1	25
I - Rationale: cancer prevalence.....	26
II - Nuclear medicine	34
III. Glycosaminoglycans.....	55
A – Composition and structure.....	56
B – Role of GAGs in cancer.....	57
C – Interest of GAGs for Nuclear Medicine	60
References.....	63
Chapter 2	68
I. Introduction.....	69
II. Exopolysaccharides and heparin.....	70
III. Scandium	101
References.....	110
Chapter 3	115
I. Introduction	116
References.....	117
II. Marine Exopolysaccharide Complexed with Scandium Aimed as Theranostic Agents.....	118
Chapter 4	142
I. Introduction	143
II. Chemistry of Europium.....	144
III. Time resolved laser fluorescence spectroscopy (TRLFS)	145
References.....	147

Table of contents

IV. Luminescence spectroscopic investigations of europium(III) complexation with exopolysaccharides from a marine bacterium.	149
Chapter 5	161
I. Introduction	162
II. In vitro cytotoxicity and cell viability assays	162
A. X-CELLigence technology and cell index	163
B. MTT assay	165
References:.....	165
III. Antiproliferative Properties of Scandium Exopolysaccharide Complexes on Several Cancer Cell Lines.....	167
Conclusions and perspectives.....	189

List of Figures

Figure 1. 2020 cancer incidence and mortality [2].....	26
Figure 2. The steps of metastasis and opportunities for therapeutic intervention [13].	31
Figure 3. Oncogenesis mechanisms involved in cancer. Adapted from Hanahan and Weinberg [16].....	32
Figure 4. Oncogenesis mechanisms and relative biomarkers. Adapted from Alam et al, 2014.	33
Figure 5. Principles of RIT. Adapted from Ménager et al. 2016 [30].....	41
Figure 6. Schematic design of a radiopharmaceutical [32].	43
Figure 7. Isotopes of current and emerging interest for imaging and therapy applications ordered from short to long half-life, matching the <i>in vivo</i> half-life of small molecules, peptides, proteins, and monoclonal antibodies [34].	44
Figure 8. Illustration of an archetypal radiometal-based radiopharmaceutical agent containing a bifunctional chelator (BFC) conjugated to a targeting vector (<i>e.g.</i> antibody, peptide, nanoparticle) using a variety of conjugation methods (<i>e.g.</i> isothiocyanate–amine coupling, peptide coupling, maleimide– thiol coupling, activated ester amide coupling, click-coupling) and then radiolabeled with a radiometal ion (<i>e.g.</i> $^{111}\text{In}^{3+}/^{177}\text{Lu}^{3+}/^{86/90}\text{Y}^{3+}$) [35].	46
Figure 9. Illustration of GAG location and interaction on endothelial cells [61].	56
Figure 10. Chemical structure of heparin, one of the most employed GAG in therapy, and heparan sulfate, normally expressed on the ECM surrounding human cells. Figure adapted from Capila et al. 2002 [63].	57
Figure 11. Selectins and integrins contribute to metastatic spread. (a) Schematic presentation of selectin- and integrin-mediated cancer cell interactions with several blood constituents (<i>e.g.</i> , platelets, leukocytes, and endothelial cells) during hematogenous metastasis. (b) Heparin application in mouse models blocks both P- and L-selectin-mediated; and VLA4-mediated interactions of cancer cells within blood circulation thereby affecting metastasis [12].	58
Figure 12. Structure of the pentasaccharide sequence of heparin fundamental for the anticoagulant activity. Figure adapted from Capila et al. 2002 [3].	70
Figure 13. Schematic illustration of a fermenter. Figure adapted from Microbiology notes [8].	72
Figure 14. Proposed structure of EPS DRS and major sulfated sites after over-sulphation reaction. Other sulphation positions are certainly expected to be present, but they have not been displayed so far. Figure adapted from Chopin et al. 2015 [9].	74
Figure 15. Schematic functioning of a MALS detector. Figure taken from Azo Material website.	78

Figure 16. Example of Debye plot [24].	79
Figure 17. Schematic illustration of the main parts forming the A4F channel. Figure adapted from a Wyatt Technology presentation [27].	80
Figure 18. Illustration of the A4F channel components and the principal steps for the analysis for mixed populations of particles differing in size. The accumulation wall (membrane) is permeable, which allows flow through the bottom of the channel. Note that this scheme is not to scale. In A4F normal mode elution the separation process occurs in the lower 10% of the channel height [28].	82
Figure 19. Schematic representation of different types of elution in A4F [29].	83
Figure 20. Polymer expansion and contraction according the quality of solvent. Figure adapted from Taylor et al. 2017 [35].	90
Figure 21. a) Schematic structure of a U-tube viscometer. A and B are respectively the upper and lower marks to be considered for measuring the liquid flow time. C indicates the maximum volume of liquid that has to be poured into the glass capillary. b) Principle of rolling ball viscometer and main forces acting on the descending ball. F_G is the gravitational force; F_B is the buoyancy force and F_V is the viscous force. Figure adapted from Anton-Paar website.	92
Figure 22. Potentiometric titration of heparin at $5 \cdot 10^{-4}$ M with NaOH at 0.1M.	98
Figure 23. SEC-MALS analysis to check the hydrolysis in the pH range of 3-7.3. Heparin's concentrations: $1 \cdot 10^{-3}$ (triangles), $5 \cdot 10^{-4}$ (squares), and $1 \cdot 10^{-4}$ mol L ⁻¹ (circles).	100
Figure 24. Pourbaix diagram of europium in aqueous solution: $[\text{Eu}]_{\text{tot}} = 10^{-5}$ M, $[\text{NaClO}_4] = 0.1$ M [11].	145
Figure 25. Diagram relating energy levels of Eu^{3+} . Figure adapted from Lourenço 2008 [15].	146
Figure 26. Energy level of aquo-ion Eu^{3+} and relative transitions. Figure adapted from Lourenço 2008 [15].	147
Figure 27. A. A simplified cartoon of an E-plate 96 and the gold microelectrodes embedded within each well (top view of a single well) is shown on the left. The number and size of the gold microelectrodes are not representative of the actual set-up and are for illustrative purposes only. The E-plate 96 is placed within the RTCA SP Station (1), which is kept in a humidified incubator and is connected to the RTCA Analyzer (2) and RTCA Control Unit (3). B. Workflow of an xCELLigence adhesion assay. Figure adapted from Hamidi et al. 2017.[5].	164
Figure 28. Metabolism of MTT to a formazan salt by viable cells as shown in a chemical reaction (A) and in a 96-well plate (B). Figure adapted by SIGMA-ALDRICH's protocol guide for MTT assay.	165

List of Tables

Table 1. Radionuclides of interest for PET imaging [20].....	37
Table 2. Radionuclides of interest for radiotherapy [27].....	40
Table 3. Chelators of interest and some example of radionuclide matches. [33]	48
Table 4. Vectors of interest for delivering radionuclides: their applications and relative pros (in green) and cons (in red). [44].....	51
Table 5. Optimized parameters for EPS characterization.....	85
Table 6. Comparison between A4F-MALS and SEC-MALS about the characterization in terms of molar mass and dispersity. The values in the brackets correspond to the uncertainties.....	88
Table 7. Stability constants of organic acids complexes with scandium. Adapted from Horovitz, 1999 [52].	101
Table 8.. Known chelators for scandium.	103

Glossary

Acronym	Meaning
A4F	Asymmetrical Flow Field-Flow Fractionation
AAZTA	1,4-bis(hydroxycarbonyl methyl)-6-[bis(hydroxylcarbonylmethyl)]Amino-6-methyl perhydro-1,4-diAZepine
BFC	BiFunctional Chelator
BSA	Bovine Serum albumin
CaCO ₃	Calcium Carbonate
CDx	Diagnostic Companions
CE-ICP-MS	Capillary Electrophoreses - Inductively Coupled Plasma Mass Spectroscopy
CI	Cell Index
CS	Chondroitin Sulphate
CSC	Cancer Stem Cells
CT	Computed Tomography
dRI	differential refractive index
DNA	DeoxyriboNucleic Acid
Dn/dc	Refractive index increment
DOTA	1,4,7,10-tetra-azacycloDodecane-1,4,7,10-Tetraacetic Acid
DS	Dermatan Sulphate
DTPA	DiethyleneTriaminePentaacetic Acid
DMF	N,N-DiMethylFormamide
EBRT	N,N-DiMethylFormamide
EC	Exchange Chromatography
ECM	Extra-Cellular Matrix
EPS	ExoPolySaccharides
EPS DR	Radical Depolymerized EPS
EPS DRS	Radical Sepolymerized and Sulphated EPS
EGFR	Epidermal Growth Factor Receptor
FDA	Food and Drug Administration
FDG	FluoroDeoxyGlucose
F-DOPA	FluoroDihydrOxyPhenylAlanine
FISRE	Free Ion Selective Radiotracer Extraction
FLT	FLuoroThymidine
F-MISO	FluoroMISONidazole
GAG	GlycosAminoGlycans
G-CSF	Granulocyte Colony-Stimulating Factor

Glossary

GPC	Gel Permeation Chromatography
HAS	Haute Autorité de Santé
HDR	High Dose Rate
HEHA	1,4,7,10,13,16-HExaazacyclo-hexadecane-N,N'',N''',N''''',N''''''-Hexaacetic Acid
HF	Hydrofluoric Acid
HOS	Human OSteosarcoma
HPAEC	High Performance Anionic Exchange Chromatography
HPLC	High Performance Liquid Chromatography
HS	Heparan Sulphate
ICP-OES	Inductively Coupled Plasma Optical Emission Spectroscopy
IO	ImmunoOncology
KS	Keratan Sulphate
LC	Liquid Chromatography
LDR	Low Dose Rate
LET	Linear Energy Transfer
LMWD	Low Molecular Weight Derivatives
LMWF	Low Molecular Weight Derivatives
LS	Light Scattering
LS-EPS	Low Sulphated Exopolysaccharides
MALS	Multi Angle Light Scattering
MHS	Mark-Houwink-Sakurada
MRI	Magnetic Resonance Imaging
MTT	3-(4,5-diMethylThiazol-2-yl)-2-5-diphenylTetrazolium bromide
NaCl	Sodium Chloride
NADH	Nicotinamide Adenine Dinucleotide
NaNO ₃	Sodium Nitrate
NCI	Normalized Cell Index
NETA	{4-[2-(bis-carboxymethylamino)-Ethyl]-7carboxymethyl-[1,4,7]Triazonan-1-yl}-Acetic acid
NMR	Nuclear Magnetic Resonance
NOTA	1,4,7-triazacyclononane-1,4,7-Triacetic Acid
NP	NanoParticle
OS	Ostrosarcoma
OS-EPS	Over-Sulphated Exopolysaccharides
PAA	PolyAcrylic Acid
PEPA	1,4,7,10,13-Pentaazacyclopentadecane-N,N',N'',N''',N''''-Pentacetic Acid
PES	PolyEther Sulphate
PET	Positron Emission Tomography
PEPA	1,4,7,10,13-Pentaazacyclopentadecane-N,N',N'',N''',N''''-Pentacetic Acid
PES	PolyEther Sulphate

Glossary

PET	Positron Emission Tomography
PDI	PolyDispersity Index
PSA	Prostate Specific Antigen
PSMA	Prostate Specific Membrane Antigen
RID	RadioImmunoDiagnostics
RIT	RadioImmunoTherapy
RNA	RiboNucleic Acid
RMS	Mean-Square-Radius
RTCA	Real-Time Cellular Analysis
SEC	Size Exclusion Chromatography
SO ₃ Py	Sulfur triOxide PYridine
SPECT	Single Photon Emission Computed Tomography
TCMC	1,4,7,10-Tetrakis(CarbomoylMethyl)-1,4,7,10-tetraazaCyclododecane
TETA	1,4,8,11-TEtra-azacyclotetradecane-1,4,8,11-Tetacetic Acid
TEL	Transfer of Linear Energy
TEMP	Tomigraphy of Emission MonoPhotonics
TLC	Thin Layer Chromatography
TRAP	1,4,7-TRiazAcyclononane-1,4,7-tris[methyl(2-carboxyethyl) Phosphinic acid
TRLFS	Time-Resolved Laser Fluorescence Spectroscopy
TRT	Targeted Radiotherapy
UV	UltraViolet
WHO	World Health Organization

Résumé long en français

Résumé long en français

L'ostéosarcome est la tumeur osseuse maligne primitive la plus courante chez les enfants et les jeunes adultes. C'est un type de cancer très agressif avec un pronostic faible ; mais le mécanisme moléculaire des métastases a été identifié pour concevoir de nouvelles stratégies thérapeutiques dans le cadre de la médecine personnalisée. Parmi les biomarqueurs considérés, les glycoaminoglycanes (GAG) sont une caractéristique liée à la croissance et à la propagation du cancer. Les GAG pourraient être utilisés dans de nouveaux systèmes de délivrance de médicaments pour délivrer des composés actifs à des fins thérapeutiques. Une approche théranostique, c'est-à-dire la combinaison d'un biomarqueur prédictif avec un agent thérapeutique, a été développée dans ce travail. L'objectif de cette thèse est d'évaluer les exopolysaccharides naturels en tant que ligand potentiel en théranostique et de déterminer s'ils pourraient être couplés aux radionucléides de scandium.

Dans la première partie de ce manuscrit, un état de l'art sur les approches récentes en cancérologie et la justification de ce travail a été présenté. Les glycosaminoglycanes (GAG) tels que l'héparine non fractionnée et ses dérivés de bas poids moléculaire (LMW) sont généralement utilisés pour la prévention ou le traitement de la thromboembolie veineuse qui survient fréquemment chez les patients cancéreux. L'héparine est composée d'acide glucuronique ou iduronique, de glucosamine et a une teneur en soufre d'environ 10% (de 8% à 13% selon la préparation d'héparine). Un taux de survie amélioré a été montré, ce qui pourrait être dû à l'héparine car elle est capable d'interférer avec certaines des étapes biologiques importantes de la propagation des métastases. Malheureusement, ce type de molécules présente des inconvénients tels qu'un risque hémorragique et pourrait présenter une contamination par des protéines prion ou du sulfate de chondroïtine sursulfaté. Ce risque limite considérablement l'utilisation de l'héparine en thérapie. En fait, le nombre d'études sur l'exploration des molécules mimétiques de l'héparine a augmenté ces dernières années. Parmi les molécules possibles, les polysaccharides pourraient être une nouvelle source de molécules de type héparine. Les polysaccharides d'algues ou bactériens traditionnels offrent une alternative valable aux GAG de mammifères. De plus, les polysaccharides extraits d'eucaryotes et de procaryotes vivant en milieu marin pourraient potentiellement révéler un meilleur rapport bénéfice / risque comme observé dans les études préliminaires sur les animaux. Dans le passé, les polysaccharides d'algues tels que les fucoïdanes - et en particulier la préparation de fucoïdane de bas poids moléculaire (LMWF) - se sont avérés présenter des propriétés de type héparine avec un risque hémorragique très faible. Les polysaccharides marins de source bactérienne présentent également un potentiel élevé en thérapie cellulaire et en génie tissulaire. Ils peuvent être produits dans des conditions totalement contrôlées dans des bioréacteurs par rapport à d'autres polysaccharides d'eucaryotes.

Parmi ces polysaccharides marins, un exopolysaccharide (EPS) d'intérêt est extrait du bouillon de culture d'une bactérie nommée *Alteromonas infernus*. L'unité répétitive de cet EPS est constituée d'un nonasaccharide monosulfaté. Il présente un poids moléculaire élevé ($> 10^6$ g mol⁻¹) et une faible teneur en sulfate (<10%). Cet EPS natif a démontré une activité anticoagulante très faible par rapport à l'héparine. Afin de favoriser ses activités biologiques et de fournir un composé mimétique GAG, l'EPS natif a été modifié par d'abord une dépolymérisation radicalaire (EPS DR) puis une étape de sursulfation (EPS DRS), ces deux modifications chimiques permettent une réduction de son poids avec une augmentation de sa teneur en sulfate. L'activité anticoagulante de ce dérivé d'EPS hautement sulfaté est améliorée par rapport à celle de son précurseur natif mais reste inférieure à la fois à l'héparine non fractionnée et à l'héparine, 10 et 5 fois moins, respectivement. Cette catégorie de polysaccharides pourrait ouvrir la voie au développement de nouveaux systèmes de délivrance

d'agents chimiothérapeutiques conventionnels, ainsi que de nouvelles stratégies en oncologie osseuse, dans le domaine de la médecine personnalisée.

La médecine nucléaire implique l'utilisation d'isotopes radioactifs dans le diagnostic et le traitement des maladies. La théranostique - un domaine de la médecine qui combine une thérapie ciblée spécifique et diagnostic grâce à des marqueurs biologiques spécifiques. Parmi les radionucléides disponibles, le scandium possède deux radionucléides émettant des radiations β^+ , ^{44}Sc ou ^{43}Sc , ce qui en fait des candidats appropriés au diagnostic TEP / CT (tomographie par émission de positrons), en raison de leur demi-vie d'environ 4 heures et de leur désintégration en Ca stable. Le ^{47}Sc , qui peut être utilisé pour la thérapie ciblée et le ^{44}Sc ou ^{43}Sc offrent une opportunité pour les calculs dosimétriques. Le couplage de l'exopolysaccharide avec ce couple de radionucléides théranostiques est donc intéressant.

Il est important de caractériser ces molécules, en particulier leurs masses moléculaires, au moyen de techniques de fractionnement flux-force (A4F) couplées à des détecteurs de réfractométrie différentielle (dRI) et de diffusion de lumière multi-angles (MALS). Un autre paramètre important qui pourrait influencer la complexation est la conformation du polymère. Ainsi, le deuxième chapitre de ce travail a abordé la caractérisation des exopolysaccharides et notamment leurs propriétés fonctionnelles (pK_a), et leurs propriétés rhéologiques (viscosité, conformation). Comme il a été démontré que ces EPS présentent des propriétés semblables à celles de l'héparine. L'héparine étant un polysaccharide, une partie de mon travail a été consacrée à celle-ci, en tant que référence des GAG. Deux constantes de protonation ont été déterminées. La première valeur de $pK_{a1} = 3,82 \pm 0,03$ correspond au groupe carboxylique de l'acide iduronique du disaccharide de l'héparine. La deuxième constante de protonation a été trouvée à $pK_{a2} = 7,53 \pm 0,03$, qui a été attribuée à l'atome d'azote du groupe sulphamino, qui est un donneur plus fort que les autres groupes sulfatés.

Nous avons confirmé que l'AF4 est très utile pour la séparation des (bio) polymères et lorsqu'il est couplé au MALS, il permet la détermination des masses molaires du polymère, remplaçant facilement la SEC-MALS. Le dérivé sur-sulfaté EPS-DRS, obtenu à partir de l'EPS natif, présentait un \overline{M}_w de 56,9 kDa tandis que pour l'EPS DR, le dérivé dépolymérisé radicalairement, \overline{M}_w était de 25,6 kDa. Certaines divergences ont été remarquées par rapport à la détermination SEC-MALS. Les poids moléculaires \overline{M}_w de EPS-DR et -DRS ont été sous-estimés en SEC-MALS car elle a été utilisée avec des valeurs moyennes de $\partial n / \partial c$ pour les deux EPS. Dans ce travail, nous avons déterminé des valeurs précises de $\partial n / \partial c$ pour chaque EPS. En outre, une dégradation potentielle existe lors de l'analyse de polymères linéaires à longue chaîne par SEC, en raison des gradients de vitesse générés pendant l'écoulement. Le polymère est allongé et les liaisons positionnées près du milieu de la chaîne s'étirent et peuvent se rompre si les taux de cisaillement sont suffisamment élevés. Les segments d'extrémité d'une chaîne conservent leur forme enroulée ; alors, la contrainte maximale est fréquemment concentrée près du centre du polymère.

Ce travail a également examiné le rayon viscosimétrique ($R\eta$) et la conformation des polymères. Pour les deux EPS, une diminution du volume hydrodynamique V_h a été observée avec l'augmentation de la force ionique. Cette diminution était légèrement plus élevée pour EPS-DR et -DRS que pour l'héparine, ce qui signifie que EPS-DR et -DRS sont plus sensibles aux changements de force ionique. Ceci a été expliqué en considérant les charges globales entourant les chaînes EPS-DR ou -DRS qui sont plus importantes par rapport à celles de l'héparine. EPS-DR et -DRS présentent plus de groupes fonctionnels ionisés qui pourraient être protégés par les contre-ions de l'électrolyte de fond, conduisant au repliement de la chaîne polymère. La diminution de la viscosité intrinsèque avec l'augmentation de la force ionique

traduit un changement de conformation : l'expansion de la chaîne polymère est clairement affectée par l'ajout d'ions qui semblent rendre inaccessibles les fonctions ionisées du polymère. Avec notre approche rhéologique, nous avons mis en évidence que les deux échantillons d'EPS présentent des tailles nanométriques qui correspondent à un indicateur quantitatif de conformation moléculaire. Ce dernier permettrait un contrôle amont des médicaments à administrer. Avec un R_G allant de 44 à 58 nm, ces EPS permettraient une circulation *in vivo* et une clairance rénale rapides.

Pour une utilisation en approche théranostique, le complexe scandium-exopolysaccharide doit être thermodynamiquement stable et cinétiquement inerte. Les constantes de stabilité des complexes Sc-EPS ont été évaluées par une méthode d'extraction sélective à base de résine échangeuse d'ions (FISRE) et l'influence de la teneur en soufre sur la complexation avec le scandium a été examinée. La méthode FISRE a été utilisée pour la détermination de la stabilité thermodynamique des produits métallo-radiopharmaceutiques contenant Y^{3+} , ou pour les complexes Sc^{3+} avec plusieurs ligands chélatants, comme EDTA, DTPA, NOTA et DOTA. D'autres techniques, telles que les titrages potentiométriques et CE-ICP-MS, ont été considérées comme moins adaptées à l'analyse des complexes Sc-EPS. Les titrages potentiométriques pourraient affecter l'intégrité de la chaîne polymère, en l'exposant à une hydrolyse à pH très acide ou très alcalin ; alors que l'électrophorèse capillaire couplée à l'ICP-MS (CE-ICP-MS) n'a pas pu être utilisée en raison des complexes polysaccharides-métal hautement chargés, ce qui conduirait à une interprétation difficile de la spéciation. La méthode FISRE évite l'hydrolyse potentielle des ligands EPS. Pour chaque ligand, un seul type de site de complexation a été mis en évidence avec une stoechiométrie 1:1 dans nos conditions expérimentales. Les constantes de complexation peuvent être calculées en ajustant $\log K_{dnorm}$ en fonction de la concentration en ligand.

Pour l'héparine, le complexe monoligand $MHep^{2-}$ était l'espèce prédominante dans les gammes de pH faiblement acide, neutre et faiblement basique. Avec l'augmentation du pH, une hydrolyse des métaux se produit. Des molécules d'eau sont présentes dans la sphère de coordination interne du métal et sont progressivement remplacées par des complexes hydroxo lorsque le pH augmente. Les constantes de stabilité suivantes ont été trouvées pour EPS : $K_{ScEPS-DR} = 9,30$ et $K_{ScEPS-DRS} = 7,85$. Les constantes de stabilité trouvées pour EPS-DR et -DRS étaient plus élevées que celles de la littérature sur les acides glucuronique et galacturonique, ce qui pourrait suggérer la présence de complexes hydroxo de Sc pour les deux EPS. En termes de spéciation, les deux ligands semblent complexer quantitativement le scandium dans des conditions proches de celles physiologiques. En termes de charges, l'EPS-DRS présente trois charges négatives supplémentaires, liées aux trois groupes sulfate générés par la réaction de sur-sulfatation. La présence des groupes sulfate a retardé la complexation, probablement en raison d'un encombrement stérique plus élevé avec les monomères de EPS-DRS causé par les sulfates. À force ionique plus élevée, ces groupes sont protégés, ce qui fait que le polymère se plie en une bobine aléatoire plus contractée. Néanmoins, les complexes Sc-EPS semblent moins stables que ceux entre le scandium et les chélates classiques utilisés dans les produits radiopharmaceutiques, tels que le DOTA et le DTPA ($K_{ScDOTA} = 30,79$; $K_{ScDTPA} = 27,43$). A partir des valeurs publiées, nous avons calculé la constante de complexation apparente pour le DTPA et DOTA respectivement avec du scandium à pH = 6,1. Nous avons trouvé respectivement 16,93 et 16,98. Même si ces valeurs sont bien supérieures à celles déterminées pour l'héparine, l'EPS-DR et l'EPS -DRS (soit 6,38; 7,07 et 5,62 respectivement), la complexation du scandium avec ces ligands est totale.

Le scandium est un métal de la première série de transition avec un rayon ionique de 0,75 Å (+3); il est classé comme élément des terres rares et, pour cette raison, son comportement chimique est assez proche de celui des lanthanides. En solution aqueuse, seul le degré d'oxydation (+3) est stable. Les ions lanthanides se trouvent dans les organismes vivants à l'état de traces et sont considérés comme jouant un rôle biologique. Ils interagissent avec des matériaux biologiques et en raison de leur analogie chimique avec les actinides à leur état redox + III, ils peuvent également agir comme sondes de substitution pour les actinides Pu (III), Am (III) ou Cm (III). De plus, il a été cliniquement prouvé que les acides polygalacturoniques ou les acides polyuroniques pouvaient être efficaces comme médicaments en cas d'empoisonnement aux métaux lourds. Dans ce travail, le potentiel de ces EPS et de l'héparine à complexes métaux des terres rares, en particulier les lanthanides, a été évalué. La complexation de Eu^{3+} avec ces deux EPS et l'héparine a été étudiée par spectroscopie de fluorescence induite par laser à résolution temporelle (TRLFS). La TRLFS est un outil très pratique pour détecter et caractériser la spéciation des lanthanides fluorescents - et en particulier l'euprotium (III) -, à des concentrations traces. Cette méthode est sensible aux changements dans l'environnement chimique du métal par des modifications des spectres de fluorescence et du temps de décroissance de l'état excité. Les données spectroscopiques obtenues - c'est-à-dire les spectres, les maxima des pics, les intensités et les temps de décroissance - donnent des informations précieuses identifiant la spéciation d'éventuels complexes Eu (III) -polysaccharides. Des travaux similaires ont été menés sur l' α -D-glucose 1-phosphate, sur le glucose 6-phosphate, le fructose 6-phosphate, les lipopolysaccharides ou sur le peptidoglycane avec de l'uranium (VI), qui est un autre élément fluorescent.

Pour l'EPS-DR et l'EPS-DRS, nous avons observé une décroissance de la luminescence mono-exponentielle, tandis que pour l'Eu-Héparine, une bi-exponentielle était nécessaire. Pour EPS-DR et EPS-DRS, la durée de vie de la luminescence est supérieure à 150 μs , indiquant la formation d'une seule espèce pour le complexe Eu(III)-EPS. Pour l'héparine, le temps de désintégration semble au contraire augmenter avec la concentration d'Euprotium et donc la viscosité. Cela pourrait s'expliquer par la conformation du polymère qui s'étend (viscosité plus élevée) qui devrait révéler plus de groupes fonctionnels, donc moins de molécules d'eau autour du métal et donc un temps de désexcitation plus élevé. Pour le système Eu (III) -héparine, deux sites de complexation ont été nécessaires pour modéliser l'isotherme alors qu'un seul site était nécessaire pour modéliser les données pour les complexes Eu(III)-EPS-DR et Eu(III)-EPS-DRS. Les deux sites observés sur le système Eu-héparine correspondaient aux deux acides uroniques, en accord avec les données de Fuks et Bünzli sur la complexation du La(III) avec l'acide glucuronique et l'acide galacturonique. Par rapport au scandium, les ions Eu (III) sont des accepteurs durs et forment des complexes forts avec des ligands durs contenant des atomes donateurs hautement électronégatifs tels que le carbonate, le phosphate, l'hydroxyde, le fluorure et le sulfate. Les liaisons entre les ions Eu^{3+} et les ligands durs tels que CO_3^{2-} ou F^- sont principalement de caractère électrostatique et les électrons 4f ne semblent pas participer dans une large mesure à la liaison. Une autre conséquence de la nature principalement électrostatique de la liaison est que le nombre de coordination et la géométrie des ions des éléments de terres rares sont moins contraints que ceux des ions de métaux de transition.

Enfin, les dérivés d'exopolysaccharides (EPS) ont montré des propriétés antimétastatiques sur différentes lignées cellulaires cancéreuses. De plus, ces dérivés n'avaient aucun effet significatif sur le cycle cellulaire et n'avaient aucun effet pro-apoptotique sur les cellules d'ostéosarcome. Pour garantir les propriétés biologiques nécessaires pour cibler les cellules cancéreuses, des complexes scandium-EPS ont été testés *in vitro* sur des lignées cellulaires HOS. Des expériences utilisant la technologie xCELLigence RTCA ont été menées pour suivre

la cinétique de prolifération de ces cellules pendant 160 heures d'abord avec les EPS seuls et le scandium seul, puis avec des complexes scandium-EPS. La viabilité cellulaire après 160 heures a également été évaluée par des tests MTT.

Les complexes EPS-Sc et Heparine-Sc ont montré un effet anti-prolifératif. Cet effet était plus efficace pour ralentir la cinétique de prolifération que les polysaccharides seuls. Cette augmentation des propriétés antiprolifératives pourrait s'expliquer par un changement de conformation des EPS lors de la complexation avec le scandium en raison de leur nature polyélectrolyte. Ce changement de conformation pourrait moduler positivement ou négativement l'effet cytotoxique. Concernant la cause de l'effet cytotoxique, il ne peut pas être expliqué par une altération du métabolisme cellulaire puisque la viabilité cellulaire reste élevée. En effet, la viabilité cellulaire était élevée avec tous les composés testés après 160 heures, ce qui suggère qu'un effet cytostatique pourrait se produire plutôt qu'un effet cytotoxique. Plus probablement, des altérations de la signalisation du récepteur du facteur de croissance, ainsi qu'une interférence de l'adhésion cellule-cellule médiée par des protéines transmembranaires spécifiques pourraient être la principale cause de l'effet antiprolifératif.

Ces résultats sont très encourageants dans une perspective théranostique pour deux raisons : 1) le tropisme intrinsèque de ces EPS pour les cellules cancéreuses est maintenu même après la complexation et 2) l'effet anti-prolifératif pourrait être modulé par le degré de complexation. La perspective future serait de réaliser une campagne plus large pour étudier l'influence du degré de complexation pour mieux voir quels sont les meilleurs rapports metal-ligand en termes d'efficacité. En outre, le test xCELLigence réalisé avec les EPS pourrait être étendu à d'autres lignées cellulaires connues pour être sensibles aux propriétés biologiques des GAG, en utilisant parallèlement de nouveaux tests pour cibler d'autres mécanismes cellulaires impliqués dans la toxicité cellulaire.

A partir de ces résultats, il serait possible de conclure que les EPS ont clairement le potentiel d'être couplés à $^{43/44/47}\text{Sc}$ pour obtenir un outil théranostique efficace. Les protocoles de marquage doivent permettre des rendements de marquage élevés, avec une pureté radiochimique et une activité spécifique élevées également. La production de $^{44\text{m}}/^{44}\text{Sc}$ est déjà établie à Arronax et permet de produire des lots de haute pureté. Dans la perspective de ce travail, l'optimisation du radiomarquage de ces EPS avec le ^{44}Sc notamment devra être réalisée. L'efficacité du radiomarquage des ligands est généralement testée à différents pH, différentes températures et des concentrations variables de ligands (ou plus exactement à différents rapports molaires métal-ligand). Ce radiomarquage est suivi en fonction du temps afin d'être optimisé. Pour tester le rendement de radiomarquage, une radio-chromatographie sur couche mince (CCM) est généralement effectuée en déposant un aliquote de solution sur une plaque de CCM et en éluant avec une solution de développement. Parmi les paramètres d'optimisation, la composition de la solution d'éluant en est un. La plaque CCM est ensuite révélée sur un système autoradiographique. Les valeurs de R_f pour les conjugués $^{44}\text{Sc-EPS}^+$ et ^{44}Sc libre sont ensuite déterminées. Le principal enjeu avec les EPS de ce travail sera la composition de la solution d'éluant et le suivi de la migration des EPS seuls sur les plaques CCM. Pour contourner ce problème, la technique d'AF4-MALS pourra être utilisée et couplée à un détecteur de rayons γ . En effet, l'AF4-MALS- γ s'est révélé être un outil puissant pour suivre la taille et l'intégrité de liposomes ainsi que l'incorporation d'émetteurs alpha de haute énergie, ainsi que pour suivre la stabilité des liposomes radiomarqués au ^{212}Bi dans le sérum.

General introduction

The use of radionuclides in medicine is based largely on the discoveries of two critical concepts, the “tracer principle” and the “magic bullet”. In 1913, George de Hevesy developed the tracer approach and was the first to recognize that radionuclides could be used as tracers to follow how the native element or compound containing the element was distributed either in plants or animals [1]. He based his theory on the principle that radioactivity has the advantage of being easily detected at very low quantities, allowing for the introduction of minute quantities, nano- to pico-moles, that will not perturb the system. Thus, the radiolabeled tracer allows for non-invasive measurement of distribution and function in a biological system. Paul Ehrlich later developed the “magic bullet” concept highlighting how biomolecules, particularly antibodies, could be utilized as targeting molecules to transport toxins selectively to cancerous tissues [2]. For example, radionuclides can be attached to antibodies that are selective for receptors that are over-expressed on certain disease site such as tumor cells. The first example of antibodies coupled with medical radionuclides was proposed by Pressman and Keighley in the 50s [3]. The concept of the “magic bullet” has been expanded to include a host of nanocarriers, from small molecules such as folic acid to peptides and proteins, microspheres and most recently nanoparticles. Both concepts have been utilized to develop radiopharmaceuticals. They can be used either as diagnostics for the non-invasive imaging of disease or as therapeutics to deliver a toxic payload selectively, for instance, to a tumor site. Most of the development and optimization of radiopharmaceuticals occurs when designing or modifying the target selectivity of the molecule, not the mechanism of action, as with other drugs. Natural polysaccharides like glycosaminoglycans (GAGs), like heparin, have raised a growing interest these past decades in cancer research, but with some limitations such as haemorrhagic and contamination risks [4]. GAGs mimetics have paved the way to new approach and among these, an exopolysaccharide (EPS) from marine bacteria could provide many valid alternatives to traditional polysaccharides [5,6].

As the development of drugs that target specific pathways advanced, the use of the same targeting biomolecule or organic ligand for both imaging and therapy began, however with attachment to two different radionuclides. One radionuclide would be used to image individual patient disease states and evaluate their receptor expression, metabolic rate, clearance and handling, and a second radionuclide would be used for therapy. A new term has been coined for these drugs: “theranostics” [7]. Among the radionuclides considered, the scandium radionuclides have recently received considerable interest, providing personalised adjustment of radiation characteristics to optimize the efficiency of medical care or therapeutic benefit for

particular groups of patients [8]. Radionuclides of scandium, namely scandium-43 and scandium-44 ($^{43/44}\text{Sc}$) as positron emitters and scandium-47 (^{47}Sc), beta-radiation emitter, seem to fit ideally into the concept of theranostic pair. $^{44}\text{Sc}/^{47}\text{Sc}$ or $^{43}\text{Sc}/^{47}\text{Sc}$ pairs could be thus envisaged as true theranostic pairs.

In this context, the aim of this thesis is to evaluate natural exopolysaccharides as potential ligand for theranostics and to determine if they could be further coupled to scandium radionuclides. The characteristics related to the applicability of these EPSs in theranostics will be particularly studied, for example the rheological behaviour of the polymers. This stability will depend on the chemical composition of the suspensions, but also on the size and size distribution of the molecules and their surface charge. The first objective of this work will therefore be to establish the state of the art on the use of exopolysaccharides for medical use as well as on their characterizations. This work will present the characterization tools that allow us to study these properties. The methodology developed will ensure the control of the composition, size, shape and surface characteristics of the EPS for further potential in vivo injections. The second objective of this work is to reach to the most comprehensive description of the interaction of these EPSs with scandium, that is chemically similar to Y^{3+} and the heaviest lanthanides. But each metal is unique and is defined by its oxidation state, coordination number, hard-soft characteristics, kinetic inertness or lability, and redox stability. Therefore, the particular coordination chemistry of scandium to these EPSs must be accurately studied. Finally, the biological behavior of these EPSs will be assessed on different cancer cell lines, being coupled or not with scandium to further evaluate their potency for Nuclear Medicine. Thus, the work carried out in the context of this thesis will be presented in the following five axes.

We will briefly present in the first part, the characteristics of cancer and more specifically of osteosarcoma and the treatments currently used. Then, we will focus on the contribution of Nuclear Medicine for osteosarcoma diagnosis and therapy and the interest of GAGs to this aim. Finally, the objectives of this thesis will be clarified.

A second part will be dedicated to present the biology and chemistry of EPSs, as well as their production and purification. Since scandium is the element of interest for theranostics, its chemistry, coordination and production will be presented as well in this second chapter. Particular attention will be paid to the tools recommended for determining the physical and chemical parameters of polymers such as chemical composition, morphology, size, as well as the surface properties and the conformation of these EPSs. The morphology and size of the

EPS will be studied using several complementary characterization tools. For example, the precise chemical composition of the polymers will be studied, viscometry will determine the conformation of the macromolecules, and methods of dynamic light diffusion (DLS) will determine the hydrodynamic diameter of the EPS. In addition, the development of Flow Field-Flow Fractionation techniques (AF4) coupled with the Multiple Light Scattering Technique (MALS) will provide additional information on the molecular weight distribution of these EPSs.

In a third section, we will present the methods developed for the study of the interaction of scandium with these EPSs. The surface charge and the conformation that influences the complexation of scandium with EPS will be described as well.

The fourth axis will address the molecular characterization of lanthanide-EPS interactions. To this aim Time-Resolved Laser-Induced Spectroscopy has been employed. In this case, Europium was used as a molecular probe. Sc-EPS and Eu-EPS systems will be compared and discussed.

The fifth and final part of this work will deal with a preliminary *in vitro* evaluation of cytotoxicity of EPS-Sc complexes and compared to EPS themselves, as well as scandium, alone. This has been evaluated on different cell lines of osteosarcoma. The potential synergetic effect of scandium on the biological activity of these EPSs will be discussed.

Finally, the conclusions of this work will be drawn up and some perspectives on the use of the EPS together with scandium in a theranostic approach will be given.

References

- [1] Cockcroft, J.D. George de Hevesy. 1885-1966. *Biogr. Mem. Fellows R. Soc.* **1967**, *13*, 125–166.
- [2] Bordon, Y. The Many Sides of Paul Ehrlich. *Nat. Immunol.* **2016**, *17*, S6–S6, doi:10.1038/ni.3601.
- [3] Pressman, D.; Keighley, G. The Zone of Activity of Antibodies as Determined by the Use of Radioactive Tracers; the Zone of Activity of Nephritotoxic Antikidney Serum. *Journal of Immunology* **1948**, *59*, 141–146.
- [4] Afratis, N.; Gialeli, C.; Nikitovic, D.; Tseggenidis, T.; Karousou, E.; Theocharis, A.D.; Pavão, M.S.; Tzanakakis, G.N.; Karamanos, N.K. Glycosaminoglycans: Key Players in Cancer Cell Biology and Treatment: GAG Targeting in Cancer Cell Biology. *FEBS J.* **2012**, *279*, 1177–1197, doi:10.1111/j.1742-4658.2012.08529.x.
- [5] Senni, K.; Pereira, J.; Gueniche, F.; Delbarre-Ladrat, C.; Sinquin, C.; Ratiskol, J.; Godeau, G.; Fischer, A.-M.; Helley, D.; Collic-Jouault, S. Marine Polysaccharides: A Source of Bioactive Molecules for Cell Therapy and Tissue Engineering. *Mar. Drugs* **2011**, *9*, 1664–1681, doi:10.3390/md9091664.
- [6] Jouault, S.C.; Chevolut, L.; Helley, D.; Ratiskol, J.; Bros, A.; Sinquin, C.; Roger, O.; Fischer, A.-M. Characterization, Chemical Modifications and in Vitro Anticoagulant Properties of an Exopolysaccharide Produced by *Alteromonas infernus*. *Biochim. Biophys. Acta* **2001**, *11*.
- [7] Mango, L. Theranostics: A Unique Concept to Nuclear Medicine. *Arch. Cancer Sci. Ther.* **2017**, *1*, 001–004, doi:10.29328/journal.acst.1001001.
- [8] Huclier-Markai, S.; Alliot, C.; Sebti, J.; Brunel, B.; Aupiais, J. A Comparative Thermodynamic Study of the Formation of Scandium Complexes with DTPA and DOTA. *RSC Adv.* **2015**, *5*, 99606–99617, doi:10.1039/C5RA16736A.

Chapter 1

Cancer, Nuclear Medicine and interest of Glycosaminoglycans (GAGs)

I - Rationale: cancer prevalence

Cancer is the second cause of death in the world. The prevalence of cancer is actually increasing every year. In the United States, 1,700,000 people have been diagnosed with cancer, and around 600,000 of them succumbed to disease [1]. The cancer burden in Europe is estimated to have risen to 2.7 million new cases (all types, excluding non-melanoma skin cancer) and 1.3 million deaths in 2020 [2].

These estimates reveal that cancer affects men slightly more than women, with 54% of new cases and 56% of deaths. As is well known, cancer mostly affects older adults. The 2020 estimates reveal that 62% of estimated new diagnoses and 76% of estimated deaths occur in people over 65 years old.

Female breast cancer is the most commonly diagnosed cancer (see Figure 1). Over 355,000 women in the EU-27 are estimated to be diagnosed with breast cancer in 2020 (13.3% of all cancer diagnoses). This is followed by colorectal (341,000, 12.7%), prostate (336,000, 12.5%) and lung cancer (318,000, 11.9%).

[No copyright permission was obtained for this figure]

Figure 1. 2020 cancer incidence and mortality [2].

The most common causes of death are from cancers of the lung (20.4% of all cancer deaths), followed by colorectal (12.4%), female breast (7.3%) and pancreatic cancer (7.1%). Higher incidence rates are estimated in the Nordic countries. However, mortality rates for all cancers combined are estimated to be higher in Eastern countries, for both men and women.

Besides the affected individuals, all cancers have a large effect on the costs to national healthcare systems [3].

By contrast, osteosarcoma is the most common primary malignant bone tumor in children and young adults and accounts for 5% of all pediatric malignancies. It is a very aggressive type of cancer, but the majority of patients can be cured with a combination of chemotherapy and surgery. The standard regimen of chemotherapy is a combination of doxorubicin, cisplatin, and methotrexate. In limited resource settings, a combination of doxorubicin, carboplatin, and ifosfamide may be considered. In addition, complete surgical resection of the primary bone tumor and all detectable metastatic lesions should be pursued. Radiation therapy does not have a role in the primary treatment of conventional osteosarcoma. The overall survival for children

with localized disease is approximately 70%, while those with metastatic disease have an outcome close to 20% [4].

While osteosarcoma is a relatively rare cancer, it is the eighth most common cancer in children and adolescents, and it is the most common of the bone cancer [5]. In 2009, a US-based study estimated the global incidence rate of osteosarcoma in children to be between 3 to 4.5 cases per 1 million children, adolescents, and young adults (0-24 years of age) per year. The incidence rates were estimated to be relatively consistent throughout the world, with Italy, parts of Latin America, Sudan, and Uganda reporting slightly higher rates than in other regions. In those aged 0 to 24, osteosarcoma affects males at a rate of 3–5 per million and females at a rate of 2-4 per million. The onset of osteosarcoma tends to occur at younger ages in females than in males around the world. The incidence in the US in 2009 was found to be highest among Asian and Pacific Islander ethnic groups, suggesting that these groups are more susceptible to the disease [6]. A possible risk factor is rapid bone growth, which suggests a link between adolescent growth spurts and the onset of the disease [5]. Osteosarcoma (OS) is a vascularized tumor characterized by typical osteoid matrix formed by cancer cells. OS is characterized by a high potency to generate lung metastases that represent the main cause of death because micro-metastases are undetectable at initial diagnosis.

Several models have been suggested to explain the origin of osteosarcoma. One of the most discussed models involves cancer stem cells (CSC). In this perspective, tumors are considered to be hierarchically organized in a subpopulation of self-renewing cells, which are seen as tumor starters. Here, CSC are proposed to be the unique subsets of clones responsible for tumor propagation, resistance to treatments and metastasis spread. The CSC assumption suggests that tumors are maintained by these conditions and drug resistance and tumor recurrence are caused by the incomplete removal of this population of tumor-initiating stem cells. CSC were discovered for the first time in hematologic tumors like leukemia: they showed to initiate the pathology when transplanted into immunodeficiency mice. These discoveries were rapidly followed by similar outcomes regarding a subpopulation of tumor cells that could restart growing inside tumors in breast, brain, colon and many other organs. CSC have two essential properties in common with normal stem cells: the capacity for self-renewal and differentiation [7].

Unfortunately, the high level of heterogeneity characteristic of osteosarcoma makes more difficult the study of this kind of cells. Despite that, various methods have been drawn up to identify and isolate CSC based on their self-renewal features. Functional *in vitro* assays are

applied very often as initial step to enrich for CSC. The standard method to assess CSC potentiality *in vivo* is the transplantation of isolated enriched CSC into immunocompromised mice to evaluate the tumorigenic effect at low cell number. Both the *in vivo* and *in vitro* functional assays have the disadvantage that truly quiescent CSC will probably not be detected. A method for detecting cell population a higher tumorigenic potential is represented by an assay that evaluate how Hoechst 33342 dye or rhodamine-123 are exported from the tumor cell. This characteristic of increased efflux of dyes is normally due to increased expression of the ABC transporter family which are linked to increased efflux of chemotherapeutics and increased resistance [8].

When OS is suspected, histologic analysis of tumor tissue obtained by biopsy is required for diagnosis. Biopsy should be undertaken by an orthopedic surgeon experienced in orthopedic oncology, and who will likely perform the definitive surgery. Core needle biopsy by an interventional radiologist may be performed after discussion with the orthopedic surgeon about the appropriate biopsy tract. Plain radiographs of the primary site are the initial investigation of choice in a patient with symptoms suggestive of a bone tumor. Once osteosarcoma is suspected, a contrast enhanced MRI (magnetic resonance imaging) of the entire length of the involved bone should be obtained [9]. There are no specific blood tests for osteosarcoma, but lactate dehydrogenase and alkaline phosphatase levels may serve as a surrogate to track tumor burden. Additional imaging studies should be obtained at diagnosis to assess the extent of primary tumor and for the presence of metastatic disease. Computed tomography (CT) scan of the chest and radionuclide bone scan are used to detect lung (most common) and bone metastases, respectively [10,11]. Organ function measurements prior to starting chemotherapy include complete blood counts, liver function tests, renal function tests, evaluation of hearing capacity (audiogram) and cardiac function (commonly by echocardiogram to estimate ejection and shortening fractions).

Chemotherapy should be administered in a cancer centre with capacity for intravenous chemotherapy infusion and monitoring. Cisplatin can cause severe nausea and vomiting and requires administration of prophylactic anti-emetics. Doxorubicin extravasation can lead to local tissue injury and necrosis. Methotrexate-containing regimens require frequent monitoring of methotrexate levels, intravenous hydration, urinary alkalinization, and folinic acid rescue. Due to the high cumulative dose of doxorubicin in osteosarcoma treatment regimens, and the subsequent risk of cardiac toxicity, co-administration of dexrazoxane should be strongly considered (when available). Supportive care with G-CSF (Granulocyte colony-stimulating

factor) administration may be required to ensure timely therapy, especially towards the end of treatment. Patients should be monitored for treatment response and adverse effects of therapy. Disease evaluation scans should be performed pre-surgery and at approximately every 3 months. Patients should be monitored regularly for bone marrow suppression with blood counts, hearing loss with audiological examination, cardiac dysfunction with echocardiogram, and for liver and renal toxicity.

Although the OS survival has increased during the past decades, the prognosis has been only slightly improved. Today, still more than half of the OS population eventually succumbs to the disease despite the current multimodal primary treatments as well as second-line chemotherapy and surgery. The inclusion of additional drugs and new treatments to all patients does not yield a convincing survival benefit.

Recent studies focused on treating metastasis to increase the OS survival and have finally identified molecular mechanism of metastases in order to help identifying new therapeutic strategies [5,12].

A – Molecular pathways in cancer

Cancer originates from the abnormal proliferation of any type of cells in the body, that is determined by changes at cellular, genetic and epigenetic levels. Cell division, or mitosis, is a physiological process that takes place in almost all tissues in the body. Usually, the equilibrium between proliferation and programmed cell death, or apoptosis, is maintained to guarantee the normal functioning of tissues and organs. Several factors contribute to cancer and several mechanisms have been identified.

The genetic mechanism is probably one of the most affecting factors in cancer. If cells start dividing in an uncontrolled way, genes that regulate cell growth may have been altered. Gene mutations can cause several dysregulations that are implied in oncogenesis mechanisms. There are three main categories of genes that are affected by these changes. Oncogenes, that usually favor cell growth, may be present as normal genes that are disproportionally expressed, or altered genes that have acquired new properties. Oncogenes act through the production of mitogens: small proteins that induce cell division. Then, proto-oncogenes, that are the normally quiescent partners of oncogenes. When a mutation occurs, the proto-oncogenes turn into oncogenes, and this transition throws off the normal equilibrium of cell cycle regulation, making uncontrolled mitosis possible. Lastly, tumor suppressor genes, instead, are genes able to block cell division and survival of cancer cells. Normally, tumor suppressors are

transcription factors that are activated by cellular stress or DNA damage. However, cancer-promoting genetic changes often disable tumor suppressor genes. When enough proto-oncogenes have mutated into oncogenes, and enough tumor suppressor genes are deactivated or damaged, then the signals for cell growth overwhelm the signals to control it and mitosis rapidly gets out of control. Moreover, the role of certain infections has been discovered, especially those carried out by viruses that contain an oncogene. These viruses are considered as oncogenic because they activate the growth of tumorous tissues in the human host.

In both cases, mutation or infection, expression of these genes enhances the malignant phenotype of cancer cells. The resulting cancer cells develop several additional mechanisms that enhance the pathological picture. Those additional mechanisms include:

- *Angiogenesis*: the tumor help building new blood vessels surrounding it. These becomes new biological infrastructures for nutrients and new starting points for metastasis;
- *Accelerated metabolism*: the abnormal mitosis characterizing tumors requires enormous energies to malignant cell. Indeed, it is well-established that cancer cell needs very high levels or simple sugars, such as glucose;
- *Insensitivity to immune system*: because of a malignant phenotype, cancer cell would not exhibit anymore transmembrane proteins, particularly the ones used by immune system to identify abnormal cells;
- *Inflammation*: certain cancer environment become hostile because of pro-inflammatory cytokines that alter the surrounding tissues, facilitating cancer invasion and impeding the arrival *in situ* of chemotherapeutics.

Metastasis is simplified by cell-cell interactions between tumor cells and endothelium in distant tissues but also by blood cells in bloodstream, such as platelets and leukocytes. These cells are the same cells involved in the coagulation cascade. As shown in Figure 2, tumor metastasis is a multistep process. It starts with the local invasion of cancer cells around the primary tumor site running towards blood vessels. Next steps are the surviving of those cells in systemic circulation, and then the extravasation in secondary sites. The establishment of growing metastatic lesions is observed then.

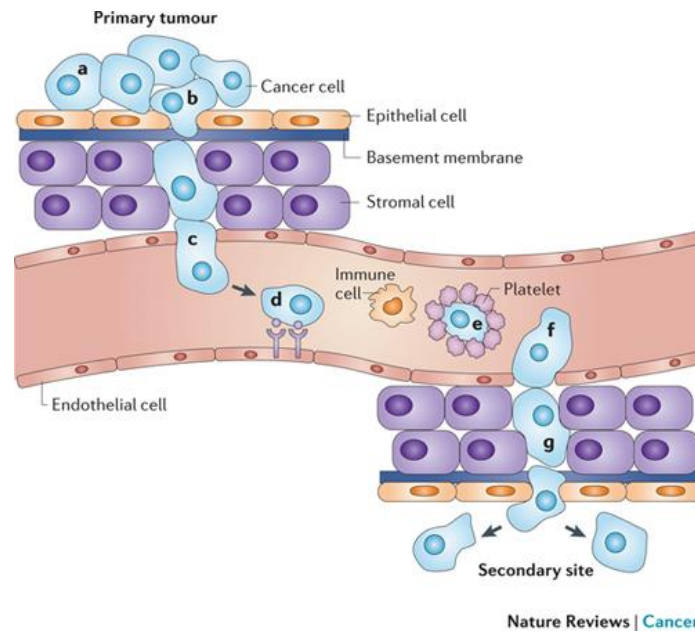


Figure 2. The steps of metastasis and opportunities for therapeutic intervention [13].

Cell-adhesion macromolecules, such as selectins and integrins, play a key role in metastasis arising. They are transmembrane glycoproteins, that are expressed on the surface of leukocytes, platelets, and endothelium cells. Metastasis seed exploits these glycoproteins to form a thrombus, a blood vessel complication. This complication is used by the tumor to carry itself in the blood flow, and also to make the metastasis extravasation possible. While cell-cell interactions are essential steps in the metastatic pathway because they facilitate tumor cell adhesion in the blood vessels of specific organs, the inhibition of these interactions represent a therapeutically useful target for mitigation of metastases [12].

In the past fifty years, conventional chemotherapy was the main choice to treat primary tumors and their metastasis. Conventional chemotherapy includes the administration of one or few drugs at one time, often combined with other cancer treatments (radiation therapy, surgery, etc.). Frequently, several cycles of chemotherapy are necessary to reach effective results. In general, chemotherapeutic is efficiently blocking the fast proliferating cells and prevent mitosis by interfering with DNA synthesis or other steps involved in cell cycle process. Alkylating agents, that substitute alkyl groups for hydrogen atoms on DNA, are the oldest chemotherapeutic compounds that have been used since the late 1940s. Even if classical chemotherapy is the key concept to control cancer proliferation, drawbacks in its administration are considerable. Difficulty in dosage selection, lack of specificity (which produces cytotoxicity to normal cells as well), rapid drug metabolism, and dangerous side effects drastically limit its success in oncology [14]. All these drawbacks of conventional

chemotherapy are due to the absence of precision that target tumor cell but also a significant number of healthy cells and tissues. In fact, the main targets of this kind of therapy is the cell-cycle, pathological accelerated in tumor cells but also physiological enhanced in certain healthy tissues.

Every tumor is unique, and different tumors from the same tissue may have completely distinct molecular characteristics. That was firstly described in 1976 [15] but then overlooked. The formation of a malignant tumor is a succession of mutations that confers a selective advantage, under pressure from the microenvironment, treatments... followed by periods of clonal expansion (so called the Darwinian model of oncogenesis). Each type of cancer includes subtypes with signatures different biological distinguish by their clinical prognosis and their response to treatment. In the last decades, significant efforts have been made to identify molecular pathways involved in cancer (Figure 3). This has paved the way to a new approach in medicine: personalized medicine.

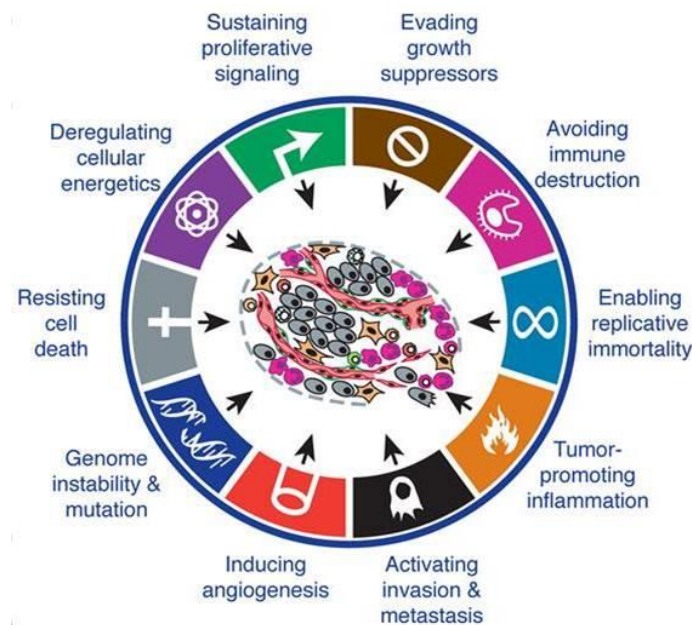


Figure 3. Oncogenesis mechanisms involved in cancer. Adapted from Hanahan and Weinberg [16].

In personalized medicine, the care is individualized. Each patient receives adapted optimal treatment, given the specificities and the molecular characteristics of his/her tumor. The need to establish the phenotype/identity card of anatomical, biological, genetic characteristics, metabolic, functional... is thus relevant. Therefore, biomarkers consist in reliable process indicators or response to treatment.

B – Biomarkers

In cancer, particular biomolecules, such as DNA, RNA, proteins, and enzymes, could be over produced, or altered in their structure, by the tumor or from a specific response of the body induced by the presence of cancer. These altered or over-produced biomolecules are defined as “biomarkers” and they are an objective indication of the presence of disturbances in the body mechanisms. The World Health Organization (WHO) has defined biomarker as “*any substance, structure or process that can be measured in the body or its products and influence or predict the incidence of outcome or disease*”.

Biomarkers in oncology consist in biological parameters to characterize a pathological condition and are based on the fundamental oncogenesis mechanisms (see Figure 4).

Depending on their function, they allow:

- i) assessing a risk of developing a medical condition (risk biomarker) – biomarkers represent a quantitative way to determine if persons are predisposed to particular types of cancer –;
- ii) realizing accurate diagnosis (diagnostic biomarker) – biomarkers aim to establish if tumors are of primary or of metastatic origin –;
- iii) predicting or tracking the course of a pathology (prognostic biomarker) – they can be used to measure the aggressiveness of a detected tumor as well as its likelihood of responding to a given treatment –;
- iv) predicting therapeutic response (predictive biomarker) – cancer biomarkers have also shown an importance in monitoring how responsive is a treatment over time [17].

A number of gene and proteins have been identified and are currently used in clinics as cancer biomarkers, of which Figure 4 gives a summary. Just to quote, BCR-ABL (chronic myeloid leukemia), HER-2 (breast cancer), KIT (gastrointestinal stromal tumor) and PSA (prostate cancer) are some of the biomarkers currently used in clinics.

[No copyright permission was obtained for this figure]

Figure 4. Oncogenesis mechanisms and relative biomarkers. Adapted from Alam et al, 2014.

Relevant biomarkers are thus necessary to help selecting patients for therapy in the frame of personalized medicine, and for predicting the response to treatments. They will serve to study the biodistribution of therapy in order to predict its effectiveness: so called a companion test. Finally, they are used for studying the biodistribution of a targeted molecule, added with an

imaging agent and then a therapeutic agent, named a theranostic agent. These concepts have been fully explored and developed in the field of Nuclear Medicine, which concepts are developed afterwards.

II - Nuclear medicine

The localization or selective destruction of cancer cells by a biological vector coupled with radionuclide is a simple and particularly attractive concept. Postulated by Ehrlich at the turn of the 20th century [18], this concept is most often based on the use of antigen recognition properties associated with antibody cancerous tumors [19]. These antibodies can specifically carry organic substances within the tumor mass in order to locate or destroy it (medical imaging). The molecules carrying the radioelements generally differ according to the radionuclide used but also and above all according to the desired purpose: imaging or therapy. The work of Pressman and Keighley [20] has shown the feasibility of this concept. However, the low availability of purified polyclonal antibodies and especially monoclonal antibodies has long limited the effectiveness of this technique. It was not until 1975, with the discovery of the technique of cell hybridization by Kohler and Milstein [21], that this concept has been developed. From then on, doctors had an interesting tool for the specific vectoring of non-toxic substances for imaging and toxic for therapy.

From a historical point of view, his first contributions were mainly in the field of oncology, but nuclear medicine today allows studying virtually all the systems of the human body and thus finds applications in all medical specialties, always including oncology but also neurology, cardiology, endocrinology, nephrology, gastroenterology, pneumology, infectious diseases, various disciplines... I will focus on the part of medicine dedicated to oncology.

The principle of nuclear medicine is to inject radioactive isotopes into the patient and target an organ or place of the body for the purpose of diagnosing or treating diseases. The main areas of application are:

- in vivo functional imaging that consists of the administration of a radioactive tracer to the patient allowing its external detection, *i.e.* scans (gamma radiation emission) or PET scans (positron emission tomography);
- In vitro biological diagnosis, *i.e.* radioimmunology;
- Metabolic radiation therapy.

Since the early 1980s, a technological revolution has profoundly changed the outlook for nuclear medicine. This technological revolution has allowed the introduction of PET imaging with the use of fluorodeoxyglucose (FDG) tracer marked with fluoride-18 (^{18}F -FDG) in routine practice of nuclear cancer. At the same time, significant progress has been made in the development of vectored radiotherapy. All these advances open up broad prospects with the availability of many vector molecules that are currently being evaluated in preclinical and clinical studies. In this context, new needs for original radioisotopes, positrons transmitters for PET imaging diagnosis and transmitters β^- and α for therapy.

The choice of the type of transmitter depends on the specifics of the cancer to be treated. For example, particles β^- are well adapted to the treatment of small tumors because they have a path in the body of a few millimeters with a low transfer of linear energy (TEL). TEL is similar to the stopping power of a particle in an environment except that it does not take into account radiative energy losses, such as braking radiation. It is therefore a parameter related to the therapeutic effect of radiation.

Particles α are particularly well suited to the treatment of scattered tumors because the decay of a α emitter results in a particle that has a path that is about 100 times smaller than beta particles and with a large transfer of linear energy, about 100 to 1000 times more than that of beta particles.

A - Radionuclides for Nuclear Imaging

The radioactive isotope used to make a radiotracer must meet two main characteristics:

- the radiation emitted must be able to be detected outside the patient; it is therefore necessary to have highly penetrating radiations such as photons γ ; photons γ are the most energetic electromagnetic radiation and can pass through the human body with a relatively low energy (20 to 600 keV) thus allowing the location of radionuclide;
- it should not be accompanied by abundant harmful emissions.

Depending on the type of radioisotope emissions used, photons γ can be obtained:

- by annihilation of a positron with an electron; in this case, PET technique is used;
- when decays a nucleus in a state of energy higher than its fundamental state; TEMP/SPECT scan and imaging technique is used.

1 - Positron Emission Tomography (PET)

Positrons emission tomography (PET) is a medical imaging modality that measures the three-dimensional distribution of a molecule labelled with a positron emitter.

Fluor-18 is now the most widely used β emitter in PET imaging. It is produced in cyclotrons by bombardment of water enriched with oxygen-18 by protons. FDG is a molecule with a structural appearance close enough to glucose to be picked up by sugar-intensive tumor cells. Because fluor-18 is radioactive, the radiation emitted is captured by a gamma camera and produces a hyper-fixation image (very marked) in glucose-consuming places such as the heart, brain or tumors. Other vectors using ^{18}F , including FLT (fluorothymidine), F-MISO (fluoromisonidazole), F-Choline (fluorocholine), F-DOPA (fluorodihydroxyphenylalanine), have been clinically evaluated and some have been granted marketing authorization for routine use (F-DOPA and F-Choline). In addition, fluoridated molecules have a small size and as a result, a rapid distribution kinetic after intravenous injection, which is consistent with the relatively short physical period of fluorine-18 (110 minutes). In addition, this short physical period of fluor-18 requires production in a cyclotron located a short distance from each user center. However, for larger vector molecules, such as antibodies or more generally immunoconjugates, blood kinetics are much slower and maximum tumor fixation is observed relatively late, a few hours or days after intravenous injection. This time interval is not consistent with the short physical period of 110 minutes of fluor-18. For this new application in PET imaging, called immuno-PET, new radioisotopes, with longer physical periods, are then needed as for example iodine-124 with a physical period of 4.2 days. Copper-64, with a physical period of 12.7 hours, is another transmitter of positrons of great interest that is envisaged for routine production.

2 - MonoPhotonic Emission Tomography (TEMP)

In 1976, John Keyes proposed the Tomography of Emission MonoPhotonics (TEMP) [22], based on the principle of the scanner. It is better known internationally as SPECT (Single Photon Emission Computed Tomography). The TEMP/ SPECT is based on the emission of a photon when a nucleus of the excited state returns to the fundamental state. After the injection of a radiotracer into the patient and its fixation on the target organ, gamma photons can be detected at well-defined energies and characteristic of the injected radioisotope.

In cardiology, thallium-201 and technetium-99m-MIBI (Cardiolite®) have been used in routine practice for decades for the diagnosis of myocardial ischemia. In 1977, the New England Nuclear Society received approval from the U.S. Food and Drug Administration (FDA) for the

distribution of thallium-201 for TEMP/SPECT imaging [23]. The Tl-201 has a radioactive period of 72.9 hours. It disintegrates by electronic capture (100%) and emits a 167 keV γ -photon (10%). Ten years later, technetium-99m was approved by the FDA for the diagnosis of apoplexy, the visible effect of stroke [24]. Technetium-99m, with its short six-hour period and γ -photon emitted at an energy of 141 keV during its decay, is now the most commonly used. For the marking of immunoconjugates and peptides, the most considered pairs of radioisotopes are iodine-124/iodine-131 and yttrium-86/yttrium-90. However, for the latter pair, the high energy of gamma radiation, emitted in abundance by yttrium-86, is a major drawback for the routine use of this radioisotope. Another pair of radioisotopes used is copper-64/copper-67 thanks to the favorable characteristics of the two radioisotopes. Among other positrons, gallium-68 is the subject of numerous studies. The interest of gallium-68 comes from its mode of production. Unlike fluor-18 or copper-64 that require a cyclotron, gallium is produced using a germanium-68 decay generator. Finally, gallium is a trivalent metal cation that can also be complexed in a stable way by chelate agents of the poly-amino-carboxylate family.

Table 1. Radionuclides of interest for PET imaging [25].

Radionuclide	$T_{1/2}$	Radiations		
		Type of emission	Energy (keV)	Abundance (%)
^{11}C	20.4 min	β^+	960.5	99.8
^{13}N	10 min	β^+	1198.5	99.8
^{15}O	2.1 min	β^+	1735.0	99.9
^{18}F	109.7 min	β^+	633.3	96.9
^{68}Ga	67.7 min	β^+	1899.1	87.4
		γ	1077.3	3.2
			1883	0.1
^{64}Cu	12.7 hrs	β^+	579.4	38.5
		β^-	653.1	17.6
		γ	1345.8	0.5
^{86}Y	14.7 hrs	β^+	1220	11.9
		γ	1077	82.5
			628	32.6
^{89}Zr	78.4 hrs	β^+	902	22.7
		γ	909	99
			1713	0.7
^{124}I	4.18 days	β^+	1532	25.6
		γ	2135	74.4

radionuclide in TEMP/SPECT imaging. It is obtained from a generator system, by decreasing molybdenum-99.

In the same year, Medi-Physics received FDA approval to market iodine-123 for TEMP/SPECT imaging [26]. Iodine-123 is an isotope of interest for thyroid imaging. It disintegrates by electronic capture in ^{123}Te with a half-life of 13.2 hours. The 159 keV γ -photon emitted allows its use in TEMP/SPECT imaging. When radioactive iodine-123 is administered to the patient it attaches naturally to the thyroid, emits its γ -photons and allows the detection of a functional abnormality of the thyroid. Technetium-99m is also used for the diagnosis of thyroid cancer and is picked up by the thyroid in a similar way to iodine. It is an optimal gamma energy emitter for imaging (gamma radiation of 140 Kev).

Finally, rubidium-82 is a positron-emitting radioisotope that is picked up by the myocardial muscle given its analogy with potassium. Rubidium-82 has a very short radioactive period (75 seconds) and is produced as a generator by degrowth of strontium-82, which has a period of 25.5 days. This very short radioactive period of rubidium-82 allows the imaging to be carried out in the stress and rest phase in less than 30 minutes compared to a few hours with SPECT imaging using thallium-201 or technetium-99m-MIBI more beneficial to the patient. Finally, the fact that it is a PET transmitter improves the quality of the image and therefore the diagnosis.

With the advent of biomarkers, molecular imaging has become a leading role in nuclear medicine examinations. The objective of molecular imaging is to best monitor the natural history of the disease and to evaluate *in vivo* possible therapeutic interventions.

B - Vectorized radiotherapy

Two treatment techniques using radionuclides can be used:

- brachytherapy, which is an internal therapy technique designed to place a sealed radioactive source or source near or directly in the area to be treated;
- metabolic therapy (or vectorized internal radiotherapy), which involves administering a drug containing a radioactive nucleus attached to a vector capable of targeting cells of interest and destroying them by emitted radiation (particles α or electrons).

Several vectors can be used depending on the target cells such as a molecule, a peptide or an antibody. The time taken by these vectors to reach the target is different depending on their size (the antibody will be slower than the molecule). The radioactive period of the radionuclide

attached to this vector must therefore be adapted so that the maximum number of decays is carried out at the targeted site and not along its route.

At this stage, we must mention the existence as well of External Beam RadioTherapy (EBRT). It is normally prescribed as a treatment of several sessions over days or weeks. External radiotherapy usually involves patient visits to a hospital or center specialized in cancer therapies. Through a particular machine, a high-energy radiation, usually gamma-rays, irradiate the cancer site and a small area of normal tissue surrounding it. The patient is positioned horizontally on a couch and then the radiation beam is directed precisely at the area to be treated, often from different angles. Currently, most radiation treatments are performed using machines called particle accelerators (in this case, linear accelerators). These equipment generate and deliver radiations using electric fields rather than radioactive material. EBRT can handle many cancer types, including breast cancer, colorectal cancer, and melanoma. Adverse reactions during or after radiotherapy may be caused by many factors. These include the strength of the radiation dose, the part of the body being irradiated, and what tissues and organs are involved in that part. The most common side effects are skin changes, nausea, hair loss and, in most cases, are only temporary.

1 - Characteristics of particles used in targeted therapy

The three radioisotopes currently used in the clinic for therapy are iodine-131, yttrium-90 and lutecium-177 (see Table 2). They cover a range of energy β -adapted to small tumors. In addition, yttrium-90, a high-energy β -emitter, is attached by the bone marrow after release from a chelating agent coupled with the vector molecule. The result is irradiation of the bone marrow that limits the activity injected. In addition, yttrium-90 does not emit associated gamma radiation for pre-therapeutic imaging, and yttrium-86 emits a high percentage of high-energy gamma radiation (82.5%) for a routine practice that causes large doses. A radioisotope of interest, with favorable radiophysical and biological characteristics, is copper-67 (physical period: 61.5 hours), which has been evaluated in preclinical and clinical studies for more than two decades. Compared to iodine-131 and yttrium-90 in a limited number of clinical studies, copper-67 showed the highest therapeutic index. Finally, it can be coupled to copper-64 for imaging.

Scandium radioisotopes are interesting for both radiotherapy and diagnosis. Specifically, scandium isotopes 44 and 47 have been identified as promising for the implementation of β -immunotherapy, in addition to the $^{64}\text{Cu}/^{67}\text{Cu}$ couple. The ^{47}Sc has a half-life of 3.35 days and emits a particle β^- (0.6 MeV average energy, 100% emission) and γ radiation (159 keV, 68%

emission intensity) comparable to ^{67}Cu , making it a promising radionuclide for targeted therapy. The ^{44}Sc is a β transmitter (632 keV, 94.27%) with energy comparable to ^{18}F , but with a longer half-life of 3.97 h. It is the β congener of ^{47}Sc , which allows a dosimetric study associated with ^{47}Sc therapy by being coupled with biological vectors. Finally, the $^{44}\text{Sc}/^{47}\text{Sc}$ torque allows later imaging with the use of the $^{44\text{m}}\text{Sc}$. Other transmitters have also been identified as of interest in β therapy, such as rhenium-186 [27] and holmium-166 [28].

The electrons from the β^- decay will deposit their energy over a high distance, resulting in a low transfer of linear energy (LET). Alpha particle-emitting radioisotopes are increasingly being considered for their use in targeted alpha therapy due to their high energy transfer (LET), which gives them a high cytotoxic effect especially for small tumor cells. Some alpha particle-emitting radioisotopes are usable, including radium-223 (a drug Xofigo on the market for the treatment of castration-resistant prostate cancer with bone metastases), astatine-211, lead-212/bismuth-212 and actinium-225/bismuth-213.

Table 2. Radionuclides of interest for radiotherapy [29].

Radionuclide	$T_{1/2}$	Type of emission	Radiations Energy (keV)	Abundance (%)
^{32}P	14.26 days	β^-	1710	-
^{89}Sr	50.53 days	β^-	1496	100.0
^{90}Y	64.10 days	β^-	2280.1	100.0
^{131}I	8.02 days	β^-	606	89.3
^{177}Lu	6.73 days	β^-	497.8	100.0
^{186}Re	3.72 days	β^-	1069.5	92.5
^{223}Ra	11.44 days	α	5972.2	-
^{211}At	7.2 hrs	α	7500	-

Radio-immunotherapy involves injecting into the patient's blood a specific antibody of cancer cells to which a radioactive element is attached (see Figure 5). This radio-marked antibody, capable of recognizing cancer cells and attaching to their surface, allows the tumor to be irradiated in a very localized way in order to destroy it. Radio-immunotherapy is of great interest in the treatment of solid tumors, including metastatic tumors.

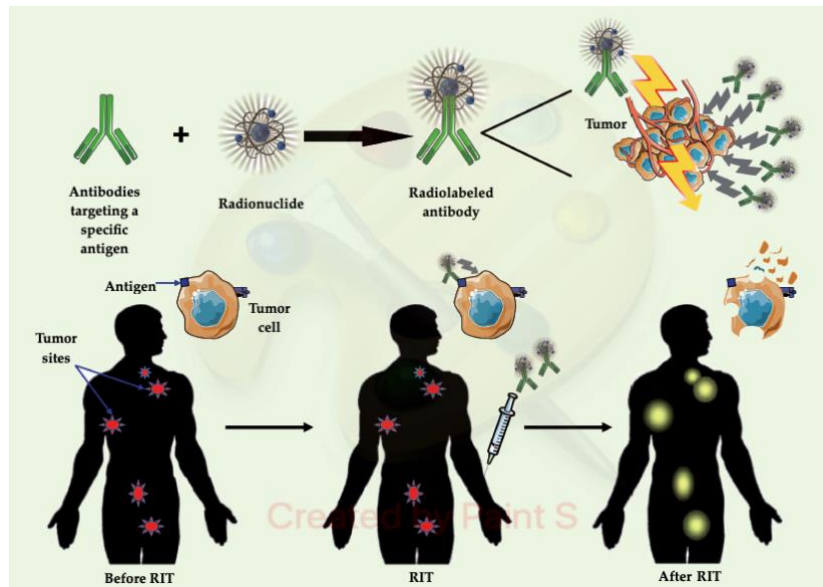


Figure 5. Principles of RIT. Adapted from Ménager et al. 2016 [30].

External radiation therapy methods often cause radionecrosis of surrounding healthy tissues, resulting in various side effects and even death in some cases. In order to reduce the side effects of conventional radiotherapy and to improve the effects of treatment on malignant tumors, current developments tend to place radiation locally and very precisely in the targeted tumor zone: this is brachytherapy, which we will address.

2 - Brachytherapy

Brachytherapy is an alternative cancer treatment technique that has been used for many years. It is based on the use of β -emitting radioactive isotopes. These isotopes are arranged on contact, or implanted in the tumor, to deliver a high dose of irradiation in a target volume limited to contact or within the tumor in order to directly target the area affected by the cancer [31].

Brachytherapy accounts for 4.3% of total radiotherapy activity in France with just over 7,500 patients treated per year. The most conventional approach is to surgically implant grains or wires containing radioisotope. The rapid drop in the dose delivered on the periphery spares the nearby radiosensitive organs. Compared to external radiotherapy techniques, this technique minimizes the risk of radio-induced cancer.

Many tumor locations accessible from the body surface can be treated by this technique. Cancers of the cervix and uterine body are major indications. Treatment may be pre- or post-surgical or combined with external radiotherapy to create a larger localized dosage. Prostate tumors have also been the subject of important work. The aim is either to overdose during prostate radiotherapy while protecting the surrounding organs, or to treat the prostate volume entirely. Skin cancers are too extensive for surgical treatment that may be mutilating, or contact

radiotherapy that is too superficial, and are also an interesting indication for brachytherapy. Finally, brachytherapy can be applied to breast cancers that are too large for resection [14].

There are two types of brachytherapy in oncology:

- for intra-cavity treatment, radiation sources are introduced into a natural cavity near the tumor such as the vagina, uterus or trachea;
- for interstitial treatments, the sources are placed in the tumor (intratumoral) or in the remaining cavity after the removal of the tumor.

Intra-cavity treatments are always temporary, short-term, while interstitial treatments may be temporary or permanent. Temporary implants are inserted using manual or remote loading procedures. Other less common forms of brachytherapy treatments include applications of superficial, intraluminal plaque (intestinal cavity), intraoperative and intravascular. For these treatments, radiation-emitting sources γ or β^- are used.

The physical advantage of brachytherapy treatments over external radiotherapy is the improvement in localized distribution of the dose to the target volume of interest. The downside is that brachytherapy can only be used in cases where the tumor is well localized and relatively small. In a typical radiotherapy department, about 10 to 20% of patients are treated with this method.

Brachytherapy treatments are categorized according to dose rate. There is no universal definition of these dose classes, but the following is common use. A dose between 0.4 and 2 Gy/h is a low dose rate (LDR). Low-dose brachytherapy is beneficial because it allows cells to recover better. A dose between 2 and 12 Gy/h is equivalent to a medium dose rate (MDR). Many cervical cancer treatments are given at about 1.5-2 Gy/h. Finally, doses above 12 Gy/h (0.2 Gy/min) correspond to a high dose rate (HDR).

For a brachytherapy technique to be effective, it must ensure control of the dose delivered, *i.e.* maximize the effective radioactive dose delivered to tumor cells and minimize the radioactive dose delivered to healthy tissues.

Although radiotherapy uses radiation to damage cells for the benefit of patient care, this damage is a limitation for diagnostic employment. The purpose of diagnostic radiations is to display and not to kill cells. In general, radiation dosages for clinical indications are optimized according preliminary studies. To understand the effects of radiation on a healthy organ, it is important to measure the quantity of radiation energy deposited/absorbed in that organ, which is called radiation absorbed dose. Correct dosages are adjusted through careful studies of pharmacokinetics, physico-chemical properties of radionuclide, drug pharmacodynamics and

metabolism. Radiochemical-toxicity and side effects must be well understood before an optimal and safe dosage.

One major limitation of cancer radiotherapy is represented by the maximum tolerated dose to adjacent normal tissues. For this reason, an effective radiotherapy takes into consideration to maximize cancer cell killing within the range of acceptable dose that adjacent healthy tissues can tolerate from irradiation. This aspect can be implemented by considering the properties of the radionuclide (type of decay, energy, half-life, etc.) as well as the characteristics of biological vector and its covalently attached linker. Concerning the radionuclide, clinical needs are driving the research towards radionuclides with a type of decay and the range of radiations penetration should guarantee the highest toxicity exclusively to cancer cells. Additionally, suitable half-life adapted to the medical approach (diagnosis, therapy or both) is required to match the biological half-life of the biomolecular vector.

C - Radiopharmaceuticals

As described in the previous sections, the drugs that are developed for diagnosis and/or therapy and that contain radioisotopes are called radiopharmaceuticals. Schematically, radiopharmaceuticals are constituted of three main parts (see Figure 6):

- 1) *carrier*, or *vector*, which allows selecting any known molecular target for site-specific delivery of the radioactive “payload” to specific cells, tissues or organs;
- 2) *linker*, normally represented by a *bifunctional chelator (BFC)*, which must be carefully matched with the radiometal for optimal stability. There are different types of bioconjugation reactions and linkages;
- 3) *radionuclide*, which changes the radioactive emission properties and half-life (γ for SPECT, β^+ for PET, and β^- or particles, or Auger electrons, for therapy).

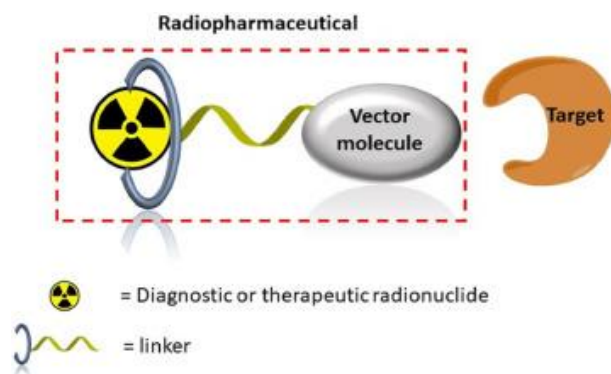


Figure 6. Schematic design of a radiopharmaceutical [32].

1 – The radionuclide

The half-life of a radionuclide is a key factor. It is involved at different steps of the radiopharmaceutical development.

1. *Production.* The shorter the half-life is, the higher the production yield must be in order to compensate the decay of radioactivity. The distance between the production site and hospitals must be also taken into account.
2. *Radiolabeling.* It consists of tagging (a hormone, enzyme, or other substance) with a radioactive tracer. The radiolabeling must provide the highest yield in a time frame compatible with the half-life, in order to deliver the maximum activity to the patient accordingly to the clinical need aimed.
3. *Clinical Efficacy.* It is fundamental that the half-life of the radionuclide matches the biological half-life of the molecular vector used (see Figure 7). Few hours are usually suitable for assessing diagnostic requirement, while several days are necessary for targeted radiotherapy with antibodies. For instance, if the half-life of the radionuclide is longer than the vector biodistribution and clearance, excessive irradiation of the patient could occur [33] as well as inactivation of biological ligand.

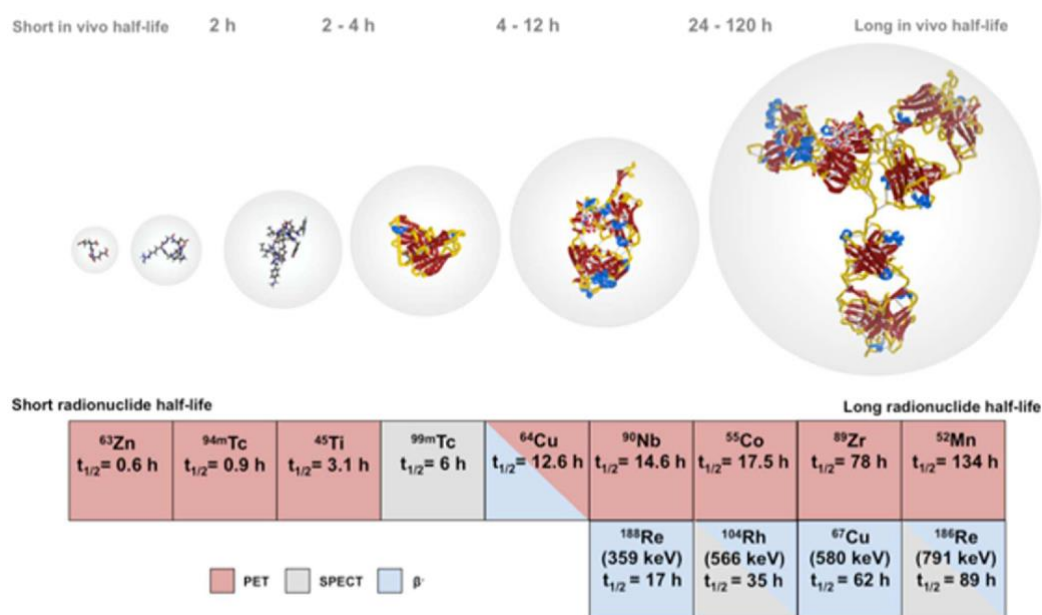


Figure 7. Isotopes of current and emerging interest for imaging and therapy applications ordered from short to long half-life, matching the *in vivo* half-life of small molecules, peptides, proteins, and monoclonal antibodies [34].

2 – The chelate

Radiometal nuclides can serve as diagnostic markers in molecular imaging or can be used in therapeutic settings for a rising number of human afflictions. For the targeted delivery of these

medically interesting ions, appropriate chelating agents forming stable complexes are of fundamental importance. For different metal ions exhibiting different physical and chemical properties, resulting in different coordination chemistries and therefore differing requirements on the chelator used, a broad variety of chelating agents has been developed over the years. Not only the chemical properties of the metal ion determine the choice of the chelator, but also the desired *in vivo* behaviour of the resulting molecular imaging or therapeutic compound influence the choice of the complexation agent. Furthermore, the conjugation chemistry for the introduction of the chelator into the biologically active compound, and the complexation reaction of the metal ion, can affect the choice of the appropriate chelator.

As highlighted by Price and Orvig [35], each radiometal ion has different chemical demands, including ligand donor atom preferences (*e.g.* N, O, S, hard/ soft), coordination number, and coordination geometry; however, there are many key design considerations that can be applied universally. Ligand synthesis should be relatively simple and avoid stereoisomers and non-enantio/diastereospecific reactions. Modularity should be incorporated in BFC synthesis as much as possible to allow for incorporation of different bioconjugation handles, and modular synthesis also should allow for tuning of denticity and physical properties by changing the polarity and charge of the chelate – the degree of polarity can be assessed by octanol–water partition coefficients ($\log P$) –, so that biodistribution properties can be adjusted.

When designing new chelators, a historical glance at previous work reveals that macrocycles are generally more kinetically inert than acyclic chelators, even if their thermodynamic stabilities have been determined to be very similar. Macrocyclic chelators require minimal physical manipulation during metal ion coordination, as they possess inherently constrained geometries and partially pre-organized metal ion binding sites, thereby decreasing the entropic loss experienced upon metal ion coordination. To contrast this, acyclic chelators must undergo a more drastic change in physical orientation and geometry in solution in order to arrange donor atoms to coordinate with a metal ion, and subsequently they suffer a more significant decrease in entropy than macrocycles (thermodynamically unfavorable).

The thermodynamic driving force towards complex formation is therefore greater for macrocycles in general, a phenomenon referred to as the macrocycle effect. A crucial property where most acyclic chelators excel and most macrocycles suffer is in the coordination kinetics and radiolabeling efficiency. The ability to quantitatively radiolabel/coordinate a radiometal in less than 15 minutes at room temperature is a common property of acyclic chelators, whereas macrocycles often require heating to 60–95 °C for extended times (30–90 minutes). Fast room

temperature radiolabeling becomes a crucial property when working with BFC-conjugates of heat sensitive molecules such as antibodies and their derivatives, or when working with short half-life isotopes such as ^{68}Ga , $^{212/213}\text{Bi}$, ^{44}Sc , and ^{64}Cu (see Figure 8).

[No copyright permission was obtained for this figure]

Figure 8. Illustration of an archetypal radiometal-based radiopharmaceutical agent containing a bifunctional chelator (BFC) conjugated to a targeting vector (*e.g.* antibody, peptide, nanoparticle) using a variety of conjugation methods (*e.g.* isothiocyanate–amine coupling, peptide coupling, maleimide–thiol coupling, activated ester amide coupling, click-coupling) and then radiolabeled with a radiometal ion (*e.g.* $^{111}\text{In}^{3+}/^{177}\text{Lu}^{3+}/^{86/90}\text{Y}^{3+}$) [35].

The structure and physical properties of the radiometal–chelate complex have a large impact on the overall pharmacokinetic properties of a radiopharmaceutical, with many radiometal complexes being very hydrophilic and subsequently leading to rapid renal excretion when attached to small vectors like peptides and nucleotides. It has been observed in peptide conjugates that keeping the radiometal ion and peptide constant and changing only the chelator can have drastic effects on biodistributions.

a. Thermodynamic stability

In vivo thermodynamic stability and kinetic inertness is undoubtedly the most essential aspect to be considered when evaluating a chelator-radionuclide interaction in the development of a radiopharmaceutical. Thermodynamic stability, represented by formation constants for the reaction



is frequently and easily determined in an experimental way by potentiometric/spectroscopic titrations. Additional techniques to study and quantify the complexation between metal and ligand are *capillary electrophoreses* paired to *inductively coupled plasma mass spectroscopy* (CE-ICP MS) and *free ion selective radiotracer extraction* (FISRE). Potentiometric titrations are commonly used to determine the stability constants of metal-ligand complexes, but they require high amounts of both components and, especially, a chemical stability of ligand in a wide pH range (often very acidic). Concerning spectroscopic titrations, when an NMR spectrum shows a shift in the resonance frequency as a function of changing concentration, it may be caused by the complexation [36]. CE-ICP MS allows the direct speciation of the system studied at trace concentrations, but for determining the stability constants it requires a significant variation of the complex charges. FISRE may be an alternative and safe method,

due to the low amounts of sample to use (compatible with radionuclides conditions as well). In contrast to CE-ICP MS, FISRE cannot determine different complex species since it is considered as an indirect method [37]. Stability constants for certain metal ligand complexes are determined in presence of a chelating resin; the chelating resin competes with the ligand to complex the metal.

Evaluating kinetic inertness under conditions related to *in vivo* applications may be much more problematic than studying the stability from a thermodynamic point of view. Thermodynamic stability constants are considered a handy tool to initially study the complexation between several chelators with different metal ions, but they do not provide any relevant information concerning the *in vivo* stability. Thermodynamic stability from a biological point of view is more frequently related to another parameter, pM value (or $-\text{Log}[M]_{\text{Free}}$). The pM value is the negative log of the concentration of free metal ion that remains uncomplexed by a given chelator under specific conditions. What makes interesting pM is the fact that it is a parameter dependent by many conditions, such as ligand basicity, metal ion hydrolysis, physiological pH, and ligand:metal ratio. Stability constants and pM values are able to quantify the direction and magnitude of the equilibrium in a metal–chelate coordination reaction but they offer no kinetic information, such as the the rate of dissociation. The kinetic inertness of a radiometal complex, in fact, is definitely affected by the *in vivo* rate of dissociation affects the kinetic inertness of a radiometal complex, independently of thermodynamic stability. Dissociation's rates are mainly due to the fact that micro- or nanograms of a radiopharmaceutical are diluted into the blood stream (according Le Chatelier's principle). Added to this, there is a physiological larger presence in the blood stream of many strong native biological chelators (e.g transferrin, ceruloplasmin, and metallothionein, ferritin, etc.) and competing metals that can transchelate radiometals from BFC-conjugates. This broad range of complicating factors demonstrates that a single *in vitro* assay is typically not accurate to predict *in vivo* stability.

b. Kinetics – acid dissociation and competitive radiolabeling

Relative kinetic inertness of a metal complex is frequently measured in acidic conditions. The reason of that resides in the fact that most complexes are found to dissociate quickly in acidic pH (notably pH 2). Dissociation experiments, that evaluate the rate of dissociation at a constant pH, have to be assessed to compare and examine chelators with a particular metal ion. In this kind of experiments, dissociation could be easily displayed over time with well-established techniques such as high-performance liquid chromatography (HPLC), thin layer chromatography (TLC), and nuclear magnetic resonance (NMR). Normally, the obtained

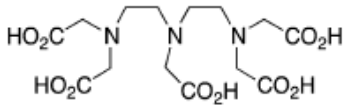
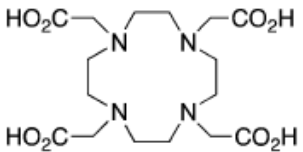
results do not offer a precise estimation of the *in vivo* kinetic inertness. Low pH, in fact, does not occur in the blood or most organs, that usually possess neutral pH. Moreover, in the case of radiometal dissociation, it typically takes place via transchelation to serum proteins and enzymes, and it is not acid mediated. Competitive radiolabeling experiments can be realized by adding to a radiometal solution an excess of non-radioactive ions, such as Na^+ , Ca^{2+} , Zn^{2+} , or Fe^{3+} , followed by addition of a chelator to study the impact of these competing ions on radiolabeling yields. Thus, it is possible to prove the radiolabeling selectivity of a chelator for a specific radiometal ion, when other biologically relevant competing ions are present. An alternative way to assess transchelation stability involves the addition of a radiometal complex, pre-formed under metal-free radiolabeling conditions, to a mixture containing these competing ions.

Since chelate-based radiopharmaceuticals are normally radiolabeled in rigorous metal-free conditions, these experiments may not provide relevant information for predicting *in vivo* stability. The way of producing and purifying a radionuclide can highly affect its specific activity, but also the concentrations of impurities. Radiometals are used in very tiny amounts and under highly dilute conditions; besides, any impurity metal ions present (even nanomole amounts) can result as the most accounting metal in solution, making the competitive binding problematic.

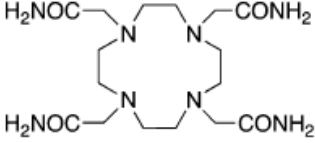
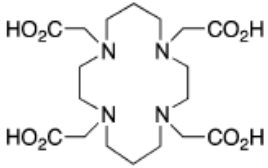
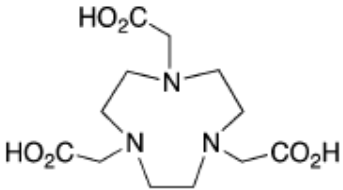
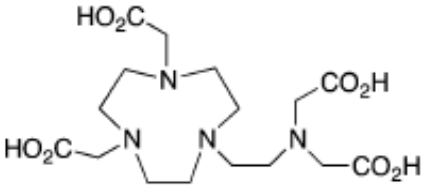
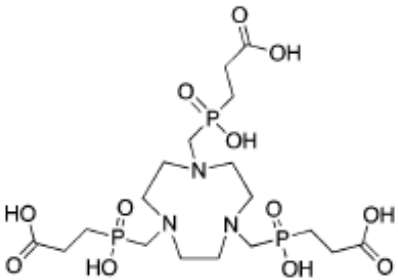
c. Chelates of choice

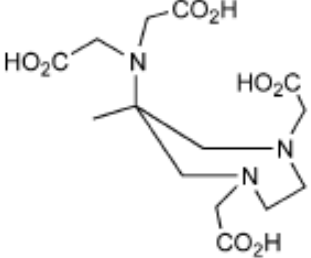
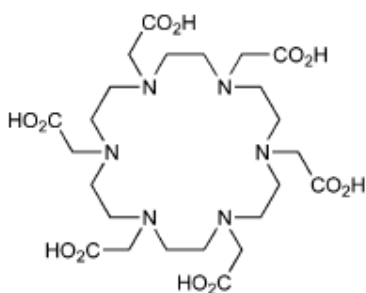
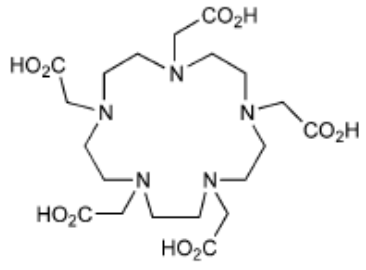
A survey of radiometal chelators has been undertaken [35]. The following Table 3 summarizes their work.

Table 3. Chelators of interest and some example of radionuclide matches. [35]

Chelator	Radionuclide	Log k_{MI}	Radiolabeling conditions
 DTPA, diethylenetriaminepentaacetic acid	$^{64}\text{Cu}^{2+}$	21.4	40°C, 60 min, pH 5.5 [38]
	$^{44/47}\text{Sc}^{3+}$	27.4 [37]	25°C, 10 min, pH 6
	$^{177}\text{Lu}^{3+}$	22.6	25°C, 60 min, pH 5.5 [39]
 DOTA, 1,4,7,10-tetra-azacyclododecane-1,4,7,10-tetraacetic acid	$^{64}\text{Cu}^{2+}$	22.2	40°C, 60 min, pH 5.5 [38]
	$^{44/47}\text{Sc}^{3+}$	30.8 [37]	70°C, 30 min, pH 4
	$^{177}\text{Lu}^{3+}$	23.5 (pM 17.1)	25°C, 60 min, pH 5.5

Chapter 1

 <p>TCMC, 1,4,7,10-tetrakis(carbomoylmethyl)-1,4,7,10-tetraazacyclododecane</p>	$^{212}\text{Pb}^{2+}$	>19	37°C , 30 min, pH 5-6 [40]
 <p>TETA, 1,4,8,11-tetra-azacyclotetradecane-1,4,8,11-tetacetic acid</p>	$^{64}\text{Cu}^{2+}$ $^{111}\text{In}^{3+}$ $^{177}\text{Lu}^{3+}$	21.9 21.9 (pM 16.3) 15.3	25°C , 60 min, pH 5-7 - -
 <p>NOTA, 1,4,7-triazacyclononane-1,4,7-triacetic acid</p>	$^{64}\text{Cu}^{2+}$ $^{67/68}\text{Ga}^{3+}$ $^{44/47}\text{Sc}^{3+}$	21.6[41] 31.0 (pM 27.9) 16.5 (pM 19.2)	40°C , 60 min, pH 5.5 [38] 95°C , 5 min, pH 3.2 [42] 95°C , 20-30 min, pH 4
 <p>NETA, {4-[2-(bis-carboxymethylamino)-ethyl]-7carboxymethyl-[1,4,7]triazonan-1-yl}-acetic acid</p>	$^{177}\text{Lu}^{3+}$ $^{86/90}\text{Y}^{3+}$ $^{212}\text{Pb}^{2+}$	- - -	25°C , 5 min, pH 4.5 25°C , 5 min, pH 4 25°C , 5 min, pH 4
	$^{67/68}\text{Ga}^{3+}$ $^{44}\text{Sc}^{3+}$ $^{86/90}\text{Y}^{3+}$	26.24[41] - 8.89	95°C , 5 min, pH 3.2 [42] 95°C , 5 min, pH 2 [42] -

TRAP, 1,4,7-triazacyclononane-1,4,7-tris[methyl(2-carboxyethyl) phosphinic acid]			
 <p>AAZTA, 1,4-bis(hydroxycarbonyl methyl)-6-[bis(hydroxylcarbonylmethyl)]amino-6-methylperhydro-1,4-diazepine</p>	$^{67/68}\text{Ga}^{3+}$ $^{44}\text{Sc}^{3+}$ $^{177}\text{Lu}^{3+}$	- - -	25°C, 10 min, pH 4.5 [43] 25°C, 5-10 min, pH 4 [44] 25°C, 10 min, pH 4.5 [43]
 <p>HEHA, 1,4,7,10,13,16-hexaazacyclo-hexadecane-N,N',N'',N''',N''''-hexaacetic acid</p>	$^{225}\text{Ac}^{3+}$	-	37-40°C, 30 min, pH 5.8-7
 <p>PEPA, 1,4,7,10,13-pentaazacyclopentadecane-N,N',N'',N''',N''''-pentacetic acid</p>	$^{225}\text{Ac}^{3+}$	-	37-40°C, 30-60 min, pH 5.8-7

To evaluate properly the stability and kinetic inertness of a chelate in vivo, a suitable vector must be attached (e.g. peptide, antibody, nanoparticle) so that the radiometal–chelate complex is made to persist in blood circulation for a substantial period of time, and can be monitored

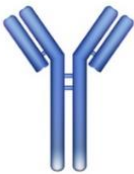
over several hours or days (depending on isotope half-life and the subsequent imaging/ therapy window)

3 – The biological vector

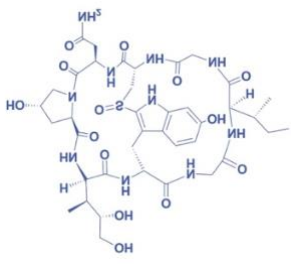
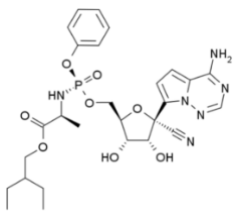
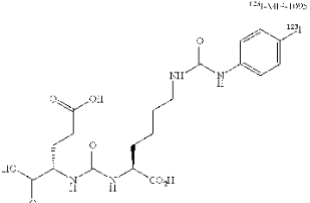
The specificity and selectivity required for screening and pinpointing tumor cells for cell-kill has been made possible by targeted ligands based on 'magic bullet' and tracer principle- theories nearing a century. Overexpression of certain receptors has been exploited using biomolecules for targeting. The pragmatic analysis, however, is not as promising compared with the theoretical knowledge of available gamut of vectors and targets. The presence of a biological vector is intended to target tumor area, to limit the irradiation of healthy tissues. A huge range of carrier compounds have been tested for the systemic biodistribution of radiopharmaceuticals. The range includes small organic or inorganic molecules, sugars, vitamins, hormones, enzymes, peptides, oligonucleotides, nanoparticles or macromolecules, such as liposomes, polymeric gels, and monoclonal antibodies. Antibodies demonstrated to be efficient vectors to carry radionuclides thanks to their exclusive interactions with cancer antigens. However, they could easily be degraded in certain tumor environmental conditions because of their peptidic nature [45]. This targeting is achieved by means of recognition between grafted biomolecule, and the surface of the malignant area.

The complex interplay of in vitro and in vivo parameters, and the effect of radionuclides involve a systematic assessment of radiopharmaceuticals as diagnostic and therapeutic agent. Different vectors with their pros and cons, present status are presented in Table 4 [46].

Table 4. Vectors of interest for delivering radionuclides: their applications and relative pros (in green) and cons (in red). [46]

Vectors of interest	Application and examples	Radionuclides delivered	Salient points
 <p>Antibodies</p>	<p>Radioimmunotherapy (RIT) and Radioimmunodiagnosis (RID).</p> <p>Some examples: anti-prostate specific membrane (PSMA)-antibodies in prostate cancer, anti- epidermal growth factor</p>	<p>^{131}I, ^{111}In, $^{99\text{m}}\text{Tc}$ (SPECT)</p> <p>^{177}Lu (RIT)</p> <p>$^{124}\text{I}/^{131}\text{I}$, $^{64}\text{Cu}/^{67}\text{Cu}$ $^{86}\text{Y}/^{90}\text{Y}$ (Theranostics)</p>	<p>Excellent cellular surface targeting.</p> <p>Large size limits bioavailability.</p> <p>Temperature sensitive.</p>

Chapter 1

	receptor (EGFR)-antibodies in colon and lung cancer, anti-human epidermal growth factor 2 (HER2)-antibodies in breast cancer...		Irreversible denaturation.
 <p>Peptides</p>	<p>Nuclear imaging and Targeted radiotherapy (TRT).</p> <p>Some examples of peptides: somatostatin receptor targeting peptides, gastrin releasing peptide, glucagon like peptide 1...</p>	^{111}In , $^{99\text{m}}\text{Tc}$ (SPECT) ^{68}Ga (PET) ^{177}Lu , ^{90}Y (TRT)	<p>Broader range of targets, well-defined chemistry.</p> <p>Fast clearance, good pharmacokinetics, good tissue perfusion.</p> <p>Low metabolic/in vivo stability.</p>
 <p>Nucleic-acid-based vectors</p>	<p>Targeted radiotherapy (TRT).</p> <p>Some examples: VEGF165-targeted aptamer and nucleolin-targeted aptamer.</p>	$^{99\text{m}}\text{Tc}$ (SPECT) ^{18}F , ^{64}Ga (PET)	<p>Broader range of targets.</p> <p>High specificity and affinity</p> <p>Good stability only when lyophilized</p>
 <p>Small molecules</p>	<p>Nuclear imaging Targeted radiotherapy (TRT).</p> <p>Some examples: kinase inhibitors, pyridine-based ligands, PSMA inhibitors...</p>	^{131}In , $^{99\text{m}}\text{Tc}$ (SPECT) ^{18}F , ^{64}Ga (PET) ^{177}Lu (TRT)	<p>Low toxicity</p> <p>Good pharmacokinetic and pharmacodynamic profile</p> <p>Less specific targeting than other vectors</p>

4 – Concept of companion diagnostic and theranostic approach

Nuclear medicine through its TEMP and PET imaging instruments, and their gradual integration into morpho-functional hybrid imaging, is a major participant in the evolution of personalized medicine by providing quantitative biomarkers of molecular signatures.

Radiolabelling confers optimal sensitivity performance with sub-picomolar detection after introduction of a very small amount of tracers, without disturbing the environment to be explored. These biomarkers are positioned today to select patients, and also from a medico-economic perspective to guide, predict, evaluate the most appropriate treatments, based on the individual characterization of the molecular signatures of the disease and lesions.

This molecular complexity is closely related to the prognosis of the disease, but also to the specific treatments developed to be directed to the same pathophysiological target for diagnosis and treatment, with the concept of companion diagnostic and theranostic.

a. Companion diagnostic

According to the Haute Autorité de Santé (HAS, France), a companion test is a diagnostic test to select, based on their status for a predictive marker identified by this test, only patients in whom treatment is likely to bring a benefit among those diagnosed with a disease. The test is therefore "companion" to the use of the administration of the treatment.

A companion test is a diagnostic test permitting selection of only patients in whom a treatment is likely to provide a benefit among those diagnosed with a given illness, according to their status for a predictive marker identified by this test. For this reason, the test is considered a "companion" to the use on the treatment. CDx have four potential applications:

- 1) Selection of patients for a specific targeted treatment;
- 2) Staging markers to adapt the therapeutic strategy;
- 3) Predictive markers for drug efficacy, resistance and safety;
- 4) Follow-up markers to check the therapeutic response (therapy monitoring) and to adjust therapy (alternative, dosing, duration) if required [47].

b. Theranostic concept

In parallel, the term *theranostics* is today perceived as the combination of a predictive biomarker with a therapeutic agent. The idea of using a radioactive compound for diagnostic imaging, target-expression confirmation, and radionuclide therapy dates back to 1946, when Seidlin et al. published the first study on radioiodine therapy for metastatic thyroid cancer [48]. A phase III randomized, controlled trial provided unequivocal evidence of the remarkable effectiveness of ^{177}Lu -DOTATATE for treatment of neuroendocrine tumors [49], and there

have been multiple reports of advanced prostate cancer responding dramatically to treatment with radiolabeled ligands targeting prostate-specific membrane antigen [50]. These theranostic applications of nuclear medicine in neuroendocrine tumors and prostate cancer have significant economic potential, with a possible yearly revenue of several billion U.S. dollars.

With the tremendous success of the clinical trial [49] in well-differentiated midgut neuroendocrine tumors and the impressive clinical results of lutetium-177- and actinium-225-based prostate-specific membrane antigen (PSMA) treatments, there is rising clinical attention and exposure of these promising therapeutic methods [51,52].

These important successes also leveraged nuclear medicine as one of the most promising partners in the oncological treatments of cancer patients. However, in parallel to the evolution in targeted radionuclide therapy, intense research in immune oncology brought forth a variety of different checkpoint inhibitor treatments or other immune-modulating anti-cancer agents. It is an open question, if and how these two worlds, which seem to develop in parallel as very promising methods, can be used synergistically and learn from each other.

In unconventional radiotheranostics, using the same metal would result in more precise indication of the therapeutic window. Indeed, the two radionuclides of the same metal possess identical pharmacokinetic properties that determine the same behavior in vivo. In this way, the information collected on the biodistribution of the diagnostic radionuclides could be translated to the therapeutic one since they are identical. Until now, different matched pairs of radionuclides have been suggested for this unconventional theranostic approach. One known example is $^{124}\text{I}/^{131}\text{I}$, which has been used for decades in SPECT/PET imaging as well as for β^- radiotherapy of thyroid diseases. Other examples are yttrium pair $^{86}\text{Y}/^{90}\text{Y}$ and copper pair $^{64}\text{Cu}/^{67}\text{Cu}$ or scandium pair $^{43,44}\text{Sc}/^{47}\text{Sc}$ that are radionuclides pairs useful for clinical PET imaging and for β^- radioimmunotherapy. Terbium nuclides $^{152/155}\text{Tb}/^{149/161}\text{Tb}$ have been proposed recently for PET and SPECT imaging as well as for α and β^- radiotherapy [53].

Immunotheranostics combines synergistically the principle of immunooncology (IO) and theranostics by imaging and modulating the tumor microenvironment. Immunotheranostics is of course much more complex than classical theranostics and needs more in-depth biological understanding of a changing heterogeneous cellular, local, and possibly systemic target over time. However, especially in this challenge, we see one of the main opportunities in nuclear medicine providing whole-body IO molecular imaging and therapeutic systemic radiopharmaceuticals for the following years.

Theranostic systems have drawn increasing attention over the past decade and further growth is expected in the near future due to the prospects for non-invasive, self-modulating drug release with traceable therapeutic response [54]. Supramolecular biomaterials are highly adaptable platforms to combine treatment and diagnosis for the personalized therapy envisioned for theranostic medicine. Supramolecular theranostics could facilitate improved treatment through the possible modification of self-assembling subunits, such that increased circulation time, tissue-specific accumulation, and cell penetration properties can be encoded with ease into nanostructures. It can be well expected that supramolecular theranostics would have a vital impact both in the clinic and the laboratory, where diagnostic data might provide physicians with early stage treatment options and empower scientists with better knowledge with which to optimize future drug formulations [54].

In this frame, biocompatible chelators and drug vectors, such as polysaccharides are drawing the attention of researchers because of their power to skip altered defense mechanisms of several tumors but especially for their wide surface full of functionalization sites. Their surface, rich in chelating groups (i.e. carboxylic, sulphate, acetate and amino groups) make them chelator and vectors at the same time, guaranteeing a versatile organic ligand. Glycosaminoglycans, also called GAGs, are heterogeneous polysaccharides implied in a multitude of biological processes. They are present on the surface of almost all the cells in the human body and thus play a key role in binding different protein targets.

III. Glycosaminoglycans

GAGs are known to be involved in multiple signaling cascades through the interaction with chemokines, cytokines, and growth factors implied in cell proliferation, differentiation, and cell-cell interaction (see Figure 9) [55]. These interactions determine important physiological effects in inhibiting coagulation, inflammation, tumor extravasation, metastasis formation, etc. Therapeutic efficacy of GAGs to treat several diseases, such as tumor progression, infection, inflammation, lung diseases, and Alzheimer's disease, has been published [56–59]. Another interest of GAGs is in biotechnological applications, particularly in the field of regenerative medicine. GAGs are common components of cell-surfaces and the extra-cellular matrix (ECM). After a damage, they modulate the arrival of skin and bone precursor cells and their subsequent differentiation and gene expression, as well as they regulate the activity of proteins crucial to bone and skin regeneration [60].

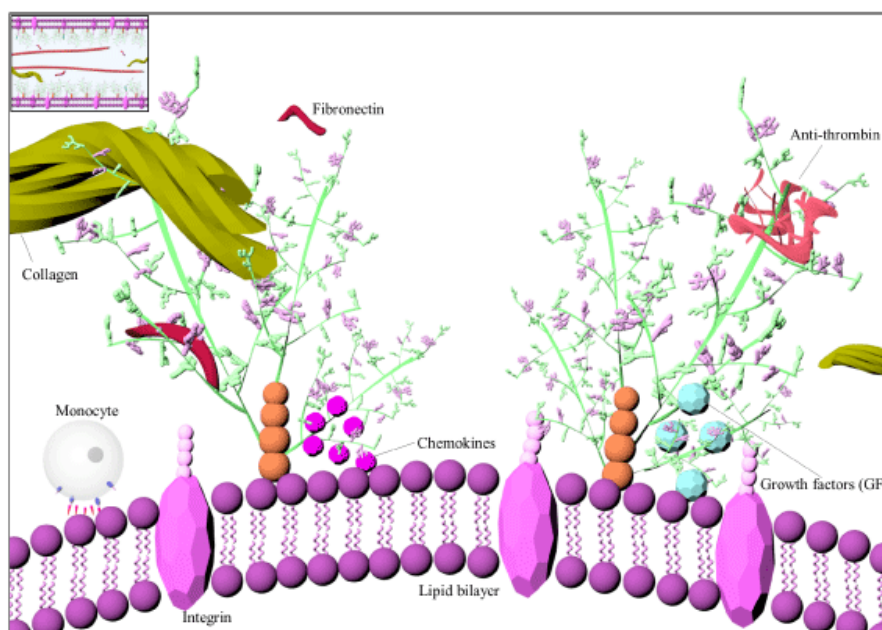


Figure 9. Illustration of GAG location and interaction on endothelial cells [61].

A – Composition and structure

GAGs are linear and negatively charged polysaccharides, which have molecular weights that range between 10 and 100 kDa. GAGs are divided into two main classes, non-sulphated and sulphated ones. An example of non-sulphated GAGs is hyaluronic acid (HA), whereas the sulphated large type includes heparin, heparan sulphate (HS), keratan sulphate (KS), chondroitin sulphate (CS) and dermatan sulphate (DS). Their chains consist of disaccharide repeating units: each unit is composed of uronic acids and amino sugars. Uronic acids include D-glucuronic acid and L-iduronic acid, whereas amino sugars comprise D-galactosamine and D-glucosamine. Units composition and the geometry of the glycosidic linkage (α and β) between these units differ among GAGs (see Figure 10). Sulphation frequently occurs on carbons 3 or 6 of the amino sugar or on the amino group itself. However, the repeating units of GAGs can be sulphated at various positions so one GAG may exhibit over a million of different sulphation patterns where major sequences are alternated to variable sequences. At neutral pH (6-7), all the function groups forming GAGs are ionized, generating very high negative charge densities along their chains that brings them to occupy a great hydrodynamic volume in solution [62].

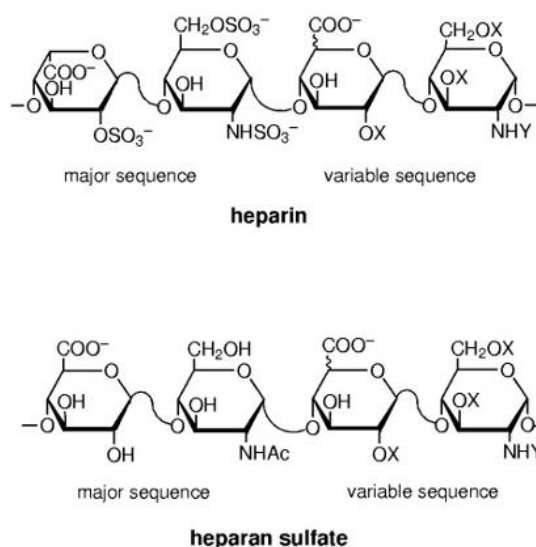


Figure 10. Chemical structure of heparin, one of the most employed GAG in therapy, and heparan sulfate, normally expressed on the ECM surrounding human cells. Figure adapted from Capila et al. 2002 [63].

B – Role of GAGs in cancer

Alterations of GAGs expression, as well as of enzymes involved in their biosynthesis and degradation, are involved in a number of steps of tumor progression and spread. GAGs bind to different protein targets, primarily via electrostatic interactions between negatively charged uronic acids and sulfate groups and positively charged amino acids in the protein. These interactions lead to profound physiological effects at various levels but, to date, the most investigated one is related cancer. For instance, Heparin and its low-molecular weight derivatives (LMWD), generally administered to prevent or treat venous thromboembolism in patients with cancer, showed an improved survival in a number of retrospective and prospective studies. It could be possible because heparin is able to interfere with some of the important steps in the metastatic process (see Figure 11). The reason why the anticoagulant activity affects tumor progression and metastasis seeding must be found in the decrease thrombin generation and fibrin formation. Since coagulation factors attract platelets and leukocytes, the negative regulation, caused by heparin, of factor Xa and thrombin-mediated proteolysis, as well as platelet activation, may partly explain the antimetastatic properties [64].

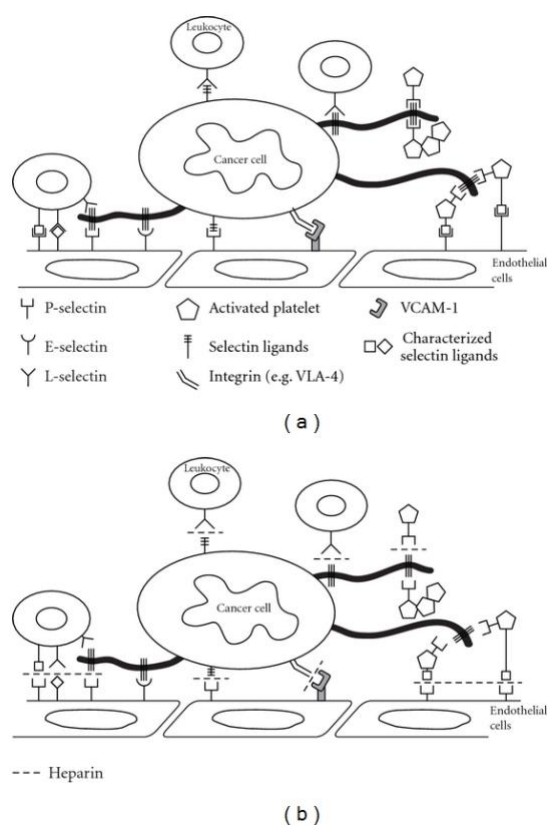


Figure 11. Selectins and integrins contribute to metastatic spread. (a) Schematic presentation of selectin- and integrin-mediated cancer cell interactions with several blood constituents (e.g., platelets, leukocytes, and endothelial cells) during hematogenous metastasis. (b) Heparin application in mouse models blocks both P- and L-selectin-mediated; and VLA4-mediated interactions of cancer cells within blood circulation thereby affecting metastasis [12].

Although its biological activity may contribute to the antitumoral properties of heparin, the strong anticoagulation represents a potential adverse effect in cancer treatment. Adverse bleeding complications, such as the increase of haemorrhagic risk, make heparin and its low-molecular-weight derivatives bad candidates to treat cancer metastasis [65]. To steer around this clinical obstacle in the development of GAGs as therapeutics, multiple strategies have been established to design GAG mimetics. The exploration of therapeutic potential of GAG mimetics is now increasing. Marine environment offers a great biodiversity, which lead to polysaccharides presenting a various chemical diversity that is largely species specific. Exploring the biological properties of the polysaccharides from marine eukaryotes and marine prokaryotes revealed that the polysaccharides from the marine environment could provide a valid alternative to traditional polysaccharides such as GAGs [66]. This aspect will be developed in more details in the next chapter.

Four therapeutic actions of GAGs in cancer have been identified so far to be:

- 1) *Cancer biomarkers*. Since glycosylation is one of the most common kinds of post-translational modifications, the presence and the structure of GAGs can affect protein role and location. An anomalous glycosylation, including the altered structure and expression of GAGs, is a hallmark related with cancer growth and spread [67]. For instance, it has been observed, in both retrospective and prospective studies relating renal cell carcinoma, that the composition and levels of plasma and urine GAGs were considerably abnormal compared to healthy standards [68]. GAGs found in the blood circulation are the products of many types of cells, tissues, and organs, healthy and not. The quantitative and qualitative changes of GAGs reflect the complexity of system lesion and the degree of involvement of the healthy districts. For this reason, plasma or serum GAGs represent the one of the most innovative and versatile cancer biomarkers for modern cancer diagnosis.
- 2) *Anti-metastatic agents*. The ability of cancer cells to disseminate in surrounding health tissues requires changes in the expression of cell-surface glycoproteins and the presence of (ECM)-degradative enzymes. Glycosaminoglycans are the main constituents of the ECM and changes in expression of these macromolecules is able to reduce cell-cell adhesion and promote cancer cell dissemination. Enzymes like heparanase promote extravasation and metastasis settlement by degrading heparin sulphate chains in the cell surface as well as in the extracellular matrix [69]. Many studies have been conducted using heparin and chondroitin sulphate, their derivatives, and other GAGs, such as dextran sulphate. Heparin is a potent anticoagulant used for decades to prevent and treat venous thromboembolism. Oncological patients on therapy with heparin have shown an increase of survival and an improvement of prognosis. Several animal studies suggest that its antimetastatic activity of GAGs is based on their anticoagulant activity, inhibition of heparanase, interference with cell membrane glycoproteins, which lead to a negative effect on tumor cell adhesion and blood motility [64].
- 3) *Target therapy vectors*. The prognosis of patients with cancer has improved considerably in the past years with the development of drugs targeting cell surface adhesive receptors. The discovery of these new targets has paved the way to the development of new anticancer agents using GAGs as drug vectors. Indeed, cell surface adhesive receptors, such as integrins and selectins, are susceptible to many important interactions with GAGs. This kind of new vectors is particularly designed to overcome conventional chemotherapy. Insolubility, system toxicity and drug resistance represent

the main limitations of conventional chemotherapy efficacy, all of them aggravated by debilitating side effects such as fatigue, nausea, neuropathy and organ failure. An effective solution to bypass these limitations is to deliver cancer drugs through biocompatible vectors such as polymeric formulations like polysaccharides [70,71].

- 4) *GAG-functionalized nanoparticle (NPs)*. Recent studies revealed that functionalization or hybridization of drug-carrying nanocarriers can significantly improve their therapeutic efficacy and biopharmaceutical properties. Moreover, surface decoration of nanoparticles has shown promising improvement in percutaneous permeation of drug-encapsulated nanoparticles through non-conventional administration routes [72]. Recently HA was used to functionalize different kinds of NPs since its very high affinity for CD44 receptors, which are over expressed in several cancer cells [73].

C – Interest of GAGs for Nuclear Medicine

GAGs could be employed in new drug delivery systems to deliver active compounds for therapeutic uses, treating a variety of pathologies even different from cancer, such as glaucoma and burns. Moreover, polysaccharidic vectors could be an alternative to classical peptide vectors, such as antibodies, especially in those physiological media that can easily degrade them. Natural linear polysaccharides, such as chitosan, and branched ones, such as dextran, have already been used for delivery of diagnostic radionuclides. Several formulations based on radiolabeled chitosan and dextran have been considered. The $^{99m}\text{Tc}/^{131}\text{I}$ -labeled chitosan derivatives were used as SPECT/PET imaging agent. In this aim, ^{99m}Tc -labeled chitosan derivatives have been employed for nuclear imaging of liver cancer and its metastasis. Radiolabeling of chitosan derivatives was also assessed using ^{66}Ga linked to a DTPA chelator. ^{66}Ga , with its half-life of 9.5 hours, is more suitable to investigate longer periods as compared to short-lived ^{68}Ga . The use of DTPA for complexation with ^{66}Ga allowed to achieve the highest efficiency to prevent radionuclide leakage. They have been tested as carriers for intratumor administration in fibrosarcoma in mice models. Literature reported an easy method to label PEGylated-chitosan nanoparticles with ^{64}Cu , using azide-functionalized chitosan and DOTA derivatives with appending dibenzyl cyclooctyne moieties. Such chitosans derivatives are much better than protein/peptides that go to degradation in liver very quickly so they may be employed as liver-targeted agents for radiotherapeutic applications. Dextran is also effectively used for targeted delivery of radionuclides. Moreover, dextran-based carriers were proved to be effective in clinical studies of oral cavity squamous cell carcinoma patients

confirmed the detection and accurate prediction of the pathology without false negative results [74].

Those previous examples demonstrate that GAGs could be considered as great candidates for becoming radionuclides vectors, especially in the theranostic field, which is constantly looking for new targeted carriers. For instance, the attention of researchers have been recently focused on marine microorganism, seaweed, and bacteria that have demonstrated a great potential for biotechnology and pharmaceutical applications [66]. Indeed, a patent deposited on 2010 showed fucoidans as ligands for the diagnosis of degenerative pathologies, with a major focus on coupling them with diagnostic radionuclides. Fucoidans are sulphated polysaccharides that can be extracted from a number of marine sources, such as sea cucumbers and brown algae. Fucoidan's biological target is represented by selectins, those glycoproteins expressed on the cellular surface and being overexpressed in certain tumor lesions. In this patent, it was described the coupling of fucoidans with SPECT radionuclides such as ^{99m}Tc and ^{68}Ga , as well PET radionuclides like ^{11}C , ^{13}N , ^{15}O and ^{18}F [75]. The reason that fucoidans could bind diagnostic radionuclides does not preclude to these sulphated polysaccharides to bind also therapeutic radiometals, so even theranostics. In fact, fucoidans could be coupled to almost all the radionuclides in nuclear medicine. Their wide chemical surface, functionalized with sulphate groups may be considered as a fusional system of vector and linker together, resulting as a breakthrough the radiopharmaceutical field.

These previous examples demonstrate that GAGs could be considered as great candidates for becoming radionuclides vectors, especially in the theranostic field, which is constantly looking for new targeted carriers. the antimetastatic properties of GAGs could act in synergy with the diagnostic and therapeutic features of radionuclides. Not to mention, together with the anti-metastasis effect, the regenerative properties of GAGs at bone level make them very interesting candidates in bone tumors, as well as their metastasis. Because of their chemical structure enriched in functional groups, such as carboxylic and sulphate groups, GAGs and their mimetics, can account for new potential ligand for radionuclides.

The goals of my work are to evaluate the feasibility coupling GAGs with an attractive theranostic pair of radionuclides: $^{44}\text{Sc}/^{47}\text{Sc}$.

The breakthrough of this work resides on two main aspects:

- 1) The possibility to combine the antimetastatic properties of the GAG vectors to targeted radiotherapy. This effect in preventing metastasis formation will be particularly useful in fight malignant cancer, such as osteosarcoma, which are characterized by high

metastasis spread. In fact, this sort of synergy between the GAG vector and the theranostic pair $^{44}\text{Sc}/^{47}\text{Sc}$ would help to display, monitor and treat the metastatic seeds scattered into the body as well the primary bone tumor, normal tropism of this vector. This approach represents an overcoming of standard RIT which focuses mainly on primary tumors.

- 2) The possibility of using a chemical identical theranostic pair, which will make easier to develop a correct dosimetry for the organs. The fact of working with only one element chemistry will results in more predictable coordination chemistry.

References

- [1]. Hassanpour, S.H. Review of cancer from perspective of molecular. 9.
- [2]. <https://ec.europa.eu/jrc/en/news/2020-cancer-incidence-and-mortality-eu-27-countries>.
- [3]. Kiss, A.; Meryn, S. Effect of sex and gender on psychosocial aspects of prostate and breast cancer. *BMJ* **2001**, *323*, 1055–1058, doi:10.1136/bmj.323.7320.1055.
- [4]. PROPOSED LIST OF CANCER MEDICINES Union for International Cancer Control 2014 Review of Cancer Medicines on the WHO List of Essential Medicines.
- [5]. Heymann, D.; Ruiz-Velasco, C.; Chesneau, J.; Ratiskol, J.; Sinquin, C.; Collicec-Jouault, S. Anti-Metastatic Properties of a Marine Bacterial Exopolysaccharide-Based Derivative Designed to Mimic Glycosaminoglycans. *Molecules* **2016**, *21*, 309, doi:10.3390/molecules21030309.
- [6]. Bruland, Ø.S.; Pihl, A. On the current management of osteosarcoma. A critical evaluation and a proposal for a modified treatment strategy. *Eur. J. Cancer* **1997**, *33*, 1725–1731, doi:10.1016/S0959-8049(97)00252-9.
- [7] Arif, A.; Hansen, M. F.; Alander, C. B.; Monson, D.K; Reimer, N.B.; Drissi, H. *Techniques in Orthopaedics* **2019**, *34*, 275-286.
- [8]. Brown, H.K.; Tellez-Gabriel M.; Heymann D. Cancer stem cells in osteosarcoma. *Cancer Lett.* **2017**, *386*,189-195.
- [9]. Nascimento, D.; Suchard, G.; Hatem, M.; de Abreu, A. The role of magnetic resonance imaging in the evaluation of bone tumours and tumour-like lesions. *Insights Imaging* **2014**, *5*, 419–440, doi:10.1007/s13244-014-0339-z.
- [10]. Kim, S.J.; Choi, J.-A.; Lee, S.H.; Choi, J.Y.; Hong, S.H.; Chung, H.W.; Kang, H.S. Imaging findings of extrapulmonary metastases of osteosarcoma. **2004**, *10*.
- [11]. Kundu, Z. Classification, imaging, biopsy and staging of osteosarcoma. *Indian J. Orthop.* **2014**, *48*, 238, doi:10.4103/0019-5413.132491.
- [12]. Bendas, G.; Borsig, L. Cancer Cell Adhesion and Metastasis: Selectins, Integrins, and the Inhibitory Potential of Heparins. *Int. J. Cell Biol.* **2012**, *2012*, 1–10, doi:10.1155/2012/676731.
- [13]. Schroeder, A.; Heller, D.A.; Winslow, M.M.; Dahlman, J.E.; Pratt, G.W.; Langer, R.; Jacks, T.; Anderson, D.G. Treating metastatic cancer with nanotechnology. *Nat. Rev. Cancer* **2012**, *12*, 39–50, doi:10.1038/nrc3180.
- [14]. Mondal, J.; Panigrahi, A.K.; Khuda-Bukhsh, A.R. Conventional Chemotherapy: Problems and Scope for Combined Therapies with Certain Herbal Products and Dietary Supplements. *Austin J. Mol. & Cell. Biol.* **2014**, *1*, 10.
- [15]. Nowell, P. The clonal evolution of tumor cell populations. *Science* **1976**, *194*, 23–28, doi:10.1126/science.959840.
- [16]. Hanahan, D.; Weinberg, R.A. Hallmarks of Cancer: The Next Generation. *Cell* **2011**, *144*, 646–674, doi:10.1016/j.cell.2011.02.013.
- [17]. Zhang, S.Y.; Zhang, S.Q.; Nagaraju, G.P.; El-Rayes, B.F. Biomarkers for personalized medicine in GI cancers. *Molecular Aspects of Medicine* **2015**, *45*, 14–27.
- [18]. Ehrlich, F. Ueber das natürlliche Isomere des Leucins. **1904**.
- [19]. Lipsztein, R.; Dalton, J.F. Antibody-mediated radiotherapy. *55*, 5.
- [20]. Pressman, D.; Keighley, G. The zone of activity of antibodies as determined by the use of radioactive tracers; the zone of activity of nephritotoxic antikidney serum. *Journal of Immunology* **1948**, *59*, 141–146.
- [21]. Köhler, G.; Milstein, C. Continuous cultures of fused cells secreting antibody of predefined specificity. *Nature* **1975**, *256*, 495–497, doi:10.1038/256495a0.
- [22]. Zimmermann, R. *La Médecine nucléaire: la radioactivité au service du diagnostic et de la thérapie*; EDP Sciences, 2012;

- [23]. Budinger, T.F.; Lebowitz, E.; Ansari, A.N.; Greene, M.W.; Fairchild, R.G.; Ellis, K.J. Thallium-201 for Medical Use. Part 3: Human and Physical Imaging Properties. *J. Nucl. Med.* **1988**, *29*, 137–144.
- [24]. Ketchum, L.E. FDA Justifies Limiting Physician-Sponsored INDs To Hasten Drug Approval Process. **1988**, *29*, 137–144.
- [25]. Chu, S.Y.F.; Ekström, L.P.; Firestone, R.B. *Isotope Explorer “Nuclear data a mouse-click away”*; 2003;
- [26.] Ketchum, L. Nuclear Medicine Faces Bright Future When New Diagnostic Agents Reach Market. *J Nucl Med.* **1986**, *27*, 1–8.
- [27]. Argyrou, M.; Valassi, A.; Andreou, M.; Lyra, M. Dosimetry and Therapeutic Ratios for Rhenium-186 HEDP. *ISRN Mol. Imaging* **2013**, *2013*, 1–6, doi:10.1155/2013/124603.
- [28]. Klaassen, N.J.M.; Arntz, M.J.; Gil Arranja, A.; Roosen, J.; Nijssen, J.F.W. The various therapeutic applications of the medical isotope holmium-166: a narrative review. *EJNMMI Radiopharm. Chem.* **2019**, *4*, 19, doi:10.1186/s41181-019-0066-3.
- [29]. Yeong, C.-H.; Cheng, M.; Ng, K.-H. Therapeutic radionuclides in nuclear medicine: current and future prospects. *J. Zhejiang Univ. Sci. B* **2014**, *15*, 845–863, doi:10.1631/jzus.B1400131.
- [30]. Ménager, J.; Gorin, J.-B.; Fichou, N.; Gouard, S.; Morgenstern, A.; Bruchertseifer, F.; Davodeau, F.; Kraeber-Bodéré, F.; Chérel, M.; Gaschet, J.; et al. Radio-immunothérapie alpha: Principes et intérêts en immunité antitumorale. *médecine/sciences* **2016**, *32*, 362–369, doi:10.1051/medsci/20163204014.
- [31]. Skowronek, J. Current status of brachytherapy in cancer treatment – short overview. *J. Contemp. Brachytherapy* **2017**, *9*, 581–589, doi:10.5114/jcb.2017.72607.
- [32]. Vermeulen, K.; Vandamme, M.; Bormans, G.; Cleeren, F. Design and Challenges of Radiopharmaceuticals. *Semin. Nucl. Med.* **2019**, *49*, 339–356, doi:10.1053/j.semnuclmed.2019.07.001.
- [33]. Serganova, I.; Ponomarev, V.; Blasberg, R.G. Radionuclide-based reporter gene imaging: pre-clinical and clinical implementation and application. *Nucl. Med. Rev.* **2012**, *15*, 17.
- [34]. Boros, E.; Packard, A.B. Radioactive Transition Metals for Imaging and Therapy. *Chem. Rev.* **2019**, *119*, 870–901, doi:10.1021/acs.chemrev.8b00281.
- [35]. Price, E.W.; Orvig, C. Matching chelators to radiometals for radiopharmaceuticals. *Chem Soc Rev* **2014**, *43*, 260–290, doi:10.1039/C3CS60304K.
- [36]. Macomber, R.S. An introduction to NMR titration for studying rapid reversible complexation. *J. Chem. Educ.* **1992**, *69*, 375, doi:10.1021/ed069p375.
- [37]. Huclier-Markai, S.; Alliot, C.; Sebti, J.; Brunel, B.; Aupiais, J. A comparative thermodynamic study of the formation of scandium complexes with DTPA and DOTA. *RSC Adv.* **2015**, *5*, 99606–99617, doi:10.1039/C5RA16736A.
- [38]. Pyo, A.; Yun, M.; Kim, H.S.; Kim, T.-Y.; Lee, J.; Kim, J.Y.; Lee, S.; Kwon, S.Y.; Bom, H.-S.; Kim, H.-S.; et al. ⁶⁴Cu-Labeled Repebody Molecules for Imaging of Epidermal Growth Factor Receptor-Expressing Tumors. *J. Nucl. Med.* **2018**, *59*, 340–346, doi:10.2967/jnumed.117.197020.
- [39]. Ehlerding, E.B.; Lacognata, S.; Jiang, D.; Ferreira, C.A.; Goel, S.; Hernandez, R.; Jeffery, J.J.; Theuer, C.P.; Cai, W. Targeting angiogenesis for radioimmunotherapy with a ¹⁷⁷Lu-labeled antibody. *Eur. J. Nucl. Med. Mol. Imaging* **2018**, *45*, 123–131, doi:10.1007/s00259-017-3793-2.
- [40]. Westrøm, S.; Generalov, R.; Bønsdorff, T.B.; Larsen, R.H. Preparation of ²¹²Pb-labeled monoclonal antibody using a novel ²²⁴Ra-based generator solution. *Nucl. Med. Biol.* **2017**, *51*, 1–9, doi:10.1016/j.nucmedbio.2017.04.005.

- [41]. Šimeček, J.; Zemek, O.; Hermann, P.; Wester, H.-J.; Notni, J. A Monoreactive Bifunctional Triazacyclononane Phosphinate Chelator with High Selectivity for Gallium-68. *ChemMedChem* **2012**, *7*, 1375–1378, doi:10.1002/cmdc.201200261.
- [42]. Notni, J.; Pohle, K.; Wester, H.-J. Comparative gallium-68 labeling of TRAP-, NOTA-, and DOTA-peptides: practical consequences for the future of gallium-68-PET. *EJNMMI Res.* **2012**, *2*, 28, doi:10.1186/2191-219X-2-28.
- [43]. Pfister, J.; Summer, D.; Rangger, C.; Petrik, M.; von Guggenberg, E.; Minazzi, P.; Giovenzana, G.B.; Aloj, L.; Decristoforo, C. Influence of a novel, versatile bifunctional chelator on theranostic properties of a minigastrin analogue. *EJNMMI Res.* **2015**, *5*, 74, doi:10.1186/s13550-015-0154-7.
- [44]. Sinnes, J.-P.; Nagel, J.; Rösch, F. AAZTA5/AAZTA5-TOC: synthesis and radiochemical evaluation with ⁶⁸Ga, ⁴⁴Sc and ¹⁷⁷Lu. *EJNMMI Radiopharm. Chem.* **2019**, *4*, 18, doi:10.1186/s41181-019-0068-1.
- [45]. Kontoghiorghes, G.J. Advances on Chelation and Chelator Metal Complexes in Medicine. *Int. J. Mol. Sci.* **2020**, *21*, 2499, doi:10.3390/ijms21072499.
- [46]. Chaturvedi, S.; Mishra, A.K. Vectors for the delivery of radiopharmaceuticals in cancer therapeutics. *Ther. Deliv.* **2014**, *5*, 893–912, doi:10.4155/tde.14.57.
- [47]. Bolognesi, M.L.; Gandini, A.; Prati, F.; Uliassi, E. From Companion Diagnostics to Theranostics: A New Avenue for Alzheimer's Disease?: Miniperspective. *J. Med. Chem.* **2016**, *59*, 7759–7770, doi:10.1021/acs.jmedchem.6b00151.
- [48]. Seidlin, S.M.; Marinelli, L.D.; Oshry, E. Radioactive iodine therapy. Effect on functioning metastases of adenocarcinoma of the thyroid. *Journal of the American Medical Association* **1946**, *132*, 838.
- [49]. Strosberg, J.; El-Haddad, G.; Wolin, E.; Hendifar, A.; Yao, J.; Chasen, B.; Mittra, E.; Kunz, P.L.; Kulke, M.H.; Jacene, H.; et al. Phase 3 Trial of ¹⁷⁷Lu-Dotatate for Midgut Neuroendocrine Tumors. *N. Engl. J. Med.* **2017**, *376*, 125–135, doi:10.1056/NEJMoa1607427.
- [50]. Liu, C.; Liu, T.; Zhang, J.; Baum, R.P.; Yang, Z. Excellent Response to ¹⁷⁷Lu-DOTATATE Peptide Receptor Radionuclide Therapy in a Patient With Progressive Metastatic Castration-Resistant Prostate Cancer With Neuroendocrine Differentiation After ¹⁷⁷Lu-PSMA Therapy: *Clin. Nucl. Med.* **2019**, *44*, 876–878, doi:10.1097/RLU.0000000000002780.
- [51]. Kratochwil, C.; Haberkorn, U.; Giesel, F.L. ²²⁵Ac-PSMA-617 for Therapy of Prostate Cancer. *Semin. Nucl. Med.* **2020**, *50*, 133–140, doi:10.1053/j.semnuclmed.2020.02.004.
- [52]. Khreish, F.; Ebert, N.; Ries, M.; Maus, S.; Rosar, F.; Bohnenberger, H.; Stemler, T.; Saar, M.; Bartholomä, M.; Ezziddin, S. ²²⁵Ac-PSMA-617/¹⁷⁷Lu-PSMA-617 tandem therapy of metastatic castration-resistant prostate cancer: pilot experience. *Eur. J. Nucl. Med. Mol. Imaging* **2020**, *47*, 721–728, doi:10.1007/s00259-019-04612-0.
- [53]. Muller, C.; Bunka, M.; Haller, S.; Koster, U.; Groehn, V.; Bernhardt, P.; van der Meulen, N.; Turler, A.; Schibli, R. Promising Prospects for ⁴⁴Sc-/⁴⁷Sc-Based Theragnostics: Application of ⁴⁷Sc for Radionuclide Tumor Therapy in Mice. *J. Nucl. Med.* **2014**, *55*, 1658–1664, doi:10.2967/jnumed.114.141614.
- [54]. Bhuivan, Z.H.; Anderson, C.F.; Cui, H. 24 - Self-assembling biomaterials for theranostic applications. In *Self-assembling biomaterials. Molecular Design, Characterization and Application in Biology and Medicine*; Woodhead Publishing, 2018; pp. 533–561.
- [55]. Volpi, N. Therapeutic Applications of Glycosaminoglycans. *Curr. Med. Chem.* **2006**, *13*, 1799–1810, doi:10.2174/092986706777452470.
- [56]. Morla, S. Glycosaminoglycans and Glycosaminoglycan Mimetics in Cancer and Inflammation. *Int. J. Mol. Sci.* **2019**, *20*, 1963, doi:10.3390/ijms20081963.
- [57]. Parish, C.R. The role of heparan sulphate in inflammation. *Nat. Rev. Immunol.* **2006**, *6*, 633–643, doi:10.1038/nri1918.

- [58]. Panagos, C.G.; Thomson, D.S.; Moss, C.; Hughes, A.D.; Kelly, M.S.; Liu, Y.; Chai, W.; Venkatasamy, R.; Spina, D.; Page, C.P.; et al. Fucosylated Chondroitin Sulfates from the Body Wall of the Sea Cucumber *Holothuria forskali*: Cconformation, Selectin Binding and Biological Activity. *J. Biol. Chem.* **2014**, *289*, 28284–28298, doi:10.1074/jbc.M114.572297.
- [59]. Scholefield, Z.; Yates, E.A.; Wayne, G.; Amour, A.; McDowell, W.; Turnbull, J.E. Heparan sulfate regulates amyloid precursor protein processing by BACE1, the Alzheimer's β -secretase. *J. Cell Biol.* **2003**, *163*, 97–107, doi:10.1083/jcb.200303059.
- [60]. Salbach, J.; Rachner, T.D.; Rauner, M.; Hempel, U.; Anderegg, U.; Franz, S.; Simon, J.-C.; Hofbauer, L.C. Regenerative potential of glycosaminoglycans for skin and bone. *J. Mol. Med.* **2012**, *90*, 625–635, doi:10.1007/s00109-011-0843-2.
- [61]. Yavuz O, U.; Matthias, T. Glycosaminoglycans as Novel Targets for in vivo Contrast-Enhanced Magnetic Resonance Imaging of Atherosclerosis. *J. Cardiol. Cardiovasc. Med.* **2020**, *5*, 080–088, doi:10.29328/journal.jccm.1001091.
- [62]. Gandhi, N.S.; Mancera, R.L. The Structure of Glycosaminoglycans and their Interactions with Proteins. *Chem. Biol. Drug Des.* **2008**, *72*, 455–482, doi:10.1111/j.1747-0285.2008.00741.x.
- [63]. Capila, I.; Linhardt, R.J. Heparin-Protein interactions. *Angew. Chem. Int. Ed.* **2002**, *41*, 390–412.
- [64]. Belting, M. Glycosaminoglycans in cancer treatment. *Thromb. Res.* **2014**, *133*, S95–S101, doi:10.1016/S0049-3848(14)50016-3.
- [65]. Afratis, N.; Gialeli, C.; Nikitovic, D.; Tsegenidis, T.; Karousou, E.; Theocharis, A.D.; Pavão, M.S.; Tzanakakis, G.N.; Karamanos, N.K. Glycosaminoglycans: key players in cancer cell biology and treatment: GAG targeting in cancer cell biology. *FEBS J.* **2012**, *279*, 1177–1197, doi:10.1111/j.1742-4658.2012.08529.x.
- [66]. Senni, K.; Pereira, J.; Gueniche, F.; Delbarre-Ladrat, C.; Siquin, C.; Ratiskol, J.; Godeau, G.; Fischer, A.-M.; Helley, D.; Collic-Jouault, S. Marine Polysaccharides: A Source of Bioactive Molecules for Cell Therapy and Tissue Engineering. *Mar. Drugs* **2011**, *9*, 1664–1681, doi:10.3390/md9091664.
- [67]. Li, G.; Li, L.; Joo, E.J.; Son, J.W.; Kim, Y.J.; Kang, J.K.; Lee, K.B.; Zhang, F.; Linhardt, R.J. Glycosaminoglycans and glycolipids as potential biomarkers in lung cancer. *Glycoconj. J.* **2017**, *34*, 661–669, doi:10.1007/s10719-017-9790-7.
- [68]. Gatto, F.; Blum, K.A.; Hosseini, S.S.; Ghanaat, M.; Kashan, M.; Maccari, F.; Galeotti, F.; Hsieh, J.J.; Volpi, N.; Hakimi, A.A.; et al. Plasma Glycosaminoglycans as Diagnostic and Prognostic Biomarkers in Surgically Treated Renal Cell Carcinoma. *Eur. Urol. Oncol.* **2018**, *1*, 364–377, doi:10.1016/j.euo.2018.04.015.
- [69]. Yip, G.W. Therapeutic value of glycosaminoglycans in cancer. *Mol. Cancer Ther.* **2006**, *5*, 2139–2148, doi:10.1158/1535-7163.MCT-06-0082.
- [70]. Yao, V.J.; D'Angelo, S.; Butler, K.S.; Theron, C.; Smith, T.L.; Marchiò, S.; Gelovani, J.G.; Sidman, R.L.; Dobroff, A.S.; Brinker, C.J.; et al. Ligand-targeted theranostic nanomedicines against cancer. *J. Controlled Release* **2016**, *240*, 267–286, doi:10.1016/j.jconrel.2016.01.002.
- [71]. Misra, S.; Hascall, V.C.; Atanelishvili, I.; Moreno Rodriguez, R.; Markwald, R.R.; Ghatak, S. Utilization of Glycosaminoglycans/Proteoglycans as Carriers for Targeted Therapy Delivery. *Int. J. Cell Biol.* **2015**, *2015*, 1–25, doi:10.1155/2015/537560.
- [72]. Hussain, Z.; Pandey, M.; Choudhury, H.; Ying, P. C.; Xian, T.M.; Kaur, T.; Jia, G.W.; Gorain, B. Hyaluronic acid functionalized nanoparticles for simultaneous delivery of curcumin and resveratrol for management of chronic diabetic wounds: fabrication, characterization, stability and in vitro release kinetics. *Journal of Drug Delivery Science and Technology* **2020**, *57*, 1–8.

- [73]. Nairi, V.; Magnolia, S.; Piludu, M.; Nieddu, M.; Caria, C.A.; Sogos, V.; Vallet-Regi, M.; Monduzzi, M.; Salis, A.; Mesoporous silica nanoparticles functionalized with hyaluronic acid. Effect of the biopolymer chain length on cell internalization. *Colloids Surf B Biointerfaces* **2018**, *168*, 50-59.
- [74]. Peltek, O.O.; Muslimov, A.R.; Zyuzin, M.V.; Timin, A.S. Current outlook on radionuclide delivery systems: from design consideration to translation into clinics. *J. Nanobiotechnology* **2019**, *17*, 90, doi:10.1186/s12951-019-0524-9.
- [75]. Michel, J.-B.; Letourneur, D.; Chaubet, F.; Bachelet, L.; Rouzet, F.; Meulemans, A. Fucoidans as ligands for the diagnosis of degenerative pathologies.

Chapter 2

Substrates of interest

I. Introduction

In the frame of Nuclear Medicine, GAGs could be considered as great candidates for becoming radionuclides vectors, especially in the theranostic field. Because of their chemical structure enriched in functional groups, such as carboxylic and sulphate groups, GAGs and their mimetics, can account for new potential ligand for radionuclides. As mentioned in Chapter 1, GAGS of interest of this work are from a marine source and especially from a bacterial source. Polysaccharides are polymeric carbohydrate molecules composed of long chains of monosaccharide units bound together by glycosidic bonds. Natural occurring polysaccharides exhibit distinct structural features in terms of molecular weight, monosaccharide composition, glycosidic linkage patterns, configuration (α or β), charging properties, degree of branching, etc. These diversified structural properties determine the functional properties of polysaccharides, such as solubility and rheological properties, which in turn benefit their extensive applications drug delivery, already demonstrated in HA-functionalized NPs.

The first part of this chapter will be thus dedicated to present the production of these polysaccharides of interest. Their characterization will be also addressed and notably their functional properties (pKa), and their rheological properties (viscosimetry, conformation). It has been shown that the influence of coordination on the structure and rheology of polymer solutions has been extensively studied in the literature. Since these EPS have been evidenced to exhibit heparin like properties, and since heparin is a polysaccharide, part of my work will also be dedicated to heparin, as a reference for GAGs.

Since, the goal of my work are to evaluate the feasibility coupling GAGs with a theranostic pair of radionuclide: $^{44}\text{Sc}/^{47}\text{Sc}$; A second part of this chapter will be dedicated to the ^{44}Sc production with the associated quality control.

Finally, metal cations may coordinate with polymer ligands forming interchain and intrachain links. Metal coordination leads to drastic changes of polymer morphology, formation of clusters that affect the solution rheology. Although metal coordination is ubiquitous in polymeric systems, the physical mechanisms of coordination inducing morphological and rheological changes must be understood due to the multiscale nature of this phenomenon [1]. The presentation of the interactions experiments as well as the characterization of their rheological behavior will be presented in the dedicated chapters (i.e. Chapters 3 and 4).

II. Exopolysaccharides and heparin

Since this work proposes EPS as GAG mimetics to replace heparin (the most used GAG in oncology), it is important to present the polysaccharide that will be the reference molecule for these novel GAG mimetics.

Heparin consists of a linear polysaccharide that tends to have an extended conformation in solution because of its highly hydrophilic nature, which comes from its large degree of sulphation. Heparin chains are composed of long, highly sulphated segments interrupted with under-sulphated domains; molecular weight of these chains varies from 2,000 to 40,000 Da. Composition in terms of disaccharide sequences is considerably heterogeneous. Chemical analysis of all the disaccharides occurring in heparin revealed that a monomeric unit of heparin may be either non sulphated or contain from one to three sulphate groups (see Figure 12) [2, 3].

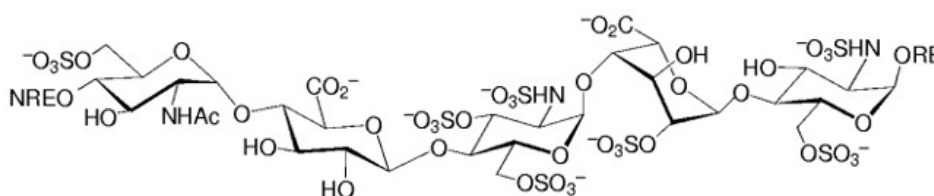


Figure 12. Structure of the pentasaccharide sequence of heparin fundamental for the anticoagulant activity.
Figure adapted from Capila et al. 2002 [3].

Heparin is one of the most acidic polyanionic macromolecules found in nature. There are three kinds of acidic functional groups in the heparin polymer. The sulphate monoesters and the sulphamido groups are both highly acidic, with pK_a values from 0.5 to 1.5. Less acidic are the carboxylate groups of the variously sulphated uronic acid units with pK_a values between 2 and 4. Depending on the physiological environment, these weaker acids could exist as both protonated and non-protonated forms. They have also been demonstrated to be essential in heparin binding to biologically important proteins, such as antithrombin III in the coagulation cascade [4].

Medical heparins are commonly extracted in large quantities from porcine intestines. The disaccharide composition may also differ according to the part of the intestine used. Some porcine intestinal heparin is prepared from porcine intestinal mucosa, while other preparations use the whole intestine. The whole intestine contains differing amounts of heparan sulphate that can end up into the final pharmaceutical product [5]. In the last decade, this contamination caused several deaths. Therefore, alternative methods of controlling the heparin production are urgently needed to prevent the occurrence of poly-pharmacologic agents. Although natural

polysaccharides can be extracted from animals or plants, microorganisms like bacteria and fungi represent the most employed source to obtain bioactive compounds.

A – Production of EPS

The search for new alternative GAGs has conducted the researchers into the deep sea literally, revealing the potential of marine GAG mimetics, such as an exopolysaccharide (EPS) produced by *Alteromonas Infernus*. This marine bacterium, originating from a hydrothermal deep-sea environment, has been classified as a non-pathogenic microorganism by the Pasteur Institute. This bacterium has shown to produce a water-soluble slightly branched acidic polysaccharide, when growing in a carbon rich medium. The native polysaccharide can be chemically modified to provide over-sulphated derivatives with interesting biological activities. In vitro studies demonstrated that over-sulphated EPS inhibits the proliferation of bone marrow stem cells during osteoblastic differentiation and the early steps from osteoclast precursor adhesion to cell fusion. In vivo studies, in mice models, revealed a cancellous loss bone, which increases the process of bone resorption. Put together, these results show different levels of bone resorption regulation by over-sulphated EPS, most of them leading to pro-resorptive effects. Additionally, EPSs are GAG-like compounds, possessing, then, all the biological properties of heparin. The fact that EPS can interact with the bone tissue, as well as with the bloodstream cells [6] make them the best candidate to treat lung metastasis generated by osteosarcoma. A recent study has underlined that an over-sulphated derivative of this polysaccharide could effectively inhibit both migration and invasiveness of osteosarcoma cells in vitro. Moreover, this compound is very efficient at inhibiting the establishment of lung metastases in vivo [7]. These interesting discoveries brought us to envisage the use of these GAG-mimetics as new synergic ligands for radiotheranostics.

Advances were made recently in developing powerful bacterial engineering tools, such as large-scale bioreactors, allowing a production of EPS that is more accessible and economic.

1. Bioreactors

The use of bioreactors is necessary to recreate and maintain certain biochemical conditions required to bacterial growth. Bioreactors are apparatus in which a biological reaction or process is carried out, especially at an industrial scale. Bioreactors are referred as fermenters when the process relate microbial cell culture. Fermenters are able to simulate the natural biochemical environment required for an optimal growth of cells. They can range from 1 L benchtop units up to 10,000 L systems for large scale industrial uses. The appropriate control of certain parameters (e.g. temperature, pH, humidity, oxygen, substrates) will allow obtaining the

required characteristics concerning cell growth and productivity. The schematic structure of a fermenter is showed in Figure 13.

[No copyright permission was obtained for this figure]

Figure 13. Schematic illustration of a fermenter. Figure adapted from Microbiology notes [8].

EPS are provided through collaboration by Laboratoire Ecosystèmes Microbiens et Molécules Marines pour les Biotechnologies from the Institut Français de Recherche pour l'Exploitation de la Mer (IFREMER). EPS production is realized at 25°C and pH 7.4 in a 30 L fermenter. The fermenter is filled with a marine culture medium prepared with 5 g/L of bactopeptones (proteins obtained by enzymatic digestion), 1 g/L of yeast extract, 35 g/L of sea salts and 30 g/L of glucose, which represent the carbohydrate source necessary for the biosynthesis of EPS. Then, 2 L of cell suspension inoculum are added to the medium. Once the fermentation process is finished, the EPS is recovered from the growth medium by centrifugation and ultracentrifugation steps, ending with freeze-drying [9]. All these production steps have been realized at IFREMER.

NMR and infrared spectroscopy led to propose a possible structure of the repeating unit of the native EPS (see Figure 14, page 74). The structural characterization given here comes from previous papers of IFREMER team [10, 11]. It consists of a mono-sulfated branched nonasaccharide composed of three uronic acids (two glucuronic acids and one galacturonic acid) and six neutral hexoses (four glucoses and two galactoses) whereby the galacturonic acid unit is the only one bearing a sulphate group. It presents a high molecular weight ($>10^6$ g.mol⁻¹) and a low sulphate content (<10%).

2. Radical depolymerization, sulphation and purification of EPS

All the following chemical steps of this section have been realized by our IFREMER colleagues as well. To promote its biological activities and to provide a GAG mimetic compound, native EPS has undergone a free radical depolymerization and then over-sulphation: it causes a decrease in the molecular weight and an increase in the sulphate content [12].

Free radical depolymerization consists in the formation of free radicals from the reaction between EPS and hydrogen peroxide with copper acetate as catalyst. The basic principle sees the action of OH• generated *in situ* with a Fenton reaction, in which Cu²⁺ is a very efficient catalyst [13]. For this process, 2.5 g of native EPS was dissolved overnight in 350 mL of water, without stirring. At the complete dissolution, copper acetate was added to the solution and the

mixture was maintained at pH 7.5 and 60°C. The relative amount of H₂O₂, so the radicals, is one of the keys to control depolymerization. A continuous addition of a diluted hydrogen peroxide solution has revealed to be much better than a one-step initial addition. After depolymerization, the polysaccharide chains are stabilized by an overnight reduction with sodium borohydride. To remove the copper employed for the radical depolymerization, the solution passes through a column containing a Chelex 20 resin, leaving it as sodium salt. The excess of sodium borohydride is neutralized with a 10 mol/L acetic acid solution. The resulting solution is ultra-filtered before being freeze-dried.

The sulfation of EPS DR (Radical Depolymerized EPS) is realized in anhydrous dimethyl formamide (DMF). Normally, hydrophilic polysaccharides present a low solubility in organic solvents. To overcome this obstacle, the sodium salt of EPS is previously converted in its pyridinium salt form using *exchange chromatography* (EC). The pyridinium salt form of EPS DR has demonstrated to be soluble in DMF. The solubilization of 50 mg of EPS DR in 100 mL of DMF is assessed for 2 hours at 45°C under continuous stirring. Once it has completely dissolved, 250 mg of sulfur trioxide pyridine (SO₃Py) was added to the mixture; the sulphation is conducted for 2 hours at 45°C; 20 mL of water is then added and the solution is left cooling to room temperature. The pH is then adjusted to 7-8 by 3 mol/L NaOH. The obtained solution is dialyzed against distilled water for 72 hours and freeze-dried.

In order to obtain a homogeneous fraction of DRS with a particular low molecular weight and low polydispersity, a population of polysaccharide chains is selected using *gel permeation chromatography* (GPC). The column is filled with 500 mL Superdex 30 preparative gel; samples are loaded through a superloop and eluted with ultrafiltered water. The purified solution is collected, dialyzed and freeze dried.

Despite sulphation seems to be a one-step reaction, the synthesis of sulfated macromolecules is challenging. The addition of a single sulfate group can drastically alter the chemical and physical properties of the macromolecules. Two common problems of sulphation are the lability of sulfate groups to acidic conditions and the lack of regioselectivity. [14]. Sulphation of D-galactose in fact, has already demonstrated to occur on 2-O, 3-O, as well as 4-O, 6-O. Primary alcohols like the one in C-6 could be preferred since the lower steric hindrance [15]. Obtaining poly-sulfated macromolecules is complicated since the generation of significantly higher negative charge cloud: as the number of alcoholic moieties rise, sulphation decreases progressively due to intense anionic crowding [14].

On the EPS nonasaccharide, every primary and secondary alcohols could represent a possible site of sulphation, especially those on the side chain which are the most accessible ones. Despite that, we are not sure of which alcohols have been sulphated since it is hard to fully analyse the complex highly charged structure of EPS. Moreover, the possibility of different sites of sulphation among all the nonasaccharides must be encountered. The assumed possible structure of EPS DRS was proposed by IFREMER [9] and is presented in Figure 14: it is displayed which are the most common sites bearing sulfate groups after the over-sulphation reaction according to NMR spectroscopy and mass spectrometry realized by the IFREMER team. These three common sulfated sites indicated in the figure are normally maintained among every nonasaccharide. Therefore, these studies indicated that sulphation normally occurs in the 6-O position of a glucose unite and in the 4-O position of a galactose unite, which are both in the branch, and in the 3-O position of a galactose unite in the linear chain. [10, 11, 16]. Other sulphation positions are certainly expected to be present, but they have not been displayed so far. The determination of the linked sulfate groups is made by high performance anion exchange chromatography (HPAEC), while total sulfate content is determined by elemental analysis. Usually, using this protocol of sulphation, the sulfur content \cong 16 wt%, while the sulfate content \cong 40 wt%.

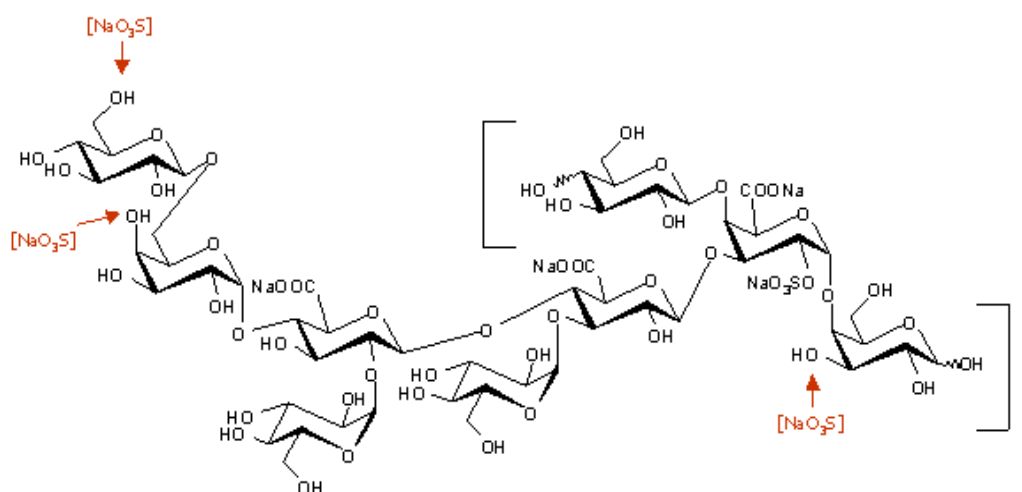


Figure 14. Proposed structure of EPS DRS and major sulfated sites after over-sulphation reaction. Other sulphation positions are certainly expected to be present, but they have not been displayed so far. Figure adapted from Chopin et al. 2015 [9].

B – Characterization of EPS and heparin

Molar mass and molar mass distribution are the most important characteristics that affect chemical and physical properties of polymers. These characteristics have tight relation with many other properties, such as solubility, viscosity, elasticity, chemical resistance, etc. In

specific applications such as drug delivery (of radionuclides or NPs), an accurate monitoring of the size of polymer chains is required to control all their chemical and physical characteristics [17].

Moreover, molar mass and chemical structure can also modulate the immunogenic effect of polymers, synthetic and natural. Polysaccharides are complex natural polymers and a small change in their chemical structure can determine a major change in the overall properties. Conformational changes can result in an increase/decrease of hydrophobicity. Glycosylation, for instance, can modify the immunological properties of macromolecules by acting as cell surface receptors for antibodies, toxins, etc. On the contrary, PEGylation may shield immunogenicity. Concerning the influence of molar mass, physical degradation of the polymer can activate an immune response. In addition, aggregates have also demonstrated to enhance the immunogenicity of various macromolecules, resulting in a key factor for antibody response. The high abnormal dimensions would appear to increase the time required to metabolize the molecule, revealing in the meanwhile new epitopes recognized as non-self by immune system [18].

1. Molecular weight

Polysaccharides are usually polydisperse in molecular weight. Therefore, the molecular weight of polysaccharides is mostly described in a statistic way, such as number average molecular weight (M_n), weight average molecular weight (M_w), and zeta average molecular weight (M_z), as shown in the below equations (Eqs. 1–3). Here C_i refers to the concentration of molecules that having molecular weight of M_i . The molecular distribution of polysaccharides can be described by the polydispersity index (Eq. 4). For monodispersed polymers, $PDI = 1$, while PDI less than 1.2 and above 2 are generally regarded as narrow disperse and wide disperse, respectively. Most natural occurring polysaccharides demonstrated high PDI value (above 2).

$$M_n = \frac{\sum C_i}{\sum C_i / M_i} \quad \text{Eq. 1}$$

$$M_w = \frac{\sum M_i C_i}{\sum C_i} \quad \text{Eq. 2}$$

$$M_z = \frac{\sum M_i^2 C_i}{\sum M_i C_i} \quad \text{Eq. 3}$$

$$\text{PDI} = M_w / M_n \quad \text{Eq. 4}$$

Number average molar mass (M_n), for instance, is mostly sensitive to fraction of low molar masses, while the *weight average molar mass* (M_w) is sensitive fraction of high molar masses. The ratio M_w/M_n is commonly called *polydispersity index* (PDI). It measures how the molar mass of each fraction varies in the polymer population. For absolute monodisperse polymer, this value is equal to 1 meaning that the two average molar masses are identical. This ratio increases at increasing the dispersity of the polymer [19].

Molar mass of polymers can be determined by various methods (e.g. osmometry, ultracentrifugation). Currently, the most popular technique is *size exclusion chromatography* (SEC). SEC, or *gel permeation chromatography* (GPC), presents a relatively simplicity of use, versatility and possibility to determine the complete distribution of the molar masses. *Asymmetrical Flow Field-Flow Fractionation* (A4F) coupled to *Differential Refractive Index* (dRI), and *Multi Angle Light Scattering* (MALS) detectors is also a well-known suitable technique for the characterization of molar mass distribution of synthetic and natural polymers [20].

Usually, M_w values of the two EPS are routinely determined by SEC-MALS, right after their production in bioreactor. In the present chapter, we have characterized the two EPS through A4F-MALS.

a. Determination of dn/dc

Refractive index (RI) increment $\partial n/\partial c$ is an important parameter to be considered for the accurate determination of molar mass averages and distribution of macromolecules [21], especially polysaccharides, when light scattering is coupled to separative techniques upstream. It varies among chemical species, as well as when changing experimental conditions, i.e. solvent, temperature, and wavelength of measurements.

The calculation of all molecular parameters from the light scattering, viscometer, and UV detectors is dependent on knowing the sample concentration, as indicated in the equations below. When the $\partial n/\partial c$ value is known, a sample of unknown concentration can be analyzed and the dRI signal can be used to determine the concentration.

Experimentally, the dn/dc can be determined using a differential refractometer (dRI). An Optilab rEX from Wyatt Technology (Germany), associated with ASTRA[®] software was used

to determine dn/dc of EPS DR and DR. The temperature of the device is set to 25°C and a wavelength (λ_0) of 660 nm is chosen.

To obtain accurate determinations, pure samples are required. Moreover, the sample solution must be the same of the one contained in the reference cell of the refractometer. In case of a lack of literature data for our experimental conditions, an *offline batch mode* can be assessed to determine the dn/dc . The term “offline” refers to the fact that every sample is directly injected into the dRI, without passing through the HPLC pump, or the column/channel or other detectors. Multiple concentrations from 0.25 up to 2 mg/mL were used to measure the dn/dc of EPS DR and DRS. The solvent used is ultrapure distilled water that allow to make comparisons with the dn/dc of common polysaccharides dissolved in water. The dn/dc is equal to the slope of the dependence of dRI signal intensity of polymer solution as a function of its concentration [22].

The dn/dc of both EPS-DR and -DRS, has been determined: results, interpretation and experimental conditions will be presented and discussed in the Chapter 3 of this manuscript.

The values of dn/dc are crucial to obtain accurate molar masses and dispersity values.

b. SEC-MALS

The basic principle of this separation technique is called *steric exclusion*. The chromatographic columns are packed with a porous material (stationary phase) and the mobile phase containing the sample flows through the porous phase. The small particles permeate deeper through the pores. Largest particles cannot penetrate the smaller pores, so, they are excluded and eluted first, followed by particles with decreasing molecular size.

Usually, SEC-MALS is employed for the absolute determination of molar mass for a wide range of macromolecules, including proteins, polysaccharides and nucleic acid complexes. A common characteristic of SEC measurements is the great short-term repeatability, while reproducibility is often considerably poorer, especially when comparing experiments from different laboratories.

A chromatographic system for SEC consists of a solvent reservoir, a degassing unit, a solvent delivery pump, an injector, a separative column, one or more detectors, and a computer for data acquisition and elaboration. *High performance liquid chromatography* (HPLC) pumps can be used in the SEC setup. Usually, a *differential refractive index* (dRI) and/or an *ultraviolet* (UV) detector are used to monitor the concentration of the sample that elutes out from the column [23].

For the characterization of EPS by SEC, the equipment is composed of a pre-column Aquagel-OH-Mixed (diameter 7.5 mm and length 50 mm) and a column PL Aquagel-OH-Mixed 8 μ m (diameter of 7.5 mm and length of 300 mm) from Agilent Technology.

The eluent used for the characterization of EPS is ammonium acetate 0.1 mol/L + NaN₃ 0.03%: the first one ensures a pH fixed to 7 and the second one prevents microbial proliferation. Concentration of salt and pH of the resulting solution may affect the solubility of biopolymers. Moreover, the ionic strength can influence the conformation and the size of polyelectrolytes: they expand at lower salt concentrations and they contract at higher concentration of salt, creating random coil conformations.

In liquid chromatography, detectors are normally employed to monitor the molecules of solute eluting from the separative device. The dRI and UV are the most common detector in SEC, converting the change in the mobile phase composition into an electrical signal that can be processed by a software. In the characterization of EPS, SEC columns are simultaneously couple online with an UV-visible spectrophotometer ($\lambda = 254$ nm) from Shimadzu Technology and a differential refractometer Optilab rEX from Wyatt Technology. The reason of using a dRI detector is because the difference between the light refracted by the sample solution and that of only solvent is directly proportional to the concentration of the sample.

Light scattering (LS) detectors are almost exclusive of SEC, especially those of *multi-angle light scattering* (MALS). Basic principles of LS and functioning of this kind of detectors are shown in following paragraph.

c. Light Scattering (coupled to either SEC or AF4)

According LS, the intensity of light scattered by a dilute polymer solution, called Rayleigh ratio, is directly proportional to the concentration and molar mass of polymer molecules. The angular variation of the scattered light intensity is related to the size of scattering molecules. In MALS, the scattered light is registered by a multitude of detectors positioned at 360° around the incident light (see Figure 15).

[No copyright permission was obtained for this figure]

Figure 15. Schematic functioning of a MALS detector. Figure taken from Azo Material website.

The most common equation that relates the intensity of scattered light with the characteristics of dilute polymer solutions is the following [20]:

$$\frac{K^*c}{R_\theta} = \frac{1}{MP_\theta} + 2A_2c \quad (\text{Eq. 5})$$

where R_θ is the Rayleigh ratio, c is the concentration of the polymer in solution (g/mL), M is the molar mass, A_2 is the second virial coefficient, K^* is an optical constant and P_θ is the particle scattering factor. The subscript term θ relates to the angle between the scattering direction and the incident light beam. Equation 1 is also called *Zimm formalism*.

The specific refractive index increment (dn/dc) is an essential parameter for processing the LS data obtained by MALS detector, normally coupled to SEC and A4F separative techniques. The dn/dc is related to the optical constant according the following Equation 6:

$$K^* = \frac{4\pi^2 n_0^2 (\partial n / \partial c)^2}{\lambda_0^4 N_A} \quad (\text{Eq. 6})$$

where n_0 is the refractive index of the solvent at the incident wavelength, λ_0 is the wavelength of the incident radiation and N_A is Avogadro's number. The dn/dc is also used to calculate the absolute concentration of polymer when using MALS detectors. The dn/dc is a constant for a given polymer in a given solvent and depends on the wavelength and temperature. This factor reflects the unique interaction that the polymer establishes with a certain solvent.

During the MALS detector acquisition, a software can plot the light scattering intensity versus the angle of observation at a given concentration. The Rayleigh ratio, then, can be extrapolated to zero angle, so ignoring the concentration dependence. This kind of plot is called *Debye's plot* and it shows a linear function (see Figure 16). Normally, $2A_2$ is given by the slope of the straight line, while the weight average molar mass is obtained by the intercept. Then, M_n and M_w may be obtained from equations 1 and 2, respectively.

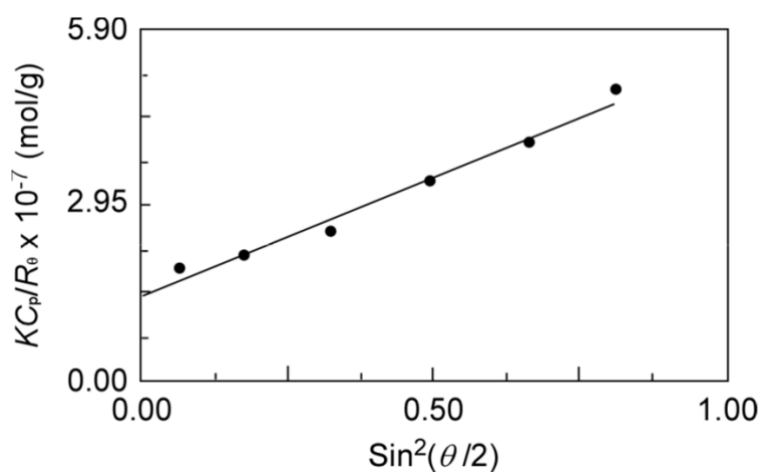


Figure 16. Example of Debye plot [24].

Coupling MALS with an on-line concentration detector, such as dRI, allows calculating the molar mass of the eluting sample coming from a separation technique. Light scattering is considered an absolute method for the determination of molar mass and its accuracy depends on the accuracy of the Rayleigh ratio, as well as on the accuracy of the concentration. An inconvenience of light scattering experiments is that they are very sensitive to higher size fraction particles, which can be presented both in the sample solution and the eluent. For this reason, a *clarification* of sample is required to remove dust, paying attention to not losing too much sample amount necessary to realise the analysis. Moreover, the accuracy of MALS depends also on the cleaning of the flow cell. Impurities attached on the flow cell can increase the background signal, affecting the analysis.

d. Asymmetrical Flow Field-Flow Fractionation (AF4)

Asymmetrical flow field flow fractionation (A4F) is the most technically developed kind of field flow fractionation (FFF), a separation technique invented by Giddings and its team [25]. A4F allows numerous applications, such as the characterization of natural and synthetic polymers, colloidal particles, proteins and nanoparticles.

The main difference between A4F and liquid chromatography (LC) is the absence of stationary phase: in fact, the separation of compounds in A4F is obtained only by a flow in an empty channel where another flow is applied perpendicularly. The longitudinal flow is called *detector flow*, while the perpendicular flow is named *cross flow*. The said channel is formed by two plates combined together that are separated using a Teflon spacer. The bottom plate is constituted by porous frit covered with a semipermeable membrane with a usual pores dimension of 5 or 10 kDa permeable to the solvent, holding the sample particles to be separated in the channel. A simple scheme of the main parts composing an A4F channel are showed in Figure 17 [26].

[No copyright permission was obtained for this figure]

Figure 17. Schematic illustration of the main parts forming the A4F channel. Figure adapted from a Wyatt Technology presentation [27].

Unlike SEC, the sample is not injected directly in the principal stream coming from the HPLC pump, but it has a different entry at the beginning of the asymmetrical channel. Channel cross section appears rectangular, and its dimensions decrease passing from the channel inlet to the channel outlet. The flow inside the channel is laminar. Its parabolic profile allows the particles

present in the middle of the channel to move faster than those situated closer to the border of channel. Initially, the particles move horizontally with the detector flow, but immediately they are driven by the cross flow towards the bottom wall of the channel.

The increase of concentration close to the membrane determines a concentration gradient. At this moment, a diffusion process begins, and smaller particles move closer to the middle of the channel because of their higher diffusion coefficient. This phenomenon is called *Brownian separation*. The balance of the two counteracting transports (cross flow and diffusion) creates a cloud of particles, which are positioned vertically according their diffusion coefficient. The separation is based on the Stokes-Einstein principle that inverse proportionality between the particle radius and the diffusion coefficient, as follows:

$$r = \frac{kT}{6\pi\eta D} \quad (\text{Eq. 7})$$

where k is the Boltzmann constant ($1,38 \cdot 10^{-19} \text{ kg} \cdot \text{cm}^2 \cdot \text{K}^{-1} \cdot \text{s}^{-2}$), T is the temperature, η is the dynamic viscosity, and D the diffusion coefficient.

Since the axial flow in the middle of the channel is faster, the small particles are eluted first, then followed by the larger ones that have a lower diffusion coefficient. Particles are then separated according to their *retention ratio*, which represents the retention of the molecule of given diffusion coefficient (t_R) compared to the same molecule unretained by the applied cross flow [26]:

$$R = \frac{t_0}{t_R} \quad (\text{Eq. 8})$$

$$t_R = \frac{t_0 V_c w^2}{6V_0 D} \quad (\text{Eq. 9})$$

where t_0 is the dead volume, corresponding to the crossing of the eluent filling the channel, V_0 is the volume of the channel, w is the thickness of the channel, D the diffusion coefficient and V_c is the cross flow rate.

A scheme showing the separation in the channel is showed in Figure 18.

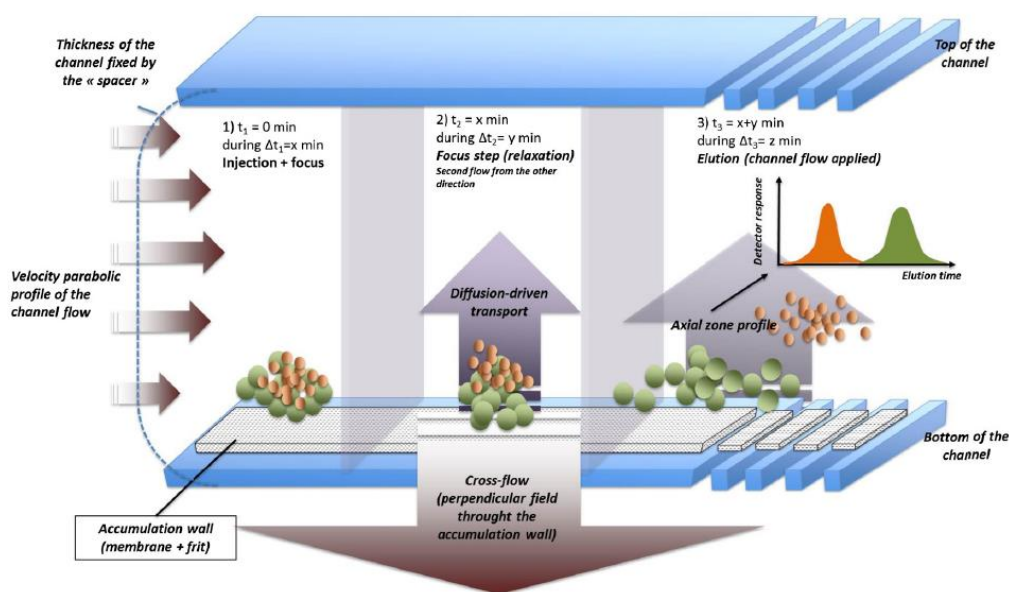


Figure 18. Illustration of the A4F channel components and the principal steps for the analysis for mixed populations of particles differing in size. The accumulation wall (membrane) is permeable, which allows flow through the bottom of the channel. Note that this scheme is not to scale. In A4F normal mode elution the separation process occurs in the lower 10% of the channel height [28].

Every A4F analysis is composed of three steps:

1. *Injection.* A part of the flow coming from the HPLC pump is split and it goes through an injection loop, filled of sample, and deliver its content towards the injection port of the channel.
2. *Focusing and relaxation.* Before the injection, the flow coming from the HPLC pump is split in two flows that enter into the channel from the inlet and outlet, meeting each other in proximity of the injection port. During the injection, the sample solution is pumped into the channel, at a certain distance from the inlet entry (focusing line); the eluent moves only according the cross flow, permeating the membrane and leaving the channel from a specific exit. At this moment, the sample starts moving and it is focused on the focusing line for certain time. Samples must reach their equilibrium positions before starting their migration through the channel. This process, called *relaxation*, consists in the temporary stoppage of longitudinal migration (only cross-flow is applied). In this way, the distribution of the sample may start.
3. *Elution.* After a Focus period, the eluent starts flowing from the channel inlet to the channel outlet, which is connected to the detector. During this period, the cross flow is maintained to let the distribution of the particle happen as a function of their size.

Generally, there are three different modes of elution that depend on the type and size of the sample, as well as on the cross flow applied.

- 1) *Normal or Brownian mode*. As already mentioned before, with this modality particles are separated according their diffusion coefficient. They are eluted in ascending order of size (see Figure 19a).
- 2) *Steric mode*. This kind of elution occurs when the diffusion of particles become neglected due to their very high dimensions (several micrometers) compared to the applied cross flow. All the particles are placed close to the membrane, where the repulsion forces play a key role in the separation. Even with this modality, the position of the particles in the channel is determined by their size. Bigger particles are eluted first, followed by the smaller ones (see Figure 19b).
- 3) *Hyperlayer mode*. This modality relates particle size bigger than the micrometer, appearing very similar to the steric mode. Here the repulsion forces depend on the size of the particles and the elution results on the contrary of the normal mode; particles are eluted in descending order (see Figure 19c).

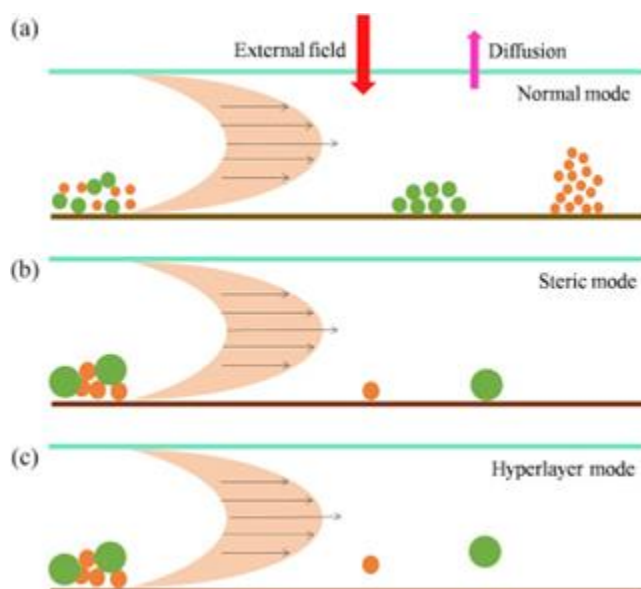


Figure 19. Schematic representation of different types of elution in A4F [29].

Very often, steric and hyperlayer modes are put together due to their similarities, forming a single mode called *steric-hyperlayer*. The transition between normal and steric-hyperlayer mode is called *inversion*. Inversion can occur when analysing samples with a very broad range of size, causing issues within the separation of particles.

The analytical system for A4F requires a solvent reservoir, a degassing unit, an HPLC pump, a device able to split the HPLC pump flow in multiple flows (chassis), an injector, the asymmetrical channel, one or more detectors, and a computer for data acquisition and elaboration. For the characterization of EPS, the A4F instrumentation employed is the one manufactured by Wyatt Technology.

The solvent reservoir usually contains the carrier solution; for the characterization of EPS, the same eluent used in SEC has been used: ammonium acetate 0.1 mol/L + NaNO₃ 0.03%. The choice of the ammonium acetate 0.1 mol/L prevents sample-sample and sample-membrane repulsion as well as sample-membrane adsorption. This, then is forced through the vacuum degasser a Shimadzu HPLC pump that has an online filter of 0.1 μm. The Wyatt technology uses a single HPLC to create the three separate flow streams that are detector flow, cross flow, and injection flow. To make this happen, a device called Eclipse 3 has been associated to the Shimadzu HPLC pump. Through several motor-driven switching valves, the main flow coming from the HPLC pump is split and directed during the three phases of the A4F separation in the channel (focusing/relaxing, injection and elution).

The channel is usually a trapezoid with two conical ends. The top and bottom channel walls must be parallel in order to ensure a uniform parabolic flow during all the analysis. The internal surface of the channel is smooth except for the bottom wall that is rough because of the membrane porosity. Frequently, a regenerated cellulose membrane is employed for its versatility (compatible with organic and aqueous solvents), but other materials like polyether sulfone and cellulose acetate are available. Usually, the solvent does not interact with the membrane, so the only important parameters to be considered are the membrane cut-off (5, 10 and 30 kDa), and the species that have to be separated.

In the determination of EPS molar mass and dispersity, the employed channel is a long channel (291mm) and the membrane contained is made of polyether sulfone (PES) with a porous size of 5 kDa. This porous size is very small compared to the one of EPS, that ranges 25-50 kDa. During EPS analysis, the presence of 0.1 mol/L of ionic strength prevents sample-membrane repulsion, while allowing enough sample-membrane interaction to ensure the separation. Solutions were prepared at 2 mg/mL and filtered with a 13 μm syringe before the injection. The separation conditions will be presented in Chapter 3.

Coupling a MALS detector to A4F allows characterizing natural and chemical polymers in terms of molar mass and dispersity. A DAWN HELEOS II of 18 angles from Wyatt Technology is employed; to calibrate and normalise all the angles of the detector, a previous

injection of a bovine serum albumin (BSA) 1 mg/mL solution of known molar mass ($M_w = 67,000$ g/mol) is required. The choice of using BSA are: (i) the fact that it is possible to well display from the monomer to the tetramer of this protein, which possess unique molar masses; (ii) because the very small dimensions of BSA (less than 10 nm) diffuses the light in an isotropic way, allowing all the detectors to see the same amount of scattered light at whatever scattered angle. In contrast to SEC, where the solubility of the sample is a mandatory, A4F permits to analyse insoluble particles. To allow that, the complete dispersibility of the sample in the solvent is required, preventing any aggregation or sedimentation. For this kind of analysis, the particle size must be calculated from the retention time. Verification tests can be assessed using polymer standards as particle with known dimensions. A verification test using several polystyrene standards of different sizes (30, 50, 70 and 100 nm) has been assessed to check the separative system.

Several parameters can be optimized in order to obtain an optimal separation of EPS:

- Sample concentration
- Focus flow rate and time
- Cross flow rate and time
- Thickness of channel
- Type and porous size of membranes
- Eluent

Table 5 shows the optimized parameters for EPS characterization by A4F-MALS.

Table 5. Optimized parameters for EPS characterization.

Optimized parameters	Values
Sample concentration (mg/ml)	2
Focus flow rate (ml.min ⁻¹)	2
Focus flow time (min)	5
Cross flow rate (ml.min ⁻¹)	1.5
Eluent	ammonium acetate 0.1 mol/L + NaNO ₃ 0.03%
Membrane	PES 5 kDa

Apparently, the analytical system looks like the SEC one except for the channel, which replaces the column, and the specific device that manages all the different flows in the column by splitting the main one coming from the HPLC pump. In this way, the A4F instrumental setup

may be easily and quickly converted into the SEC one by disconnecting the channel+chassis and connecting the column, and vice versa. A4F may present some advantages in comparison with SEC:

- 1) No enthalpic interactions of macromolecules (often polyelectrolytes) with the column packing. Despite the absence of enthalpic interactions between the analysed molecules and the stationary phase, in real SEC, several types of interactions may often play a significant role. Nonetheless, many proteins and polyelectrolytes possess polar functional groups that would show strong interactions with the SEC column, cancelling the size-based separation. Besides, amino groups and carboxyl groups may increase the probability of interaction. In this way, the fractions that are eluted in the end on the separation contain the smaller molecules plus those large, branched molecules (delayed by column packing interactions). This phenomenon is called *anchoring* [30].
- 2) Better managing of dilute injection volumes. In A4F, since the injection phase is located between two focus time, the particles do not go through the channel immediately. This advantage is particularly used when dealing with large and diluted injection volumes (e.g. environmental samples), allowing to concentrate the sample during the Focus+Inject phase.
- 3) Easier way to control the resolution. With A4F there is no need to change columns dimensions or column packing content to control the resolution. All the separation condition can be controlled through the channel.
- 4) Fast changing solvent. Changing the solvent in SEC, normally requires a huge amount of time. In the gel forming the packing column, a long time is required to replace the old solvent with the new one. In A4F, this changing is really fast due to the absence of stationary phase.
- 5) No bleeding. Since there is no stationary phase, the dRI detector signal is not disturbed by column bleeding (release of eluent not necessary for the analysis).
- 6) Robustness and practicality. SEC columns are fragile, and they could be damaged very easily. In contrast, the A4F channel is basically unbreakable, while the membrane can be replaced frequently at affordable prices.

As all the analytical technique, even A4F has its drawbacks.

One of these is probably the *overloading*. In most cases, the separation takes place in a relatively thin layer near the accumulation wall. During the relaxation phase, if the concentration injected are really high, sample molecules can affect each other. This is due to a

steric effect resulting from a reduction of physical space necessary for the molecule to reach the equilibrium. The results is that relaxation equilibrium may be not reached, affecting the retention time, so the shape of the fractogram. Additional effects resulting from too high concentration injected are aggregation/repulsion of particles, entanglement of chains and adsorption on the membrane.

A second drawback is the possible formation of aggregates during the analysis. Aggregation of particles is a serious problem that has to be taken into account to ensure the stability of injectable biopharmaceuticals. This process, that remains unclear, can occur at any moment during the lifetime of a therapeutic macromolecule (especially proteins), from its synthesis, purification up to its shipping, storage, and delivery. There are various different analytical techniques that can be used to investigate the presence of aggregates within the micrometer range. To detect and quantify the presence of aggregates at an early stage MALS coupled to SEC or A4F can be used. Despite that, the use of Dynamic Light Scattering (DLS) can be considered more useful to characterize aggregates since phenomena like dilution and shear degradation can encounter in A4F and SEC, causing a disassociation of aggregates. DLS is a technique used to study the distribution profile of small particles in suspension or polymer in solutions. DLS is commonly employed in colloidal and protein sciences and it is based on the analysis of scattered light fluctuations that occur as a result of the Brownian motion of particles. These fluctuations are lately converted into particle size kinetic analysis using mathematical algorithms [31]. Different measurement configurations are available for commercial DLS systems, nonetheless, each of these options requires to manipulate the sample prior and during the analysis. To prevent this problem, a DLS system coupled to a special optical fiber has been designed to make direct and contactless measurements.

Last but not least, the possibility of sample-membrane interactions has to be encountered. Normally, these interactions are not considered in the A4F theory, so they can deviate from theory and causing incorrect size particle analysis. Some additives, such as salts, buffers and surfactants can be added to control those interactions. It is known that sample-membrane can occur if the ionic strength is too low, while particle adsorption can occur if the ionic strength is too high. Fortunately, there is wide evidence in the literature that sample-membrane interactions can be neglected for the analysis of most compounds with the use of proper additives to the eluent [32].

e. M_w characterization through SEC-MALS and A4F-MALS

Thanks to the recent development of new A4F-MALS devices, this technique has reached a mature condition where it can be used in a routinely way as SEC-MALS. Molar mass and dispersity determined by A4F-MALS and SEC-MALS for the two EPS of interest of this work have been compared. Results are summarized in Table 6.

Table 6. Comparison between A4F-MALS and SEC-MALS about the characterization in terms of molar mass and dispersity. The values in the brackets correspond to the uncertainties.

		M_w (kDa)	M_n (kDa)	PDI
DR	AF4-MALS	25.6 (3.2)	18.8 (2.8)	1.41
	SEC-MALS	17.9 (0.3)	10.9 (0.2)	1.64
DRS	AF4-MALS	56.9 (8.1)	39.1 (4.1)	1.46
	SEC-MALS	25.1 (1.0)	15.1 (0.4)	1.65

Concerning both M_w and M_n , yields are higher in A4F-MALS than SEC-MALS. A4F achieves slightly higher M_n due to higher resolution in lower molar mass region in linear polymers; also, the permeation of oligomeric fractions through semi-permeable membrane may result in a higher M_n . Concerning M_w , a slight increase of this value, when using A4F, is due to the fact that the concentration of sample in A4F is normally lower compared to SEC columns, resulting in a lower error by neglecting the virial coefficient A_2 in Eq. 5. A higher increase of M_w in A4F analysis, instead, may result from the absence of stationary phase and significantly lower pressure in the A4F channel (normally this pressure is of 10-11 bars); in these conditions, shearing degradation and anchoring are reduced or even avoided in high and ultra-high molar mass region [28].

In fact, flow velocities and pressures used in HPSEC are usually five times stronger than standard SEC. Because of velocity gradients generated during flow, a polymer gets elongated. Bonds situated close to the middle of the chain become stretched and can break if shear rates are high enough. The end segments of a chain maintain their coiled shape; then, the maximum stress is frequently focused near the centre of the polymer [33]. Even controlling all the SEC separation conditions, the possibility of shearing degradation can never be totally eliminated. Then, it has been assumed that the increase of M_w and M_n , in A4F analysis may be due to a possible shear degradation of EPS occurring in the SEC ones.

Despite the fact that, in A4F, polymers are in contact with the semi-permeable membrane of the bottom wall channel, the contact surface is much lower compared the column packing and

the enthalpic interactions are far less intense than SEC ones. EPS are branched polymers and this anchoring effect may explain the increase of polydispersity index when analysing those polysaccharides using SEC-MALS.

A4F-MALS represents an alternative to SEC-MALS to analyse a broad variety of linear and branched polymers with the advantage of reducing significantly the shearing degradation and the anchoring effects. Major details and experimental conditions are given in the Chapter 3.

f. RMS radius

In the theory of LS, the scattered light gives additional information on the analytical sample. For small angles, the particle scattering function can be resumed as the following:

$$\lim_{\theta \rightarrow 0} P(\theta) = 1 - \frac{16\pi^2}{3\lambda^2} R^2 \sin^2(\theta/2) = 1 - \frac{\mu^2}{3} R^2 \quad (\text{Eq. 10})$$

Where λ is the wavelength of the incident light in a given solvent, R^2 is the mean-square radius, and μ is the scattering vector. When $P(\theta)$ is plotted against $\sin^2(\theta/2)$, the slope of the resultant linear function is directly proportional to R^2 . This means that the slope of the angular variation of the scattered light intensity at angle zero yields the root mean square (RMS) radius, or R . The RMS radius indicate the distribution of particle mass around its center of gravity. If we consider a polymer as a particle, its physical mass results from component of mass m_i and RMS radius is determined by the square root of the weight-average of r_i for all the mass component, as shown below:

$$R = \left(\frac{\sum m_i r_i^2}{\sum m_i} \right)^{1/2} \quad (\text{Eq. 11})$$

where r_i is the distance of the i^{th} mass element of mass m_i from the center of gravity. In comparison with other parameters characterising the size, the RMS radius gives no information on the particle shape. This is because this size parameter is obtained by light scattering data that can be collected even when the concentration of the particle is not known. As a result, Eq. 11 is valid only for rigid particles. Natural and synthetic polymer are structurally more complex. A random coil conformation, for instance, accounts as the most typical shape for both types of polymers. Random coil is a flexible structure that can determine several conformations.

In polymer physics, the RMS radius corresponds to the *radius of gyration* (R_g) and is used to describe the dimensions of a polymer chain. The chain conformations of a polymer sample could be considered infinite in number, constantly change over time. Then, R_g should be understood as a mean over all polymer molecules of the sample and over time. R_g cannot

provide any information on the particle shape until it is compared with the hydrodynamic radius (R_h). R_h represents the radius of the “equivalent” sphere when taking into consideration the interactions between polymer and solvents. In reality, solutions of polymers and their complexes cannot be imagined as solid sphere, so R_h reflects more closely the apparent size adopted by the solvated polymer. Through viscometrical analysis, it is possible to understand that kind of interactions, obtaining new parameters needed for the determination of R_h .

2. Viscometry

Measurements of dilute solution viscosities can provide information about polymer flexibility, branching and polymer dimensions and conformation. In an ideal behavior, chain polymer conformation would expect a random walk of the monomer units, ignoring any kind of interactions among monomers. However, this behavior cannot occur because of steric effects. In fact, real polymer chains can be represented by a self-avoiding walk, meaning that, for instance, two chain segments cannot occupy the same space in solution. This brings to the formation of an *excluded volume* that makes the polymer expanding. Chain conformation is also influenced by the nature of the solvent. The interactions between polymer chains and their surrounding solvent molecules can be considered energetically favorable or not. Solvents that favorably promote these interactions polymer-solvent, causing an expansion of polymer coils, are called *good solvent*. Instead, solvents where interactions polymer-polymer are preferred, causing a contraction of polymer coils, are called *poor solvents*. When a solvent is poor enough to eliminate the effects of the excluded volume (ideal chain), it is called *theta solvent*. A schematic view is showed in Figure 20. The quality of the solvent is affected by both the chemical composition of the polymer (e.g. neutral polymer, polyelectrolytes) and solvent (e.g. aqueous or organic), as well as the temperature of solution [34].

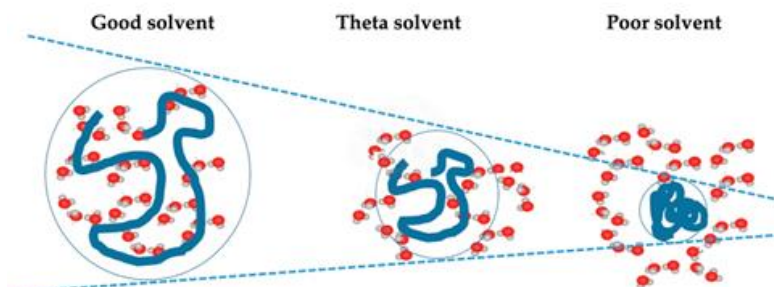


Figure 20. Polymer expansion and contraction according to the quality of solvent. Figure adapted from Taylor et al. 2017 [35].

The size and conformation of the polymer chains in a dilute solution can influence the viscous properties of the solution.

The chemical structure of a polymer is able to influence the interactions between polymer and solvent, so the hydrodynamic volume. These interactions result in the solvation of polymer chain, that has a strong impact on the polymer's expansion. Ionic groups situated along the polymer chain affect in a significant way the intrinsic viscosity. In dilute solutions, the polymer chain can expand due to the electrostatic repulsive forces between the ionic groups and this results in an increase of viscosity. This coil expansion results from the degree of dissociation of ionic groups, that also depends on the pH of the solution. Indeed, one of the most significant properties that come out from the study of polyelectrolyte solutions is the shape dynamics as affected by the degree of ionization. The study of the viscometrical behaviour of acidic polymers at different pH values led to a definite view of the interaction of the electrostatic field caused by the ionization and the random rearrangement of the polymeric chain. The general trend of the curves may be summarised as follows: at low degrees of ionization (pH=2-3), the viscosity is basically small and the change in solution is not appreciable. At increasing degree of ionization, a rapid increase in viscosity can be observed that reaches its maximum at 50% of ionization. From hydrodynamic point of view, this means that at low degrees of ionization the molecules are more or less hyper-coiled rigid spheres; they open up with increasing ionization and assume the form of freely knobby strings at initial ionization and, finally, at high degrees of ionization, stretch to rod-like filaments [36]. Moreover, the expansion of the polyelectrolyte chain is highly impacted by addition of salt. The free ions of the added electrolyte represent opposite charges to the functional groups placed on the polymeric chain, that shields charged groups. For this reason, they are attracted by the rod-like polymer and cause a shield effect, which diminishes the electrostatic repulsion of the ionized functional groups. At sufficiently high ionic concentrations, the stretching effect vanishes, and the molecules become normal, random coils, as observed in strongly alkaline solutions [35]. Generally, at increasing the salt concentration, the coil expansion decreases so the viscosity decreases as well. This behavior has already been investigated for heparin [37], showing a reverse relationship between ionic strength and intrinsic viscosity.

This aspect will be displayed more in detail in the Chapter 3, where the hydrodynamic volume of EPS and heparin have been determined as a function of salt concentration. The hydrodynamic volume trend in solution will allow predicting what kind of conformation is adopted by the polymer according to the solvent in which it is dissolved. This will help us understanding the polymer behavior in relation to additional chemical features like the complexation with metals.

a. Intrinsic viscosity

Intrinsic viscosity displays the potential of a polymer chain to enhance the viscosity of the solvent and depends on polymer size and shape. It represents an important feature to depict the behavior of a polymer in solution and its molecular structure. Many kinds of viscometer are available to measure viscosity.

Standard laboratory viscometers for liquids include glass capillary U-tube viscometers and falling/rolling ball ones. The first ones are constituted by a U-shaped capillary with two bulbs, placed up and down in the device. Normally, the liquid to examine is drawn into the upper bulb by suction and allowed to flow down through the capillary into the lower bulb. Two marks situated above and below the upper bulb indicate a known volume; the time necessary to the liquid to flow through those marks is proportional to the viscosity (see Figure 21a). In falling/rolling ball viscometers, instead, the rolling or falling time of a ball is measured, where gravity acts as the driving force. A ball of known dimensions rolls inside a closed glass capillary filled of sample solution. An inclination angle is preset to adjust the driving force. The time needed by the ball to roll a defined distance within the fluid is related to its viscosity (see Figure 21b). In this section, the determination of viscosities will be related to this last type of viscometer.

[No copyright permission was obtained for this figure]

Figure 21. **a)** Schematic structure of a U-tube viscometer. A and B are respectively the upper and lower marks to be considered for measuring the liquid flow time. C indicates the maximum volume of liquid that has to be poured into the glass capillary. **b)** Principle of rolling ball viscometer and main forces acting on the descending ball. F_G is the gravitational force; F_B is the buoyancy force and F_V is the viscous force. Figure adapted from Anton-Paar website.

When viscosity is used to characterize polymers, it is important to calculate the one determined by the presence of polymer molecules rather than the absolute viscosity of the solution. This property refers to the *specific viscosity* (η_{sp}) or *relative viscosity* (η_{rel}) according the Equation 12 [20]:

$$\eta_{sp} = \frac{\eta - \eta_0}{\eta_0} = \frac{t - t_0}{t_0} = \eta_{rel} - 1 \quad (\text{Eq. 12})$$

Where η and η_0 are the viscosities of dilute polymer solutions and pure solvent, respectively. In this way, the viscosity values can be replaced by the time needed by the ball to roll within a certain distance in the polymer solution filled capillary (t) and in the pure solvent filled one. Two other quantities of interest are the *reduced viscosity* and the *inherent* (or *logarithmic*)

viscosity, respectively Equations 13 and 14, that take in consideration the concentration, c , of the polymer solution.

$$\eta_{red} = \frac{\eta_{sp}}{c} ; \eta_{inh} = \frac{\log \eta_{rel}}{c} \quad (\text{Eq. 13 and Eq. 14})$$

In the limit of infinite dilution, both quantities provide respectively the *intrinsic viscosity* (Equations 15 and 16).

$$[\eta] = \lim_{c \rightarrow 0} \frac{\eta_{sp}}{c} ; [\eta] = \lim_{c \rightarrow 0} \frac{\eta_{rel}}{c} \quad (\text{Eq. 15 and Eq. 16})$$

Graphically, the most used and reliable procedure to determine the intrinsic viscosity is to plot $\frac{\eta_{sp}}{c}$ or $\frac{\eta_{rel}}{c}$ or both and to project the intercept that gives $[\eta]$.

Infinite dilute solutions of flexible polymers may be imagined as system in which polymeric “particles” are scattered in the solvent and almost never touch each other or interpenetrate. Therefore, the individual chains are well separated from one another and are free to move independently. In this case, the total rheological response of the solution can be considered as the sum of the individual contribution of the chains. Increasing the concentration gradually determines an increase in the statistical probability of intermolecular interactions: the collision between polymeric particles becomes more frequent and causes the chains to overlap or interpenetrate. At these conditions, we can imagine a system the polymeric particles begin to touch one another throughout the solution [38].

When intermolecular interactions are increased, polymers, especially branched ones, can form cross-links between the chains, which lead to a network of molecules. The system reduces its fluidity and viscosity becomes very important. Then, the solution undergoes to a gel transition (also called *gelation*) forming a polymeric hydrogel. In physically cross-linked hydrogels, ionic interactions, hydrogen bond and hydrophobic interactions are involved in their formation. Through ionic interactions, hydrogels can be cross-linked under mild conditions, at room temperature and physiological pH. When metallic ions are present in solution, stronger hydrogels can be obtained. For example, sodium alginate solution can form hydrogels in the presence of calcium ions, allowing to form ionic bonds that act like bridges between alginate chains. Other examples of polymers which form physically cross-linked gels relate collagen and agarose. Natural polysaccharides such as chitosan, dextran and pullulan are reported in the literature to form hydrogels by hydrophobic interactions [39].

b. Hydrodynamic radius and Hydrodynamic volume

Intrinsic viscosity is linked to molar mass according the Mark-Houwink-Sakurada (MHS) equation, as following.

$$[\eta] = K M_v^a \quad (\text{Eq. 17})$$

The molar mass concerned in this equation is the *viscosity average molar mass*, which is placed in the middle of molar masses distribution: $M_n < M_v < M_w$. In the MHS equation, K and a are constants for a given polymer, solvent, and temperature. For many polymers, these MHS constants can be found in the literature. Otherwise, they can be determined experimentally by selecting different sizes of the same polymer, that possess well-known values of intrinsic viscosity and molar mass. Then, the logarithm of the intrinsic viscosity is plotted against the logarithm of the molar mass and the MHS constants K and a are obtained by the intercept and slope, respectively [40].

MHS constants K and a for GAG, like heparin, or GAG mimetics, like EPS are not-known. In fact, to determinate these constants, no matter in what temperature or solvent, different sizes of heparin and EPS should have been used. This requirement is not practical since different sizes of polysaccharide should be bought or produced, demanding a certain cost. To estimate these values a universal calibration can be realized using a particular standard that can mimic the viscometrical behavior of our polysaccharides of interest. Polyacrylic acid (PAA) has already demonstrated to represent a simple model of those extracellular polymeric substances produced by bacteria [41]. This consideration resides in the importance of carboxylate groups found on macromolecules secreted by bacteria that are fundamental to promote their biological properties. Linear PAA can be considered a weak acid polyelectrolyte model since its pKa equal to 4.54 [42]. At low pH, PAA adopt a compact, but not totally collapsed, globular conformation. However, when increasing the pH, the ionization of its carboxylic groups occurs and the polymer expands into a fully solvated and open conformation. A set of different sizes of PAA can be easily found or bought by many laboratories in contrast to natural polysaccharides that are more difficult to obtain. Experimental conditions of the PAA calibration will be shown in Chapter 3.

Exponent a can provide information on the polymer conformation. When a range from 0 to 0.5, the macromolecule results into a compact sphere. In theta solvents, a is equal to 0.5. Normally, flexible polymers in thermodynamically good solvents show an exponent a ranging from 0.65 to 0.75, while values exceeding 1 can be found for certain expanded rodlike polyelectrolytes. The maximum value of a is 2 and it refers to rigid rods.

To calculate R_g , the Flory-Fox and Ptitsyn-Eizner equations can be used:

$$R_g = \frac{1}{\sqrt{6}} \left(\frac{[\eta]M}{\Phi} \right)^{\frac{1}{3}} \quad (\text{Eq. 18})$$

$$\Phi = 2.86 \times 10^{21} (1 - 2.63\varepsilon + 2.86\varepsilon^2) \quad (\text{Eq. 19})$$

$$\varepsilon = \frac{2a-1}{3} \quad (\text{Eq. 20})$$

where a is the exponent of Mark-Houwink-Sakurada (MHS) Equation and Φ is the Flory's universal constant for non-theta conditions. ε is a correction parameter: it is equal to 0 for theta solvents, while for thermodynamically good solvents it is correlated to the MHS exponent.

$$R_h = \left(\frac{3[\eta]M}{10\pi N_A} \right)^{\frac{1}{3}} \quad (\text{Eq. 21})$$

Both R_g and R_h can be used to find insights on polymer structure. Since R_g is determined using Φ and a , it is slightly more dependent on the structure of the analysed molecule than R_h . But it is the ratio R_g/R_h that really provides shape information. For a globular polymer, $R_g/R_h = 0.8$ while it is > 1 for flexible/elongated polymers.

The dimensions of intrinsic viscosity, mL/g, indicate that this property is also related to volume occupied by the polymer chain in solution. This volume is called *hydrodynamic volume* and it also takes consideration the volume of the expanded polymer plus the water molecules involved in its solvation. The hydrodynamic volume V_h is calculated using Equation 22 [43].

$$V_h = \frac{4\pi[\eta]M}{\mu} \quad (\text{Eq. 22})$$

with $\mu = 10\pi \times N_A$, where N_A is the Avogadro's number, $[\eta]$ and M are the intrinsic viscosity and the viscosity-average molar mass, respectively.

The hydrodynamic volume (and indirectly the molecular weight) strongly affects the systemic pharmacokinetics and pharmacodynamics of certain polymers. As mentioned in the previous chapter and developed in the introduction of this one, GAG mimetics have been proposed as vectors for radiopharmaceuticals. Normally, the higher dimensions, compared to other vectors such small molecules, have already displayed superior pharmacokinetic and pharmacodynamic. Different sizes of the same polymer may result in a different hydrodynamic volume and pharmacokinetic profile. For instance, PEGylated polymers larger than 30 kDa typically demonstrate a prolonged circulation time in the bloodstream and high accumulation in solid tumors. Generally, higher dimensions of molecules require more time to be oxidated by the liver (metabolism) and eliminated by kidneys (renal clearance) [44]. For these reasons, it is important to understand and quantify the interactions between polymer and its solvent in terms of hydrodynamic volume.

3. Protonation constants (pK_a)

The determination of protonation constants, pK_a , is necessary to predict the deprotonated complex species in equilibrium that is supposed to interact with metal. To be suitable for

nuclear medicine purpose, a metal-polymer complex must exhibit a high thermodynamic stability together with kinetic inertness. These criteria ensure a strong interaction of the metal with the molecule while preventing the dissociation of the complex. The determination of stability constants for Sc-EPS complexes is thus required. To this aim, the determination of protonation constants pK_a , is assessed in order to calculate the number of ionized groups available for complexation. For extreme acidic and basic pH ranges, hydrolysis of EPS chains could occur [45]. Nonetheless, potentiometric titrations of heparin were conducted in the literature suggesting its stability in extreme pH ranges [46].

Commonly, potentiometric titrations are conducted to this aim. All samples considered in this Section were titrated with an automatic titrator (702 SM Titrino, Metrohm, France) and monitored by the accompanying software (Tiamo Metrohm, France). The titration procedure was a dynamic titration with the highest available precision (titration speed “slow”) and a delay of at least 20 s at each titration point before measuring. The dosing rate of the delivery system of titrant was set at 0.1 mL/min and the volume increment registered by the electrode was set at 0.02 mL. It was checked that the solution was allowed to reach equilibrium between each stepwise addition of titrant. The potentiometric titration experiments were carried out under inert gas atmosphere (argon) at 25 ± 1 °C and a constant background electrolyte solution of 0.1 M (NaCl). In each case, the starting volume was 20 mL.

The pH values were measured with an Ag/AgCl electrode (Metrohm) which was calibrated before each experiment by titration of degassed HCl 0.1M solution by freshly prepared free carbonate NaOH 0.1 M solution to maintain constant ionic strength equal to 0.1 M. The electrode was calibrated using OPIUM software with the following equation:

$$E = E^0 + S \times \log[H^+] \quad (\text{Eq. 23})$$

where the additive term E^0 contains the standard potentials of the electrodes used and contributions of inert ions to the liquid junction potential, S corresponds to the Nernstian slope, the value of which should be close to the theoretical value. No significant deviation was observed in very acidic acid solution and alkaline solution and no corrections was taken into consideration.

a. Heparin's pK_a

For Heparin titration (3 measurements), a 5 mmol of sodium-Heparin converted to acid form by HCl (2.43 equivalent) was prepared in NaCl 0.1 M solution. The 20 mL final solution was then titrated with fresh free carbonate NaOH solution 0.053 M. Since the titration commonly involves a constant addition of titrant solution, the control of the ionic strength is not

straightforward. The obtained titration curve was fitted using OPIUM software to determine pK_a of Heparin.

The experimental data corresponded to a classical acid/base titration curve (Figure 22). As already said, heparin was initially acidified, and the number of protons added in the initial solution was taken into account for the modelling. From the experimental data, it was possible to extrapolate the protonation constants. Two protonation constants were found. The first value was found to be pK_{a1} = 3.82 ± 0.03, which corresponded to a weak acid. This value was attributed to the carboxylic group of iduronic acid of heparin disaccharide (see Figure 22) [47]. The second protonation constant was found at pK_{a2} = 7.53 ± 0.03, that was attributed to the nitrogen atom of the sulphamino group, which is a stronger donor than the other sulphated groups. This value was higher than the one previously determined by Karpukhin et al [48]. An explanation of that could reside in a possible *N*-sulphate cleavage at the starting acidic pH, leaving only the amine linked to the sugar pyranose ring. The *O*-ring and the -OH groups attached can make more acidic the amine pK_a by inductive effect. This hypothesis will be taken into consideration later on in this chapter.

Four kinds of acidic functional groups are present in heparin. Sulphates and sulphamido are both strongly acidic since their pK_a vary from 0.5 to 1.5 [49]. Less acidic moieties are the carboxylate groups, with a pK_a value ranging from 2 to 4, and the nitrogen proton from the sulphamino portion. [47]. According to Karpukhin *et al.* [48] four protonation stages are possible for heparin dimers in the pH range of 2.3-6.1. Standard potentiometric titrations were incapable of distinguishing between the different carboxy groups within the heparin polymer. Additionally, the *pKa* determined by standard titration could only provide a weighted average of the pK_a value for each α and β anomeric forms of constitutive sugars of GAGs.

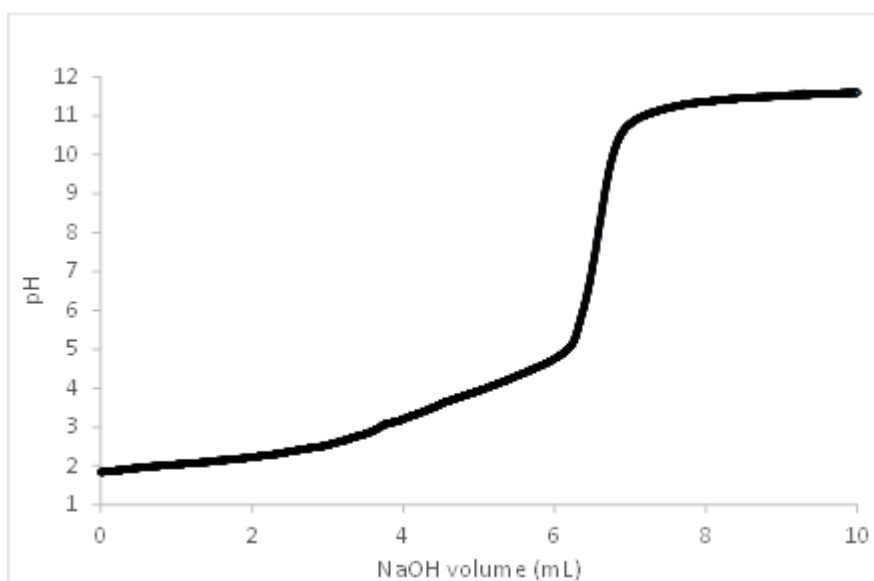


Figure 22. Potentiometric titration of heparin at $5 \cdot 10^{-4}$ M with NaOH at 0.1M.

Nonetheless, based on Karpukhin *et al.* [48] results, we assumed that the dominant heparin species at pH 3.5-6 was H_2L^{2-} , in which the two protons were attached to the carboxylate group and to the amine group (at pH around 6). At pH = 6-7, heparin was present as the unprotonated anionic form HL^{3-} , where only the -NH moiety was protonated. From the experimental data, the protonation constant of heparin species H_2L^{2-} , was determined by the means of Opium software from the potentiometric titration curve (not presented here). We assumed that the protonation constant determined corresponded to the carboxylate moiety. In the literature, the pK_a of galacturonic acid and glucuronic acid, were respectively 3.51 and 3.28 [50]. It was assumed that the determined pK_a of iduronic acid system (i.e. the galacturonic and glucuronic acids) from heparin could be transposed to the ones present on EPS DR and EPS DRS.

b. Heparin's carboxylic groups

Carboxylic groups from iduronic acid portion have displayed their important role in binding blood proteins, such as antithrombin III, responsible of the anticoagulant effect [51]. It was also evidenced, from NMR studies, that carboxylic groups of polysaccharides were the main interaction site for ions such as Na^+ , Ca^{2+} , Mg^{2+} [52]. Their quantification was thus required. In addition to the pK_a determination, the number of carboxylic moieties per chain of heparin was determined from the equivalent volume. This value was found to be 29.5. Then, it was considered only one carboxylic group by disaccharide unit. The number of disaccharide units was calculated by dividing the M_w of heparin by the M_w of the disaccharide. For the heparin sodium salt with $M_w = 27,250$ kDa, the number of carboxylic groups was found to be 40.1. This number of carboxylic groups titrated is lower than the real number of groups in the

polymer. It was assumed that, in our experimental conditions, some of these carboxylic groups were not accessible to titration. The solvent composition, *i.e.*, ionic strength, could influence the structural shape of the polymer, there was some hindrance of some functional groups to the titration. This means that an absolute quantification of carboxylic groups is not possible when an external ionic strength is added.

c. Heparin's hydrolysis

There was a possibility that hydrolysis of polymer could occur during the titration, precisely in the pK_a region (*i.e.* 3.82) and up the most alkaline conditions of the titration (*i.e.* $pH = 7.5$). Thus, the molecular weight was determined using SEC-MALS in order to check if there was a possible reduction of M_w induced by hydrolysis. SEC-MALS was used for determining the M_w of Na-heparin *vs.* pH . The choice to run the experiment by SEC-MALS derived from the choice of avoiding *overloading*, that normally occurs more easily in A4F-MALS when working at high concentration of sample. In SEC-MALS, indeed, a maximal sample concentration of 0,25 (% w/v) for polymer of approximately $25000 \text{ g}\cdot\text{mol}^{-1}$ may be reached without overloading the column. The equipment was composed of a pre-column Aquagel OH mixed (Agilent, \varnothing 7.5 mm, length 50 mm) and a column PL Aquagel-OH-Mixed $8 \mu\text{m}$ (Agilent, \varnothing 7.5 mm, length 300 mm). Ammonium acetate 0.1 mol L^{-1} + NaN_3 0.03% was the eluent. All the samples were filtered through a $0.45 \mu\text{m}$ filter before injection in the SEC column. Samples were prepared at the following pH values: 3, 3.5, 4, 6, 7, 7,2 and 7,3. For each pH value, 3 different concentrations of heparin (*i.e.* 10^{-3} , $5\cdot 10^{-4}$, and $10^{-4} \text{ mol L}^{-1}$) were prepared. Samples were maintained at 20°C for one week before being analysed.

It was shown that the values of M_w were quite constants over the pH range considered and for all concentrations considered (see Figure 23).

For the acidic pH range as for the most alkaline pH range considered, it was evidenced that M_w were lower compared to the initial value of M_w . A slight drop of the M_w was observed when decreasing the pH from 6.5 to 3, as well as with an increase in pH from 6.5 up to 7.3. These results were in agreement with published data on heparin showing that its molecular weight dropped in mild acidic conditions [53]. There might be a slight hydrolysis occurring, but the differences observed could be attributed as well to the experimental error and the uncertainties. Another reason of this decrease may reside in the possible shearing degradation linked to the separation system (previously described), that can be added to a possible slight hydrolysis.

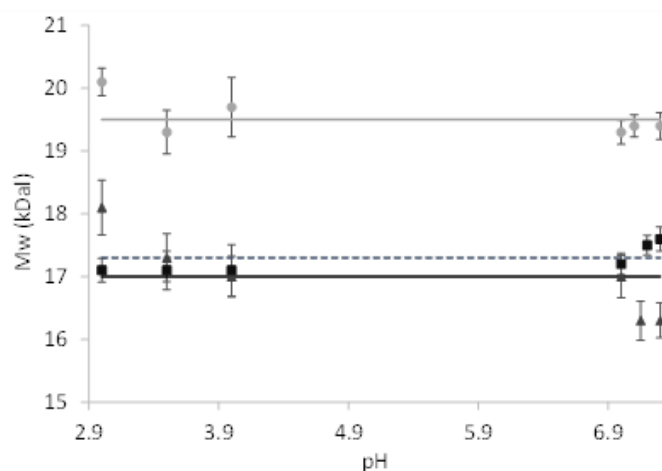


Figure 23. SEC-MALS analysis to check the hydrolysis in the pH range of 3-7.3. Heparin's concentrations: 1.10^{-3} (triangles), 5.10^{-4} (squares), and 1.10^{-4} mol L $^{-1}$ (circles).

Usually, chain fragmentation strongly occurs in polysaccharides containing glycosidic bounds [54], even if the presence of carboxyl or amino groups in certain GAGS could reduce the hydrolysis of the glycoside bounds [55]. Thus for heparin, a cleavage of *O*-sulphate and *N*-sulphate groups could occur, slightly reducing the M_w value without causing chain fragmentation [56]. Sulphate esters are easily degraded by both mild acid and alkali hydrolysis. Normally, ester formed on equatorial secondary hydroxyl groups are more easily hydrolysed than those on axial secondary hydroxyl groups. The latter, in turn, can be more promptly degraded than sulphate esters placed on primary hydroxyl groups. Moreover, *N*-sulphate (also called sulphamino) groups are much more unstable in acidic medium than the *O*-sulphate ones [57].

The fact that a possible hydrolysis of heparin may occur brings to take with caution the collected pKa information. If we consider a cleavage of sulphates involved in the decrease of M_w , the resulting (reduced) charged surface may interact differently with the ionic strength of the solution. This could determine differences in the polymer conformation which could reveal, or not, more carboxylic groups to the solvent. Moreover, this pH-sensitivity limit significantly the number of analytical techniques to be envisaged to determine the stability Sc-polysaccharides constants. In the Chapter 3, a less common technique will be proposed to this aim since it allows to work at fixed pH. The pH of all the complexation studies will be set to 6, allowing to prevent mild acidic and alkaline hydrolysis.

III. Scandium

A – Chemistry of the element

Scandium is a silvery white, mildly soft metal. It is relatively stable in air but slowly oxidizes to a yellowish color because of the formation of Sc_2O_3 oxide on its surface. Scandium gradually dissolves in diluted acids except hydrofluoric acid (HF), where a protective trifluoride layer stops further reactions. Scandium is paramagnetic from $-273\text{ }^\circ\text{C}$ to its melting point of $1,541\text{ }^\circ\text{C}$.

Scandium is located in the third column of the periodic table and it exists mainly under its +III oxidation state in water. Scandium is a metal from the first-transition series with an ionic radius of 0.75 \AA (+3); it is classified as a rare-earth element and, for this reason, its chemical behaviour is pretty close to lanthanides. In aqueous solution, only the degree of oxidation (+3) is stable. However, the ionic form Sc^{3+} is stable in acidic conditions below pH 4. Between $\text{pH} > 4$ and $\text{pH} < 5.5$, Sc undergoes hydrolysis forming $[\text{Sc}(\text{OH})]^{2+}$ ($\log\beta^{\circ}_1 = -4.16 \pm 0.05$) followed by hydrolysis in the form $[\text{Sc}(\text{OH})_2]^+$ ($\log\beta^{\circ}_2 = -9.71 \pm 0.30$) at pH range 5.5-6.5. This latter further hydrolyses to $\text{Sc}(\text{OH})_3$ ($\log\beta^{\circ}_3 = -16.8 \pm 0.30$) at pH range 7-10. Above pH 10, very rare in nature, the amphoteric nature of $\text{Sc}(\text{OH})_3$ is revealed and the scandate $[\text{Sc}(\text{OH})_4]^-$ is formed ($\log\beta^{\circ}_4 = -26.7 \pm 0.3$) [58]. The acidic nature of its trivalent state, along with its short atomic radius and its strong electronic charge, brings the metallic ion to coordinate with electron-rich ligands: oxygen and nitrogen donors like hydroxyl, carboxylate, phosphate and sulphate groups. Scandium forms with these ligands complexes in which the metal has a coordination number that is greater than 6 and up to 9 although the octahedral geometry is the most common. In nature, scandium exists in the form of one stable isotope, ^{45}Sc .

Scandium is a “hard” acceptor, with a main preference for oxygen donor atoms. These oxygen donor atoms are contained into proteins, peptides, carbohydrates, nucleotides and other biologically active molecules. The most common ligands for scandium are carboxyl, phosphate and amino groups, but also carbonyl, hydroxyl and sulphate groups. These potential ligands may be involved in the coordination sphere of the metal ions. In this work, GAGs and their mimetics are proposed as ligands for Sc. In the past, a GAG ligand, such as hyaluronate, has shown to bind scandium ions [59]. Moreover, lipopolysaccharide and peptidoglycans forming the envelope of *Escherichia coli* have demonstrated to bind significant amounts of scandium and other metals from aqueous solutions [60]. Organic carboxylic, dicarboxylic and polycarboxylic acid have already proved to be possible ligand for scandium, as shown in Table 7.

Table 7. Stability constants of organic acids complexes with scandium. Adapted from Horovitz, 1999 [59].

Organic acid anion	Log β_1 at 20°C
Acetate	3.14 ± 0.16
Lactate	3.77 ± 0.11
Oxalate	8.12 ± 0.13
Iminodiacetate	9.80 ± 0.17
Sulphosalicylate	11.23 ± 0.08
Salicylate	14.20 ± 0.05
Tartrate	17.60 ± 0.13
Citrate	21.62 ± 0.17

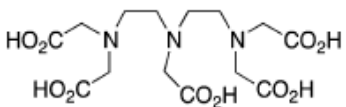
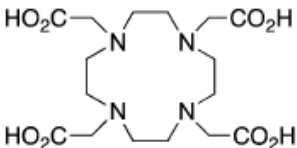
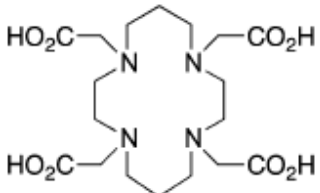
Those ligands have paved the way to the study of polyamino-polycarboxylic acids as ligands for scandium, whose have been highly investigated in the last two decades. Thermodynamic data for scandium(III) complexes with polyamino-polycarboxylic ligands, such as NOTA, EDTA or TETA have been determined using potentiometric titration and free ion selective radiotracer extraction (FISRE) method and the values of stability constants were found to be in the order TETA < NOTA < EDTA < DTPA < DOTA. DOTA derivatives with phosphinic/methylphosphonic acid pendant arms (i.e. DO₃A; DO₃AP^{PrA}, DO₃AP^{ABn}) were also investigated showing that the stability constants of the monophosphate analogues were somewhat lower than that of the Sc(DOTA) complex [61]. The thermodynamic stability constant of recently developed chelating agent AAZTA (1,4-bis (carboxymethyl)-6-[bis (carboxymethyl)]amino-6-[pentanoic-acid]perhydro-1,4-diazepine), Sc(AAZTA) was reported to be lower than that of Sc(DOTA) but the striking difference was observed on the radiochemical yield at 25°C indicating that AAZTA quickly incorporated ⁴⁴Sc [62]. Another chelator, H₄pypa (N₅O₄) has been shown to exhibit high complexation constant with Sc (log K = 27) as well as with In, Lu, Y, and La, as determined by potentiometric titration and UV spectrometer [63,64]. Further search on chelators enabling Sc chelation at room temperature led to the development of the small-cavity triaza-macrocyclic-based, picolinate-functionalized chelator H₃mpatcn. Spectroscopic and radiochemical studies established the [Sc(mpatcn)] complex as kinetically inert and appropriate for biological applications. As a proof-of-concept bifunctional conjugate targeting the prostate-specific membrane antigen (PSMA), picaga-DUPA, chelated ⁴⁴Sc to form ⁴⁴Sc(picaga)-DUPA at room temperature with an apparent molar activity of 60 MBq μmol⁻¹. H₃mpatcn and its bifunctional analogue picaga

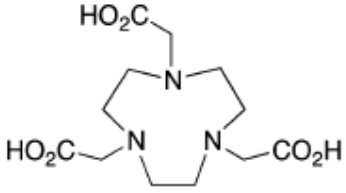
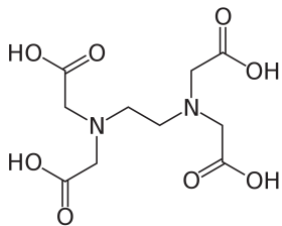
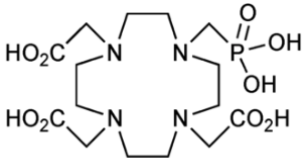
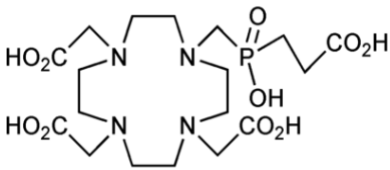
represent new additions to the chelator toolbox for the emerging $^{44/47}\text{Sc}$ theragnostic isotope pair [65].

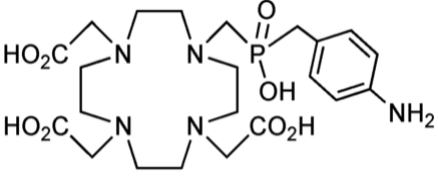
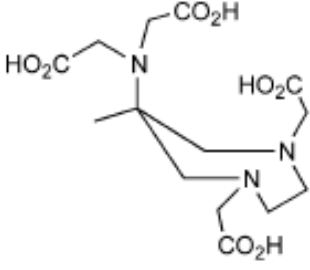
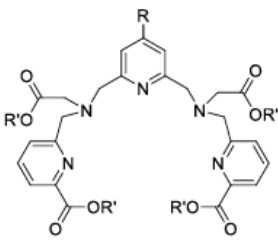
Scandium also displays favorable physical properties and chemistry for conjugation to mAb-chelate systems. Since it is chemically similar to ^{90}Y and close to ^{177}Lu , the same ligands developed for ^{90}Y or ^{177}Lu can be used for chelating ^{47}Sc .

Table 8 provides a summary of the main chelates that have been evaluated, with the corresponding formula and the measured value of the complexation constant with scandium. The table reports values reported in the original manuscripts, the uncertainties of which is not homogeneous across the data. For the sake of simplicity, the uncertainties (available only for selected studies) are not reported in this table.

Table 8. Known chelates for scandium.

Chelate	Log k_{MI}	Reference
 <p>DTPA, diethylenetriaminepentaacetic acid</p>	27.4	[66]
 <p>DOTA, 1,4,7,10-tetra-azacyclododecane-1,4,7,10-tetraacetic acid</p>	30.8	[67]
 <p>TETA, 1,4,8,11-tetra-azacyclotetradecane-1,4,8,11-tetacetic acid</p>	18.0	[67]
	18.5	[67]

Chelate	Log k_{MI}	Reference
 <p>NOTA, 1,4,7-triazacyclononane-1,4,7-triacetic acid</p>		
 <p>EDTA, 2,2',2'',2'''-(Ethane-1,2-diyl)dinitrilo)tetracetic acid</p>	21.0	[67]
 <p>H₅DO3AP, 1,4,7,10-tetraazacyclododecane-1,4,7,10-triacetic-10-methylphosphinic acid</p>	28.6	[61]
 <p>H₄DO3AP^{PrA}, 2-[[2-carboxyethyl]hydroxyphosphoryl]methyl]-1,4,7,10-tetraazacyclododecane-1,4,7-triacetic acid</p>	25.9	[61]
	26.4	[61]

Chelate	Log k_{MI}	Reference
 <p>H₄DO3AP^{ABn}, 1,4,7,10-tetraazacyclododecane-4,7,10-tri-acetic-1-{methyl[(4-aminophenyl)methyl]phosphinic acid}</p>		
 <p>AAZTA, 1,4-bis(hydroxycarbonyl methyl)-6-[bis(hydroxycarbonylmethyl)]amino-6-methylperhydro-1,4-diazepine</p>	27.7	[62]
 <p>H₄pypa</p>	27.1	[62]

B – Production of ⁴⁴Sc

Generally, the production of radionuclides is assessed through nuclear reactors as well as cyclotrons. Neutron activation occurs in a nuclear reactor: neutrons are used to bombard stable nuclides to form other radioactive nuclides. Cyclotrons, on the other side, are used to accelerate charged particles, such as α particles, deuterons (d), protons (p), and tritons (t), to high speed which are then employed to break nuclei. Generally, the reactor produced radionuclides have an excess of neutrons and they mainly decay by β^- particles emission. The cyclotron produced

radionuclides, instead, are typically neutron deficient and decay mainly by β^+ emission [68]. ^{44}Sc , as well as other radionuclides used in PET are produced in cyclotron facilities.

1. Method of production used in Arronax

In the previous chapter the interest towards $^{44\text{m}}\text{Sc}/^{44}\text{Sc}$ generator has been highlighted. Several different ways have been looked into to produce ^{44}Sc and $^{44\text{m}}\text{Sc}$. It is known that ^{44}Sc can be achieved via the decay of ^{44}Ti ; this system is already known as $^{44}\text{Ti}/^{44}\text{Sc}$ generator, but through this way no $^{44\text{m}}\text{Sc}$ can be obtained [69]. In this work, the chemical process used to obtain ^{44}Sc refers to the employment of irradiation target made of ^{44}Ca . In the past, many authors have developed processes to purify Sc from Ca using solvent extraction [70–72]. Recently, the use of an irradiation target made of 96.9% enriched $^{44}\text{CaCO}_3$, instead of natural calcium, has been developed to limit contaminants due to the production, such as ^{46}Sc , ^{47}Sc , and ^{48}Sc [73].

In the following protocol, the target is made of 500 mg of $^{44}\text{CaCO}_3$ that has been pressed under 10000 tons to form a disk with a diameter of 20 mm and a thickness of 0.6 mm. To maintain the integrity of the target during the irradiation, the pressed disk was fixed between two 75 μm Kapton foils. For the irradiation, a deuteron beam with energy of 16.9 MeV and intensity of 0.3 μA has been chosen. With this energy of deuterons, it is possible to obtain a higher $^{44\text{m}}\text{Sc}/^{44}\text{Sc}$ ratio, producing also a $^{44\text{m}}\text{Sc}$ with activity 3 times higher compared to protons. When deuterons pass through this foil, their energy decreases until reaching the target with an energy of 15 MeV and an output energy of 7.5 MeV. The time necessary to irradiate the target depends on the required activity [74].

After irradiation, the $^{44}\text{CaCO}_3$ target is dissolved in 10 mL of 4 mol/L HCl. The resulting solution is poured onto a column of DGA resin that has been previously conditioned. Resin conditioning consists in leaving an amount on resin (approximately 100mg) immersed in 10 mL of 4 mol/L HNO_3 acid, stirred for 24 hours. The resin is then transferred into a small plastic chromatographic column: the 4 mol/L HNO_3 is eluted and the resin is conditioned with the addition of, first, 20 mL of 0.1 mol/L HCl and, in a second time, 20 mL of 4 mol/L HCl. DGA resin has a high affinity for trivalent rare earths and actinides; Sc is retained by the resin whereas other metals, such as Ca, are rejected. A first elution of 20 mL of 4 mol/L HCl allow to recover ^{44}Ca , that can be recycled for further productions, as well as to remove the major impurities. A second elution of 20 mL of 1 mol/L HNO_3 is necessary to eliminate the most persistent metallic impurities, that are Al, Fe and Zn. After that, 5 mL of 6.10^{-2} mol/L HF are used to release $^{44\text{m}}\text{Sc}/^{44}\text{Sc}$ from the DGA resin and, then, evaporated to obtain a dry residue.

This dry residue is recovered in 400 μL of 0.1 mol/L HCl, obtaining the radionuclide in the form of $^{44\text{m}/44}\text{ScCl}_3$ [75].

After the extraction and purification processes, it is essential to determine the radiochemical and radionuclide purity. Radionuclide purity control can be assessed using a *gamma spectrometer*. For this work, a gamma spectrometer coupled to a germanium detector of AMETEK Technology has been used. Samples have been prepared in nitric acid 1%. When irradiation works perfectly, an activity of approximately 100 MBq may be reached from this production protocol.

The chemical purity control enables to quantify the amounts of metallic impurities resulting from the production and purification process. This kind of analysis can be performed by *inductively coupled plasma optical emission spectroscopy* (ICP-OES). For the quality control of ^{44}Sc , an ICP spectrometer iCAP 6000 of Thermo Scientific Technology has been used. For the ICP-OES, samples are prepared in nitric acid 1% and run through an auto sampler ASX-520 (Cetac). The calibration for Sc and other metals is normally done in the range 0-30ppb using a multi element standard solution (PlasmaCAL, SCP Science) containing several metals at the concentration of 10 $\mu\text{g}/\text{mL}$. This analytical technique can be used for the qualitative and quantitative detection of chemical elements. Being a kind of emission spectroscopy, ICP-OES utilizes the inductively coupled plasma to produce excited atoms and ions. In response to an exciting state, those atoms and ions emit electromagnetic radiation at wavelengths that are characteristic of certain elements. The intensity of the emissions from various wavelengths of light is proportional to the concentration of the elements within the sample. Al^{3+} , Fe^{3+} and Zn^{3+} are most accounting impurities in the final product of $^{44\text{m}/44}\text{Sc}$. Knowing the concentration of those impurities is crucial for the radiolabelling step, since they can compete with Sc^{3+} in the complexation with the chelator (that could have normally a high affinity for trivalent metals). The most important thing when producing radionuclides for medical use is to obtain a final product having a high specific activity, high radionuclide and chemical purity. It allows obtaining a great amount of radionuclide compared with non-radioactive isotopes that will allow to realize a good quality PET imaging. Moreover, those requirements will be fundamental once the radiolabelling process will be assessed. Quantifying the concentration of medical radionuclide, as well as the concentration of all the possible impurities, will allow to select the lowest amount of ligand necessary to complex the radiometal of interest.

2. Radiolabelling

Labeling protocols should allow high labeling yields, radiochemical purity and specific activity. Nevertheless, the reported data are often difficult to compare. To overcome this problem, the recommendations on consensus nomenclature rules for radiopharmaceutical chemistry should be followed. According to SI convention, the term ‘specific’ refers to a physical property as a function of the mass of the material in question. Since in chemistry the amount of material (mass) is most often denoted in moles, related chemical properties are indicated in ‘molar’ units; e.g. molar volume. Because of this possible source of confusion, the following terms are to be used correctly

- Specific activity: the measured activity per gram of compound; measured in Bq/g or GBq/mg etc.; symbol: As.
- Molar activity: the measured radioactivity per mole of compound; measured in Bq/mol or GBq/ μ mol, etc.; symbol: Am.

Besides in the occasional situation, where the molecular weight cannot be determined, or in the context of radionuclide development (such as the activity of irradiated target material), the term ‘specific activity’ is to be used instead of the term ‘molar activity’.

- Activity yield (AY). It is defined as the amount of a radioactive product expressed in Bq, which is obtained from a starting amount of activity, e.g. primary cyclotron product, secondary synthon or labelled intermediate etc., and is not corrected for decay.
- Radiochemical yield (RCY) is the amount of radioactivity in the product expressed as the percent of related starting radio-activity used in the corresponding synthesis (step). The quantity of both must be decay corrected to the same point in time before the calculation is made.

Labelling efficiency of ligands is usually tested at different solution pH’s, temperatures and ligand concentrations (or more correctly, at different radiometal-to-ligand molar ratios) and monitored as a function of time in order to optimize the radiolabeling. Herein, we discuss the development of labelling methods that were developed for radio scandium.

Most of the published works dealt with ^{44}Sc . These studies have shown the importance of a high chemical purity of the final ^{44}Sc fraction. Given that the presence of other metals may interact with the DOTA-chelator (or any other chelator) it can compromise the radiolabeling yield. The concentration of common environmental contaminants (Al(III), Cu(II), Pb(II), Zn(II), Fe(III)) in ^{44}Sc is frequent. The most problematic is Fe^{3+} , for which the stability with the DOTA ligand is greater than that for Sc^{3+} . By contrast, the influence of divalent metal

cations (considered as contaminants) is negligible due to the much lower stability of DOTA complexes. Although DOTA forms very stable complexes, the slow formation kinetics at room temperature, though it can be increased by heating, remains an important obstacle for efficient labelling of heat-sensitive molecules such as antibodies. In contrast to DOTA, from an old study, monoclonal antibodies conjugated with DTPA have demonstrated to be efficiently radiolabeled with ^{46}Sc with exceed the temperature of 37°C [76]. Recently, in prostatic cancer, DOTA-DUPA and picaga-DUPA conjugates were subjected to radiolabeling with ^{44}Sc , testing both time and temperature dependence. $^{44}\text{Sc}(\text{picaga})\text{-DUPA}$ produced high radiochemical yields (83%), against the 96% at 80°C , while ^{44}Sc with DOTA-DUPA reached the 87% only heating at 95°C [65].

On the other side of the complexation, the one relating the ligand, few information can be found on the radiolabeling of GAGs. One example of GAG radiolabeling displayed the possibility to add covalently [^3H]acetylated residues to the N-unsubstituted hexosamine residues of heparin and heparan sulphate without no major rearrangement of the polysaccharide molecules [77].

Another example sees the use of fluorescein to create dextran-fluorescent intermediate that can be radiolabeled with ^3H or ^{131}I [78]. Unfortunately, the scientific literature on the radiolabeling of GAG without using any additional linker is very poor. In fact, more recent studies [79] have demonstrated the radiolabeling of chitosan and dextran by covalently attaching a BFC to the polysaccharidic vector. In my work, there will be no BFC attached to EPS. The aim of this choice resides on the possibility to exploit the surface of the exopolysaccharide reach in oxygen donor atoms to complex scandium.

References

- [1] Santo, K.P.; Vishnyakov, A.; Kumar, R.; Neimark, A.V. Elucidating the Effects of Metal Complexation on Morphological and Rheological Properties of Polymer Solutions by a Dissipative Particle Dynamics Model. *Macromolecules* **2018**, *51*, 4987–5000, doi:10.1021/acs.macromol.8b00493.
- [2]. Lima, M.; Rudd, T.; Yates, E. New Applications of Heparin and Other Glycosaminoglycans. *Molecules* **2017**, *22*, 749, doi:10.3390/molecules22050749.
- [3]. Capila, I.; Linhardt, R.J. Heparin-Protein interactions. *Angew. Chem. Int. Ed.* **2002**, *41*, 390-412.
- [4]. Wang, H.M.; Loganathan, D.; Linhardt, R.J. Determination of the pKa of glucuronic acid and the carboxy groups of heparin by ¹³C-nuclear-magnetic-resonance spectroscopy. *Biochem. J.* **1991**, *278*, 689–695, doi:10.1042/bj2780689.
- [5]. Liu, H.; Zhang, Z.; Linhardt, R.J. Lessons learned from the contamination of heparin. *Nat. Prod. Rep.* **2009**, *26*, 313, doi:10.1039/b819896a.
- [6]. Ruiz Velasco, C.; Baud'huin, M.; Siquin, C.; Maillason, M.; Heymann, D.; Collic-Jouault, S.; Padrines, M. Effects of a sulfated exopolysaccharide produced by *Alteromonas infernus* on bone biology. *Glycobiology* **2011**, *21*, 781–795, doi:10.1093/glycob/cwr002.
- [7]. Heymann, D.; Ruiz-Velasco, C.; Chesneau, J.; Ratiskol, J.; Siquin, C.; Collic-Jouault, S. Anti-Metastatic Properties of a Marine Bacterial Exopolysaccharide-Based Derivative Designed to Mimic Glycosaminoglycans. *Molecules* **2016**, *21*, 309, doi:10.3390/molecules21030309.
- [8]. Pandey, A. Overview of bioreactor or fermenters. *Microbiol. Notes* 2020.
- [9]. Chopin, N.; Siquin, C.; Ratiskol, J.; Zykwincka, A.; Weiss, P.; Cérantola, S.; Le Bideau, J.; Collic-Jouault, S. A Direct Sulfation Process of a Marine Polysaccharide in Ionic Liquid. *BioMed Res. Int.* **2015**, *2015*, 1–9, doi:10.1155/2015/508656.
- [10]. Roger, O.; Kervarec, N.; Ratiskol, J.; Collic-Jouault, S.; Chevolut, L. Structural studies of the main exopolysaccharide produced by the deep-sea bacterium *Alteromonas infernus*. *Carbohydr. Res.* **2004**, *339*, 2371–2380, doi:10.1016/j.carres.2004.07.021.
- [11]. Raguénès, G.H.C.; Peres, A.; Ruimy, R.; Pignet, P.; Christen, R.; Loaec, M.; Rougeaux, H.; Barbier, G.; Guezennec, J.G. *Alteromonas infernus* sp. nov., a new polysaccharide-producing bacterium isolated from a deep-sea hydrothermal vent. *J. Appl. Microbiol.* **1997**, *82*, 422–430, doi:10.1046/j.1365-2672.1997.00125.x.
- [12]. Guezennec, J.; Pignet, P.; Lijour, Y.; Gentric, E.; Ratiskol, J.; Collic-Jouault, S. Sulfation and depolymerization of a bacterial exopolysaccharide of hydrothermal origin. *Carbohydr. Polym.* **1998**, *37*, 19–24, doi:10.1016/S0144-8617(98)00006-X.
- [13]. Petit, A.-C.; Noiret, N.; Siquin, C.; Ratiskol, J.; Guézennec, J.; Collic-Jouault, S. Free-radical depolymerization with metallic catalysts of an exopolysaccharide produced by a bacterium isolated from a deep-sea hydrothermal vent polychaete annelid. *Carbohydr. Polym.* **2006**, *64*, 597–602, doi:10.1016/j.carbpol.2005.11.016.
- [14]. Al-Horani, R.A.; Desai, U.R. Chemical sulfation of small molecules-advances and challenges. *Tetrahedron* **2010**, *66*, 2907-2918.
- [15]. Peat, S.; Bowker, D.M.; Turvey, J.R. Sulphates of monosaccharides and derivatives. Part VI: D-Glucose 2-sulphate, DGalactose 2- and 3-Sulphate, and D-Galactose 2,3-Disulphate. *Carbohydrate Research* **1968**, *7*, 225-231.
- [16]. Jouault, S.C.; Chevolut, L.; Helley, D.; Ratiskol, J.; Bros, A.; Siquin, C.; Roger, O.; Fischer, A.-M. Characterization, chemical modifications and in vitro anticoagulant properties of an exopolysaccharide produced by *Alteromonas infernus*. *Biochim. Biophys. Acta* **11**.

- [17]. Konno, M.; Nagao, D. Monodisperse Polymer Particles: MONODISPERSE POLYMER PARTICLES. In *Encyclopedia of Polymer Science and Technology*; John Wiley & Sons, Inc., Ed.; John Wiley & Sons, Inc.: Hoboken, NJ, USA, 2014; pp. 1–26 ISBN 978-0-471-44026-0.
- [18]. Hermeling, S. Structural aspects of the immunogenicity of therapeutic proteins. Utrecht University, 2005.
- [19]. Podzimek, S. 1- Polymers. In *Light Scattering, Size Exclusion Chromatography and Asymmetric Flow Field Flow Fractionation*; Wiley, 2011.
- [20]. Podzimek, S. Truths and myths about the determination of molar mass distribution of synthetic and natural polymers by size exclusion chromatography. *J. Appl. Polym. Sci.* **2014**, *131*, n/a-n/a, doi:10.1002/app.40111.
- [21]. Striegel, A.; Yau, W.; Kirkland, J.; Bly, D. *Modern size- exclusion liquid chromatography: practice of gel permeation and gel filtration chromatography, 2nd edition.*; 2009;
- [22]. Podzimek, S. 2- Light Scattering. In *Light Scattering, Size exclusion Chromatography and Asymmetric Flow Field Flow Fractionation*; Wiley, 2011.
- [23]. Podzimek, S. 3- Size Exclusion Chromatography. In *Light Scattering, Size Exclusion Chromatography and Asymmetric Flow Field Flow Fractionation*; Wiley, 2011.
- [24]. Yukioka, S.; Kitadume, T.; Chatterjee, S.; Ning, G.; Ooya, T.; Yusa, S. Amphiphilic Block Copolymers Bearing Hydrophobic γ -Tocopherol Groups with Labile Acetal Bond. *Polymers* **2019**, *12*, 36, doi:10.3390/polym12010036.
- [25]. Giddings, J.C. Field-flow fractionation of macromolecules. *J. Chromatogr. A* **1989**, *470*, 327–335, doi:10.1016/S0021-9673(01)83561-5.
- [26]. Podzimek, S. 5- Asymmetric Flow Field Flow Fractionation. In *Light Scattering, Size Exclusion Chromatography and Asymmetric Flow Field Flow Fractionation*; Wiley, 2011.
- [27]. Podzimek, S.; Johann, C. Comparison of Polymer Separation by Size Exclusion Chromatography and Asymmetric Flow Field Flow Fractionation.
- [28]. Gigault, J.; Pettibone, J.M.; Schmitt, C.; Hackley, V.A. Rational strategy for characterization of nanoscale particles by asymmetric-flow field flow fractionation: A tutorial. *Anal. Chim. Acta* **2014**, *809*, 9–24, doi:10.1016/j.aca.2013.11.021.
- [29]. Zhang, X.; Li, Y.; Shen, S.; Lee, S.; Dou, H. Field-flow fractionation: a gentle separation and characterization technique in biomedicine. *Trends in Analytical Chemistry* **2018**, *108*, 231–238.
- [30]. Podzimek, S. 6- Characterization of Branched Polymers. In *Light Scattering, Size exclusion Chromatography and Asymmetric Flow Field Flow Fractionation*; Wiley.
- [31]. Berne, B.J.; Pecora, R. *Dynamic Light Scattering*; Wiley, New York, 2nd edition, 2000.
- [32]. Du, Q.; Schimpf, M.E. Correction for particle-wall interactions in the separation of colloids by flow field-flow fractionation. *Anal. Chem.* **2002**, *74*, 2478-2485.
- [33]. Barth, H.G.; Carlin, F.J. A Review of Polymer Shear Degradation in Size-Exclusion Chromatography. *J. Liq. Chromatogr.* **1984**, *7*, 1717–1738, doi:10.1080/01483918408068832.
- [34]. Hiemenz, P.; Lodge, T. *Polymer Chemistry*; CRC Press: Boca Raton, 2007;
- [35]. Taylor, M.; Tomlins, P.; Sahota, T. Thermoresponsive Gels. *Gels* **2017**, *3*, 4, doi:10.3390/gels3010004.
- [36]. Katchalsky, A. Solutions of polyelectrolytes and mechanochemical systems. *J. Polym. Sci.* **1951**, *7*, 393–412, doi:10.1002/pol.1951.120070403.
- [37]. Chung, M.C.M.; Ellerton, N.F. Viscosity at low shear and circular dichroism studies of heparin. *Biopolymers* **1976**, *15*, 1409–1423, doi:10.1002/bip.1976.360150713.
- [38]. Lapsin, R.; *Rheology of industrial polysaccharides: theory and applications.* Springer US. 1995.

- [39]. Maitra, J.; Shukla, V.K. Cross-linking in hydrogels – A review. *Americal Journal of Polymer Science* **2014**, *4*, 25-31.
- [40]. Beer, M.U.; Wood, P.J.; Weisz, J. A simple and rapid method for evaluation of Mark–Houwink–Sakurada constants of linear random coil polysaccharides using molecular weight and intrinsic viscosity determined by high performance size exclusion chromatography: application to guar galactomannan. *Carbohydr. Polym.* **1999**, *39*, 377–380, doi:10.1016/S0144-8617(99)00017-X.
- [41]. Sparks, D.J.; Romero-González, M.E.; El-Taboni, E.; Freeman, C.L.; Hall, S.A.; Kakonyi, G.; Swanson, L.; Banwart, S.A.; Harding, J.H. Adsorption of poly acrylic acid onto the surface of calcite: an experimental and simulation study. *Phys. Chem. Chem. Phys.* **2015**, *17*, 27357–27365, doi:10.1039/C5CP00945F.
- [42]. Swift, T.; Swanson, L.; Geoghegan, M.; Rimmer, S. The pH-responsive behaviour of poly(acrylic acid) in aqueous solution is dependent on molar mass. *Soft Matter* **2016**, *12*, 2542–2549, doi:10.1039/C5SM02693H.
- [43]. Rudin, A.; Choi, P. *Practical aspects of molecular weight measurements*; 2013;
- [44]. Khor, S.Y.; Hu, J.; McLeod, V.M.; Quinn, J.F.; Williamson, M.; Porter, C.J.H.; Whittaker, M.R.; Kaminskis, L.M.; Davis, T.P. Molecular weight (hydrodynamic volume) dictates the systemic pharmacokinetics and tumour disposition of PolyPEG star polymers. *Nanomedicine Nanotechnol. Biol. Med.* **2015**, *11*, 2099–2108, doi:10.1016/j.nano.2015.08.001.
- [45]. Jang, J.; Hia, H.C.; Ike, M.; Inoue, C.; Fujita, M. Acid hydrolysis and quantitative determination of total hexosamines of an exopolysaccharide produced by *Citrobacter* sp . **2005**, 13–18.
- [46]. Feofanova, M.A.; Frantseva, Y. V.; Lapshin, S. V. Complexation in the Heparin-Metal Ion System. *Russ. J. Coord. Chem.* **2012**, *38*, 387–392.
- [47]. Wang, H.; Loganathan, D.; Linhardt, R.J. Determination of the pKa of glucuronic acid and the carboxy groups of heparin by ¹³C-nuclear-magnetic-resonance spectroscopy. **1991**, *278*, 689–695.
- [48]. Karpukhin, L.E.; Feofanova, M.A.; Nikolaeva, L.S.; Mamontov, M.N. Complexation of Magnesium and Calcium Ions with Heparin. *Russ. J. Inorg. Chem.* **2006**, *51*, 908–914.
- [49]. Jang, J.-H.; Hia, H.C.; Ike, M.; Inoue, C.; Fujita, M.; Yoshida, T. Acid hydrolysis and quantitative determination of total hexosamines of an exopolysaccharide produced by *Citrobacter* sp. *Biotechnol. Lett.* **2005**, *27*, 13–18, doi:10.1007/s10529-004-6305-y.
- [50]. Kohn, R.; Kovác, P. Dissociation constants of D-galacturonic and D-glucuronic acid and their O-methyl derivatives. **1978**, *32*.
- [51]. van Boeckel, C.A.A.; van Aelst, S.F.; Wagenaars, G.N.; Mellema, J.-R.; Paulsen, H.; Peters, T.; Pollex, A.; Sinnwell, V. Conformational analysis of synthetic heparin like oligosaccharides containing α-L-idopyranosyluronic acid. *Recl. Trav. Chim. Pays-Bas* **1987**, *106*, 19–29.
- [52]. Rabenstein, D.L.; Robert, J.M.; Peng, J. Multinuclear magnetic resonance studies of the interaction of inorganic cations with heparin. *Carbohydr. Res.* **1995**, *278*, 239–256.
- [53]. Braswell, E. Heparin: Molecular weight and degradation studies. *Biochim. Biophys. Acta* **1968**, *158*, 103–116.
- [54]. Moissev, Y.V.; Khalturinskii, N.A.; Zaikov, G.E. The mechanism of the acid-catalysed hydrolysis of polysaccharides. *Carbohydr. Res.* **1976**, *51*, 39–54, doi:10.1016/S0008-6215(00)84034-3.
- [55]. Biermann, C.J. Hydrolysis and other Cleavages of Glycosidic Linkages in Polysaccharides. In *Advances in Carbohydrate Chemistry and Biochemistry*; Elsevier, 1988; Vol. 46, pp. 251–271 ISBN 978-0-12-007246-0.

- [56]. Helbert, J.R.; Marini, M.A. Structural Studies of Heparin . I . Hydrolytic Cleavage of Sulfates *. **1963**, 2, 1101–1106.
- [57]. Bhavanandan, V.P.; Breindel, D.; Davidson, E.A. Release of O-sulfate groups under mild acid hydrolysis conditions used for estimation of N-sulfate content. *Biochim. Biophys. Acta BBA - Gen. Subj.* **1977**, 498, 250–254, doi:10.1016/0304-4165(77)90105-2.
- [58]. Brown, P.L.; Ekberg, C. Scandium, Yttrium and the Lanthanide Metals. In *Hydrolysis of Metal Ions*; Wiley-VCH Verlag GmbH & Co. KGaA: Weinheim, Germany, 2016; pp. 225–324 ISBN 978-3-527-65618-9.
- [59]. Horovitz, C.T. Interactions of Scandium and Yttrium with Molecules of Biological Interest. In *Biochemistry of Scandium and Yttrium, Part 1: Physical and Chemical Fundamentals*; Springer US: Boston, MA, 1999; pp. 235–308 ISBN 978-1-4613-6936-3.
- [60]. Beveridge, T.J.; Koval, S.F. Binding of metals to cell envelopes of Escherichia coli K-12. *Appl. Environ. Microbiol.* **1981**, 42, 325–335, doi:10.1128/AEM.42.2.325-335.1981.
- [61]. Kerdjoudj, R.; Pniok, M.; Alliot, C.; Kubíček, V.; Havlíčková, J.; Rösch, F.; Hermann, P.; Huclier-Markai, S. Scandium-complexes of monophosphorus acid DOTA analogues: a thermodynamic and radiolabelling study with ^{44}Sc from cyclotron and from a $^{44}\text{Ti}/^{44}\text{Sc}$ generator. *Dalton Trans.* **2016**, 45, 1398–1409, doi:10.1039/C5DT04084A.
- [62]. Nagy, G.; Szikra, D.; Trencsényi, G.; Fekete, A.; Garai, I.; Giani, A.M.; Negri, R.; Masciocchi, N.; Maiocchi, A.; Uggeri, F.; et al. AAZTA: An Ideal Chelating Agent for the Development of ^{44}Sc PET Imaging Agents. *Angew. Chem. Int. Ed.* **2017**, 56, 2118–2122, doi:10.1002/anie.201611207.
- [63]. Li, L. [nat/ ^{44}Sc (pypa)]–: Thermodynamic Stability, Radiolabeling, and Biodistribution of a Prostate-Specific-Membrane-Antigen-Targeting Conjugate. *Inorg. Chem.* 11.
- [64]. Li, L.; de Guadalupe Jaraquemada-Pelaez, M.; Kuo, H.-T.; Merkens, H.; Choudhary, N.; Gitschtaler, K.; Jermilova, U.; Colpo, N.; Uribe-Munoz, C.; Radchenko, V.; et al. Functionally Versatile and Highly Stable Chelator for ^{111}In and ^{177}Lu : Proof-of-Principle Prostate-Specific Membrane Antigen Targeting. *Bioconjug Chem.* **2019**, 30, 1539–1553.
- [65]. Vaughn, B.A.; Ahn, S.H.; Aluicio-Sarduy, E.; Devaraj, J.; Olson, A.P.; Engle, J.; Boros, E. Chelation with a twist: a bifunctional chelator to enable room temperature radiolabeling and targeted PET imaging with scandium-44. *Chem. Sci.* **2020**, 11, 333–342, doi:10.1039/C9SC04655K.
- [66]. Pniok, M.; Kubíček, V.; Havlíčková, J.; Kotek, J.; Sabatie-Gogová, A.; Plutnar, J.; Huclier-Markai, S.; Hermann, P. Thermodynamic and Kinetic Study of Scandium(III) Complexes of DTPA and DOTA: A Step Toward Scandium Radiopharmaceuticals. *Chem. - Eur. J.* **2014**, 20, 7944–7955, doi:10.1002/chem.201402041.
- [67]. Huclier-Markai, S.; Sabatie, A.; Ribet, S.; Kubíček, V.; Paris, M.; Vidaud, C.; Hermann, P.; Cutler, C.S. Chemical and biological evaluation of scandium(III)-polyaminopolycarboxylate complexes as potential PET agents and radiopharmaceuticals. *Radiochim. Acta* **2011**, 99, 653–662, doi:10.1524/ract.2011.1869.
- [68]. Currie, G.; Wheat, J.; Davidson, R.; Kiat, H. Radionuclide production. *Radiographer* **2011**, 58, 46–52, doi:10.1002/j.2051-3909.2011.tb00155.x.
- [69]. Filosofov, D.V.; Loktionova, N.S.; Rösch, F. A $^{44}\text{Ti}/^{44}\text{Sc}$ radionuclide generator for potential application of ^{44}Sc -based PET-radiopharmaceuticals. *Radiochim. Acta* **2010**, 98, doi:10.1524/ract.2010.1701.
- [70]. Radhakrishnan, K.P.; Owens, T.C. Separation of Scandium and Calcium by Liquid-liquid Extraction Using Tri-n-butyl Phosphate as Solvent. 5.
- [71]. Hill, M. Rapid Radiochemical Separations of Strontium-90-Yttrium-90 and Calcium-45-Scandium-46 on a Cation Exchange Resin. **1966**, 38, 4.

- [72]. Duval, J.E.; Kurbatov, M.H. Separation of Carrier-free Scandium from a Calcium Target. *J. Am. Chem. Soc.* **1953**, *75*, 2246–2248, doi:10.1021/ja01105a065.
- [73]. Alliot, C.; Kerdjoudj, R.; Michel, N.; Haddad, F.; Huclier-Markai, S. Cyclotron production of high purity $^{44m,44}\text{Sc}$ with deuterons from $^{44}\text{CaCO}_3$ targets. *Nucl. Med. Biol.* **2015**, *42*, 524–529, doi:10.1016/j.nucmedbio.2015.03.002.
- [74]. Alliot, C.; Kerdjoudj, R.; Mokili, M.; Michel, N.; Haddad, F.; Huclier-Markai, S.; Barbet, J. Processing of $^{44m}/^{44}\text{Sc}$ generator for potential medical applications: production and chemistry aspects. *Appl. Rad. Isot.* **2013**.
- [75]. Kerdjoudj, R. Complexes de Scandium: étude physico-chimique et évaluation des stabilités in vitro et in vivo pour des applications en médecine nucléaire, University of Nantes Angers Le Mans, 2014.
- [76]. Anderson, W.T.; Strand, M. Stability, Targeting, and Biodistribution of Scandium-46- and Gallium-67- labeled Monoclonal Antibody in Erythroleukemic Mice. **1985**, *45*, 6.
- [77]. Hook, M.; Riesenfiels, J.; Lindahl, U. N-[^3H]Acetyl-Labeling, a convenient method for Radiolabeling of Glicosaminoglycans. *Analytical Biochemistry* **1982**, *119*, 236–245.
- [78]. Prigent-Richard, S.; Cansell, M.; Vassy, J.; Viron, A.; Puvion, E.; Jozefonvicz, J.; Letourneur, D. Fluorescent and radiolabeling of polysaccharides: Binding and internalization experiments on vascular cells. 7.
- [79]. Peltek, O.O.; Muslimov, A.R.; Zyuzin, M.V.; Timin, A.S. Current outlook on radionuclide delivery systems: from design consideration to translation into clinics. *J. Nanobiotechnology* **2019**, *17*, 90, doi:10.1186/s12951-019-0524-9.

Chapter 3

**Evaluation of the complexation of
exopolysaccharides with scandium**

I. Introduction

Previous published examples demonstrated that GAGs could be considered as promising candidates to serve as vectors, especially in nuclear medicine, either for molecular imaging or for targeted therapy. The anti-metastatic properties of GAGs could act in synergy with the diagnostic and therapeutic features of radionuclides, that could be combined to these vectors. Because of the chemical structure of GAGs with carboxylic and sulphate groups, they can serve as chelating agents for radiometals. Among different radionuclides, the theranostic pair of Scandium isotopes $^{44}\text{Sc}/^{47}\text{Sc}$ has been considered for this work; and the goal is to evaluate the feasibility of coupling GAGs with scandium.

The scandium-exopolysaccharide complex must be thermodynamically stable and kinetically inert, and those systems will be compared to the reference polysaccharide, i.e. heparin.

The polysaccharides chemistry, morphology, and polydispersity play an important role on their biodistribution, and when coupled to radionuclides, it could lead to irradiation of healthy tissues. Moreover, identical polymers, but of diverse sizes, could interact drastically differently with cells. In addition to this, the polysaccharides of interest are produced in bioreactors, thus it is important to monitor the reproducibility of their rheological properties from one production to the other. One aspect of this work, presented in this chapter, has dealt with setting suitable and robust tools in order to characterize these macromolecules.

Among parameters that are important to characterize, the molecular masses is crucial. In this work, Asymmetrical Flow Field-Flow Fractionation (A4F) coupled to Differential Refractive Index (dRI), and Multi Angle Light Scattering (MALS) detectors were used. Usually, SEC-MALS is used for the determination of M_w of macromolecules [1] but A4F has been recognized since long to be a suitable technique for the characterization of molar mass distribution of synthetic and natural polymers [2-4] as well as for nanoparticle [5], that are considered as drug delivery systems in antitumor and anti-metastasis therapy approaches [6].

The polymer conformation could influence the complexation [29 from marine drugs]. The viscosimetric behavior of polyelectrolytes could help better understanding the relationship between the electrostatic field induced by the ionization of functional groups and the random rearrangement of the polymeric chain. The change in conformation was monitored through the polymer's intrinsic viscosity in solution, by varying the ionic strength of solvent for both EPS-DR and heparin.

The FISRE method has been used for the determination of thermodynamic stability of metallo-radiopharmaceuticals containing Y^{3+} [7], or for Sc^{3+} complexes with several chelating ligands,

i.e, EDTA, DTPA, NOTA, and DOTA [8] instead. Other techniques, such as potentiometric titrations and CE-ICP-MS were considered being less suitable to analyze Sc-EPS complexes. Indeed, EPS are very sensitive to pH edges leading to hydrolysis, leading to avoid titration for determining the stability constants. Capillary Electrophoresis (CE) could be another technique but since these polymers are highly charged, the technique won't be a useful speciation tool in this case.

All the work dealing with EPS rheological tools and the interactions with Sc has been proposed as an article in *Molecules*.

Additional work by the means of SEC-MALS, was performed at Ifremer on EPS themselves and in order to monitor potential hydrolysis at acidic pH values (i.e. pH =4). Just to note, a hydrolysis of EPS ranging from 36% to 67 % was determined, confirming thus the choice of FISRE for studying Sc-EPS interactions. Fixing the samples pH to 6 will prevent mild acidic as well as alkaline hydrolysis of EPS. For sake of clarity and for consistency, these data aren't presented in the *Molecules* paper neither in this chapter.

References

- [1] Tarazona, M.P.; Saiz, E. Combination of SEC/MALS Experimental Procedures and Theoretical Analysis for Studying the Solution Properties of Macromolecules. *J Biochem Biophys Methods* **2003**, *56*, 95-116.
- [2] Viebke, C.; Williams, P.A. Determination of Molecular Mass Distribution of K-Carrageenan and Xanthan Using Asymmetrical FLOW Field-FLOW Fractionation. *Food Hydrocoll.* **2000**, *14*, 265-270.
- [3] Wittgren, B.; Wahlund, K.-G. Fast Molecular Mass and Size Characterization of Polysaccharides Using Asymmetrical Flow Field-Flow Fractionation-Multiangle Light Scattering. *J. Chromatogr. A* **1997**, *760*, 205–218.
- [4] Lou, J.; Myers, M.N.; Calvin Giddings, J. Separation of Polysaccharides by Thermal Field-Flow Fractionation. *J. Liq. Chromatogr.* **1994**, *17*, 3239–3260.
- [5] Gigault, J.; Pettibone, J.M.; Schmitt, C.; Hackley, V.A. Rational Strategy for Characterization of Nanoscale Particles by Asymmetric-Flow Field Flow Fractionation: A Tutorial. *Anal. Chim. Acta* **2014**, *809*, 9–24.
- [6] Sun, H.; Cao, D.; Liu, Y.; Wang, H.; Ke, X.; Ci, T. Low Molecular Weight Heparin Based Reduction Sensitive Nanoparticles for Antitumor and Anti-Metastasis of Orthopic Breast Cancer. *Biomater. Sci.* **2018**, *6*, 2172–2188.
- [7] Jurkin, D.; Wierczinski, B. Analysis of the Kinetic Stability of Yttrium Chelates by Free-Ion Selective Radiotracer Extraction (FISRE). *J. Radioanal. Nucl. Chem.* **2008**, *277*, 91–96, doi:10.1007/s10967-008-0714-7.
- [8] Pniok, M.; Kubíček, V.; Havlíčková, J.; Kotek, J.; Sabatie-Gogová, A.; Plutnar, J.; Huclier-Markai, S.; Hermann, P. Thermodynamic and Kinetic Study of Scandium(III) Complexes of DTPA and DOTA: A Step Toward Scandium Radiopharmaceuticals. *Chem. - Eur. J.* **2014**, *20*, 7944–7955.

II. Marine Exopolysaccharide Complexed with Scandium Aimed as Theranostic Agents.

Article published in *Molecules* (revised version, IF = 3.267).

Marine Exopolysaccharide Complexed with Scandium Aimed as Theranostic Agents

Mattia Mazza ^{1,2}, Cyrille Alliot ^{1,3}, Corinne Sinquin ⁴, Sylvia Collic-Jouault ⁴, Pascal E. Reiller ⁵ and Sandrine Huclier-Markai ^{1,2,*}

¹ GIP ARRONAX, 1 rue Aronnax, CS 10112, F-44817 Nantes, CEDEX 3, France; mattia.mazza@subatech.in2p3.fr (M.M.); alliot@arronax-nantes.fr (C.A.)

² SUBATECH, 4 rue Alfred Kastler, BP 20722, 44307 Nantes, CEDEX 3, France

³ INSERM U892-8 quai Moncoussu, BP 70721, F-44007 Nantes, CEDEX 1, France

⁴ IFREMER, Institut Français de Recherche pour l'exploitation de la mer, rue de l'Île d'Yeu, BP 21105, F-44311 Nantes, CEDEX 3, France; corinne.sinquin@ifremer.fr (C.S.); Sylvia.Collic.Jouault@ifremer.fr (S.C.-J.)

⁵ DES—Service d'Etudes Analytiques et de Réactivité des Surfaces (SEARS), Université Paris-Saclay, CEA, F-91191, Gif sur Yvette, CEDEX, France; Pascal.REILLER@cea.fr

* Correspondence: sandrine.huclier@subatech.in2p3.fr Tel.: +33-(0)51-85-85-37 or +33-(0)28-21-25-23

Abstract: (1) Background: Exopolysaccharide (EPS) derivatives, produced by *Alteromonas infernus* bacterium, showed anti-metastatic properties. They may represent a new class of ligands to be combined with theranostic radionuclides, such as ⁴⁷Sc/⁴⁴Sc. The goal of this work was to investigate the feasibility of such coupling. (2) Methods: EPSs, as well as heparin used as a drug reference, were characterized in terms of molar mass and dispersity using Asymmetrical Flow Field-Flow Fractionation coupled to Multi-Angle Light Scattering (AF4-MALS). The intrinsic viscosity of EPSs at different ionic strengths were measured in order to establish the conformation. To determine the stability constants of Sc with EPS and heparin, a Free-ion selective radiotracer extraction (FISRE) method has been used. (3) Results: AF4-MALS showed that radical depolymerization produces monodisperse EPSs, suitable for therapeutic use. EPS conformation exhibited a lower hydrodynamic volume for the highest ionic strengths. The resulting random-coiled conformation could affect the complexation with metal for high concentration. The LogK of Sc-EPS complexes have been determined and showing that they are comparable to the Sc-Hep. (4) Conclusions: EPSs are very promising to be coupled with the theranostic pair of scandium for Nuclear Medicine.

Keywords: exopolysaccharides; scandium; theranostic; characterization; complexation

Citation: Mazza, M.; Alliot, C.; Sinquin, C.; Collic-Jouault, S.; Reiller, P.E. Marine Exopolysaccharide Complexed with Scandium Aimed as Theranostic Agents. *Molecules* **2021**, *26*, 1143. <https://doi.org/10.3390/molecules26041143>

Academic Editor: Helen Osborn

Received: 25 January 2021

Accepted: 18 February 2021

Published: 20 February 2021

Publisher's Note: MDPI stays neutral with regard to jurisdictional claims in published maps and institutional affiliations.



Copyright: © 2021 by the authors. Licensee MDPI, Basel, Switzerland. This article is an open access article distributed under the terms and conditions of the Creative Commons Attribution (CC BY) license (<http://creativecommons.org/licenses/by/4.0/>).

1. Introduction

Osteosarcoma is the most common primary malignant bone tumor in children and young adults. It is a very aggressive type of cancer with a low prognosis, but molecular mechanisms of metastases have been identified for designing new therapeutic strategies in the frame of personalized medicine. Among the biomarkers considered, glycoaminoglycans (GAGs) are a hallmark related to cancer growth and spread. GAGs could be employed in new drug delivery systems to deliver active compounds for therapeutic in oncology [1]. GAGs such as unfractionated heparin, and its low-molecular weight (LMW) derivatives, are generally used for prevention or treatment of venous thromboembolism that frequently occurs in cancer patients. Heparin is composed of glucuronic or iduronic acid, glucosamine and has a sulfur content around 10% (from 8% to 13% according to the heparin preparation). An improved survival rate has been shown [2,3], which could be due to heparin, as it is able to interfere with some of the important biological steps in the metastasis spread [4]. Unfortunately, this kind of molecule exhibits drawbacks, such as hemorrhagic risk, and could present a contamination with prion proteins or oversulfated

chondroitin sulfate [5]. This hazard profile drastically limits the use of heparin in therapy. Actually, the number of studies on the exploration of heparin mimetic molecules has been raised in recent years. Among the possible molecules, polysaccharides could be a new source of heparin-like molecules. Traditional algal or bacterial polysaccharides provide a valid alternative to mammalian GAGs [6]. Additionally, polysaccharides extracted from eukaryotes and prokaryotes living in marine environment could potentially reveal a better benefit/risk ratio as observed in preliminary animal studies [6]. In the past, algal polysaccharides such as fucoidans—and especially low-molecular-weight fucoidan preparation (LMWF)—have been shown to exhibit heparin-like properties with very low hemorrhagic risk [7]. Marine polysaccharides from a bacterial source also present a high potentiality in cell therapy and tissue engineering. They can be produced under totally controlled conditions in bioreactors [8] compared to other polysaccharides from eukaryotes.

Among these marine polysaccharides, an exopolysaccharide (EPS) of interest is extracted from the culture broth of a bacterium named *Alteromonas infernus*. The repeating unit of this EPS consists of a monosulfated nonasaccharide composed of six neutral hexoses and three hexuronic acids, among those the galacturonic acid unit bears one sulfate group. It presents a high molecular weight ($> 10^6 \text{ g mol}^{-1}$) and a low sulfate content ($< 10\%$) [9–11]. This native EPS demonstrated a very weak anticoagulant activity compared to heparin. In order to promote its biological activities and to provide a GAG mimetic compound, the native EPS has been modified by first a radical depolymerization, then followed by an oversulfation step [12,13]. EPS-DR represents the native EPS that has undergone radical depolymerization, while EPS-DRS has undergone additional over-sulfation. These two chemical modifications allow for a reduction of its molecular weight along with an increase in its sulfate content. The anticoagulant activity of this highly sulfated EPS derivative is improved compared to that of its native precursor but remains lower than both unfractionated heparin and LMW heparin, 10 and 5 times less, respectively. A hypothetical structure of the oversulfated exopolysaccharide (EPS-DRS) has been proposed [12,13] and is presented in Figure 1a. In the proposed structure three hexose units could be sulfated after the oversulfation reaction according to preliminary mass spectrometry analysis, as indicated in Figure 1a [12–14].

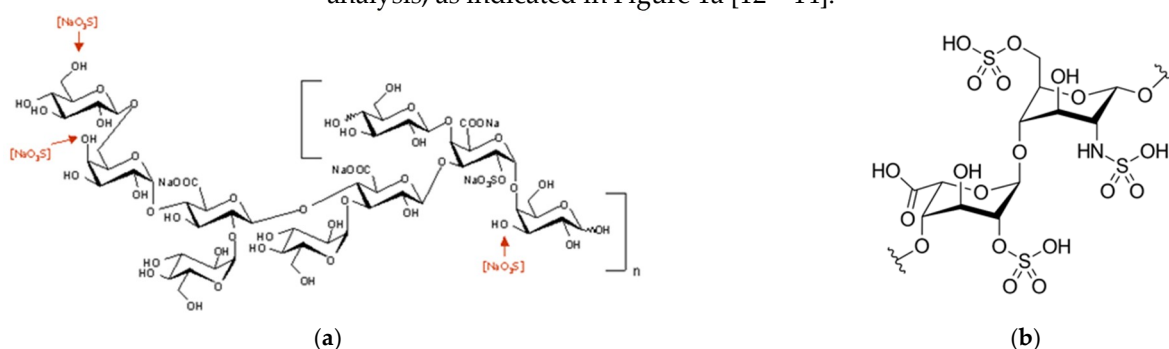


Figure 1. (a) Structure of EPS and postulated sulfated position after oversulfation reaction [12]. (b) Structure of heparin: the major repeating unit is the tri-sulfated disaccharide 2-O-sulfo- α -L-iduronic acid 1 \rightarrow 4 linked to 6-O-sulfo-N-sulfo- α -D-glucosamine.

The EPS DRS could effectively inhibit, *in vitro*, both the migration and invasiveness of osteosarcoma cells [15]. It has been shown different levels of bone resorption regulation due to the presence of over sulfated-EPSs, most of them leading to proresorptive effects [13]. Moreover, this compound has been evidenced to be very efficient at inhibiting the establishment of lung metastases *in vivo* [15]. These EPSs could pave the way for the development of new drug-delivery systems in bone oncology in the field of personalized medicine [16].

In cancer treatment, personalized medicine uses specific information about a patient's tumor to help making a diagnosis, planning treatment, finding out how well treat-

ment is working, or making a prognosis. Examples of personalized medicine include using targeted therapies to treat specific types of cancer cells, such as HER2-positive breast cancer cells, or using tumor marker testing to help diagnosing cancer [17]. Nuclear medicine enables clinicians identifying non-invasively and precisely specific molecular activity within tissues and organs of the body, facilitating the early detection of disease and the immediate monitoring of therapeutic responses. Nuclear medicine involves the use of radioactive isotopes in the diagnosis and treatment of diseases. Theranostics—a field of medicine that combines specific targeted therapy based on specific targeted diagnostic tests—uses specific biological pathways in the human body, to acquire diagnostic images and to deliver a therapeutic dose of radiation to the patient. The acquired image allows for identifying the patient response and estimating, for the responder, the dose of the therapeutic agent to be injected. With this strategy, it is possible to give the right treatment, to the right patient, at the right time, with the right dose. For that purpose, it is necessary to have access to two specific radionuclides: one for imaging and another one for therapy. Such a pair of isotopes can be of a same element—often called true theranostic pairs, e.g., $^{64}\text{Cu}/^{67}\text{Cu}$, $^{44}\text{Sc}/^{47}\text{Sc}$, $^{124}\text{I}/^{131}\text{I}$ —or of element sharing, quite similar biodistributions—e.g., $^{68}\text{Ga}/^{177}\text{Lu}$, $^{99\text{m}}\text{Tc}/^{188}\text{Re}$ [18,19]. Among the available radionuclides, scandium possesses two radionuclides emitting β^+ radiation, ^{44}Sc or ^{43}Sc , which makes them appropriate candidates in PET/CT (Positron Emission Tomography—Computed Tomography) diagnosis, due to their half-life of around 4 h and decay to non-toxic Ca. For both radionuclides, half-lives are compatible with the pharmacokinetics of a fairly wide range of targeting vectors, such as peptides, antibodies, antibody fragments, and oligonucleotides. The validity, usefulness and advantages of ^{44}Sc ($E_{\beta} = 1\,157\text{ keV}$) have been demonstrated, e.g., featuring ^{44}Sc -radiolabeled targeting vectors, including ^{44}Sc -radiopharmaceuticals, very recently used in patients [20]. Some recent studies have shown also the validity of ^{43}Sc -radiolabeled targeting vectors [21]. Finally, ^{47}Sc is a low energy β^- -emitter ($T_{1/2} = 3.34\text{ days}$; $E_{\beta} = 270\text{ keV}$; $E_{\gamma} = 159.37\text{ keV}$), which is suitable for SPECT (Single-Photon Emission-Computed Tomography) and planar imaging. ^{47}Sc , which can be used for targeted radionuclide therapy, opens the field of Sc-based vectors from diagnosis to therapy and gives a great opportunity for dosimetric calculations. These exopolysaccharides, coupled with theranostic radionuclides, may serve as new radiopharmaceuticals drugs.

For use in a theranostic approach, the scandium-exopolysaccharide complex must be thermodynamically stable and kinetically inert. Hence, the aim of this work is to obtain these data, compared to heparin, considered as a reference. It is also important to characterize EPS-DR, -DRS and heparin as reference, especially their molecular masses. Asymmetrical Flow Field-Flow Fractionation (AF4) technique coupled to differential Refractive Index (dRI), and Multi Angle Light Scattering (MALS) detectors was used. Usually, Size-Exclusion Chromatography (SEC) coupled to MALS is used for the determination of weight-average molar mass (\overline{M}_w) of macromolecules [22, 23]. However, AF4 has been recognized to be a suitable technique for the characterization of molar mass distribution of synthetic and natural polymers [24–26] as well as for nanoparticles [27], that are considered as drug delivery systems in antitumor and anti-metastasis therapy approaches [28].

Another important parameter that could influence the complexation is the polymer conformation [29]. To this aim, the hydrodynamic volume at different ionic strength was measured. Finally, to prevent the potential hydrolysis of EPS ligands, the stability constants Sc-EPS was assessed through Free Ion Selective Resin Extraction (FISRE) and the influence of sulfur content on the complexation with scandium was scrutinized. A good compromise has to be found between the complexes' stability and the sulfur content, which is inversely linked to hemorrhagic risk.

2. Results

2.1. EPS $\partial n/\partial c$

The $\partial n/\partial c$ values obtained were analyzed using the light scattering software ASTRA[®] (see experimental section). The measured dRI values are then plotted against the concentration and fitted to a linear regression (Figure 2), the slope of which corresponds to the specific refractive index increment of the analyte in the given experimental conditions.

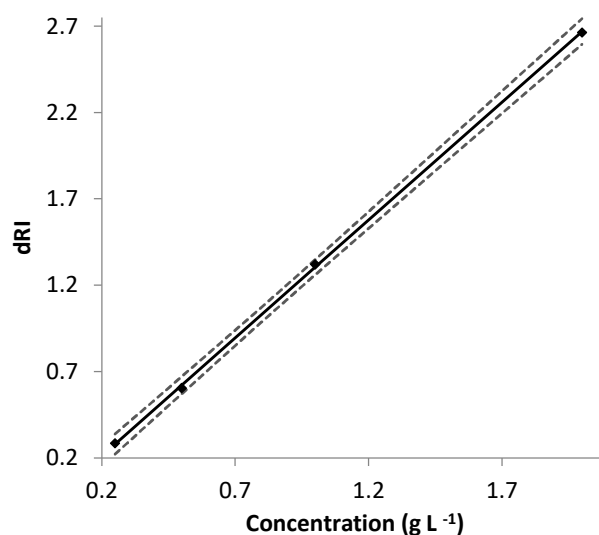


Figure 2. Determination of $\partial n/\partial c$ of EPS-DR in ultra-pure water at 25 °C; $\lambda_0 = 660$ nm. Concentrations of EPS = 0.25 – 2 mg. mL⁻¹. Measured differential refractive index dRI values ($\times 10^4$) with EPS-DR concentration. The solid line represents the linear fit; the uncertainties' hyperboles are plotted in dashed lines.

Usually, \overline{M}_w values of the two EPSs are routinely determined by SEC-MALS, after the native EPS modifications. In the present paper, we have characterized the two EPSs through AF4 coupled to MALS. Table 1 summarizes the different values of $\partial n/\partial c$ determined for the two EPS samples. In addition to the detector constant and concentration (or injected molar mass), signal intensity also relies on a sample-related constant and may be influenced by the molar mass (M^x). The molar mass exponent x is equal to 1 for a molar mass sensitive detector (such as MALS) and is 0 for a typical concentration detector (such as dRI). When using either a dRI or a MALS detector, the sample related constant is $\partial n/\partial c$. As shown in Table 1, the $\partial n/\partial c$ of EPS-DR and -DRS appears lower than the range commonly considered for polysaccharides (0.140–0.150 mL g⁻¹) [30]. The $\partial n/\partial c$ of homogeneous polymers is constant and can be considered as a contrast factor. Thus, the slightly lower $\partial n/\partial c$ value indicates a lower signal intensity than for the average range of polysaccharides. It is also important to note that, as the $\partial n/\partial c$ increases, the molar masses that can be detected is lower (under the same analytical conditions). The lower value of $\partial n/\partial c$ would probably lead to a lower accuracy and precision on the lowest molecular mass determination of EPS.

Table 1. Determination of $\partial n/\partial c$ for EPS-DR and -DRS, and heparin in water at 25 °C and the molecular masses (uncertainties between brackets).

Sample	$\partial n/\partial c$ (mL g ⁻¹)	SO ₄ ²⁻ %	\overline{M}_w (kDa)
EPS-DR	0.125 (0.001)	9	26.6 (3.2)
EPS-DRS	0.110 (0.001)	48	57.0 (8.0)
Heparin	0.133 (0.001)	30	21.4 (2.2)

2.2. Determination of EPS Molar Masses and Dispersion

The most commonly used technique for the separation and molar mass determination of polymers is SEC, whereas AF4 is very useful for the separation of (bio)polymers [31]. It can be coupled to MALS for the determination of polymer molar masses [22–24], easily replacing SEC-MALS that has been routinely used to characterize polysaccharides. AF4 is the method of choice, especially for high-molar mass samples that could avoid shearing degradation of long-chain polymers, as in SEC. In AF4, the smallest polymer chains are eluted first due to their small sizes, whereas the bigger ones are eluted last.

The fractogram of EPS-DRS is shown in Figure 3. The light scattering peak looks uneven and sharper than those in UV-VIS and dRI, which is typical of the highly charged polysaccharides analyzed with AF4-MALS [32]. The small peak shift is due to the delay from one detector to another one due to the tubing, which was not corrected in ASTRA.

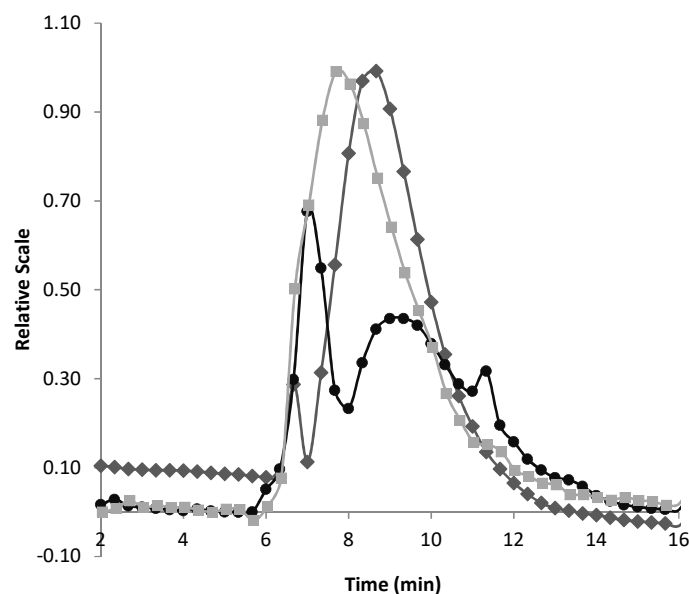


Figure 3. Fractogram of EPS-DRS (squares: UV-VIS @ $\lambda = 254$ nm; circles: dRI; diamonds: MALS @ 90°). [EPS-DRS] = 2 mg mL^{-1} ; injection volume = $20 \text{ }\mu\text{L}$; eluent = MilliQ water with 0.1% in volume of Tween 20; membrane = PES 5 kDa; canal length = 291 mm; spacer = $350 \text{ }\mu\text{m}$; cross flow = from 2 to 0 mL min^{-1} in 17 min; injection flow = 0.20 mL min^{-1} ; focalization flow = 2 mL min^{-1} ; detector flow = 1 mL min^{-1} .

During light scattering calculations, it is assumed that the value of $\partial n/\partial c$ remains constant across the given sample separation. Measurements of scattered light at different detection angles θ (Debye plot) are thus necessary. The R_θ/K^*c values are calculated from Equation (2), knowing the $\partial n/\partial c$ value and the Rayleigh ratio R_θ for the different θ . ASTRA software allows the direct extrapolation of the molecular weight of EPS-DR and -DRS from the scattered light measured after the AF4 separation.

The fractogram in Figure 4a displays the molar mass of EPS-DR extrapolated from the Debye plot (Figure 4b, with the 95% hyperboles of uncertainties). The second peak of the fractogram in Figure 4a was only considered for the Debye plot, since the first one corresponds to the void peak. For the linear regression ($r^2 = 0.9875$) of EPS-DR, the slope corresponds to R_θ , while the intercept $\overline{M}_w \cdot P(\theta)$ allows for obtaining the \overline{M}_w value. For the measurements made at low angle and infinite dilution, since $P(0) = 1$, the intercept provides the $\overline{M}_w = (26.1 \pm 3.2) \text{ kDa}$. For EPS-DRS, the regression provides an $\overline{M}_w = (57 \pm 8) \text{ kDa}$ ($r^2 = 0.9714$). The results of molar mass and dispersity determined by AF4-MALS for the two EPS are compared in Table 2. Moreover, the angular dependence scattered light at low angles can be related directly to the z-average of the "radius of gyration" (R_g). This

is the only technique that can be used to measure the dimensions of the molecules without assumptions about their shapes.

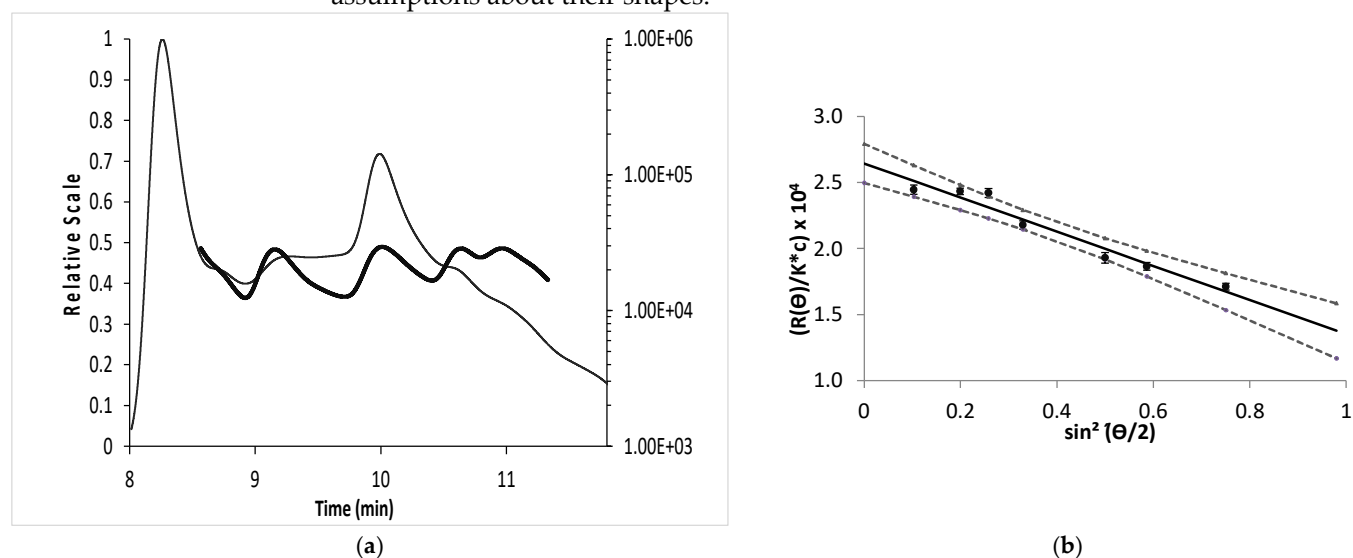


Figure 4. (a) Fractogram of molar mass of EPS-DR. The Light Scattering signal is plotted on the left Y axis, whereas the \overline{M}_w calculated from this LS signal using ASTRA is plotted on the right Y axis. (b) Debye plot measurements of light scattering intensity at (θ) angles 18° , 36° , 45° , 58° , 90° , 108° , and 135° and analyzed with ASTRA.

Table 2. AF4-MALS characterization in terms of molar mass and dispersity. The values in the brackets correspond to the uncertainties.

	\overline{M}_w (kDa)	\overline{M}_n (kDa)	PDI = $\overline{M}_w/\overline{M}_n$	R_g (nm)
DR	26.6 (3.2)	18.8 (2.8)	1.41 (0.38)	44.6 (0.1)
DRS	57.0 (8.0)	39.1 (4.1)	1.46 (0.36)	58.8 (0.1)

2.3. Polymer Conformation

The first step in the analysis of any samples is the instrument or detector calibration. The response of the detectors is calibrated to a known property by the use of a narrow standard. In our case, a water-soluble anionic polymer, such as polyacrylic acid (PAA) was used. Intrinsic viscosities $[\eta]$ of PAA solutions of different molecular weights—i.e., 2000, 8000, 10,000, and 50,000 g mol^{-1} —were measured. Mark–Houwink plots of log intrinsic viscosity as a function of log \overline{M}_w were calculated for the PAA (Table 3). From Eq. 10, a value of $a = 0.617$ was obtained for PAA in NaCl 0.1 mol L^{-1} at 20°C , which would indicate that the solvent could be considered as a good solvent— $a = 0.5$ to 0.7 being expected for a random coil polymer in a good solvent. From Equation 9, Mv was calculated together with $[\eta]$, to determine the hydrodynamic volume V_h from equation 5 (see Section 4.5) [33].

Table 3. Mark–Houwink calibration with PAA.

	PAA 2 kDa	PAA 8 kDa	PAA 10 kDa	PAA 50 kDa
Intrinsic Viscosity $[\eta]$ (dL g^{-1})	$3.03 \cdot 10^{-2}$	$5.83 \cdot 10^{-2}$	$10.32 \cdot 10^{-2}$	$21.51 \cdot 10^{-2}$

Since polysaccharides are polyelectrolytes, their viscosimetric behavior was studied as a function of the concentration in water and in dilute aqueous solutions containing variable amounts of NaCl. This is also of importance since, for polyelectrolytes, as with polysaccharides of interest, the second virial coefficient is very sensitive to ionic strength. The results of the relative viscosity $\ln \eta_r$ of EPS-DR and heparin are presented in Figure 5. In Figures 5a,b,e, the relative viscosity increases with polyelectrolyte concentration, and is progressively suppressed with the increase in the salinity of the solvent. This was in

agreement with the viscosimetric behavior of other types of polyelectrolytes [34]. The $\ln \eta_{sp}/c$ value allows for estimating $[\eta]$ according the following formula.

$$[\eta] = \lim_{c \rightarrow 0} \left(\frac{\ln(\eta_r)}{c} \right) \quad (1)$$

When plotting $\ln \eta_{sp}/c$ vs. c (Figures 5c,d,f), it is observed that, at low polyelectrolyte concentrations, $\ln \eta_r/c$ increases with decreasing c . This effect is caused by the increase in the Debye length with dilution, which reduces the screening of the charges fixed on the chain and strengthens their mutual repulsion. This is in agreement with the observation of Pavlov et al. [35] on highly charged polyelectrolytes. As a result, the size of the polyion increases. The behavior of EPS-DR and -DRS observed at the highest ionic strengths (Figure 5e), could be explained by a more important folding of the molecules induced by their larger structure.

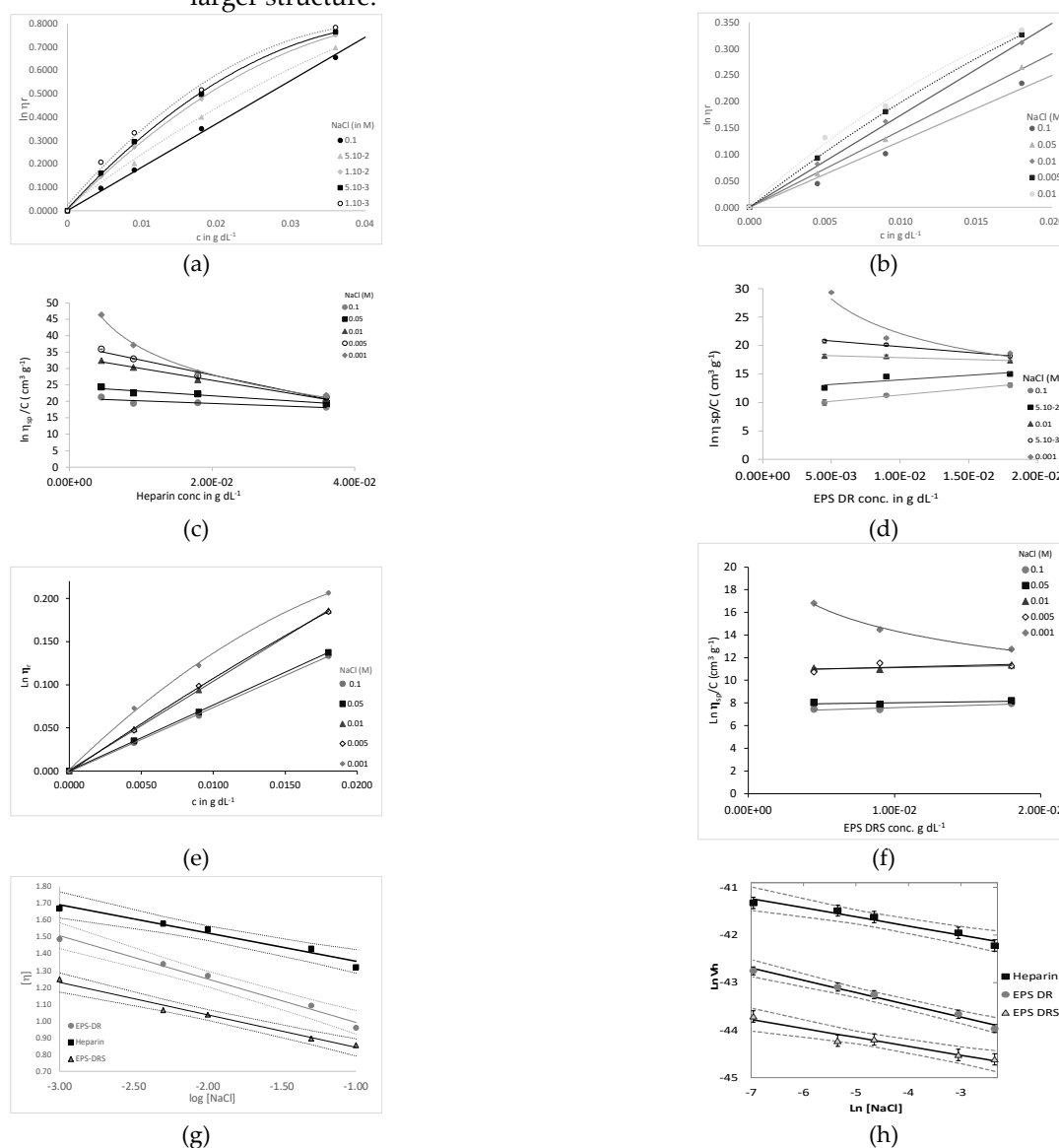


Figure 5. Relative viscosity η_r and intrinsic viscosity $[\eta]$ at different ionic strength (NaCl) of (a,c) heparin, (b,d) EPS-DR and (e,f) EPS-DRS. Concentrations of EPS-DR, -DRS and heparin: 4.5, 9, and 18 mg mL⁻¹ (additional concentration at 36 mg mL⁻¹ for heparin). NaCl concentrations: 0.1 (circles), 5 × 10⁻² (squares), 10⁻² (triangles), 5 × 10⁻³ (empty diamonds), 10⁻³ mol L⁻¹ (diamonds); (g) Intrinsic viscosity and (h) hydrodynamic volume of heparin (squares) and EPS-DR (circles) and -DRS (triangles) at different NaCl concentrations (in logarithmic scale).

The decrease in $[\eta]$ could be fitted by linear regression as followed: $\log [\eta] = 0.259 \log [\text{NaCl}] + 0.732$ ($r^2 = 0.9856$) for EPS-DR; $\log [\eta] = -0.193 \log [\text{NaCl}] + 0.649$ ($r^2 = 0.9849$) for EPS-DRS and $\log [\eta] = -0.168 \log [\text{NaCl}] + 1.186$ ($r^2 = 0.9633$) for heparin. Hence, $\log [\eta]$ is slightly higher for heparin than for EPS-DR or -DRS. The intrinsic viscosity provides information on the compaction of flexible-chain polymers on passing to the moderate polymer concentration range in solvents of various thermodynamic quality. This behavior in solution was confirmed through the determination of the hydrodynamic volume V_h of EPS-DR, -DRS, and heparin, at background electrolyte concentrations (Figure 5f). The same logarithmic trend as for $[\eta]$ was observed with $y = -0.19 \ln(x) - 42.67$ ($r^2 = 0.9856$) for EPS-DR; $y = -0.19 \ln(x) - 45.18$ ($r^2 = 0.9849$) for EPS-DRS and $y = -0.26 \ln(x) - 44.89$ for heparin ($r^2 = 0.9633$). The rate of decrease in V_h was comparable between both EPS but slightly higher than for heparin. The uncertainties on the slopes are similar for the 3 compounds, i.e., with 0.14. In addition, the V_h value is decreasing with increasing ionic strength (Figure 5f). This result could be translated when dealing with the complexation with metal ions. With decreasing ionic strength of the solution, the chain size increases due to electrostatic repulsion between charges. This aspect would be taken into consideration when evaluating the stability of polymer complexes with Sc^{3+} in the following section. For weak polyelectrolytes, with further decreasing concentration, a maximum concentration dependence of $\ln \eta_{sp}/c$ was observed, and Table 4 gives a summary of the hydrodynamic sizes from viscosimetric measurements compared to the R_g determined by AF4.

Table 4. Size information summary. The values in the brackets correspond to the uncertainties.

	$[\eta] \sim V_h$ (nm)	R_g (nm)	Mark Houwink	
				$\log K$
PAA	/	/	0.617	2.785
Heparin	41.4 (0.3)	63.6 (0.1)		
EPS-DR	42.9 (0.3)	44.6 (0.1)		
EPS-DRS	43.8 (0.3)	58.8 (0.1)		

The viscosimetric radius R_η ($\sim R_h$) values are slightly lower than the R_g . Both R_g and R_h can be used to gain insight into the third key area of polyelectrolyte characterization: structure. The characteristic R_g/R_h value for a globular protein is ~ 0.775 [36], which means that R_g is smaller than R_h . However, when molecules deviate from globular to non-spherical or elongated structures, then R_g/R_h tend to values upwards of 0.775, as R_g becomes larger than R_h . This is, thus, the case of the two EPS and heparin.

2.4. Stability Constants of Sc-EPS and Sc-Heparin Complexes

Free Ion Selective Radiotracer Extraction (FISRE) was used to obtain the apparent stability constants of Sc-EPS and -heparin complexes, as explained elsewhere [37]. Other techniques, such as potentiometric titrations and CE-ICP-MS were considered as being less suitable to analyze EPS-Sc complexes. Potentiometric titrations could affect the integrity of the polymer chain, by exposing it to very acidic and very alkaline pH hydrolysis [38,39], whereas CE-ICP-MS could not be used because of the highly charged polysaccharides-metal complexes, leading to a difficult interpretation of the speciation.

The partition coefficients normalized over the partition coefficient without organic ligands were calculated as a function of ligand concentrations (Figure 6).

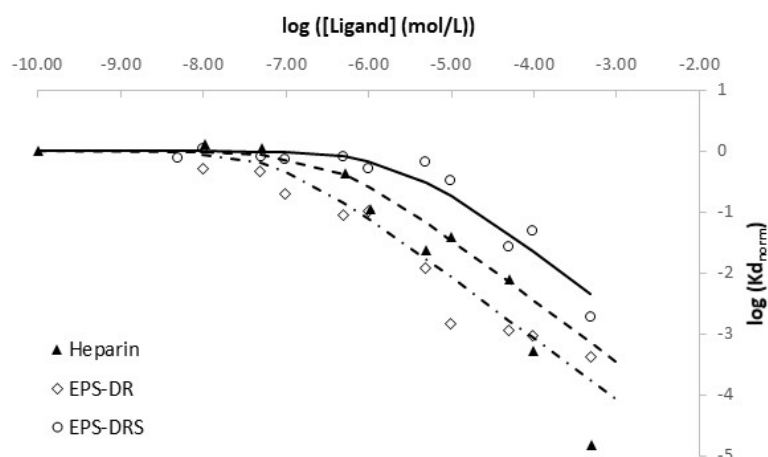


Figure 6. Ligand concentration isotherms of EPS-DR, EPS-DRS and Heparin: pH = 6.1 ± 0.1 ; 10 mg of chelex 100 resin in 5 mL of solutions; $[Sc^{3+}] = 10^{-4}$ mol L $^{-1}$, [EPS-DR], [EPS-DRS] and [Hep] ranged from 10^{-10} to $5 \cdot 10^{-4}$ mol L $^{-1}$.

As detailed in § 4.6, the number of different complexation sites is related to the number of plateaus in the isotherm, and the slope indicates the stoichiometry of sites implied in the scandium complexation with ligand. From Figure 6, for each different ligand, only one kind of complexation site was evidenced with a stoichiometry of 1:1 with regard to the free Sc^{3+} ion under our experimental conditions. Complexation constants could be calculated by the fitting of $\log Kd_{norm}$ vs. ligand concentration. As studies as a function of pH cannot be performed without potential ligand hydrolysis, the determined apparent complexation constant cannot be corrected from acid-base properties of ligand and potential H^+ implied in the reaction. Table 5 summarizes the apparent constants at pH 6.1 and the deduced ones, implying free aquo Sc^{3+} .

Table 5. Complexation constants obtained by FISRE for different ligand. Charges are omitted for the sake of simplicity.

	EPS-DR	EPS-DRS	Heparin
Apparent constant	7.07 ± 0.12	5.62 ± 0.12	6.38 ± 0.46
$\log \beta_{h,l} [H^+]^h$ (Equation (23))	9.30 ± 0.30	7.85 ± 0.30	8.61 ± 0.46

3. Discussion

The potential of polysaccharides such as GAGs in medicine has already been assessed [5], especially in tumor targeting [15,40,41], but not their coupling with theranostic radionuclides. The major interest in studying materials containing metal complexes of polymers stems from the fact that the rheological and other material properties of polymeric systems are strongly affected by complexation with metals [42].

3.1. EPS Molar Mass Determination and Polydispersity

Polysaccharides are heterogeneous substances; their chemistry, morphology, and polydispersity play an important role on their biodistribution [34,43], and when coupled to radionuclides, it could lead to the irradiation of healthy tissues. After their production in bioreactors, it is important to monitor their rheological properties to ensure reproducibility. AF4, an alternative separative technique to SEC-MALS with a higher selectivity [44], was proposed to determine the molecular weights of polysaccharides. MALS provides a direct and absolute way of measuring the \overline{M}_w value [45]. Indeed, for polysaccharides, non-ideality arising from co-exclusion and polyelectrolyte effects can be a serious problem and, if not corrected for, can lead to significant underestimates for \overline{M}_w . At the concentrations used in this work, the non-ideality effect could be neglected. The estimate

for \overline{M}_w could thus be considered within a few percent of the true or "ideal" \overline{M}_w . In order to use MALS data, the $\partial n/\partial c$ value for the studied polyelectrolytes must be accurately known.

The $\partial n/\partial c$ values determined for the two EPS samples were lower than the common range considered for other polysaccharides. The published $\partial n/\partial c$ values for various macromolecules [30], particularly for polysaccharides such as dextran and pullulan, indicated $\partial n/\partial c$ values in aqueous solution ranging between 0.14 and 0.15 mL g⁻¹, whereas the range is broader, i.e., from 0.044 to 0.218 mL g⁻¹, for non-aqueous systems [45]. For chitosan, the degree of substitution could influence the $\partial n/\partial c$ value, particularly if ionic functional groups are involved in the polysaccharide structure [46]. The presence of counter ions, such as Na⁺, together with a small chain branching, were shown to decrease the $\partial n/\partial c$ value from the general range of aqueous solutions, i.e., 0.14–0.15 mL g⁻¹ [47]. The different $\partial n/\partial c$ values between the two EPSs of this work could be explained by: (i) the differences in the sulfate contents, thus leading to different degree of ionization; by (ii) the different chain lengths of the two EPSs, as described later.

The $\partial n/\partial c$ values determined for EPS-DR and -DRS were thus used with AF4-MALS, and the \overline{M}_w were determined. EPS-DR and -DRS appeared to be monodisperse. Their \overline{M}_w were slightly higher than the ones published on low molecular weight polysaccharides, i.e., 10⁶ and 24–35 10³ g mol⁻¹, respectively [13]. Nonetheless, it was confirmed that radical depolymerization provided homogeneous polysaccharides in terms of molar mass dispersion (for both \overline{M}_n and \overline{M}_w) [48]. Monodisperse polymers have the same degree of polymerization or relative molecular mass [49], with a polydispersity index PDI = 1. For this kind of polysaccharide, the PDI found is usually around 1.5 [14], while most of the natural polysaccharides have PDI above 2 [50,51].

It can be assumed that the \overline{M}_w of EPS-DR and -DRS were underestimated in the previously published work [14] since the authors characterized these EPS by SEC-MALS with an average $\partial n/\partial c$ values for both EPS. Many commonly used SEC stationary phases may contribute to the unwanted interactions between charged analytes and column material. Another limitation of SEC is the incapability of the technique to characterize high-molar mass polymers and polysaccharides accurately ($M_w > 1 \times 10^6$ g mol⁻¹), even if SEC has been successfully used for characterization of commercial cationic hydroxyethyl cellulose derivatives [52]. Additionally, it has been well established that the potential for degradation exists when analyzing long linear polymers by SEC [53].

Finally, the use of SEC in combination with MALS or the triple detector system, where a true size exclusion from the column is not necessary in order to obtain absolute \overline{M}_w , would still give erroneous results as the $\partial n/\partial c$ for the polymer in solution would change due to the change in repeating unit composition. It was shown, for instance that loss of sulfate groups would result in the polymer assuming a less extended and more flexible conformation due to lower electrostatic intramolecular repulsion [39]. A desulfated polysaccharide molecule would, therefore, effectively behave as a smaller molecule in solution compared to another molecule of the same degree of polymerization but unchanged degree of sulfation. To some extent, the impact of this factor on elution from a SEC column could be minimized by using a mobile phase with high ionic strength, which will shield the electrostatic charges, but would definitely change the size of the polymer in solution [39].

Finally, both EPS samples exhibit nanometric sizes for their gyration radius that correspond to one quantitative indicator of molecular conformation. This last one controls the efficacy in drug delivery [54]. With R_g ranging from 44 to 58 nm, these EPS are suitable with rapid in vivo circulation, and fast clearance through the kidneys [43].

3.2. Polymer Conformation

Other useful quantitative indicators of molecular conformation are the viscosimetric radius (R_η) or the hydrodynamic radius (R_h). The hydrodynamic radius (or equivalent

sphere radius) is usually determined by dynamic light scattering. Thus, this work has examined the viscosimetric radius ($R\eta$) and the conformation of the polymers.

The viscosity of a polymer in solution is related to the polymer conformation, that could be affected by the complexation with metal ions [28]. The change in conformation was monitored through the polymer's intrinsic viscosity in solution, by varying the ionic strength of solvent for both EPS-DR and heparin. Figures 5a,b show an important decrease in the intrinsic viscosity for all concentrations considered with increasing ionic strength. These results were in agreement with results otherwise obtained on heparin [55]. A decrease in Debye length and a shield effect are caused by cations from the background electrolyte that decreased the electrostatic repulsion of the ionized groups, thus leading to a drop in viscosity [56].

Indeed, electrostatic interactions are very long-range (ca. 1000 nm) in pure water but quickly become screened in the presence of added salt (10 nm for 10^{-3} mol L⁻¹ monovalent salt). This is why, during dilution in pure water, polyelectrolytes adopt a more elongated conformation under the effect of electrostatic repulsions and the length of the chain is proportional to the number of monomers. However, the chain is not fully stretched, and it has been showed that the concept of the electrostatic blob allows for the accounting of both long-range electrostatic interactions at the monomers. When the conformation is a highly stretched chain bearing a large number of charges, thus producing an important interoperable electrostatic potential with the counter-ions.

Intrinsic viscosity, $[\eta]$ and the hydrodynamic volume V_h are related through Equation (9), where M is given by the Mark–Houwink–Sakurada equation (Equation (10)).

A universal calibration was performed first with polyacrylic acid (PAA) of different molecular weights. In this method, a set of standards are still required, but they do not have to be exactly the same. The polymer samples used for such calibration should be as narrow in distribution as possible because the width of the distribution will influence the values of K and a . Since viscosity is a function of molecular size and not strictly molecular weight, the constants K and a apply only to a given polymer at a specified temperature and solvent. They should be limited to the molecular weight range for which they were determined. The polymer must be linear, unbranched and not crosslinked. As a result, the calibration curve generated gives information about the intrinsic viscosity, molecular weight, and elution volume of a sample. Since intrinsic viscosity is the basis for this method, a universally calibrated system can be used for any polymer sample. One advantage of this method is that, unlike conventional calibration, the series of standards used do not have to be the same. Thus, a separate calibration for each type of polymer is not necessary.

In an aqueous solution at neutral pH, PAA was under an anionic form composed only of carboxylic groups ($pK_a = 4.54$ [57]). The PAA standards used were all linear. The intrinsic viscosity of each standard was determined (Table 3) and from this a calibration curve was established allowing the determination of K and a [58]. The $a = 0.617$ obtained for PAA in 0.1 mol L⁻¹ NaCl at 20 °C would indicate that the solvent is a “poor” solvent. However, NaCl has a great affinity for water and the addition of ions to aqueous solutions of polymers reduced the hydration of hydrophilic polymers [59]. The polymers are partially hydrated due to the great affinity of ions for hydration and, consequently, the polymer–polymer interactions are enhanced. This led to a low a value, as observed experimentally.

The constants K and a from Equation (10) were used to determine the viscosity average molar mass (M_v), depending on the polymer type and solute–solvent interactions. For instance, Grubisic et al. [60] calculated the V_h of different linear and branched polystyrene using the product $[\eta]\overline{M}_w$. Hamielec and Ouano [61] determined the V_h of standard polystyrenes using the product $[\eta]\overline{M}_n$. The authors concluded that inaccurate V_h values were obtained, when using \overline{M}_n or \overline{M}_w instead of M_v [62].

For the two EPS samples, a decrease in V_h was observed with increasing ionic strength. This decrease is slightly higher for EPS-DR and -DRS than for heparin, meaning

that EPS-DR and -DRS are more sensitive to the ionic strength changes. This could be explained by considering the overall charges surrounding EPS-DR or -DRS chains that are more important compared to the heparin ones. EPS-DR and -DRS exhibit more ionized functional groups that could be shielded by the counter-ions from the background electrolyte, leading to the folding of the polymer chain. The decrease in intrinsic viscosity with increasing ionic strength reflects a change in conformation: the expansion of the polymer chain is clearly affected by the addition of ions that seem to make the ionized functional groups of the polymer inaccessible. Coil expansion, and thus the intrinsic viscosity, decreased with ion concentration. This means that, with a higher V_h , the EPS polymers seem to be more elongated, exhibiting a larger portion of available ionized functional groups, i.e., carboxylate, available for the counter ion, i.e., Na^+ . By contrast, when V_h is lower, the polymer is more compact and tightly coiled, reducing the portions of ionized functional moieties for the counter ions.

Smidsrød and Haug [38] noticed that the size of the polysaccharide molecule in solution at a certain ionic strength changed depending upon the degree of desulfation (random coil to rigid rod) since the sulfate groups determine the total charge and charge distribution on the polymer. Loss of sulfate groups resulted in the polymer assuming a less extended and more flexible conformation due to lower electrostatic intramolecular repulsion. A desulfated polysaccharide molecule would, therefore, effectively behave as a smaller molecule in solution compared to another molecule of the same degree of polymerization but unchanged degree of sulfation. This is observed here between EPS-DR and -DRS. Hence, we measured the ability of polyelectrolytes to respond to changes in salt concentration by altering their hydrodynamic volume in agreement with published data on other type of polysaccharides [38].

3.3. Stability Constants of Sc-EPS and Sc-Heparin

As described by Santo et al. [42], the simplest model of complexation used in the literature is the non-bonded model, in which the metal atom interacts with the ligands simply by van der Waals and Coulombic interactions. This model cannot take into account the number and spatial arrangement of coordinating bonds specific to the particular metal, as the ligands tend to close-pack around the metal atom. In the bonded model, the metal atom is covalently bonded to ligands, and this preserves the coordination number and complex geometry. This model is applicable to stable metal-ligand complexes but cannot be used in the systems where ligand dissociation and exchange may occur.

The FISRE method has been used for the determination of thermodynamic stability of metallo-radiopharmaceuticals containing Y^{3+} [63], or for Sc^{3+} complexes with several chelating ligands, i.e., EDTA, DTPA, NOTA, and DOTA [37]. Other techniques, such as potentiometric titrations and CE-ICP-MS were considered being less suitable to analyze Sc-EPS complexes. The influence of coordination on the structure and rheology of polymer solutions has been extensively studied in the literature [42]. As written earlier, potentiometric titrations would affect the integrity of the polymer chain because of an extreme pH range that can cause chain scission. CE-ICP-MS, instead, could be used because of the complex highly charged polysaccharides-metal complexes, leading to a very difficult interpretation of the speciation.

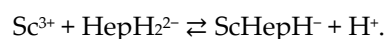
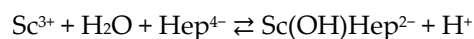
Hao et al. demonstrated using NMR and FTIR measurements that metal atom interacts with the carbonyl oxygen of the polyvinylpyrrolidone (PVP) polymer and, based on the data, hypothesized possible coordination with amine group [64]. For sugar-based moieties, it was evidenced that, in glucuronic, as well as galacturonic acid, the complexation with a trivalent ion, such as Eu^{3+} , occurred between the carboxylic moiety, the ring oxygen and the C-4 hydroxyl group [65,66].

To the best of our knowledge, there are no data on the complexation of EPS or heparin with Sc^{3+} . It was shown that, on a sulfate containing polyelectrolyte, the fixation of weakly acidic cations resembled the formation of outer-sphere complexes, in which the cation was separated from the anionic group by a solvent molecule [67]. The cation and

anion were held together by electrostatic forces, and the smaller the radius of the solvated cation, the stronger the bond. The stability constant of heparin with Ca^{2+} is $\log K = 2.09$ at $\text{pH} = 7.2$ and $I = 0.15 \text{ M}$ [67]. Feofanova et al. determined by potentiometric titration the stability constants of heparin with divalent d-transition series metals, i.e., Cu^{2+} , Zn^{2+} , Co^{2+} , Ni^{2+} and Fe^{3+} [65]. They found that the monoligand complex MHep^{2-} was the predominant species in weakly acidic, neutral, and weakly basic pH ranges. Otherwise, it was also shown that the affinity of metal ions for donor groups of low basicity is expected to decrease with increasing ionic radius of the hydrated cation. [68]. For Sc^{3+} , the ionic radius is smaller than the one of Ca^{2+} [69], so a higher complexation is expected.

With increasing pH, metal hydrolysis occurs. Water molecules are present in the inner coordination sphere of the metal that are progressively replaced by hydroxo-complexes, such as $[\text{M}(\text{OH})\text{Hep}]^{3-}$ and $[\text{M}(\text{OH})_2\text{Hep}]^{4-}$, with increasing pH. For all the metal-heparin complexes identified, these authors showed that $\log \beta$ values increased when more hydroxo-species of the metal were complexed—see Feofanova et al. [65] for application.

From a thermodynamic point of view, and with no further indication, the two following equilibria cannot be discriminated.



For EPS, these assumptions are not straightforward. Indeed, even if the literature provided some data on the complexation of polysaccharides with metals, there are very few data on the determination of their stability constants [70]. Nonetheless, considering the nonasaccharide monomer that composes EPS-DR and -DRS (Figure 1a), there are from five (DR) to eight (DRS) negative charges from its glucuronic and galacturonic acid units. Fuks and Bünzli [71] determined, by spectrophotometry, the complexation constants of these two latter uronic acids with lanthanide trivalent ions. These authors found that the complexation of La(III) with glucuronic acid and galacturonic acid lead to two complexes with respective values of $\log K_1 = 1.32$ and $\log K_2 = 3.86$ and $\log K_1 = 1.41$ and $\log K_2 = 3.94$, without consideration of La(III) hydrolysis, which is less extensive than Sc(III) [72].

Thus, for our investigated systems, the model with more than one complex was chosen, as it would be more relevant for the experimental data considered. The stability constants found for EPS-DR and -DRS were higher than those from Fuks and Bünzli [71] on glucuronic and galacturonic acids, and this could suggest the presence of hydroxo-complexes of Sc for both of them. Indeed, the hydrolysis of Sc^{3+} is more extensive than La^{3+} since it occurs at pH 5 [71].

Comparing the stability constants between two EPS, Sc-EPS-DR complexes seem to be slightly more stable than the Sc-EPS-DRS ones. However, in terms of speciation, both ligands seem to quantitatively complex scandium in conditions near physiological ones. In terms of charge, EPS-DRS present three additional negative charges, related to the three sulfate groups generated by the oversulfation reaction. The presence of the sulfate groups was awaited to enhance the complexation. The reasons for this opposite trend, instead, could be due to a higher steric hindrance with DRS monomers caused by sulfates. At higher ionic strength, those groups are shielded, which makes polymer folding into a more contracted random coil. Carboxylate moieties of EPS-DRS may be less accessible for steric reasons than those of EPS-DR. Nonetheless, Sc-EPS complexes appear to be less stable than those between scandium and classic chelate ligands used in radiopharmaceuticals, such as DOTA and DTPA ($K_{\text{ScDOTA}} = 30.79$; $K_{\text{ScDTPA}} = 27.43$) [73]. From the values published in [73], we calculated the apparent complexation constant for DTPA and DOTA, respectively, with scandium at $\text{pH} = 6.1$. We found 16.93 and 16.98, respectively. Even if these values are much higher than those determined for heparin, EPS-DR and -DRS (i.e., 6.38; 7.07 and 5.62 from Table 5), the complexation of scandium with these ligands is total. Additionally, the Sc-EPS and Sc-heparin complexes appear comparable, meaning that the

complexation behavior of those exopolysaccharides is quite similar to the traditional GAG heparin.

Regarding the Metal–Heparin complexes, a comparison could be made plotting the $\log \beta$ values vs. the inverse effective ionic radius $1/IR$ of the free metals in Shannon [69] in Figure 7. It can be seen that Sc^{3+} seems to effectively show stronger complexation than Ca^{2+} , and even stronger complexation than smaller ions, such as Zn^{2+} , Ni^{2+} or Co^{2+} . It is comparable to Mn^{2+} and Cu^{2+} , which is distorted by Jahn–Teller effect. It also shows a markedly smaller value than the trivalent Fe^{3+} complex. In effect, the comparison could be somewhat difficult as the formation of $Fe(OH)Hep$ complex—and of $Cu(OH)Hep$ to a somewhat lesser extent—is more extensive than the other first series d-transition elements [65]. Even the formation of $Sc(OH)Hep$ seems to be lower than $Fe(OH)Hep$.

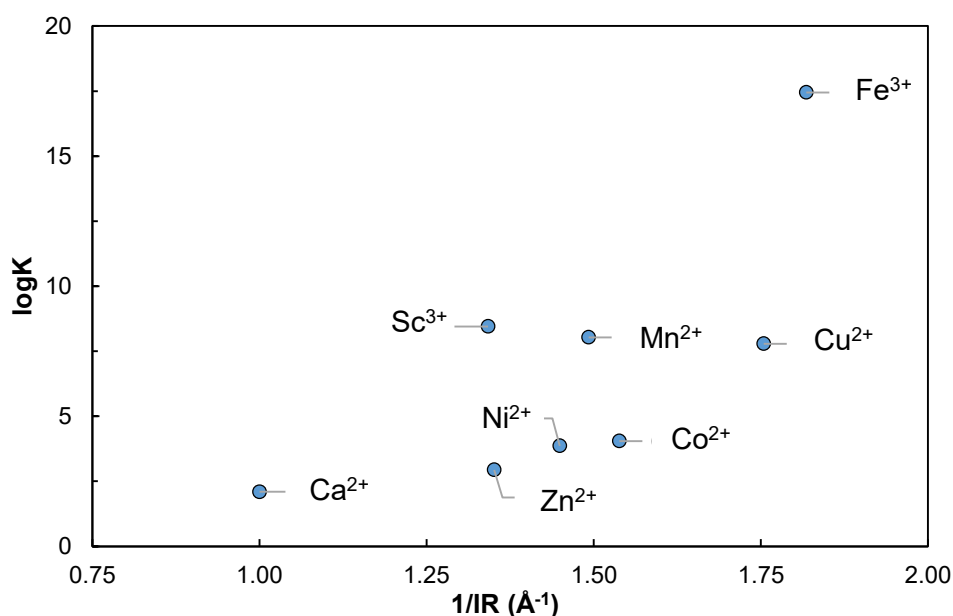


Figure 7. Comparison of $\log \beta$ for M-Heparin complexes from Feofanova et al. [65] (Zn^{2+} , Cu^{2+} , Ni^{2+} , Co^{2+} , and Fe^{3+}), Rendleman [67] (Ca^{2+}), and Sc-heparin in this work, as a function of the inverse effective ionic radius $1/IR$ [69].

The two EPSs studied are strongly complexing Sc^{3+} and thus, they can be further envisaged as carriers for the theranostic pair $^{44}Sc/^{47}Sc$.

4. Materials and Methods

4.1. Chemicals

The exopolysaccharides used in this work, namely EPS-DR and -DRS, were kindly provided by the Institut Francais de Recherche pour l'Exploitation de la MER (IFREMER) of Nantes as already described elsewhere [12]. The native EPS is produced from fermentation, and then undergoes radical depolymerization and over-sulfation [12]. The sulfate content of both polymers was determined by elemental analysis (Central Microanalysis Department of the CNRS, Gif-sur-Yvette, France). These two EPS differ from their sulfate content (SO_4^{2-} %) that were 10 and 48% for EPS-DR and -DRS, respectively. Several batches were produced in order to have sufficient amounts of EPS for performing the study. Each batch has been fully characterized using the methods described in the present paper.

Heparin sodium salt (from porcine intestinal mucose, ≥ 180 USP units mg^{-1}), scandium chloride hexahydrate (purity 99.9%), polyacrylic acid (of different \overline{M}_w , 50,000, 10,000 and 8000 $g\ mol^{-1}$) and certified bovine serum albumin (BSA) ($\overline{M}_w = 67,000\ g\ mol^{-1}$,

Sigma Aldrich, France), hydrochloric acid, sodium hydroxide, sodium chloride, ammonium acetate, and sodium azide were of analytical grade and were provided by Sigma Aldrich France. All other chemicals were pure reagent grade and used as received unless otherwise specified. Milli-Q water (18 M Ω .cm, Millipore) was used in all reactions. Heparin sulfate content was analyzed, similar to EPS, and showed 30% of SO₄²⁻.

4.2. Refractive Index Increment ($\partial n/\partial c$)

The index increment ($\partial n/\partial c$) parameter of both EPS samples and heparin was measured in order to better extrapolate the molar mass from light scattering. $\partial n/\partial c$ refers to the rate of change of the refractive index with the concentration of a solution for a sample at a given temperature, a given wavelength, and a given solvent [74]. The approach used in this article to determine $\partial n/\partial c$ is generally the most accurate one, involving the so-called offline-batch-mode dRI experiment [29]. Here, a series of solutions of increasing concentrations of polysaccharides in a certain solvent are injected directly into the dRI detector. Concentrations of EPS range from 0.25 up to 2 mg mL⁻¹ in Milli-Q water. The choice of Milli-Q water as a solvent is derived from the fact of comparing those literature values measured in H₂O. The dRI measurements were performed at 25 °C, using an Optilab rEX (Wyatt Technology, Germany) with $\lambda_0 = 660$ nm, and analyzed using the corresponding ASTRA[®] software (Wyatt Technology, Germany).

4.3. Asymmetrical Flow Field-Flow Fractionation (AF4) coupled to Multi Angle Light Scattering (MALS)

The principles and applications of the Field-Flow Fractionation methods are largely described in the literature [31,75,76]. The eluent is forced through a vacuum degasser from the HPLC chain (Shimadzu, France) and then through a 0.1 μ m on-line filter (Millipore Ltd., Watford, U.K.) into the Eclipse 3 (Wyatt Technology, Germany) before entering the flow-FFF channel (Wyatt Technology, Germany). The dimensions of the channel are 291×56×59 mm. A polyether sulfone (PES) membrane (5 kDa MWCO) with a 350 μ m mylar spacer is used. The sample is injected through a sampling loop of 20 μ L into the inlet of the channel with a 0.2 mL min⁻¹ flow. The channel outlet is connected to the detectors. The AF4 device is simultaneously coupled on-line with a UV-visible spectrophotometer (SPD-20A; Shimadzu; $\lambda = 254$ nm), a differential refractometer (Optilab rEX, Wyatt Technology, Germany), and a multi angle light scattering detector (MALS) 18 angles (DAWN HELEOS II, Wyatt Technology, Germany). The flow rates are controlled employing the Eclipse software (Wyatt Technologies, Germany). The elution flow was fixed at 1 mL/min. Focalization flow was 2 mL min⁻¹ and the cross flow was set in gradient, from 2 to 0 mL min⁻¹. The carrier solution chosen was MilliQ water with 0.1% in volume of Tween 20. Molecular weight-certified bovine serum albumin (BSA) of 67,000 g mol⁻¹ was used for calibration of the AF4 channel with a concentration of 1 mg mL⁻¹, which corresponds to 1.5×10^{-5} mol L⁻¹. To recapitulate, BSA is a protein, which is forming mono, di, tri and tetramers. The calibration performed under gentle conditions with high resolution to get complete baseline separation of the BSA monomer and the corresponding aggregates. For the polysaccharides, the concentrations were fixed at 2 mg mL⁻¹. The injection conditions are summarized in Table 6. The optimization of these different parameters is further discussed in this paper. Each sample was injected at least in triplicate. Data were analyzed using ASTRA software. ASTRA[®] is a versatile software available for the characterization (molar mass, size, conformation, conjugation, etc.) of macromolecules and nanoparticles via light scattering.

Table 6. AF4 method used to characterize EPS.

Start Time (min)	Duration (min)	Mode	Initial Cross Flow (mL/min)	Final Cross Flow (mL/min)
0.00	1.00	Elution	0.00	1.50
1.00	1.00	Focus		
2.00	2.00	Focus + Inject		
4.00	2.00	Focus		
6.00	10.00	Elution	1.50	1.50
16.00	7.00	Elution + Inject	1.50	0.00

The determination of the concentration c is usually given through the dRI detector, whereas the K^* value is determined through Equation (2):

$$K^* = \frac{4\pi^2 n_0^2}{\lambda_0^4 N_A} (\partial n / \partial c)^2 \quad (2)$$

where λ_0 is the wavelength of the incident radiation, N_A the Avogadro's number and n_0 the refractive index of the solvent.

The mass concentration determined when preparing the sample and the recovery ratio for these experiments was determined in order to get the final concentration of the sample analyzed through AF4.

The variation of MALS scattered light is directly proportional to the weight-average molecular weight, \overline{M}_w , according to the Zimm formalism [77],

$$\frac{K^* c}{R_\theta} = \frac{1}{M_w P_\theta} + 2A_2 c \quad (3)$$

where K^* is the optical constant of Equation (2), c the concentration of the compound; R_θ the Rayleigh ratio; A_2 the second virial coefficient; P_θ the form factor.

A_2 reflects solvent-solute interactions whereas P_θ describes the variation of scattered light with scattering angle θ .

The Rayleigh ratio R_θ is defined as:

$$R_\theta = \frac{I_s(\theta)}{I_0(\theta)} \quad (4)$$

This represents the ratio between the amount of light scattered by the analyte solution in excess, and the amount of light scattered by the solvent at varying scattering angle θ . When extrapolated to zero angle, and at infinite dilution, the relation between R_θ and \overline{M}_w leads to the following equation.

$$\overline{M}_w = \frac{R_\theta}{K^* c} \quad (5)$$

According to Eq. 2 and 3, the light scattered at the different angles R_θ depends on the $(\partial n / \partial c)^2$ value, whereas the molecular weight M_w depends on $(\partial n / \partial c)^{-1}$ and the form factor P_θ / M_w depends on $(\partial n / \partial c)$.

In this work, Zimm's formalism is the one used for extrapolating the physical characteristics of the polymers from light scattering data. According to this formalism, the expression of P_θ is the following:

$$P_\theta = 1 - \frac{u^2}{3} \quad (6)$$

where u is

$$u = \frac{4\pi}{\lambda} n_0 R_g \sin\left(\frac{\theta}{2}\right) \quad (7)$$

R_g represents the gyration radius of the polymer and n_0 is the refractive index of the solvent.

4.4. pH Measurements

The pH values were measured with a combined Ag/AgCl electrode (Metrohm), which was calibrated before each experiment by titration of degassed HCl 0.1 M solution by freshly prepared free carbonate NaOH 0.1 M solution to maintain constant ionic strength equal to 0.1 M. The electrode was calibrated using OPIUM software and the following equation.

$$E = E^0 + S \times \log[H^+] \quad (8)$$

where the additive term E^0 contains the standard potentials of the electrodes used and contributions of inert ions to the liquid junction potential, S corresponds to the Nernstian slope. No significant deviation was observed in very acidic acid solution and alkaline solution and no correction was taken into consideration.

4.5. Viscosity Analysis

To investigate the polymer shape, the intrinsic viscosity at different ionic strength of solvent was determined. Five batches of 2 mL solutions containing EPS-DR were prepared in NaCl solution at different concentrations (from 10^{-3} to 0.1 mol L⁻¹) and in MilliQ water. Three different concentrations of polysaccharide, i.e., 4.5, 9, and 18 mg mL⁻¹, were prepared for each ionic strength. The same kind of analysis was assessed on Na-heparin (Sigma Aldrich, $\overline{M}_w \approx 18,000$ g mol⁻¹) to have a reference of viscosity behavior in the same ionic strength conditions. Viscosimetric measurements were realized using a digital microviscosimeter Lovis 2000 M[®] (Anton Paar, France). A rolling-ball viscometer measures the rolling time of a steel ball through a glass capillary filled with transparent or opaque liquids according to Hoeppler's falling ball principle. The temperature was set at 20 °C.

The hydrodynamic volume V_h of the polymer, that represents the sum of the time-average of the molecular volume and the volume of the solvent molecules associated with it, is calculated using Equation (9) [78].

$$V_h = \frac{4\pi[\eta]M_v}{\mu} \quad (9)$$

with $\mu = 10\pi N_A$, where N_A is the Avogadro's number, $[\eta]$ and M_v are the intrinsic viscosity and the viscosity-average molar mass, respectively, that are present in the Mark-Houwink-Sakurada (MHS) equation [79].

$$[\eta] = KM_v^a \quad (10)$$

The calculation of MHS parameters is carried out by the graphic representation of the following equation:

$$\ln[\eta] = \ln K + a \ln M_v \quad (11)$$

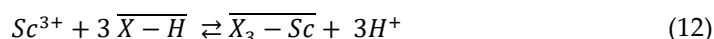
where K and a are M-H constants, depending upon the type of polymer, the solvent, and the temperature of viscosimetric determinations.

The exponent a is a function of polymer geometry varying from 0.5 to 2.0. Since MHS constants for EPS-DR, K , and a are not known, they have been estimated using the polyacrylic acid (PAA) of different \overline{M}_w , i.e., 2000; 8000; 10,000; 50,000 g mol⁻¹. These constants can be determined experimentally by measuring the intrinsic viscosity of several polymer samples for which the molecular weight has been determined by an independent method, e.g., osmotic pressure or light scattering. Using the polymer standards of PAA, a plot of $\ln[\eta]$ vs. $\ln \overline{M}_w$ usually gives a straight line, the slope of which is a and its intercept is $\ln K$ [80]. The M-H-S exponent bears the signature of a polymer chain's three-dimensional configuration in the solvent environment: a values from 0.0–0.5 reflect a rigid sphere in an ideal solvent, also called the theta solvent; those from 0.5–0.8 have a random coil in a good solvent; those from 0.8–2.0 have a rigid or rod like configuration (stiff chain) [81].

4.6. Free-Ion Selective Radiotracer Extraction (FISRE)

FISRE was used to determine the stability constants of a complex M:L, at tracer level, using a cationic exchange resin Chelex 100, which bears iminodiacetic functional groups [82]. The chelating resin competes with the ligands for Sc³⁺ complexation. FISRE was applied in batch mode, varying the concentration of polymer ligand. It allowed for determining the association processes.

The adsorption of Sc³⁺ by iminodiacetate chelating groups ($\overline{X-H}$) can be described by the following exchange equation:



Over-lined species are related to adsorbed species present on the resin. The partition coefficient K_d could be expressed as follows:

$$K_d = \frac{[Sc(III)]_{ads}}{[Sc(III)]_{sol}} = \frac{[\overline{X_3-Sc}]}{[Sc^{3+}] \alpha_{Sc(L,OH)}} = \frac{K_{ads} [\overline{X-H}]^3}{[H^+]^3 \alpha_{Sc(L,OH)}} \quad (13)$$

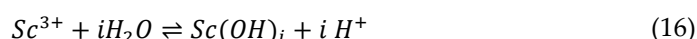
where K_{ads} is the equilibrium constant for Sc³⁺ bound to the resin (Eq.12), $\alpha_{Sc(L,OH)}$ is the complexation coefficient of Sc³⁺, which defines the ratio between the total aqueous scandium concentration $[Sc(III)]_{sol}$ and the Sc³⁺-aqua ion concentration $[Sc^{3+}]$, as shown in Equation (14).

$$\alpha_{Sc(L,OH)} = \frac{[Sc(III)]_{sol}}{[Sc^{3+}]} \quad (14)$$

When the exchange resin is used in large excess in comparison to the initial concentration of scandium, $[\overline{X-H}]$, the free concentration of ligand can be approximated to C_e , the exchange capacity of the resin. Moreover, at fixed pH, K_d (Equation (13)) can be simplified:

$$K_d = \frac{K_{ads} [\overline{X-H}]^3}{[H^+]^3 \alpha_{Sc(L,OH)}} = \frac{C1}{\alpha_{Sc(L,OH)}} \quad (15)$$

where C1 is a constant. The partition coefficient also varies only with the Sc³⁺ complexation in aqueous medium. The complexation coefficient varies with pH, ligand concentration and other complexing agents: $\beta_{OH,i}$ are the hydrolysis constants corresponding to the equilibrium [83],



$\beta_{Cl,j}$ are the chloride complexation constants corresponding to the following equilibrium [72].

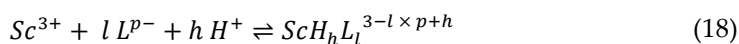


Used thermodynamic constants are summarized below in Table 7:

Table 7. Thermodynamic constants of scandium(III) complexation.

Reactions	Value	Ref
$Sc^{3+} + H_2O \rightleftharpoons Sc(OH)^{2+} + H^+$	-4.16 ± 0.05	[83]
$Sc^{3+} + 2H_2O \rightleftharpoons Sc(OH)_2^+ + 2H^+$	-9.71 ± 0.30	[83]
$Sc^{3+} + 3H_2O \rightleftharpoons Sc(OH)_3 + 3H^+$	-16.08 ± 0.30	[83]
$Sc^{3+} + 4H_2O \rightleftharpoons Sc(OH)_4 + 4H^+$	-26.7 ± 0.3	[72]
$Sc^{3+} + Cl^- \rightleftharpoons ScCl^{2+}$	1.1 ± 0.1	[72]
$Sc^{3+} + 2Cl^- \rightleftharpoons ScCl_2^+$	0.75 ± 0.10	[72]

The behavior of scandium in different systems is also influenced by the presence in solution of heparin or EPS ligands (L), due to the formation of the associated complexes. If we consider the different polymers as aqueous molecules with different potential complexation sites, an equilibrium can be defined for each reaction site,



with the associated complexation constant.

$$\beta_{h,l} = \frac{[ScH_h L_l^{3-p+i}]}{[Sc^{3+}][L^{p-}]^l [H^+]^h} \quad (19)$$

Considering all the reactions occurring in aqueous medium, the complexation coefficient $\alpha_{Sc(L,OH)}$ can be expressed as

$$\begin{aligned} \alpha_{Sc(L,OH)} &= \frac{[Sc^{3+}] + \sum_{i=0}^4 [Sc(OH)_i^{3-i}] + \sum_{j=1}^3 [Sc(Cl)_j^{3-j}] + \sum_{h,l} [ScH_h L_l]}{[Sc^{3+}]} \quad (20) \\ &= 1 + \sum_{i=1}^4 \frac{\beta_i}{[H^+]^i} + \sum_{j=1}^3 \beta_j [Cl^-]^j + \sum_{h,l} \beta_{h,l} [L]^l [H^+]^h \end{aligned}$$

As the experiments were performed at fixed pH and constant chloride concentration, the complexation coefficient varies only with the aqueous concentration of different sites on heparin or EPS ligands. This concentration cannot be considered equal to the initial concentration due to its complexation with scandium. The mass balance of these sites must be solved to determine the different complexation constant.

Complexation constants could be calculated by fitting the dependence of the distribution coefficient (K_d) of Sc(III) between the resin and the supernatant on the total ligand concentration in the supernatant. At very low concentrations of heparin or EPS ligands, they do not significantly affect the scandium speciation and the partition coefficient is also constant.

$$\log K_d \approx \log C_1 + \log \left(1 + \sum_{i=1}^4 \frac{\beta_i}{[H^+]^i} + \sum_{j=1}^3 \beta_j [Cl^-]^j \right) \quad (21)$$

When heparin or EPS ligand concentrations increase, the complexation becomes major, it can be approximated to $\alpha_{Sc(L,OH)} = \sum_{h,l} \beta_{h,l} [L]^l [H^+]^h$, where the equilibrium ligand concentration is equal to the initial ligand concentration.

$$\log K_d \approx \log C_1 + \log \left(\sum_{h,l} \beta_{h,l} [L]^l [H^+]^h \right) \quad (22)$$

$\log K_d$ vs. $\log[L]$ allows determining the slopes, which are related to the stoichiometric coefficient l . The x-intercept between these slopes and the plateau corresponding to the adsorption of scandium without ligand is related to $-\log \beta_{h,l}$.

$$\log \beta_{h,l} [H^+]^h = -l \times \log[L] \quad (23)$$

Concerning the experimental conditions, 10 mg of exchange resin were added to a final volume of 5 mL. Solutions contained fixed 10^{-4} mol L⁻¹ Sc³⁺ and varying ligand concentration from 10^{-9} to 10^{-3} mol L⁻¹. The resulting suspensions were daily monitored and adjusted to pH = 6. The separation of the solid and liquid phases was done by sedimentation. Aliquots of the supernatant from 0.4 to 1 mL were taken for ICP-AES analysis (ICP spectrometer iCAP 6000 of Thermo Scientific). For the ICP-AES, samples were prepared in nitric acid 1% and run through an auto sampler ASX-520 (Cetac). The calibration for Sc was done in the range 0–100 ppb, prepared by a dilution of a standard solution of 10.04 $\mu\text{g mL}^{-1}$ (PlasmaCAL, SCP Science). Sc was detected at 255, 366, and 424 nm. The average LQM was 0.576 ppb.

5. Conclusions

Two exopolysaccharides, a slightly sulfated named EPS-DR and a highly sulfated named -DRS, exhibiting heparin-like properties, have been characterized in terms of molar mass distribution and conformation. Their respective $\overline{dn/dc}$ values were determined for being used with AF4-MALS for reaching their \overline{M}_w values. Both EPS were monodisperse and exhibited nanometric sizes, making them suitable as targeting chelates for their further use in Nuclear Medicine. We confirmed the ability of these polysaccharides to respond to changes in salt concentration by altering their hydrodynamic volume in agreement with a polyelectrolyte's behavior. The rheological tools developed in this work, were successfully applied to monitor the repeatability of the bio-production of these polysaccharides. The complexation properties of these EPS with scandium indicated that Sc-EPS-DR and -DRS stability constants were higher than those on glucuronic and galacturonic acids, thus suggesting the presence of hydroxo-complexes of Sc for both of them. Sc-EPS complexes appear to be less stable ($K_{ScEPS-DR} = 9.14$; $K_{ScEPS-DRS} = 7.69$) than scandium complexes with DOTA and DTPA, classically used in radiopharmaceutical drugs. However, this will not consist in a limitation of further use of these EPS since they exhibit biological properties, and especially antiproliferative properties in cancer cells. Further work will thus scrutinize, through biological assays, the synergetic effect of Sc-EPS complexes on different cancer cell lines, compared to the EPS and Scandium alone. In parallel, the optimization of the EPS radiolabeling with ^{44}Sc may provide an additional purification step. The radiolabeling must provide the highest yield in a time frame compatible with the half-life of the radionuclide, in order to deliver the maximum activity to the patient, according to the clinical need. If both biological assays and radiolabeling yields are encouraging, then small animal studies will be envisaged with both Positron Emission Tomography imaging and biodistributions.

Author Contributions: Conceptualization, S.H.-M., C.A. and P.E.R.; methodology, S.H.-M., C.A. and P.E.R.; software, C.A., M.M.; validation, S.H.-M., C.A. and C.S.; formal analysis, M.M.; investigation, M.M.; resources, C.S.; data curation, S.H.-M., C.A., M.M.; writing—original draft preparation, S.H.-M., C.A., M.M., C.S., S.C.-J., writing—review and editing, S.H.; visualization, S.H.-M.; supervision, S.H.-M., C.A., C.S. and P.E.R.; project administration, S.H.; funding acquisition, S.H.-M.

Funding: This work has been supported in part by grants from the French National Agency for Research, called “Investissements d’Avenir” IRON Labex no. ANR-11-LABX-0018-01 and Arronax-Plus Equipex no. ANR-11-EQPX-0004. We acknowledge the Institut-Mines-Telecom and the Pays de la Loire council for the financial support of M. Mazza PhD grant.

Data Availability Statement: “Data available in a publicly accessible repository The data presented in this study are openly available at [doi], reference number [reference number].”

Conflicts of Interest: The authors declare no conflict of interest. The funders had no role in the design of the study; in the collection, analyses, or interpretation of data; in the writing of the manuscript, or in the decision to publish the results.

Sample Availability: Samples of the compounds are available from the authors.

Glossary: AF4: Asymmetrical Flow Field-Flow Fractionation; CE-ICP-MS: Capillary Electrophoresis coupled to Inductively Coupled Plasma-Mass Spectrometry; ICP-AES Inductively Coupled Plasma-Atomic Emission Spectroscopy/Spectrometer; FISRE: Free-ion selective radiotracer extraction; MALS: Multi-Angle Light Scattering; SEC: Size Exclusion Chromatography; $T_{1/2}$: radioactive half-life.

References

1. Bruland, S.; Pihl, A. On the Current Management of Osteosarcoma. A Critical Evaluation and a Proposal for a Modified Treatment Strategy. *Eur. J. Cancer* **1997**, *33*, 1725–1731, doi:10.1016/S0959-8049(97)00252-9.
2. Lyman, G.H. Thromboprophylaxis with Low-Molecular-Weight Heparin in Medical Patients with Cancer. *Cancer* **2009**, *115*, 5637–5650, doi:10.1002/cncr.24665.
3. Debourdeau, P.; Elalamy, I.; de Raignac, A.; Meria, P.; Gornet, J.M.; Amah, Y.; Korte, W.; Marty, M.; Farge, D. Long-Term Use of Daily Subcutaneous Low Molecular Weight Heparin in Cancer Patients with Venous Thromboembolism: Why Hesitate Any Longer? *Support. Care Cancer* **2008**, *16*, 1333–1341, doi:10.1007/s00520-008-0491-4.

4. Bendas, G.; Borsig, L. Cancer Cell Adhesion and Metastasis: Selectins, Integrins, and the Inhibitory Potential of Heparins. *Int. J. Cell Biol.* **2012**, *2012*, 1–10, doi:10.1155/2012/676731.
5. Köwitsch, A.; Zhou, G.; Groth, T. Medical Application of Glycosaminoglycans: A Review: Medical Application of Glycosaminoglycans. *J. Tissue Eng. Regen. Med.* **2018**, *12*, e23–e41, doi:10.1002/term.2398.
6. Senni, K.; Pereira, J.; Gueniche, F.; Delbarre-Ladrat, C.; Sinquin, C.; Ratiskol, J.; Godeau, G.; Fischer, A.-M.; Helley, D.; Collic-Jouault, S. Marine Polysaccharides: A Source of Bioactive Molecules for Cell Therapy and Tissue Engineering. *Mar. Drugs* **2011**, *9*, 1664–1681, doi:10.3390/md9091664.
7. Millet, J.; Jouault, S.C.; Mauray, S.; Theveniaux, J.; Sternberg, C.; Vidal, B.; Fischer, A.M. Antithrombotic and Anticoagulant Activities of a Low Molecular Weight Fucoidan by the Subcutaneous Route. *Thromb. Haemost.* **1999**, *81*, 391–395, doi:10.1055/s-0037-1614484.
8. Guezennec, J. Deep-Sea Hydrothermal Vents: A New Source of Innovative Bacterial Exopolysaccharides of Biotechnological Interest? *J. Ind. Microbiol. Biotechnol.* **2002**, *29*, 204–208, doi:10.1038/sj.jim.7000298.
9. Collic-Jouault, S.; Zanchetta, P.; Helley, D.; Ratiskol, J.; Sinquin, C.; Fischer, A.M.; Guezennec, J. Les polysaccharides microbiens d'origine marine et leur potentiel en thérapeutique humaine. *Pathol. Biol.* **2004**, *52*, 127–130, doi:10.1016/j.pat-bio.2003.05.005.
10. Roger, O.; Kervarec, N.; Ratiskol, J.; Collic-Jouault, S.; Chevlot, L. Structural Studies of the Main Exopolysaccharide Produced by the Deep-Sea Bacterium *Alteromonas Infernus*. *Carbohydr. Res.* **2004**, *339*, 2371–2380, doi:10.1016/j.carres.2004.07.021.
11. Raguénès, G.H.C.; Peres, A.; Ruimy, R.; Pignet, P.; Christen, R.; Loaec, M.; Rougeaux, H.; Barbier, G.; Guezennec, J.G. *Alteromonas Infernus* Sp. Nov., a New Polysaccharide-producing Bacterium Isolated from a Deep-sea Hydrothermal Vent. *J. Appl. Microbiol.* **1997**, *82*, 422–430, doi:10.1046/j.1365-2672.1997.00125.x.
12. Chopin, N.; Sinquin, C.; Ratiskol, J.; Zykwinska, A.; Weiss, P.; Cérantola, S.; Le Bideau, J.; Collic-Jouault, S. A Direct Sulfation Process of a Marine Polysaccharide in Ionic Liquid. *BioMed Res. Int.* **2015**, *2015*, 1–9, doi:10.1155/2015/508656.
13. Ruiz Velasco, C.; Baud'huin, M.; Sinquin, C.; Maillason, M.; Heymann, D.; Collic-Jouault, S.; Padrines, M. Effects of a Sulfated Exopolysaccharide Produced by *Alteromonas Infernus* on Bone Biology. *Glycobiology* **2011**, *21*, 781–795, doi:10.1093/glycob/cwr002.
14. Jouault, S.C.; Chevlot, L.; Helley, D.; Ratiskol, J.; Bros, A.; Sinquin, C.; Roger, O.; Fischer, A.-M. Characterization, Chemical Modifications and in Vitro Anticoagulant Properties of an Exopolysaccharide Produced by *Alteromonas Infernus*. *Biochim. Biophys. Acta* **2001**, doi:10.1016/S0304-4165(01)00185-4.
15. Heymann, D.; Ruiz-Velasco, C.; Chesneau, J.; Ratiskol, J.; Sinquin, C.; Collic-Jouault, S. Anti-Metastatic Properties of a Marine Bacterial Exopolysaccharide-Based Derivative Designed to Mimic Glycosaminoglycans. *Molecules* **2016**, *21*, 309, doi:10.3390/molecules21030309.
16. Arpicco, S.; Milla, P.; Stella, B.; Dosio, F. Hyaluronic Acid Conjugates as Vectors for the Active Targeting of Drugs, Genes and Nanocomposites in Cancer Treatment. *Molecules* **2014**, *19*, 3193–3230, doi:10.3390/molecules19033193.
17. Cutter, G.R.; Liu, Y. Personalized Medicine: The Return of the House Call? *Neurol. Clin. Pract.* **2012**, *2*, 343–351, doi:10.1212/CPJ.0b013e318278c328.
18. Smilkov, K.; Janevik, E.; Guerrini, R.; Pasquali, M.; Boschi, A.; Uccelli, L.; Di Domenico, G.; Duatti, A. Preparation and First Biological Evaluation of Novel Re-188/Tc-99m Peptide Conjugates with Substance-P. *Appl. Radiat. Isot.* **2014**, *92*, 25–31, doi:10.1016/j.apradiso.2014.06.003.
19. Weineisen, M.; Schottelius, M.; Simecek, J.; Baum, R.P.; Yildiz, A.; Beykan, S.; Kulkarni, H.R.; Lassmann, M.; Klette, I.; Eiber, M.; et al. 68Ga- and 177Lu-Labeled PSMA I&T: Optimization of a PSMA-Targeted Theranostic Concept and First Proof-of-Concept Human Studies. *J. Nucl. Med.* **2015**, *56*, 1169–1176, doi:10.2967/jnumed.115.158550.
20. Singh, A.; van der Meulen, N.P.; Müller, C.; Klette, I.; Kulkarni, H.R.; Türler, A.; Schibli, R.; Baum, R.P. First-in-Human PET/CT Imaging of Metastatic Neuroendocrine Neoplasms with Cyclotron-Produced ⁴⁴Sc-DOTATOC: A Proof-of-Concept Study. *Cancer Biother. Radiopharm.* **2017**, *32*, 124–132, doi:10.1089/cbr.2016.2173.
21. Giddings, J.C. A New Separation Concept Based on a Coupling of Concentration and Flow Nonuniformities. *Sep. Sci.* **1966**, *1*, 123–125, doi:10.1080/01496396608049439.
22. Tarazona, M.P.; Saiz, E. Combination of SEC/MALS Experimental Procedures and Theoretical Analysis for Studying the Solution Properties of Macromolecules. *J. Biochem Biophys Methods* **2003**, doi:10.1016/S0165-022X(03)00075-7.
23. Striegel, A.; Yau, W.; Kirkland, J.; Bly, D. *Modern Size-Exclusion Liquid Chromatography: Practice of Gel Permeation and Gel Filtration Chromatography*; 2nd edition.; Wiley: Hoboken, NJ, USA, 2009.
24. Viebke, C.; Williams, P.A. Determination of Molecular Mass Distribution of K-Carrageenan and Xanthan Using Asymmetrical Flow Field-Flow Fractionation. *Food Hydrocoll.* **2000**, doi:10.1016/S0268-005X(99)00066-1.
25. Wittgren, B.; Wahlund, K.-G. Fast Molecular Mass and Size Characterization of Polysaccharides Using Asymmetrical Flow Field-Flow Fractionation-Multiangle Light Scattering. *J. Chromatogr. A* **1997**, *760*, 205–218, doi:10.1016/S0021-9673(96)00777-7.
26. Lou, J.; Myers, M.N.; Calvin Giddings, J. Separation of Polysaccharides by Thermal Field-Flow Fractionation. *J. Liq. Chromatogr.* **1994**, *17*, 3239–3260, doi:10.1080/10826079408013201.
27. Gigault, J.; Pettibone, J.M.; Schmitt, C.; Hackley, V.A. Rational Strategy for Characterization of Nanoscale Particles by Asymmetric-Flow Field Flow Fractionation: A Tutorial. *Anal. Chim. Acta* **2014**, *809*, 9–24, doi:10.1016/j.aca.2013.11.021.

28. Sun, H.; Cao, D.; Liu, Y.; Wang, H.; Ke, X.; Ci, T. Low Molecular Weight Heparin Based Reduction Sensitive Nanoparticles for Antitumor and Anti-Metastasis of Orthopic Breast Cancer. *Biomater. Sci.* **2018**, *6*, 2172–2188.
29. Floor, M.; Peters, J.A.; van Bekkum, H.; Kieboom, A.P.G.; Koek, J.H.; Smeets, F.L.M.; Niemantsverdriet, R.E. Structural and Conformational Effects on the Complexation of Calcium by 2,3-Dicarboxy Derivatives of B-Cyclodextrin (Cyclomaltoheptaose), Amylose, and Cellulose. **1990**, *203*, 19–32, [https://doi.org/10.1016/0008-6215\(90\)80042-2](https://doi.org/10.1016/0008-6215(90)80042-2).
30. Theisen, C.; Johann, C.; Deacon, M.P.; Harding, S.E. *Refractive Index Increment Data Book for Polymer and Biomolecular Scientists*; Nottingham University Press: Nottingham, USA, 2000.
31. Messaud, F.A.; Sanderson, R.D.; Runyon, J.R.; Otte, T.; Pasch, H.; Williams, S.K.R. An Overview on Field-Flow Fractionation Techniques and Their Applications in the Separation and Characterization of Polymers. *Prog. Polym. Sci.* **2009**, *34*, 351–368, doi:10.1016/j.progpolymsci.2008.11.001.
32. Ratanathanawongs Williams, S.K.; Lee, D. Field-Flow Fractionation of Proteins, Polysaccharides, Synthetic Polymers, and Supramolecular Assemblies. *J. Sep. Sci.* **2006**, *29*, 1720–1732, doi:10.1002/jssc.200600151.
33. Suresha, P.R.; Badiger, M.V.; Wolf, B.A. Polyelectrolytes in Dilute Solution: Viscometric Access to Coil Dimensions and Salt Effects. *RSC Adv.* **2015**, *5*, 27674–27681.
34. DeAngelis, P. Monodisperse Hyaluronan Polymers: Synthesis and Potential Applications. *Curr. Pharm. Biotechnol.* **2008**, *9*, 246–248, doi:10.2174/138920108785161550.
35. Pavlov, G.M.; Zaitseva, I.I.; Gubarev, A.S.; Gavrilova, I.I.; Panarin, E.F. Diffusion-Viscometric Analysis and Conformational Characteristics of Sodium Polystyrenesulfonate Molecules. *Russ. J. Appl. Chem.* **2006**, *79*, 4.
36. Leszczyszyn, O. Hydrodynamic radius–radius of gyration, Size matters: Hydrodynamic Radius Vs Radius of Gyration (Rh versus Rg). Available online: <https://www.materials-talks.com/blog/2012/11/15/size-matters-rh-versus-rg> (accessed on 26 October 2020).
37. Huclier-Markai, S.; Sabatie, A.; Ribet, S.; Kubicek, V.; Paris, M.; Vidaud, C.; Hermann, P.; Cutler, C.S. Chemical and Biological Evaluation of Scandium(III)-Polyaminopolycarboxylate Complexes as Potential PET Agents and Radiopharmaceuticals. *Radiochim. Acta* **2011**, *99*, 653–662, doi:10.1524/ract.2011.1869.
38. Smidsrød, O.; Haug, A.; Larsen, B. The Influence of PH on the Rate of Hydrolysis of Acidic Polysaccharides. *Acta Chem. Scand.* **1966**, *20*, 1026–1034.
39. Karlsson, A.; Singh, S.K. Acid Hydrolysis of Sulphated Polysaccharides. Desulphation and the Effect on Molecular Mass. *Carbohydr. Polym.* **1999**, doi:10.1016/S0144-8617(98)00085-X.
40. Belting, M. Glycosaminoglycans in Cancer Treatment. *Thromb. Res.* **2014**, *133*, S95–S101, doi:10.1016/S0049-3848(14)50016-3.
41. Yip, G.W. Therapeutic Value of Glycosaminoglycans in Cancer. *Mol. Cancer Ther.* **2006**, *5*, 2139–2148, doi:10.1158/1535-7163.MCT-06-0082.
42. Santo, K.P.; Vishnyakov, A.; Kumar, R.; Neimark, A.V. Elucidating the Effects of Metal Complexation on Morphological and Rheological Properties of Polymer Solutions by a Dissipative Particle Dynamics Model. *Macromolecules* **2018**, *51*, 4987–5000, doi:10.1021/acs.macromol.8b00493.
43. Caster, J.M.; Yu, S.K.; Patel, A.N.; Newman, N.J.; Lee, Z.J.; Warner, S.B.; Wagner, K.T.; Roche, K.C.; Tian, X.; Min, Y.; et al. Effect of Particle Size on the Biodistribution, Toxicity, and Efficacy of Drug-Loaded Polymeric Nanoparticles in Chemoradiotherapy. *Nanomed.* **2017**, *13*, 1673–1683, doi:10.1016/j.nano.2017.03.002.
44. Podzimek, S. 5- Asymmetric Flow Field Flow Fractionation. In *Light Scattering, Size Exclusion Chromatography and Asymmetric Flow Field Flow Fractionation*; Wiley: Hoboken, NJ, USA, 2011.
45. Harding, S.E. Analysis of Polysaccharides by Ultracentrifugation. Size, Conformation and Interactions in Solution. In *Polysaccharides I*; Heinze, T., Ed.; Advances in Polymer Science; Springer-Verlag: Berlin/Heidelberg, 2005; Vol. 186, pp. 211–254.
46. Anthonsen, M.W.; Vrum, K.M.; Smidsrod, O. Solution Properties of Chitosans: Conformation and Chain Stiffness of Chitosans with Different Degrees of N-Acetylation. *Carbohydr. Polym.* **1993**, *22*, 193–201.
47. Greenwood, C.T.; Hourston, D.J. Specific Refractive Index Increments of Certain Polysaccharide Systems. *Polymer* **1975**, *16*, 474–476, doi:10.1016/0032-3861(75)90001-4.
48. Senni, K.; Gueniche, F.; Yousfi, M.; Fioretti, F.; Godeau, G.; Collic-Jouault, S.; Ratiskol, J.; Sinquin, C.; Raguénès, G.H.C.; Courtois, A.; et al. Sulfated Depolymerized Derivatives of Exopolysaccharides (EPS) from Mesophilic Marine Bacteria, Method for Preparing Same, and Uses Thereof in Tissue Regeneration. AU2005259078A2, Australia, 12 January 2006.
49. McNaught, A.D.; Wilkinson, A. *Compendium of Chemical Terminology*; 2nd ed.; Wiley: Hoboken, NJ, USA 1997.
50. Guo, M.Q.; Hu, X.; Wang, C.; Ai, L. Polysaccharides: Structure and Solubility. In *Solubility of Polysaccharides*; Xu, Z., Ed.; InTechOpen: London, UK, 2017.
51. Atkins, P.; De Paula, J. *Atkins' Physical Chemistry*. 9th ed.; Oxford University Press: Oxford, UK, 2010.
52. Pitkänen, L.; Tenkanen, M. Field-Flow Fractionation of Cationic Cellulose Derivatives. *Chromatographia* **2019**, *82*, 1827–1832, doi:10.1007/s10337-019-03800-2.
53. Barth, H.G.; Carlin, F.J. A Review of Polymer Shear Degradation in Size-Exclusion Chromatography. *J. Liq. Chromatogr.* **1984**, *7*, 1717–1738, doi:10.1080/01483918408068832.
54. Tande, B.M.; Wagner, N.J.; Mackay, M.E.; Hawker, C.J.; Jeong, M.; Viscosimetric, Hydrodynamic, and Conformational Properties of Dendrimers and Dendrons. *Macromolecules* **2001**, *34*, 8580–8585, doi:10.1021/ma011265g.
55. Chung, M.C.M.; Ellerton, N.F. Viscosity at Low Shear and Circular Dichroism Studies of Heparin. *Biopolymers* **1976**, *15*, 1409–1423, doi:10.1002/bip.1976.360150713.

56. Rathee, V.; Sidky, H.; Sikora, B.; Whitmer, J. Explicit Ion Effects on the Charge and Conformation of Weak Polyelectrolytes. *Polymers* **2019**, *11*, 183, doi:10.3390/polym11010183.
57. Swift, T.; Swanson, L.; Geoghegan, M.; Rimmer, S. The PH-Responsive Behaviour of Poly(Acrylic Acid) in Aqueous Solution Is Dependent on Molar Mass. *Soft Matter* **2016**, *12*, 2542–2549, doi:10.1039/C5SM02693H.
58. Sparks, D.J.; Romero-González, M.E.; El-Taboni, E.; Freeman, C.L.; Hall, S.A.; Kakonyi, G.; Swanson, L.; Banwart, S.A.; Harding, J.H. Adsorption of Poly Acrylic Acid onto the Surface of Calcite: An Experimental and Simulation Study. *Phys. Chem. Chem. Phys.* **2015**, *17*, 27357–27365, doi:10.1039/C5CP00945F.
59. Kasaai, M.R. Calculation of Mark–Houwink–Sakurada (MHS) Equation Viscometric Constants for Chitosan in Any Solvent–Temperature System Using Experimental Reported Viscometric Constants Data. *Carbohydr. Polym.* **2007**, *68*, 477–488, doi:10.1016/j.carbpol.2006.11.006.
60. Grubisic, Z.; Rempp, P.; Benoit, H. A Universal Calibration for Gel Permeation Chromatography. *J. Polym. Sci. [B]* **1967**, *5*, 753–759, doi:10.1002/pol.1967.110050903.
61. Hamielec, A.E.; Ouano, A.C. Generalized Universal Molecular Weight Calibration Parameter in GPC. *J. Liq. Chromatogr.* **1978**, *1*, 111–120, doi:10.1080/01483917808068382.
62. Kasaai, M.R. Intrinsic Viscosity–Molecular Weight Relationship and Hydrodynamic Volume for Pullulan. *J. Appl. Polym. Sci.* **2006**, *100*, 4325–4332, doi:10.1002/app.22324.
63. Jurkin, D.; Wierczinski, B. Analysis of the Kinetic Stability of Yttrium Chelates by Free-Ion Selective Radiotracer Extraction (FISRE). *J. Radioanal. Nucl. Chem.* **2008**, *277*, 91–96, doi:10.1007/s10967-008-0714-7.
64. Hao, C.; Zhao, Y.; Zhou, Y.; Zhou, L.; Xu, Y.; Wang, D.; Xu, D. Interactions between Metal Chlorides and Poly(Vinyl Pyrrolidone) in Concentrated Solutions and Solid-State Films. *J. Polym. Sci. Part. B Polym. Phys.* **2007**, *45*, 1589–1598, doi:10.1002/polb.21138.
65. Feofanova, M.A.; Frantseva, Yu.V.; Lapshin, S.V. Complexation in the Heparin-Metal Ion System. *Russ. J. Coord. Chem.* **2012**, *38*, 373–378, doi:10.1134/S1070328412040033.
66. Karpukhin, L.E.; Feofanova, M.A.; Nikolaeva, L.S.; Mamontov, M.N.; Dobrynina, N.A. Complexation of Magnesium and Calcium Ions with Heparin. *Russ. J. Inorg. Chem.* **2006**, *51*, 908–914, doi:10.1134/S0036023606060106.
67. Rendleman, A. Metal-Polysaccharide Complexes Part II. *Food Chem.* **1978**, *3*, 127–162.
68. Stokes, R.H.; Robinson, R.A. Ionic Hydration and Activity in Electrolyte Solutions. **1948**, *70*, 9.
69. Shannon, R.D. Revised Effective Ionic Radii and Systematic Studies of Interatomic Distances in Halides and Chalcogenides. *Acta Cryst.* **1976**, *32*, 751.
70. Loaëc, M. Uptake of Lead, Cadmium and Zinc by a Novel Bacterial Exopolysaccharide. *Water Res.* **1997**, *31*, 1171–1179, doi:10.1016/S0043-1354(96)00375-2.
71. Fuks, L.; Bünzli, J.-C.G. Lanthanide-Ion Complexation by D -Glucuronic and D -Galacturonic Acids. *Helv. Chim. Acta* **1993**, *76*, 2992–3000, doi:10.1002/hlca.19930760824.
72. Brown, P.L.; Ekberg, C.; Scandium, Yttrium and the Lanthanide Metals. In *Hydrolysis of Metal Ions*; Wiley-VCH Verlag GmbH & Co. KGaA: Weinheim, Germany, 2016; pp. 225–324.
73. Pniok, M.; Kubíček, V.; Havlíčková, J.; Kotek, J.; Sabatie-Gogová, A.; Plutnar, J.; Huclier-Markai, S.; Hermann, P. Thermodynamic and Kinetic Study of Scandium(III) Complexes of DTPA and DOTA: A Step Toward Scandium Radiopharmaceuticals. *Chem. — Eur. J.* **2014**, *20*, 7944–7955, doi:10.1002/chem.201402041.
74. Striegel A.M. Specific refractive index increment ($\partial n/\partial c$) of polymers at 660 nm and 690 nm. *Chromatographia.* **2017**, *80*, 989–996, doi:10.1007/s10337-017-3294-2.
75. Zhang, H.; Lyden, D. Asymmetric-Flow Field-Flow Fractionation Technology for Exomere and Small Extracellular Vesicle Separation and Characterization. *Nat. Protoc.* **2019**, *14*, 1027–1053, doi:10.1038/s41596-019-0126-x.
76. Gigault, J.; Mignard, E.; El Hadri, H.; Grassi, B. Measurement Bias on Nanoparticle Size Characterization by Asymmetric Flow Field-Flow Fractionation Using Dynamic Light-Scattering Detection. *Chromatographia* **2017**, *80*, 287–294.
77. Zimm, B.H. The Scattering of Light and the Radial Distribution Function of High Polymer Solutions. *J. Chem. Phys.* **1948**, *16*, 1093–1099, doi:10.1063/1.1746738.
78. Rudin, A.; Choi, P. Practical Aspects of Molecular Weight Measurements. In *The Elements of Polymer Science & Engineering*; Elsevier: Amsterdam, The Netherlands, 2013; pp. 89–148.
79. McCrackin, F.L. Relationship of Intrinsic Viscosity of Polymer Solutions to Molecular Weight. *Polymer* **1987**, *28*, 1847–1850, doi:10.1016/0032-3861(87)90289-8.
80. Cotte, J.-F.; Bouadam, A.; Sordoillet, A.; Jaudinaud, I.; Chambon, V.; Talaga, P. Determination of Molecular Size Parameters and Quantification of Polyacrylic Acid by High Performance Size-Exclusion Chromatography with Triple Detection. *Anal. Bioanal. Chem.* **2017**, *409*, 2083–2092, doi:10.1007/s00216-016-0155-z.
81. Masuelli, M.A. Mark-Houwink Parameters for Aqueous-Soluble Polymers and Biopolymers at Various Temperatures. **2014**, *2*, 37–43.
82. van Doornmalen, J.; Wolterbeek, H.T. Analysis of Copper Complex Lability Using ^{64}Cu -Equilibration Techniques and Free-Ion Selective Radiotracer Extraction. *Anal. Chim. Acta* **2002**, *12*.
83. Smith, R.M.; Martell, A.E. Critical Stability Constants, Enthalpies and Entropies for the Formation of Metal Complexes of Aminopolycarboxylic Acids and Carboxylic Acids. *Sci. Total Environ.* **1987**, *64*, 125–147, doi:10.1016/0048-9697(87)90127-6.

Chapter 4

Investigation of exopolysaccharides complexation through spectroscopy

I. Introduction

In the previous chapter, the complexation between scandium and EPS-DR and -DRS has been studied and quantified by FISRE, showing that these modified polysaccharides are valid chelators for the theranostic pair $^{44}\text{Sc}/^{47}\text{Sc}$. Nevertheless, no direct information on the structure of the formed complexes was available. Some techniques offer the possibility of both quantifying the interaction and approaching the structure of the formed complexes. One of these techniques, is the time-resolved laser-induced fluorescence spectroscopy (TRLFS), which allows studying the complexation of a luminescent metal ions in aqueous solutions. Scandium does not show any observable luminescence, but, as part of the rare-earth metals, is showing an analogous chemical behaviour to other luminescent lanthanides (Ln), such as europium(III). The free ion Eu^{3+} in aqueous solutions is luminescent. The luminescent properties are influenced by the change in the ligand field when a ligand is displacing water molecules in the hydration sphere. Luminescence properties of Eu^{3+} make this ion an interesting candidate to show how EPSs are behaving when complexing trivalent rare-earth ions. Moreover, in a perspective of optical imaging approach, Eu-EPS complexes – or with other luminescent lanthanides – would be suitable as luminescent probes to investigate biomolecular systems [1].

Fluorescence imaging provides an innovative approach to recognize cancer biomarkers, do imaging of *in vivo* animal models, monitor the effects of anticancer agents and guide the surgery of certain tumors with high sensitivity and specificity. Related to osteosarcoma, an *in vitro* work [2] has already demonstrated the ability of fluorescent probes to display osteogenesis, highlighting their utility as clinical tools for imaging at molecular level. Lanthanide ions are found in living organisms in trace amounts and they are considered to play a biological role [3]. They interact with biological materials and because of their chemical similarity with actinides, they may also act as substitution probes for the actinides. Additionally, it has been clinically evidenced that polygalacturonic acids or polyuronic acids could be efficient as medication drugs in case of heavy-metal poisoning, notably with Pb [4], Sr, Ba or Ra [5]. Fuks and Bunzli have evidenced that galacturonic and glucuronic acids were very efficient to complex lanthanide ions, especially Eu^{3+} .

Fundamental for fluorescence imaging is the building of fluorescent probes that are composed of two parts, a scaffold able to recognize cancer biomarkers, and a fluorophore to signal their presence. The antimetastatic effect of EPSs, would make them a biological scaffold able not only to detect metastasis but also to prevent them, allowing a therapeutic action, so a new

different theranostic approach. To be suitable as luminescent probe, it is necessary that Eu^{3+} be capable of binding strongly and retaining both their binding and luminescence properties under sample assay conditions. Eu^{3+} exhibits a strong propensity to bind negatively charged groups containing oxygen, such as hydroxide, carbonate, phosphate, and also organic carboxylate groups. Typically, these groups are changing the symmetry of the coordination sphere – the Eu(III) luminescence spectrum –, and the luminescence decay time (τ) [6].

In the first part of the following chapter, the chemistry of europium and as some basic principles of TRLFS will be presented. This part will prepare the reader to the second part of the chapter, which is concerning the complexation study between the two polysaccharides of interest, EPS and heparin, and Eu^{3+} written in the form of an article to be submitted in Dalton Transactions.

II. Chemistry of Europium

Europium is a rare-earth metal belonging to the lanthanide series of the periodic table. The electronic configuration of Eu^{3+} is $[\text{Xe}]4f^65d^06s^0$. Eu is the least dense, the softest, and the most volatile element among lanthanides. The pure metal is silvery but because of its high reactivity, metallic Eu rarely looks shiny. Eu quickly reacts with water to form europium hydroxide $\text{Eu}(\text{OH})_3$ [7]. It rapidly oxidizes in air and ignites in the range 150-180°C to form Eu(III) oxide (Eu_2O_3) [8].

Isolated in 1901, Eu was named after the continent of Europe. Being a typical member of the lanthanide series, its predominant oxidation state is +3; the oxidation state +2 is also common and stable under strongly reducing conditions. All the Ln^{3+} ions can be considered as “hard acids”: coordination occurs mostly via ionic bonding interactions, leading to a strong preference for negatively charged donor groups that are also hard bases. Water molecules and hydroxide ions are particularly strong Ln^{3+} ligands. In Ln^{3+} complexes, ligands can entirely influence primary coordination numbers and complex geometry because of a lack of directionality. Eight and nine are the most common coordination numbers of lanthanide complexes. In complexes of 8-fold or 9-fold coordination, Eu^{3+} shows a ionic radii ranging ~ 1.07-1.12 Å [9]: these numbers give us an idea of the size requirements for Eu^{3+} . Binding strengths are supposed to be less than those of transition metal ions and since its low polarizing ability, lanthanide ions do not induce significant changes in the electronic charge distributions at binding sites. Most of the coordination properties of europium(III) are pretty similar to those of divalent alkaline earth metal ions [1].

It can be recalled here that the hydroxo complexes formation of Eu(III) is less extensive than Sc(III) (See Figure 24) [10].

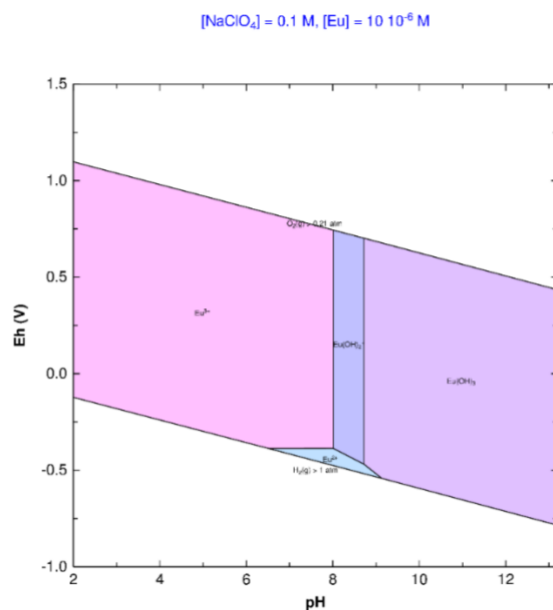


Figure 24. Pourbaix diagram of europium in aqueous solution: $[Eu]_{\text{tot}} = 10^{-5}$ M, $[NaClO_4] = 0.1$ M [11].

Unlike scandium, europium has a well-exploitable quantum fluorescence yield.

III. Time resolved laser fluorescence spectroscopy (TRLFS)

Since europium (III) is showing luminescence properties, TRLFS can be considered a suitable technique to investigate the interaction of this lanthanide in biosystems, as well as to elucidate its chemical behaviour on a molecular level [12]. TRLFS is a speciation technique for fluorescent actinide and lanthanide ions that allows discriminating, quantifying, and structurally evaluating the different species present in solution. The discrimination among species is obtained through different excitation/emission spectra and luminescence decay times of the species. Since the fluorescence intensities are proportional to their concentrations, the quantification of species is possible. Moreover, the structure of those species could be assumed by their spectral signatures and decay times [13,14].

The excited Eu³⁺ cation emits luminescence bands coming from 4f-4f intra-configuration transitions, which are the most easily relaxed. Figure 25 below represents a partial diagram of the energy levels of the Eu³⁺ ion in solution.

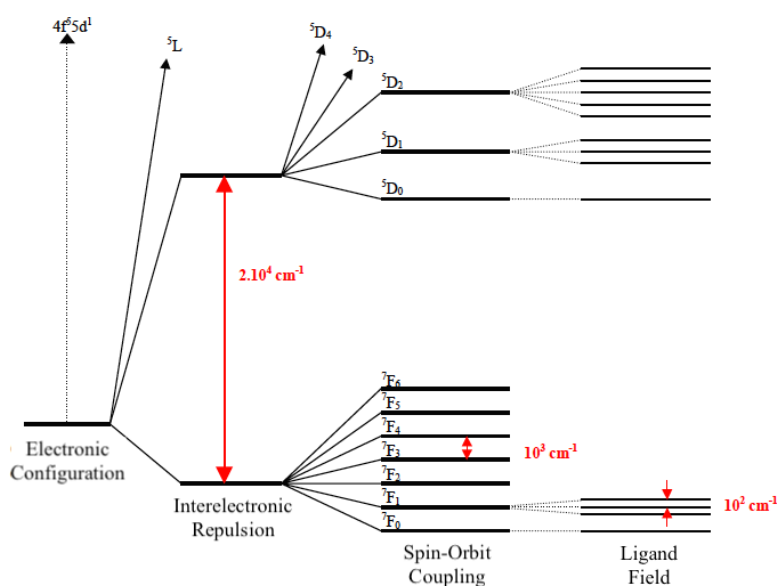


Figure 25. Diagram relating energy levels of Eu^{3+} . Figure adapted from Lourenço 2008 [15].

In TRLFS, the excited states of actinide and lanthanide ions are achieved by selective irradiation by pulsed lasers [16], usually from the 7F_0 ground state to the 5L_6 excited state – $^5L_6 \leftarrow ^7F_0$, $\bar{\nu} = 25,400 \text{ cm}^{-1}$, $\lambda = 393.70 \text{ nm}$ [17]. For europium(III) complexes in aqueous solutions, the most intense emissions are emitted from the 5D_0 level (see Figure 26) to the 7F_j ground state manifold ($0 \leq j \leq 6$). Analysis of the $^5D_0 \rightarrow ^7F_j$ transitions provide information about ion coordination. After coordination, these transitions are not situated anymore in the same energy level of previous free ion system: complexation causes a deformation of electronic cloud surrounding the ion. The $^5D_0 \rightarrow ^7F_0$ transition is nondegenerate and weakly restricted by selection rules: for single complexes with the same ligand, which show a spherical symmetry (high symmetry system), the intensity of this transition is very weak. The appearance of a split line or of multiple lines within this excitation region can occur only if the ligands surrounding the ion are qualitatively different; this change causes a loss of symmetry (low symmetry system): the greater is the change in symmetry, greater the intensity of the transition [18,19].

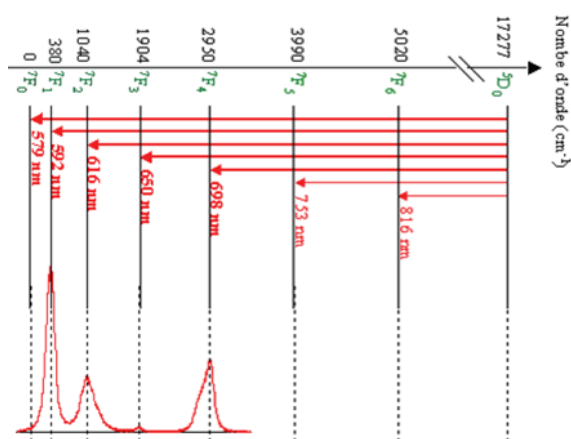


Figure 26. Energy level of aquo-ion Eu^{3+} and relative transitions. Figure adapted from Lourenço 2008 [15].

The intensities of ${}^5\text{D}_0 \rightarrow {}^7\text{F}_1$ and ${}^7\text{F}_2$ emissions, instead, are sensitive to complexation. Even in low symmetry systems the ${}^5\text{D}_0 \rightarrow {}^7\text{F}_1$ transition retains its magnetic dipole character, and its radiative transition is not much dependent on the ligand environment – except in particular instances [20]. In contrast, the ${}^5\text{D}_0 \rightarrow {}^7\text{F}_2$ and ${}^5\text{D}_0 \rightarrow {}^7\text{F}_4$ transitions have basically an electric dipole nature, and their radiative transitions are very sensitive to the detailed nature of the ligand environment [1] – ${}^5\text{D}_0 \rightarrow {}^7\text{F}_2$ is noted hypersensitive to the change in complexation symmetry.

The luminescence intensity and decay time of europium(III) species have been used to gain information on the composition and structure of the first coordination sphere of these ions in solution. The radiative constant k of europium(III) – *i.e.* the inverse of the decay time, $k = 1/\tau$ – in aqueous solution decreases linearly as the number of water molecules in the inner coordination sphere increases. This is a result of efficient energy transfer from the excited state (${}^5\text{D}_0$) of europium(III) to the O-H vibration of the coordinated water molecules [21]. In order to determine the number of water molecules, which are linked to Eu^{3+} ion in the inner hydration sphere, the empiric relationship established by Kimura *et al.* could be used [22]. Sc-EPS (from chapter 3) and Eu-EPS systems will be compared and discussed.

All the work dealing with EPS-Eu interactions has been proposed as an article in Dalton Transactions.

References

- [1] Richardson, F.S. Terbium(III) and Europium(III) Ions as Luminescent Probes and Stains for Biomolecular Systems. *Chem. Rev.* **1982**, 82, 541–552.
- [2] Lin, C.-C.; Chang, W.H.-S.; Cheng, T.-M.; Chiu, L.-H.; Wang, Y.-H.; Lin, C.-A.J.; Ho, Y.-S.; Zuo, C.S.; Wang, Y.-M.; Lai, W.-F.T. Two New, near-Infrared, Fluorescent Probes as Potential Tools for Imaging Bone Repair. *Sci. Rep.* **2020**, 10, 2580, doi:10.1038/s41598-020-59522-1.

- [3] Fuks, L.; Bünzli, J.-C.G. Lanthanide-Ion Complexation by D -Glucuronic and D -Galacturonic Acids. *Helv. Chim. Acta* **1993**, *76*, 2992–3000, doi:10.1002/hlca.19930760824.
- [4] Kohn, R. Dissociation Constants of D-Galacturonic and D-Glucuronic Acid and Their O-Methyl Derivatives. 8.
- [5] Vanderborgh, O. *Reprints on Prevention of Uptake on Incorporation of Radioactive Heavy Alkaline Earth Metals in Man, Mice, Swine*; Belgian Nuclear Centre: Mol, 1981;
- [6] Weissman, S.I. Intramolecular Energy Transfer The Fluorescence of Complexes of Europium. *J Chem Phys* **1942**, *10*, 214–217.
- [7] Ramírez-García, J.J.; Jiménez-Reyes, M.; Solache-Ríos, M.; Fernández-Ramírez, E.; López-González, H.; Rojas-Hernández, A. Solubility and First Hydrolysis Constants of Europium at Different Ionic Strength and 303 K. 5.
- [8] Ugale, A.; Kalyani, T.N.; Dhoble, S.J. Potential of europium and samarium β -diketonates as red light emitters in organic light-emitting diodes. In *Lanthanide-Based Multifunctional Materials*; Elsevier, 2018; pp. 59–97 ISBN 978-0-12-813840-3.
- [9] Shannon, R.D. Revised Effective Ionic Radii and Systematic Studies of Interatomic Distances in Halides and Chalcogenides. *Acta Cryst.* **1976**, *32*, 751.
- [10] Brown, P.L.; Ekberg, C. Scandium, Yttrium and the Lanthanide Metals. In *Hydrolysis of Metal Ions*; Wiley-VCH Verlag GmbH & Co. KGaA: Weinheim, Germany, 2016; pp. 225–324 ISBN 978-3-527-65618-9.
- [11] Hummel, W.; Berner, U.; Curti, E.; Pearson, F.J.; Thoenen, T. *Nagra/PSI Chemical Thermodynamic Data Base 01/01*; NAGRA: Wettingen, Switzerland, 2002; p. 564;
- [12] Heller, A.; Rönitz, O.; Barkleit, A.; Bernhard, G.; Ackermann, J.-U. Complexation of Europium(III) with the Zwitterionic Form of Amino Acids Studied with Ultraviolet—Visible and Time-Resolved Laser-Induced Fluorescence Spectroscopy. *Appl. Spectrosc.* **2010**, *64*, 930–935, doi:10.1366/000370210792081127.
- [13] Saito, T.; Aoyagi, N.; Kimura, T. Time-Resolved Laser-Induced Fluorescence Spectroscopy Combined with Parallel Factor Analysis: A Robust Speciation Technique for UO₂²⁺. *J. Radioanal. Nucl. Chem.* **2015**, *303*, 1129–1132, doi:10.1007/s10967-014-3465-7
- [14] Saito, T.; Sao, H.; Ishida, K.; Aoyagi, N.; Kimura, T.; Nagasaki, S.; Tanaka, S. Application of Parallel Factor Analysis for Time-Resolved Laser Fluorescence Spectroscopy: Implication for Metal Speciation Study. *Environ. Sci. Technol.* **2010**, *44*, 5055–5060, doi:10.1021/es9036995.
- [15] Lourenço, V. Etude de la Spéciation des Radionucléides avec des molécules d'intéret biologique par Approche Spectroscopométrique. 2008.
- [16] Collins, R.N.; Saito, T.; Aoyagi, N.; Payne, T.E.; Kimura, T.; Waite, T.D. Applications of Time-Resolved Laser Fluorescence Spectroscopy to the Environmental Biogeochemistry of Actinides. *J. Environ. Qual.* **2011**, *40*, 731–741, doi:10.2134/jeq2010.0166.
- [17] Carnall, W.T.; Fields, P.R.; Rajnak, K. Electronic Energy Levels of Trivalent Lanthanide Aquo Ions. IV. Eu³⁺. *Chem. Phys* **1968**, *49*, 4450–4455
- [18] Ferrand, A.-C. Complexes Luminescents de Lanthanides avec des Dérivés du Cyclène comme Briques pour l'Ingénierie de Sondes Analytiques Biomédicales, 2004.
- [19] Gallagher, P.K. Absorption and Fluorescence of Europium(III) in Aqueous Solutions. *J. Chem. Phys.* **1964**, *41*, 3061–3069, doi:10.1063/1.1725678
- [20] Colette, S.; Amekratz, B.; Madic, C.; Berthon, L.; Cote, G.; Moulin, C. Europium(III) Interaction with a Polyaza-Aromatic Extractant Studied by Time-Resolved Laser-Induced Luminescence: A Thermodynamic Approach. *Inorg. Chem.* **2004**, *43*, 6745–6751.
- [21] Lis, S.; Choppin, G.R. Luminescence Study of Europium(III) Complexes with Several Dicarboxylic Acids in Aqueous Solution. *J. Alloys Compd.* **1995**, *225*, 257–260.
- [22] Kimura, T.; Kato, Y.; Takeishi, H.; Choppin, G.R. Comparative Study on the Hydration States of Cm(III) and Eu(III) in Solution and in Cation Exchange Resin. *J. Alloys Compd.* **1998**, *271–273*, 719–722.

IV. Luminescence spectroscopic investigations of europium(III) complexation with exopolysaccharides from a marine bacterium.

Article submitted to Dalton Transactions (IF = 4.052)

Luminescence spectroscopic investigations of europium(III) complexation with exopolysaccharides from a marine bacterium

Sandrine Huclier-Markai^{a,b}, Mattia Mazza^{a,b}, Cyrille Alliot^{a,c}, and Pascal E. Reiller^d

Received 00th January 20xx,
Accepted 00th January 20xx

DOI: 10.1039/x0xx00000x

The potential of naturally occurring polysaccharides to complex heavy metals, especially lanthanides, has been assessed by time-resolved laser-induced fluorescence spectroscopy (TRLFS). Since these polysaccharides are polyelectrolytes, their conformation could affect the complexation properties, thus viscosimetric measurements were performed as a function of their concentration and the background electrolyte concentration. Polysaccharides conformation exhibited a lower hydrodynamic volume for the highest ionic strengths. The resulting random-coiled conformation could affect the complexation with metal for high concentration but no change was evidenced when increasing Europium concentration. Therefore, two sites of complexation of Eu(III) were evidenced by TRLFS on heparin whereas only one site was evidenced on two sulfated exopolysaccharides produced from a marine bacteria.

Introduction

Extracellular polymeric substances (EPS) are playing a crucial role in heavy metal bio-adsorption, but the interaction between heavy metals and EPS remains unclear. EPS are usually complex high molecular mixtures of biopolymers secreted by microorganisms and mainly consist of extracellular proteins, polysaccharides and humic substances. Heavy metal pollution has aroused intense concern, because of significant hazard posed by such metals to human health and the environment. The interaction of heavy metals with humic/fulvic substances has been a wide area of research for decades now and has led to many papers [1-5]. However, little is known about the interactions of polysaccharides with heavy metals.

The interaction between carbohydrates and their derivatives and metal ions has already been observed, but the field of sugar type complexes continued to remain largely unexplored. One of the reasons is that the quantitative characterization of metal ion coordination equilibria is difficult due to the low stability of the complexes in neutral or acidic aqueous conditions. The low electron densities on these donor oxygens case, in spite of their relatively large number in one ligand, that they do not readily substitute the water molecules bonded in the first coordination sphere of the metal ions. With increasing pH, the hydrolysis of some metal ions prevents the coordination. Complex formation

could only be expected in strongly alkaline solutions after deprotonation of alcoholic hydroxyl groups. In polysaccharides, the species are in anomeric and conformational equilibrium and isomers could interact in different ways with metal ions.

Lanthanide ions are found in living organisms in trace amounts and they are considered to play a biological role [6]. They interact with biological materials and because of their chemical analogy with actinides at their +III redox state, they may also act as substitution probes for the actinides Pu(III), Am(III), or Cm(III). Additionally, it has been clinically evidenced that polygalacturonic acids or polyuronic acids could be efficient as medication drugs in case of heavy-metal poisoning, notably with Pb [7], Sr, Ba, or Ra [8]. Fuks and Bunzli [6] have evidenced that galacturonic and glucuronic acids were very efficient to complex lanthanide ions, especially Eu³⁺.

Polysaccharides from a marine environment revealed a growing interest, notably for their biological properties in cell therapy and tissue engineering [9]. Marine polysaccharides from a bacterial source can be produced under totally controlled conditions in bioreactors⁷ compared to other polysaccharides from eukaryotes. Among these marine polysaccharides, an exopolysaccharide (EPS) extracted from *Alteromonas infernus*, has raised interest from its high potentiality in cell therapy and tissue engineering. The repeating unit of this EPS consists of a monosulphated nona-saccharide composed of six neutral hexoses acids and three uronic ones, among those the galacturonic acid unit bears a sulphate group. It shows a high molecular weight (> 10⁶ g/mol) and a low sulphate content (< 10%) [10].

The EPS has been submitted to a radical depolymerisation and then oversulphation (OS), which reduces the molecular weight with increasing the sulphate content. The hypothetical

^a GIP ARRONAX, 1 rue Aronnax, F-44817 Nantes Cedex 3, France.

^b SUBATECH, 4 rue Alfred Kastler, BP 20722, 44307 Nantes Cedex 3, France

^c INSERM U892- 8 quai Moncoussu, F-44007 Nantes Cedex 1, France.

Université Paris-Saclay, CEA, Service d'Etudes Analytiques et de Réactivité des Surfaces (SEARS), F-91191, Gif sur Yvette, France.

† Correspondence: sandrine.huclier@subatech.in2p3.fr Tel.: +33-(0)51-85-85-37 or 33-(0)28-21-25-23 (FR)

Electronic Supplementary Information (ESI) available: [details of any supplementary information available should be included here]. See DOI: 10.1039/x0xx00000x

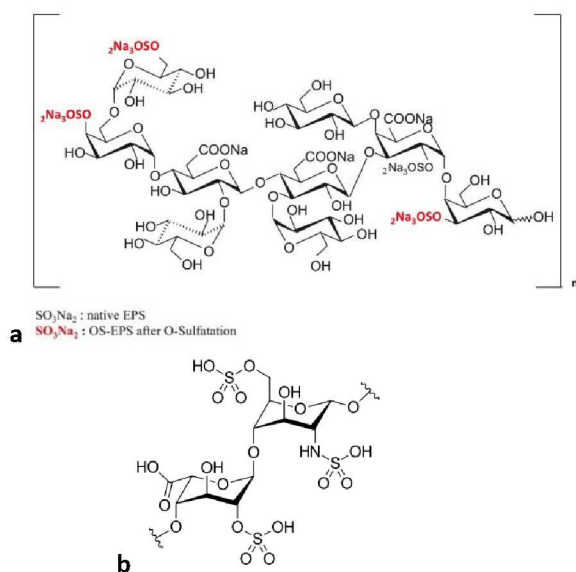


Figure 1. Structures of two GAG, respectively EPS and Heparin. (a) Proposed structure of EPS and sulphated position after over-sulphation reaction. 13 (b) Heparin: The major repeating unit is the tri-sulphated disaccharide 2-O-sulfo- α -L-iduronic acid 1⁴ linked to 6-O-sulfo-N-sulfo- α -D-glucosamine.

structure of the over-sulphated exopolysaccharide (OS-EPS), has been proposed (**Error! Reference source not found.**) [10]. A tentative structure of hexose units that could be sulphated after the oversulphation reaction according to NMR spectroscopy is also indicated in **Error! Reference source not found.** [10–11].

These compounds belong to glycosaminoglycan (GAG). Another very important GAG molecule is heparin, which is a polydisperse, highly sulphated polysaccharide molecule composed of repeated 1–4 linked uronic acid and glucosamine. Karpukhin et al. [12] have determined the protonation constant ($\log K = 3.66$) for heparin corresponding to the carboxylic group. Glycans are part of the outer membrane of bacteria. Soluble metal ions could thus interact with these polysaccharides. The understanding of the binding mechanisms at the molecular level is thus essential. Algal polysaccharides such as fucoidans – and especially their low-molecular-weight fucoidans – have been shown to complex heavy metals [13, 14].

In this work, the potential of these EPS and heparin to complex rare earth metals, especially lanthanides, has been assessed. The complexation of Eu^{3+} with these two EPS and heparin was studied by time-resolved laser-induced fluorescence spectroscopy (TRLFS). This technique has been preferred over potentiometric titrations that could affect the integrity of the polymer chain, by exposing it to very acidic and very alkaline pH hydrolysis. TRLFS is a very convenient tool for detecting and characterizing fluorescent lanthanide speciation – and especially europium(III) –, at trace concentrations. This method is sensitive to changes in the chemical environment of the metal through modifications of fluorescence spectra and decay-time of the excited state [15]. The obtained spectroscopic data – *i.e.* spectra, peak maxima, intensities, and decay-times – give valuable information identifying the

speciation of eventual Eu(III)-polysaccharides complexes. Similar works were conducted on α -D-glucose 1-phosphate, on glucose 6-phosphate, fructose 6-phosphate, lipopolysaccharides or on peptidoglycan with uranium (VI) [16–19].

As polymer conformation importantly could influence complexation [20], the viscosimetric behaviour of the polysaccharides have been studied.

Results and discussion

A – Formation of complexes

Error! Reference source not found. shows the TRLFS spectra of Eu(III) using the least dispersive grating ($300 \text{ lines mm}^{-1}$) as a function of the metal-to-ligand ratio, for the three ligands of interest (*i.e.* heparin, EPS-DR and -DRS). The intensity of the hypersensitive ${}^5\text{D}_0 \rightarrow {}^7\text{F}_2$ transition (ca. 615 nm) relative to the ${}^5\text{D}_0 \rightarrow {}^7\text{F}_1$ transition (ca. 590 nm) was significantly increased for EPS-DR and -DRS indicating the progress of Eu(III) complexation via inner-sphere complexation mechanism [21]. The final increase was comparable between EPS-DR, -DRS, and heparin complexes. All of these spectral changes indicate the complexation of Eu(III) by the polysaccharides.

The luminescence spectra of the Eu(III) EPS-DR, -DRS, and heparin complexes exhibit an additional emission band ca. 578 nm corresponding to the Laporte forbidden ${}^5\text{D}_0 \rightarrow {}^7\text{F}_0$ transition, which occurs only upon deformation of the spherical symmetry of the Eu^{3+} aqua ion [22].

The shape and barycentre of the ${}^5\text{D}_0 \rightarrow {}^7\text{F}_4$ transition (ca. 700 nm) are distinct for each polysaccharides. The ${}^5\text{D}_0 \rightarrow {}^7\text{F}_4$ transition (theoretically degeneracy of 9) is split into 4 levels in crystal field in D_3 symmetry for instance [23]. At this stage, no attempt to define the geometry of the complexes has been made due to the inevitable convolution of the spectra with the spectrometer's parameters, but these changes in ${}^5\text{D}_0 \rightarrow {}^7\text{F}_4$ transition are consistent with a decrease in symmetry of the Eu sites in polysaccharides upon complexation.

Using the \overline{M}_w of heparin, EPS-DR and -DRS were determined in our previous work [24], it is possible to calculate the number of mean carboxylic moieties per chain. This value of 19 for heparin was in agreement with the number of carboxylic groups found by Helbert and Marini for a heparin sodium salt [25]. Then, it was considered only one carboxylic group by disaccharide unit. The number of disaccharide units was calculated by dividing the \overline{M}_w of heparin by the \overline{M}_w of the disaccharide. For the heparin sodium salt with $\overline{M}_w = 18.32 \text{ kDa}$, the number of carboxylic groups was found to be 26. The same type of calculation was done for EPS-DR and -DRS in Table 1.

Table 1. characteristics of polysaccharides

Molecule	\overline{M}_w (kDa)	n_{COOH} per chain	number of disaccharide units
Heparin	18.32 (21.4)	19	26
EPS-DR	26.6	45	15
EPS-DRS	57.0	81	27

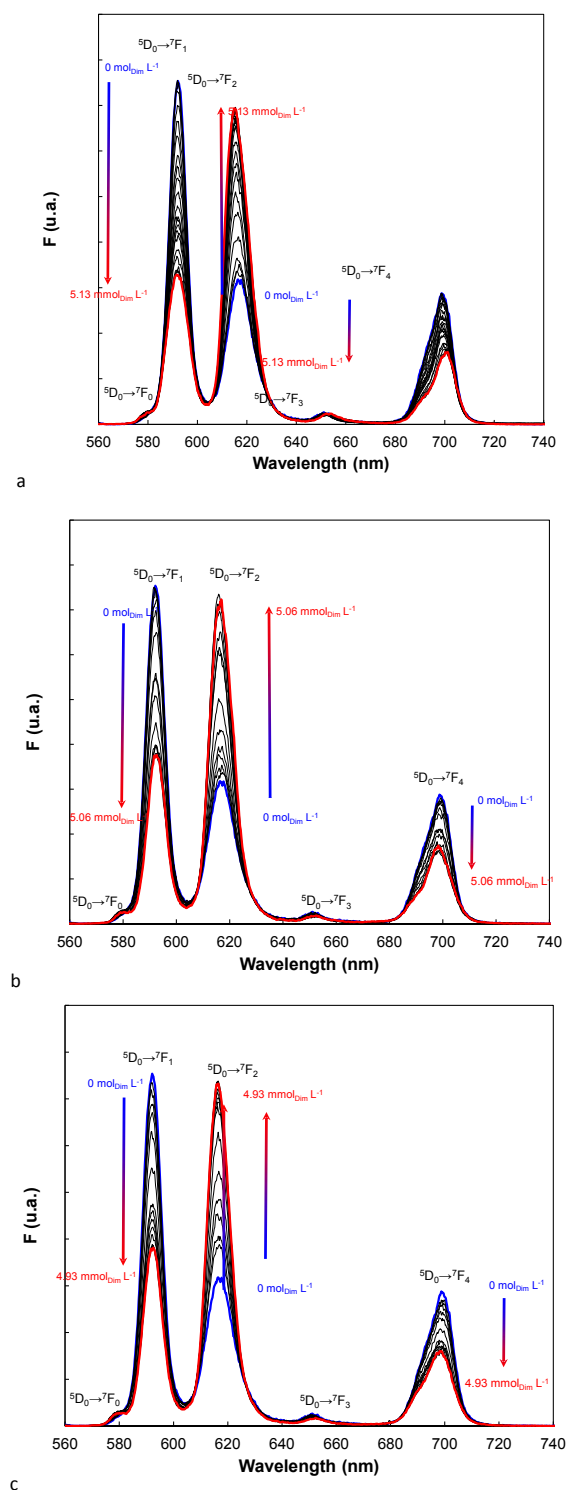


Figure 1. TRLFS spectra of Eu(III) ($[Eu^{3+}] = 10^{-5} \text{ mol L}^{-1}$) at pH = 6 normalised to the total area of (a) Heparin ($c = 2.3 \cdot 10^{-4}$ to $6.2 \cdot 10^{-8} \text{ mol L}^{-1}$), (b) EPS-DR ($c = 7.7 \cdot 10^{-8}$ to $2.9 \cdot 10^{-4} \text{ mol L}^{-1}$), (c) EPS-DRS ($c = 4.2 \cdot 10^{-8}$ to $1.6 \cdot 10^{-4} \text{ mol L}^{-1}$). Concentrations of polymers are reported in terms of monomeric units; $\lambda_{exc} = 593.8 \text{ nm}$, $D = 10 \mu\text{s}$, $W = 50 \mu\text{s}$, grating $300 \text{ lines mm}^{-1}$.

The differences of the complexation site symmetries in heparin, DR, and DRS are shown with a higher dispersive grating ($1800 \text{ lines mm}^{-1}$) in **Error! Reference source not found.** First, the non-degenerated ${}^5D_0 \rightarrow {}^7F_0$ transition seem to be more red-shifted in Eu-DR and -DRS than in Eu-heparin, which could be indicative of either a higher charged complexing entity [26] of a higher coordination [27]. It seems that the supposedly less sensitive to complexation magnetic dipole ${}^5D_0 \rightarrow {}^7F_1$ transition is relatively similar in Eu-DR and -DRS complexes but is significantly different in Eu-heparin. There is an obvious lowering of the band degeneracy in ${}^5D_0 \rightarrow {}^7F_1$, where three components could be seen in Eu-heparin spectrum, which indicates a point symmetry group C_{2v} or lower envisaged for the Eu-Heparin complex [28]. A higher symmetry could be envisaged for Eu-DR and -DRS. The analysis of the ${}^5D_0 \rightarrow {}^7F_2$ transitions is also showing different symmetries between Eu-Heparin complex, and the Eu-DR and -DRS complexes. The clear band ca. 611 nm for Eu-heparin complex only corresponds to a shoulder for Eu-DRS and can be barely distinguished for Eu-DR. The change in complexation site symmetry in heparin with Eu concentration is confirmed in the spectra of Fig. 4 acquired with the $1800 \text{ lines mm}^{-1}$ grating. The ligand field from 0.3 to $30 \mu\text{mol L}^{-1}$ of Eu(III) is clearly changed both for the supposedly less sensitive magnetic dipole ${}^5D_0 \rightarrow {}^7F_1$ transition (**Error! Reference source not found.**a) and for the hypersensitive ${}^5D_0 \rightarrow {}^7F_2$ transition (**Error! Reference source not found.**b). It can also noteworthy that the low Eu concentration spectra are very reminiscent of the ${}^5D_0 \rightarrow {}^7F_2$ spectra obtained for the Eu-DR and -DRS species (Fig. 3b). It can be then proposed that the Eu complexation sites in DR and DRS are similar to one of the heparin complexation sites.

Metal coordination can lead to drastic changes of polymer morphology, formation of clusters, and, ultimately, a sol-gel transition that affect the solution rheology. Although metal coordination is ubiquitous in polymeric systems, the physical mechanisms of coordination-induced morphological and rheological changes are still poorly understood due to the multiscale nature of this phenomenon.

B – Conformation of complexes

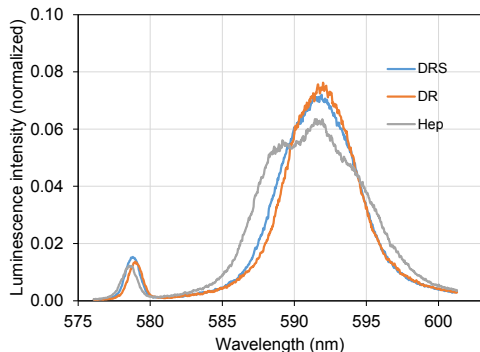
The possible change in conformation was monitored through the polymer's intrinsic viscosity $[\eta]$ in solution, by varying the ionic strength of solvent for heparin. This rearrangement was related to the hydrodynamic volume (V_h). It was calculated using the viscosity-average molar mass (M_v) and the intrinsic viscosity $[\eta]$, that were both present in the Mark-Houwink-Sakurada (MHS) equation [29-30]. Cations from the background electrolyte caused a decrease in Debye length, and a shield effect that reduced the electrostatic repulsion of the ionized groups, leading thus to a drop of the viscosity [31]. Indeed, electrostatic interactions are very long-range (about 1000 nm) in pure water but quickly become screened in the presence of added salt.

That's why, dilution in pure water, polyelectrolytes adopt an elongated conformation under the effect of electrostatic repulsions and the length of the chain is proportional to the

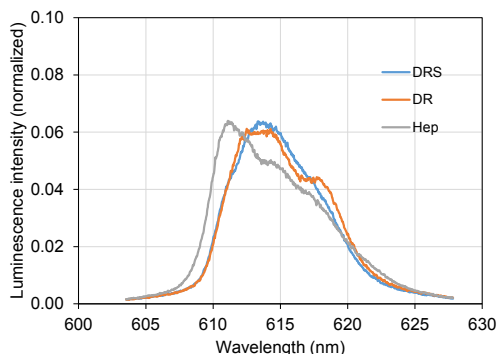
ARTICLE

Dalton transactions

number of the monomers that make it up. However, the chain is not fully stretched and it was showed that the concept of electrostatic blob allows for both account of interactions long-range electrostatic at the monomers.

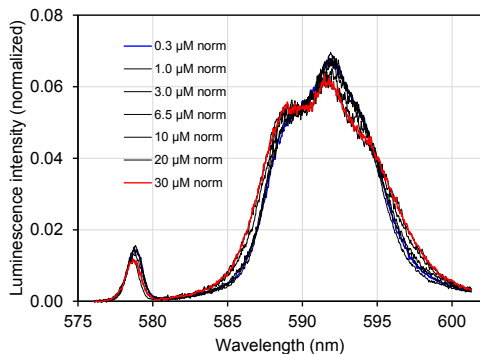


a

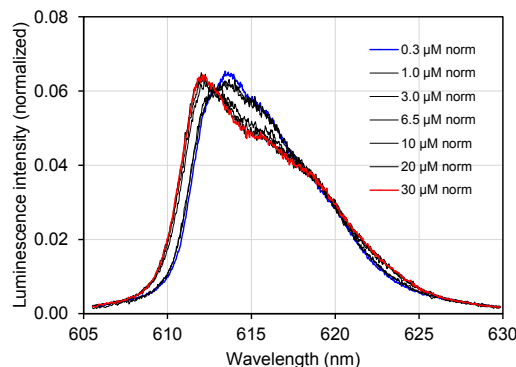


b

Figure 3. TRLFS spectra of Eu(III) ($[Eu] = 1.10^{-5} \text{ mol L}^{-1}$) at pH = 6 normalised to the total area of each spectrum of Heparin ($c = 1.7 \cdot 10^{-6} \text{ mol L}^{-1}$), DR ($C = 2.9 \cdot 10^{-4} \text{ mol L}^{-1}$) and DRS ($C = 1.6 \cdot 10^{-4} \text{ mol L}^{-1}$); $\lambda_{exc} = 593.8 \text{ nm}$, $D = 10 \mu\text{s}$, $W = 50 \mu\text{s}$, grating 1800 lines mm^{-1}



a



b

Figure 4. TRLFS spectra of Eu(III) ($[Eu] = 3.10^{-7} - 3.10^{-5} \text{ mol L}^{-1}$) at pH = 6 normalised to the total area of (a) Heparin ($c = 4 \times 10^{-4} \text{ mol L}^{-1}$); $\lambda_{exc} = 593.8 \text{ nm}$, $D = 10 \mu\text{s}$, $W = 50 \mu\text{s}$, grating 1800 lines mm^{-1}

When the polyelectrolytes are very heavily charged, the conformation is very stretched chain carrying a large number of charges creates an interoperable electrostatic potential strongly with the counter-ions. From our previous work [24], it was observed that at low polyelectrolyte concentrations, $\ln[\eta]$ increased with decreasing c . This effect was explained by the increase of the Debye length with dilution, which reduces the screening of the charges fixed on the chain and strengthens their mutual repulsion. This was in agreement with the observation of Pavlov et al. [31] on highly charged polyelectrolytes. As a result, the size of the polyion increased. The behaviour of EPS-DR and -DRS observed at the highest ionic strengths was explained by a more important folding of the molecules induced by their larger structure

The viscosimetric behaviour of Europium-heparin system was studied as a function of the metal concentration and in dilute aqueous solutions containing variable amounts of NaCl.

Results of the relative viscosity $\ln \eta_r$ heparin is presented in **Error! Reference source not found.a**. The relative viscosity increased with an increasing Europium concentration, for a constant polymer concentration, but was progressively suppressed as the salinity of the solvent rose. This was in agreement with the viscosimetric behaviour of other types of polyelectrolytes [32]. By contrast, the solution did not exhibit the same behaviour when the concentration of the background electrolyte reached 0.5 mol L^{-1} . The repulsion of the charges of the functional groups of heparin with the ones from the background electrolyte led to reduce the hydrodynamic volume. Hence, at 0.5 mol L^{-1} , the Eu-heparin system exhibited a random-coil shape, whereas at 0.1 and 0.2 mol L^{-1} , the system was more under a linear shape.

When plotting the $\ln \eta_{sp/c}$, that allowed an estimation of $[\eta]$, it was observed in **Error! Reference source not found.b** that at low ionic strength, $\ln \eta_{sp/c}$ increased with increasing $[Eu^{3+}]$. This effect was caused by the fact that with dilution, the volume in which the counterions were spread increased, thus reducing the screening of the charges fixed on the chain and strengthening their mutual repulsion. This was in agreement with the observation of Pavlov et al. [31] The behaviour of Eu(III)-heparin observed at the highest ionic strengths, as seen

in **Error! Reference source not found.**, could be explained by a more important folding of the molecule induced by its larger structure. Therefore, the absence of drastic changes in viscosity induced by europium, seems to evidence the assumption that there is no change in the conformation, or if there is a change in conformation, it does not affect the europium complexation. Nonetheless, if there is a change in the conformation with the ionic strength, the area ratio of the ${}^5D_0 \rightarrow {}^7F_2$ and the ${}^5D_0 \rightarrow {}^7F_1$ transition from TRLFS (Fig.2) would change.

C- Determination of the complexation constants

1. Isotherms

The complexation isotherms in **Error! Reference source not found.** are plotted from the normalized total area of spectra (**Error! Reference source not found.**), and the values of dimeric groups (Table 1). For each metal-to-ligand ratio, there is a well-defined spectrum and therefore a constant relationship. From the shape of the isotherm of Eu(III)-heparin

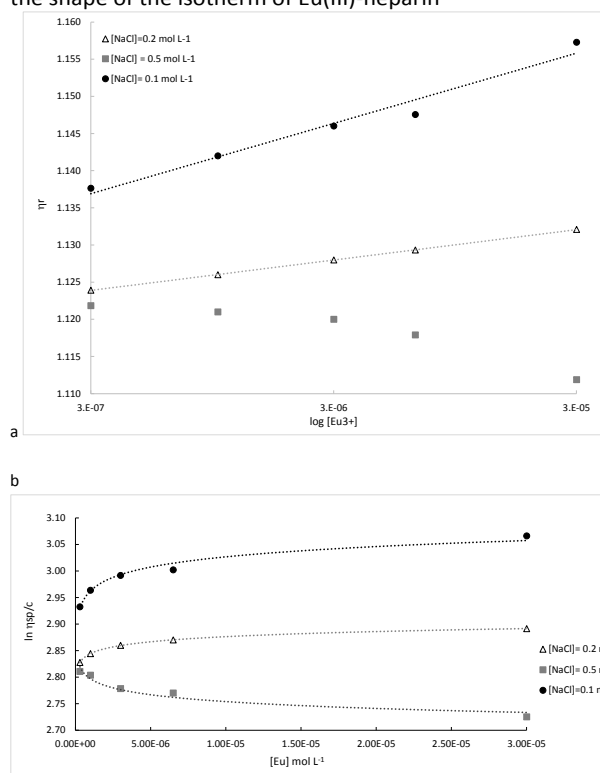


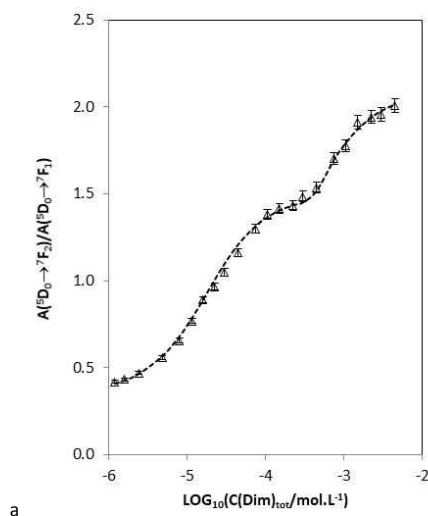
Figure 5. (a) Relative viscosity and (b) Intrinsic Viscosity of heparin ($c = 4.10^{-4}$ mol L⁻¹) as a function of Europium concentration ($[Eu^{3+}] = 3.10^{-7} - 3.10^{-5}$ mol L⁻¹) and for different background electrolyte solutions of NaCl (0.1 to 0.5 mol L⁻¹).

system (**Error! Reference source not found.a**), it seems that there is a change in the symmetry for dimer concentration higher than 10^{-3} mol L⁻¹. This change was confirmed by studying the fluorescence of europium at different concentrations but with the same stoichiometric dimer/Eu(III) ratios. Assumptions can be made to explain the origin of this change: either complex of different stoichiometry are present, or there are different complexation sites, or a conformation change occurs.

From **Error! Reference source not found.a**, for the lowest concentrations of Eu, at $I = 0.1$ M, the ratio of fluorescent peaks remains steady, and then it suddenly increased. Similar observations could be made for $I = 0.05$ M and 0.5 M. This means that the chemical environment of complex is significantly different and this applies for every ionic strength considered. This is confirmed when plotting the fluorescence intensity of the ${}^5D_0 \rightarrow {}^7F_2$ and the ${}^5D_0 \rightarrow {}^7F_1$ transition as a function of Eu concentration (Fig 7b). Luminescence increases for each ionic strength considered when increasing Eu concentration (Fig 7c), while there is a decrease in the intrinsic viscosity.

For heparin, it was noticed in **Error! Reference source not found.** that there is a slight change in the spectra meaning that the environment around Eu(III) is slightly different. It was assumed that this change is partially due to a lowering of degeneracy.

Finally, the emission decay-time varies with complexation. For EPS-DR and -DRS, we observed mono-exponential luminescence decay, while for Eu-Heparin a bi-exponential was necessary. For EPS-DR and DRS, the luminescence decay-times



a

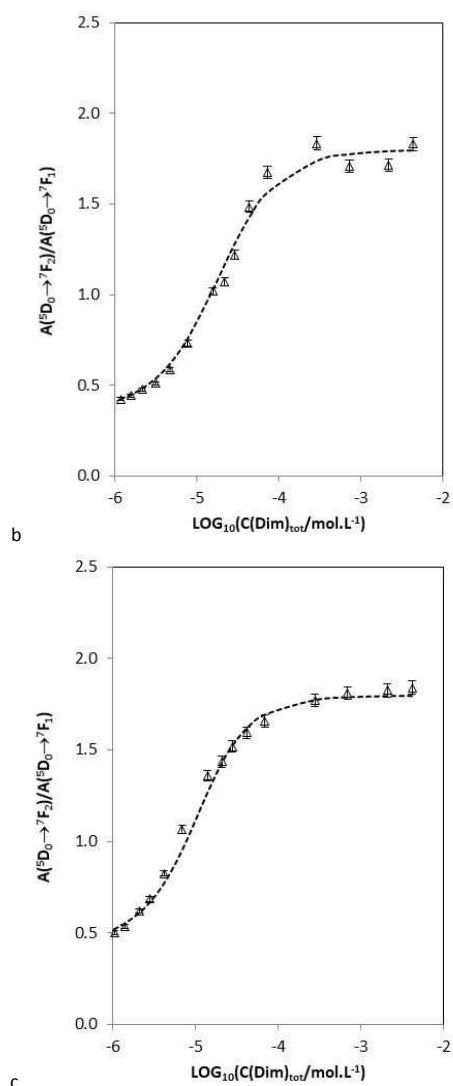


Figure 6. Isotherms of Eu(III)-polysaccharides from TRLFS normalised to the total area ($[Eu^{3+}] = 10^{-5} \text{ mol L}^{-1}$) at pH = 6 of (a) Heparin, (b) EPS-DR, (c) EPS-DRS. Concentrations of polymers are reported in terms of monomeric units.

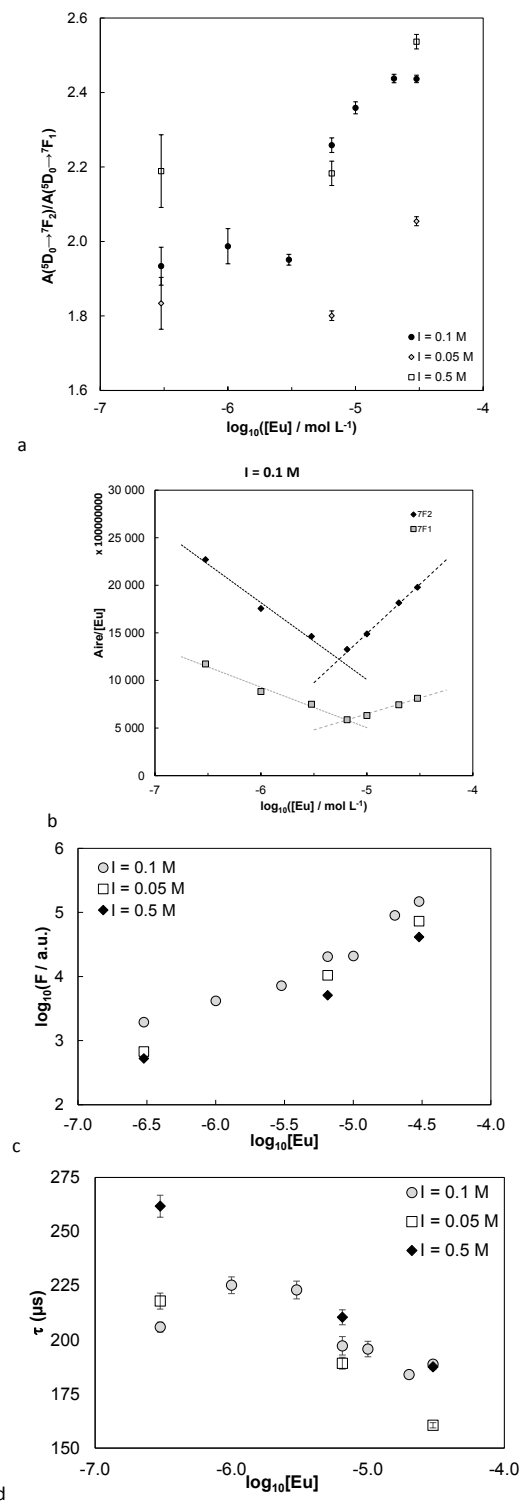


Figure 7. TRLFS spectra of Eu(III)-heparin at different ionic strengths (Heparin $c = 4 \times 10^{-4} \text{ mol L}^{-1}$; $[Eu^{3+}] = 3.10^{-7} - 3.10^{-5} \text{ mol L}^{-1}$) at pH = 6 (a) luminescence normalised to the total area (b) fluorescence intensity of the ${}^5D_0 \rightarrow {}^7F_2$ and the ${}^5D_0 \rightarrow {}^7F_1$ (c) luminescence against the Log_{10} of Eu concentration (d) decay time against the Log_{10} of Eu concentration. Concentrations of polymers are reported in terms of monomeric units.

are $230 \pm 2 \mu\text{s}$ (Fig. 8a) and $171 \pm 2 \mu\text{s}$ (Fig. 8b), respectively, and indicating the formation of single Eu(III)-EPS species. The corresponding number of water molecules remaining in the first coordination sphere can be evaluated using empirical relationships [33, 34]. As direct decay-time determinations in both H_2O and D_2O were not possible in the course of this project, the relationship from Kimura et al. [33] was directly applied (see Eq. (3)). It has been assumed that in the chemical environment considered – i.e. neither aromatic nor phenolic compound that strongly lowers the decay-time [35].

The obtained remaining number of water molecules correspond to 4.0 ± 0.5 and 5.6 ± 0.5 in the first coordination sphere of Eu-DR and -DRS, respectively. The number of sulfate groups are higher in the case of EPS-DRS than for EPS-DR, and the coordination spheres seem slightly different both from the point of view of site symmetry and decay-time. As observed by Kimura et al. [33], the biggest impact on the water molecules is noticed for the biggest functional groups for similar environments. This seems to be the case for Eu(III) complexed by EPS-DR or -DRS. For heparin, decay time, instead, seems to increase with Eu concentration and thus the viscosity (Fig. 7 d). This could be explained by the relaxed polymer conformation (higher viscosity) that should reveal more functional groups, so less water molecules around which corresponds to a higher decay time.

At $I = 0.05 \text{ M}$ for $[\text{Eu}^{3+}] = 30 \mu\text{M}$ and $[\text{Hep}] = 40 \text{ mM}$, a the bi-exponential decay leads to $\tau_1 = 125 \mu\text{s}$ and $\tau_2 = 206 \mu\text{s}$ (**Error! Reference source not found.c**), which correspond respectively to 7.9 ± 0.5 and 4.6 ± 0.5 water molecules in the first coordination sphere of Eu(III).

Nonetheless, for a fixed background solution concentration, as used for TRF experiments, no drastic change in the conformation was evidenced when increasing $[\text{Eu}^{3+}]$ concentration, meaning thus the second plateau observed in **Error! Reference source not found.a** is related to a second complex specie. It was possible then to model these isotherms in order to extract the conditional complexation constant.

2. Modelling

The log K values obtained on each system is indicated in Table 2. As studies as a function of pH cannot be performed without potential ligand hydrolysis, the determined apparent complexation constant is not corrected from acid-base properties of ligand and potential H^+ implied in the reaction.

For Eu(II)-heparin system, two sites of complexation were necessary to model the isotherm whereas only one site was necessary to model the data for Eu(III)-EPS-DR and -DRS. Fuks and Bünzli [6] determined, by spectrophotometry, the complexation constants of glucuronic and galacturonic acid units with lanthanide trivalent ions. These authors found that the complexation of La(III) with glucuronic acid and galacturonic acid lead to 2 complexes with respective values of $\log K_1 = 1.32$ and $\log K_2 = 3.86$ and $\log K_1 = 1.41$ and $\log K_2 = 3.94$, without consideration of La(III) hydrolysis [36].

We do assume that the two sites observed on Eu-heparin system corresponded to the two uronic acids, in agreement

with data from Fuks and Bünzli [6]. From a thermodynamic point of view, and with no further indication, the different

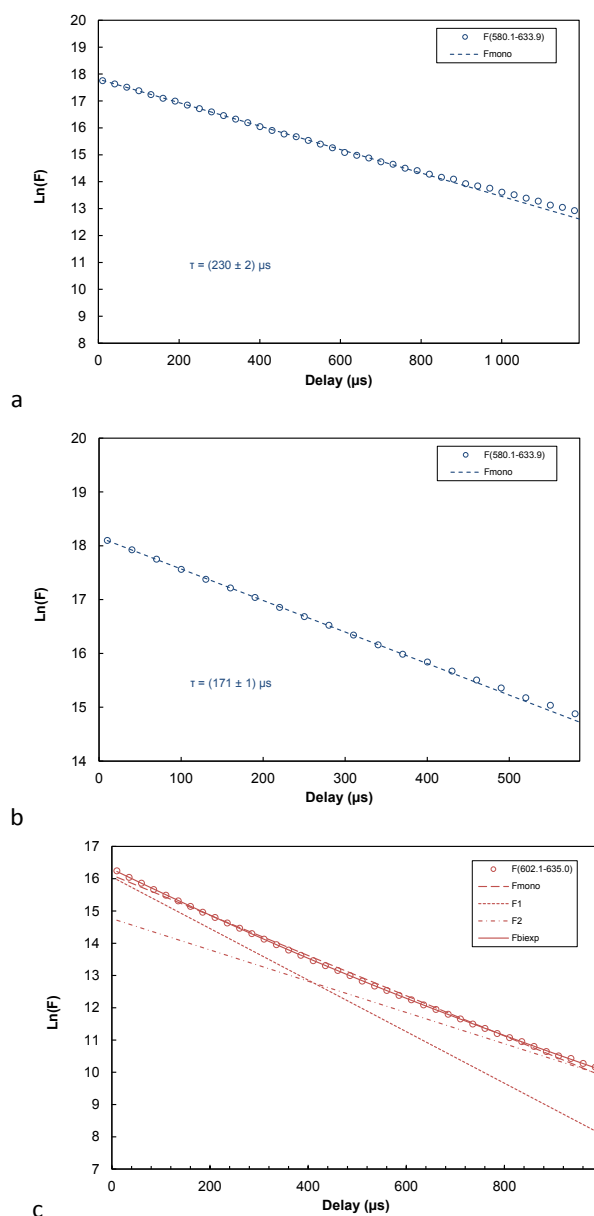


Figure 8. Decay time determination of Eu-DR (a) and -DRS (b) complexes $[\text{Eu}] = 10^{-5} \text{ M}$, $C_{\text{DR}} = ?$, $C_{\text{DRS}} = ?$; $\lambda_{\text{exc}} = 593.8 \text{ nm}$, $W = 50 \mu\text{s}$, grating $300 \text{ lines mm}^{-1}$

conceivable species ($\text{Eu}(\text{OH})\text{Hep}^{2-}$, EuHepH , EuHep^-) cannot be discriminated.

Feofanova et al. determined by potentiometric titration the stability constants of heparin with divalent d-transition series metals – i.e., Cu^{2+} , Zn^{2+} , Co^{2+} , Ni^{2+} – and Fe^{3+} [37]. They found that the monoligand complex MHep^{2-} was the predominant specie in weakly acidic, neutral, and weakly basic pH ranges. Otherwise, it was also shown that the affinity of metal ions for donor groups of low basicity is expected to decrease with increasing ionic radius of the hydrated cation [38]. With increasing pH, metal hydrolysis occurs. Water molecules are

present in the inner coordination sphere of the metal that are progressively replaced by hydroxo-complexes, such as

Table 2. Conditional complexation constants of the different Eu(III)-ligand system. Charged are omitted for the sake of simplicity

		EPS-DR	EPS-DRS	Heparin
Apparent constant	Sc ³⁺ [24]	7.07 ± 0.12	5.62 ± 0.12	6.38 ± 0.46
	Eu ³⁺	4.9 ± 0.1	5.3 ± 0.1	4.9 ± 0.1
	$\log \beta_{h,l}[H^+]^{h+2}$			3.7 ± 0.1

[M(OH)Hep]³⁻ and [M(OH)₂Hep]⁴⁻, with increasing pH. For all the metal-heparin complexes identified, these authors showed that log β values increased when more hydroxo-species of the metal were complexed [37].

Similar work was performed on another lanthanide-like metal, namely scandium, but using Free Ion Selective Radiotracer Extraction (FISRE) to obtain the apparent stability constants of Sc-EPS and -heparin complexes [24]. For comparison purpose, the data are indicated in Table 2.

The Eu(III) ions are hard acceptors and form strong complexes with hard ligands containing highly electronegative donor atoms such as carbonate, phosphate, hydroxide, fluoride, and sulphate. The bonds between Eu³⁺ ions and hard ligands such as CO₃²⁻ or F⁻ are mainly electrostatic in character and the 4f electrons do not seem to participate to a large extent in the bonding. Another consequence of the dominantly electrostatic nature of bonding is that the coordination number and the geometry of rare earth element ions are less constrained than those of transition metal ions [39].

It was shown that on a sulphate containing polyelectrolyte, fixation of weakly acidic cations resembled formation of outer-sphere complexes, in which the cation was separated from the anionic group by a solvent molecule [40]. The cation and anion were held together by electrostatic forces, and the smaller the radius of the solvated cation, the stronger the bond. Stability constant of heparin with Ca²⁺ is log K = 2.09 at pH = 7.2 and I = 0.15 M [38].

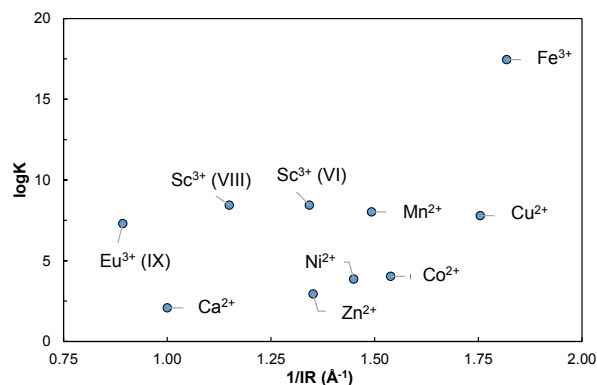


Figure 2. Comparison of log β for M-Heparin complexes from Feofanova et al. [37] (Zn²⁺, Cu²⁺, Ni²⁺, Co²⁺, and Fe³⁺), Rendleman [40] (Ca²⁺), and Sc-heparin [24], and Eu-heparin in this work, as a function of the inverse effective ionic radius 1/IR [38]. One must note that the roman numbers in the brackets indicate the number of water molecules

Regarding the M-Heparin complexes, a comparison could be done plotting the log β values vs. the inverse effective ionic radius 1/IR of the free metals in [38] in **Error! Reference source not found.** It can be seen that Eu³⁺ seems to effectively showing stronger complexation than Ca²⁺, like it was observed with Sc³⁺, and even stronger that smaller ions like Zn²⁺, Ni²⁺ or Co²⁺. It is comparable to Mn²⁺ and Cu²⁺, which is distorted by Jahn-Teller effect. It is also showing a markedly smaller value that the trivalent Fe³⁺ complex, which has a smaller effective ionic radius. Inasmuch, the comparison could be somewhat difficult as the formation of Fe(OH)Hep complex – and of Cu(OH)Hep to a somewhat lesser extent – is more extensive than the other first series d-transition elements [40]. Even the formation of Sc(OH)Hep seem to be lower than Fe(OH)Hep. Indeed, even if the literature provided some data on the complexation of polysaccharides with metals, there are very few data on the determination of their stability constants [6, 18, 19].

It should be pointed out that the primary experimental data used in these works to calculate thermodynamic values of the constants are in some cases the same, as e.g. for carbonate or phosphate complexes, but the calculation of activity coefficients to extract thermodynamic values differs. The use of a modified extended Debye-Hückel expression, assuming thus the log K values would be linear with $\sqrt{I}/(1+\sqrt{I})$, is quite acceptable for low ionic strengths and for complex formation reactions of the rare earth M³⁺ ions with high charge ligands. Nonetheless, the same cannot be expected at high ionic strengths and for monovalent ligands, since the Debye-Hückel contribution to the activity coefficient expression is not as dominant [39].

Experimental

A - Chemicals

The exopolysaccharides used in this work, namely EPS-DR and -DRS, were provided in-kind by the Institut Français de Recherche pour l'Exploitation de la MER (IFREMER) of Nantes as already described elsewhere [41]. The native EPS is produced from fermentation, and then undergoes radical depolymerisation and over-sulphation [10, 11]. The sulphate content of both polymers were determined by elemental analysis (Central Microanalysis Department of the CNRS, Gif-sur-Yvette, France). These two EPS differ for their sulphate content (SO₄²⁻%) that were 3 and 16% for EPS-DR and -DRS, respectively. Heparin sulphate content which was intermediate, was 10%.

Heparin sodium salt (from porcine intestinal mucose, ≥ 180 USP units mg⁻¹), ScCl₃·6H₂O (purity 99,9%), polyacrylic acid (of different M_w, 50 000; 10 000, 8 000, and 2 000 g.mol⁻¹) and certified bovine serum albumin (BSA) (M_w = 67 000 g.mol⁻¹, Sigma Aldrich, France), hydrochloric acid, sodium hydroxide, sodium chloride were of analytical grade (Sigma Aldrich, France) and used without further purification. Milli-Q water (18.2 MΩ.cm, Millipore) was used in all solutions.

B - Time-resolved laser-induced fluorescence spectroscopic measurements

TRLFS set up has been described in details elsewhere [42, 43]. Fluorescence data were collected either at $25 \pm 1^\circ\text{C}$ using a 355 nm tripled Nd:YAG laser (Surelite, Continuum, USA) delivering ca. 170 mJ, and an optical parametric oscillator system (Horizon, Continuum, USA). The temperature was controlled using a cuvette holder. The laser pulse energy (2–4 mJ) was monitored using a RJP-734 Joule-meter (Laser Probe, Inc.). The fluorescence emission spectra were recorded using an optical multi-channel analyzer system, consisting of an Acton monochromator, a spectrograph with a 300 lines mm^{-1} grating, and an Andor iStar ICCD camera (Andor, UK). A constant gate delay of 10 μs was applied. The selective excitation wavelength was set for the $^5\text{L}_6 \leftarrow ^7\text{F}_0$ transition (593.8 nm). For time-resolved measurements, 40–60 spectra were recorded with delay time steps between 10 and 30 μs . For Eu(III), the emission bands of the $^5\text{D}_0 \rightarrow ^7\text{F}_0$ (ca. 580 nm), $^5\text{D}_0 \rightarrow ^7\text{F}_1$ (ca. 590 nm), and $^5\text{D}_0 \rightarrow ^7\text{F}_2$ transitions (ca. 615 nm) are of special interest. The first one is a symmetry forbidden transition and, hence, it should appear only upon the rearrangement of the first coordination shell of Eu(III). The magnetic dipole transition $^5\text{D}_0 \rightarrow ^7\text{F}_1$ is only weakly influenced by complexation, while the relative intensity and the splitting pattern of the hypersensitive induced electric dipole transition $^5\text{D}_0 \rightarrow ^7\text{F}_2$ reflect changes in the local coordination environment of Eu(III).

Normalization was applied only to the peak area of the $^5\text{D}_0 \rightarrow ^7\text{F}_1$ band because the luminescence is considered to be only weakly dependent from the chemical environment of the metal ion [18, 19]. For better comparison, all Eu(III) spectra were normalized to the total area of spectra.

Additionally, the intensity ratio $R_{(E/M)}$ between the electric dipole transition $^5\text{D}_0 \rightarrow ^7\text{F}_2$ and the magnetic dipole transition $^5\text{D}_0 \rightarrow ^7\text{F}_1$ was determined as follows:

$$R_{(E/M)} = I(^7\text{F}_2) / I(^7\text{F}_1) \quad (1)$$

with I being the luminescence intensity (peak area) of the respective transition.

The lifetimes of the luminescent species were generally determined by the following equation:

$$E(t) = \sum_i E_i \times e^{-\frac{t}{\tau_i}} \quad (2)$$

where E is the total luminescence intensity at the time t , E_i is the luminescence intensity of the species i at $t = 0$, and τ_i is the corresponding luminescence lifetime. The observed decay mode was either mono- or bi-exponential. If the luminescence lifetimes of two co-existing species are very close to one another or if one species has a small contribution to the sum spectrum, it could be fitted with a subordinate exponential function, meaning that further species could not be detected.

With the luminescence lifetimes (in ms), the number of water molecules in the first coordination shell of the metal ions ($n(\text{H}_2\text{O})$) can be estimated using the following empirical equations:

$$n(\text{H}_2\text{O}) = 1.07 \times \tau^{-1} - 0.62 \quad (3)$$

The luminescence lifetime of the Eu(III) aquo ion in H_2O is $110 \pm 4 \mu\text{s}$. These values correspond to the coordination of the nine water molecules in the first coordination shell [33].

C - Viscosity measurements

To investigate the polymer shape in aqueous media, the intrinsic viscosity at different ionic strength was determined. Five batches of 2 mL solutions containing EPS-DR and -DRS coupled to Eu^{3+} were prepared in NaCl solution at different concentrations (from 0.1 to 0.5 mol L^{-1}). A fixed concentration of polysaccharide (i.e. 7.3 mg mL^{-1}) was used whereas Eu concentrations were varied from 3.10^{-7} to $3.10^{-5} \text{mol L}^{-1}$ for each ionic strength. The same kind of analysis was assessed on Na-heparin (Sigma Aldrich, $M_w \approx 18\,000 \text{g mol}^{-1}$) to have a reference of viscosity behaviour in the same ionic strength conditions. Viscosimetric measurements were realized using a digital microviscometer Lovis 2000 M[®] (Anton Paar, France). A rolling-ball viscometer measures the rolling time of a steel ball through a glass capillary filled of transparent or opaque liquids according to Hoesppler's falling ball principle. Temperature was set at 20°C .

The hydrodynamic volume V_h of the polymer, which represents the sum of the time-average of the molecular volume and the volume of the solvent molecules associated with it, is calculated using Equation 4 [29].

$$V_h = \frac{4\pi[\eta]M_v}{\mu} \quad (4)$$

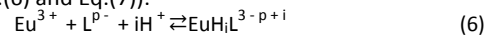
With $\mu = 10\pi N_A$, where N_A is the Avogadro's number, $[\eta]$ and M_v are the intrinsic viscosity and the viscosity-average molar mass, respectively, that are present in the Mark-Houwink-Sakurada (MHS) equation [36].

$$[\eta] = KM_v^a \quad (5)$$

A universal calibration of the viscosimeter was first performed by the use of a narrow standard. In our case, a water-soluble anionic polymer, such as polyacrylic acid (PAA) was used. Intrinsic viscosities $[\eta]$ of PAA solutions of different molecular weights – i.e. 2 000, 8 000, 10,000, and 50,000 g mol^{-1} – were measured. Mark-Houwink plots of log intrinsic viscosity as a function of log M_w were calculated for the PAA.

D - Speciation calculation

The behaviour of europium in different systems is influenced by the presence in solution of polysaccharides ligands (L) due to the formation of the associated complexes. Considering the complex formation reaction and its associated apparent constant (Eq.(6) and Eq.(7)):



$$\beta_{\text{EuH}_i\text{L}} = \frac{[\text{EuH}_i\text{L}^{3-p+i}]}{[\text{Eu}^{3+}][\text{L}^{p-}]^i[\text{H}^+]^i} \quad (7)$$

To prevent hydrolysis of polysaccharides ligands, the complexation studies were performed at constant pH. Only the apparent constants for each system can be determined (Eq. (8)).

$$\beta_{\text{EuH}_i\text{L}}^{\text{app}} = \frac{[\text{EuL}]}{[\text{Eu}][\text{L}]} \quad (8)$$

The charges of different species are omitted. $[\text{EuL}]$, $[\text{Eu}]$ and $[\text{L}]$ are the total aqueous concentration of complex, europium (excepted complex with polysaccharides) and free polysaccharides respectively.

As the fluorescence spectra is specific for each europium species, the ${}^7F_2/{}^7F_1$ ratio is equally characteristic. If we consider only the major species presented previously (Eq.(8)), the experimental one is then defined as:

$$R = \frac{\sum_i R_i [Eu]_i}{\sum_i [Eu]_i} = \frac{R_1 [Eu] + R_2 [EuL]}{[Eu]_T} \quad (9)$$

R_1 and R_2 being the ratio of Eu and EuL respectively. Considering the apparent constant presented in Eq.(8), the expression can be simplified:

$$R = \frac{[Eu]}{[Eu]_T} (R_1 + R_2 \beta_{EuHL}^{app} [L]) \quad (10)$$

For low concentration of polysaccharides, where Eu concentration is equal to total concentration of europium and EuL concentration can be neglected, the ratio is equal to R_1 , the ${}^7F_2/{}^7F_1$ ratio of “non-complexed” europium (potential hydrolysis excepted [44]). This value can be determined in the same conditions without exopolysaccharides to limit freedom degree of Eq.(10) modelling. For high concentration of polysaccharides, this ratio tends to R_2 . The apparent constant is modelled between both plateaus.

Conclusions

The selective complexation of Eu^{3+} by exopolysaccharides has been documented, although the locations of the functional group that participate in the formation of the coordination complex have not been identified. We have obtained a detailed and widespread overview of the europium binding properties with polysaccharides (PS) in the mildly acidic to neutral pH range. At very low europium concentrations, corresponding to an excess of PS and its functional groups, we observe coordination. At a higher relative amount of europium, corresponding to a reduced ratio of PS functional groups, an additional significant coordination to carboxylate groups can be observed on heparin as it was proven by TRLFS spectroscopy. Up to now, investigations, focusing on exopolysaccharides from a marine bacteria, have shown only one coordination site. The determined dissociation constants of the biomacromolecule and the appropriate stability constants of the europium complexes are important data for a better description of the interaction of bacterial surfaces with heavy metals in the biogeochemical cycle.

Conflicts of interest

There are no conflicts to declare.

Acknowledgements

This work has been supported in part by grants from the French National Agency for Research, called “Investissements d’Avenir” IRON Labex no. ANR-11-LABX-0018-01, ArronaxPlus Equipex no. ANR-11-EQPX-0004 and ISITE NExT (ANR-16-IDEX-0007).

The authors acknowledge Mrs Corinne Siquin and Mrs Sylvia Collic-Jouault, from EB3M – IFREMER Nantes, for providing the EPS of interest for this work.

Notes and references

- 1 N. Janot, M.F. Benedetti, and P.E. Reiller. Colloidal α - Al_2O_3 , Europium(III) and Humic Substances Interactions: A Macroscopic and Spectroscopic Study. *Environmental Science & Technology* 2011, 45 (8), 3224-3230. <https://doi.org/10.1021/es102592a>
- 2 N. Janot, M. F. Benedetti, P. E. Reiller. Influence of solution parameters on europium(III), α - Al_2O_3 , and humic acid interactions: Macroscopic and time-resolved laser-induced luminescence data. *Geochimica et Cosmochimica Acta* 2013, 123, 35-54. <https://doi.org/10.1016/j.gca.2013.08.038>
- 3 P. E. Reiller. Modelling metal–humic substances–surface systems: reasons for success, failure and possible routes for peace of mind. *Mineralogical Magazine* 2012, 76 (7), 2643-2658. <https://doi.org/10.1180/minmag.2012.076.7.02>
- 4 X. L. Tan, X. K. Wang, H. Geckeis, and TH. Rabung Sorption of Eu(III) on Humic Acid or Fulvic Acid Bound to Hydrous Alumina Studied by SEM-EDS, XPS, TRLFS, and Batch Techniques. *Environmental Science & Technology* 2008 42 (17), 6532-6537. DOI: 10.1021/es8007062
- 5 G. Montavon, S. Markai, I. Billard, A. Nehlig and B. Grambow. Complexation and Luminescence Spectroscopic Studies of Europium(III) with Polymaleic Acid: A Synthetic Analogue of Humic Material. *Radiochim. Acta*, 2002; 90, 289-296. https://doi.org/10.1524/ract.2002.90.5_2002.289
- 6 L. Fuks, J.-C.G. Bünzli, Lanthanide-Ion Complexation by D -Glucuronic and D -Galacturonic Acids. *Helv. Chim. Acta* 1993, 76, 2992-3000, doi:10.1002/hlca.19930760824.
- 7 P. Pellerin and M.A. O’Neil, The interaction of the pectic polysaccharide Rhamnogalacturonan II with heavy metals and lanthanides in wines and fruit juices. *Analisis Mag.* 1998, 26 (6), 32-36.
- 8 M. Loaëc. Uptake of Lead, Cadmium and Zinc by a Novel Bacterial Exopolysaccharide. *Water Res.* 1997, 31, 1171-1179, doi:10.1016/S0043-1354(96)00375-2.
- 9 Heymann, D.; Ruiz-Velasco, C.; Chesneau, J.; Ratiskol, J.; Siquin, C.; Collic-Jouault, S. Anti-Metastatic Properties of a Marine Bacterial Exopolysaccharide-Based Derivative Designed to Mimic Glycosaminoglycans. *Molecules* 2016, 21, 309, doi:10.3390/molecules21030309.
- 10 Ruiz Velasco, C.; Baud’huin, M.; Siquin, C.; Maillason, M.; Heymann, D.; Collic-Jouault, S.; Padrines, M. Effects of a Sulfated Exopolysaccharide Produced by *Altermonas infernus* on Bone Biology. *Glycobiology* 2011, 21, 781-795, doi:10.1093/glycob/cwr002.
- 11 Chopin, N.; Siquin, C.; Ratiskol, J.; Zykwiniska, A.; Weiss, P.; Cérantola, S.; Le Bideau, J.; Collic-Jouault, S. A Direct Sulfation Process of a Marine Polysaccharide in Ionic Liquid. *BioMed Res. Int.* 2015, 2015, 1-9, doi:10.1155/2015/508656.
- 12 L. E. Karpukhin, M. A. Feofanova, L. S. Nikolaeva, and M. N. Mamontov, “Complexation of Magnesium and Calcium Ions with Heparin,” *Russ. J. Inorg. Chem.*, vol. 51, no. 6, pp. 908-914, 2006.
- 13 Paskins-Hurlburt, A. J.; Skoryna, S. C.; Tanaka, Y.; Moore, W.; Stara, J. F. Fucoidan: Its Binding of Lead and Other Metals. *Bot. Mar.* 1978, 21, 13.

- 14 W. Jurkowski, M. Heilmann, A. M. Becker, R. Buchholz, and T.B. Brück. Terbium Excitation Spectroscopy as a Detection Method for Chromatographic Separation of Lanthanide-Binding Biomolecules. *ACS Omega* 2020 5 (42), 27050–27056 DOI: 10.1021/acsomega.0c02135
- 15 A. Heller, A. Barkleit, H. Foerstendorf, S. Tsushima, K. Heim and G. Bernhard. Curium(III) citrate speciation in biological systems: a europium(III) assisted spectroscopic and quantum chemical study *Dalton Trans.*, 2012, 41, 13969–13983. DOI: 10.1039/c2dt31480k
- 16 A. Koban, G. Geipel and G. Bernhard, *Radiochim. Acta*, 2003, 91, 393–396
- 17 A. Koban, G. Geipel, A. Rossberg and G. Bernhard, *Radiochim. Acta*, 2004, 92, 903–908
- 18 A. Barkleit, H. Moll and G. Bernhard Interaction of uranium(VI) with lipopolysaccharide. *Dalton Trans.*, 2008, 2879–2886
- 19 A. Barkleit, H. Moll and G. Bernhard Complexation of uranium(VI) with peptidoglycan. *Dalton Trans.*, 2009, 5379–5385.
- 20 Floor, M.; Peters, J.A.; van Bekkum, H.; Kieboom, A.P.G.; Koek, J.H.; Smeets, F.L.M.; Niemantsverdriet, R.E. Structural and Conformational Effects on the Complexation of Calcium by 2,3-Dicarboxy Derivatives of B-Cyclodextrin (Cyclomaltoheptaose), Amylose, and Cellulose. 14.
- 21 Tan et al., *Trends in Analytical Chem.*, 2014, 61, 107–132
- 22 K. Binnemans, *Coord. Chem. Rev.*, 2015, 295, 1–45.
- 23 Picayo et al., 2020, *ACS Omega*, 5, 8076–8989
- 24 M. Mazza, C. Alliot, C. Siquin, S. Collic-Jouault, P.E. Reiller, S. Huclier-Markai. Marine exopolysaccharide complexed with scandium aimed as theranostic Agents Molecules, 2021.
- 25 J. R. Helbert and M. A. Marini, "Structural Studies of Heparin: I Hydrolytic Cleavage of Sulfates *," vol. 2, no. 5, pp. 1101–1106, 1963
- 26 M. Albin and W. D. Horrocks, Jr., *Inorg. Chem.*, 1985, 24, 895–900.
- 27 G. R. Choppin and Z. M. Wang, *Inorg. Chem.*, 1997, 36, 249–252.
- 28 C. Görller-Walrand and K. Binnemans, Rationalization of crystal-field parametrization, in *Handbook on the Physics and Chemistry of Rare Earths*, eds. K. A. Gschneidner, Jr. and L. Eyring, Elsevier, 1996, vol. 23, ch. 155, pp. 121–283.
- 29 McCrackin, F.L. Relationship of Intrinsic Viscosity of Polymer Solutions to Molecular Weight. *Polymer* 1987, 28, 1847–1850, doi:10.1016/0032-3861(87)90289-8.
- 30 Cotte, J.-F.; Bouadam, A.; Sordoillet, A.; Jaudinaud, I.; Chambon, V.; Talaga, P. Determination of Molecular Size Parameters and Quantification of Polyacrylic Acid by High Performance Size-Exclusion Chromatography with Triple Detection. *Anal. Bioanal. Chem.* 2017, 409, 2083–2092, doi:10.1007/s00216-016-0155-z.
- 31 Pavlov, G.M.; Zaitseva, I.I.; Gubarev, A.S.; Gavrilo, I.I.; Panarin, E.F. Diffusion-Viscometric Analysis and Conformational Characteristics of Sodium Polystyrenesulfonate Molecules. *Russian Journal of Applied Chemistry* 2006, 79, 4.
- 32 Punith V. S., S. N. Suresha, S. Raju, et al. Laboratory Investigation of Open-Graded Friction-Course Mixtures Containing Polymers and Cellulose Fibers. *Journal of Transportation Engineering*, 2012, 138(1): 67–74.
- 33 T. Kimura and G. R. Choppin, *J. Alloys Compd.*, 1994, 213, 313–317
- 34 R. M. Supkowski and W. D. Horrocks, Jr., *Inorg. Chim. Acta*, 2002, 340, 44–48.
- 35 P. Moreau, S. Colette-Maatouk, P. Vitorge, P. Gareil and P. E. Reiller, *Inorg. Chim. Acta*, 2015, 432, 81–88.
- 36 Brown, P.L.; Ekberg, C. Scandium, Yttrium and the Lanthanide Metals. In *Hydrolysis of Metal Ions*; Wiley-VCH Verlag GmbH & Co. KGaA: Weinheim, Germany, 2016; pp. 225–324 ISBN 978-3-527-65618-9.
- 37 Feofanova, M.A.; Frantseva, Yu.V.; Lapshin, S.V. Complexation in the Heparin-Metal Ion System. *Russ. J. Coord. Chem.* 2012, 38, 373–378, doi:10.1134/S1070328412040033.
- 38 S Shannon, R.D. Revised Effective Ionic Radii and Systematic Studies of Interatomic Distances in Halides and Chalcogenides. *Acta Cryst.* 1976, 32, 751–hd
- 39 Spahiu and Bruno, Technical Report SKB, A selected thermodynamic database for REE to be used in HLNW performance assessment exercises, 1995
- 40 Rendleman, A. Metal-Polysaccharide Complexes Part II. 36.
- 41 Raguénès, G.H.C.; Peres, A.; Ruimy, R.; Pignet, P.; Christen, R.; Loaec, M.; Rougeaux, H.; Barbier, G.; Guezennec, J.G. *Alteromonas Infernus* Sp. Nov., a New Polysaccharide-producing Bacterium Isolated from a Deep-sea Hydrothermal Vent. *J. Appl. Microbiol.* 1997, 82, 422–430, doi:10.1046/j.1365-2672.1997.00125.x.
- 42 C. Shang and P. E. Reiller, *Dalton Trans.*, 2020, 49, 466–481, doi: 10.1039/C9DT03543E
- 43 C. Shang, P. E. Reiller and T. Vercoouter, *Dalton Trans.*, 2020, 49, 15443–15460, doi : 10.1039/D0DT03164J
- 44 PSI/Nagra Thermochemical Database Version 12/07

Chapter 5

***In vitro* anti-proliferative effect of
scandium-exopolysaccharide complexes on
different cancer cell lines**

I. Introduction

The anti-metastatic properties of these GAG-mimetic EPS have already been assessed, revealing that EPS can efficiently inhibit osteosarcoma cell proliferation, migration and invasiveness of murine and human osteosarcoma cell lines in both *in vitro* and *in vivo* models [1]. In the previous chapters, we have evidenced that exopolysaccharides (EPS) could complex scandium and the complexation was total. However, it is crucial to ensure that, once complexation is done, the biological properties of the vector remain intact, allowing the molecular tropism of the ligand to recognize its molecular target. So, it is of importance to assess if the biological properties of EPS evidenced on osteosarcoma cells, remain when scandium is complexed to the polymers. Moreover, the effect of EPS will be tested on three additional cancer cell lines. This is the goal of the present chapter.

In a first part, two different techniques will be presented to investigate biological aspects attributable, directly or indirectly to cytotoxicity. The first one is a cell-based assay (xCELLigence technology) where, instead of usual plates, cells are seeded in special plates with micro electrodes covering the well bottom. The purpose of these assays is to measure the impedance within the well, parameter that is affected by cell number as well as cell morphology. Colorimetric assay is the second test that will be presented and aims to measure the quantity of a biochemical marker that usual reflects a certain metabolic activity in the cell. In a second part of the chapter, the preliminary *in vitro* cytotoxicity evaluation of EPS-Sc complexes compared to the EPS alone and scandium alone will be presented. This work will be submitted in Marine Drugs.

II. In vitro cytotoxicity and cell viability assays

Cell proliferation depends on the well-working structure and function of all vital processes inside the cell. For this reason, proliferation provides an all-embracing screen for cytotoxic effects [2]. Very often chemicals can affect cell viability and its metabolism. *In vitro* cell proliferation and cell viability of cultured cells are two of the most frequent biological aspects to study when evaluating drugs and chemicals. Currently, these tests are used in oncology to examine both compound toxicity and tumor cell growth inhibition when developing drugs. Drugs can determine a toxic effect on cells through different mechanisms such as cell membrane fragmentation, proteic synthesis inhibition, enzymatic lysis, irreversible binding to receptors, etc. Potential for automation, reduced cost and speed represent some advantages of

in vitro cytotoxicity and cell viability assays, despite they are not technically advanced enough to replace animal tests [3].

A. X-CELLigence technology and cell index

The x-CELLigence technology is a real-time cellular analysis (RTCA) biosensor, allowing continuous monitoring of cell proliferation in a non-invasive way. This technology uses custom-designed plates constituted by high density gold electrode chip on which the target cells stick and grow. When cells adhere to the plate surface, they influence the electrical impedance across the chip. Impedance is measured and recorded in continuous by the xCELLigence software, and it is converted in an electrical signal reflecting the level of adhesion called *Cell Index* (CI). CI is a dimensionless parameter that follows, at least, one fundamental rule: if cells are not adhered on the electrodes, the CI is zero. Greater the cell index, greater the level of adhesion; on the contrary, lower the cell index, lower the adhesion. Basically, xCELLigence is able to quantify the cellular focal adhesion inside the well, allowing also to monitor cell morphology, cell number and movement [4]. A simplified scheme of xCELLigence technology is showed in Figure 27, while in the caption all experimental phases are presented in a comprehensive way [5].

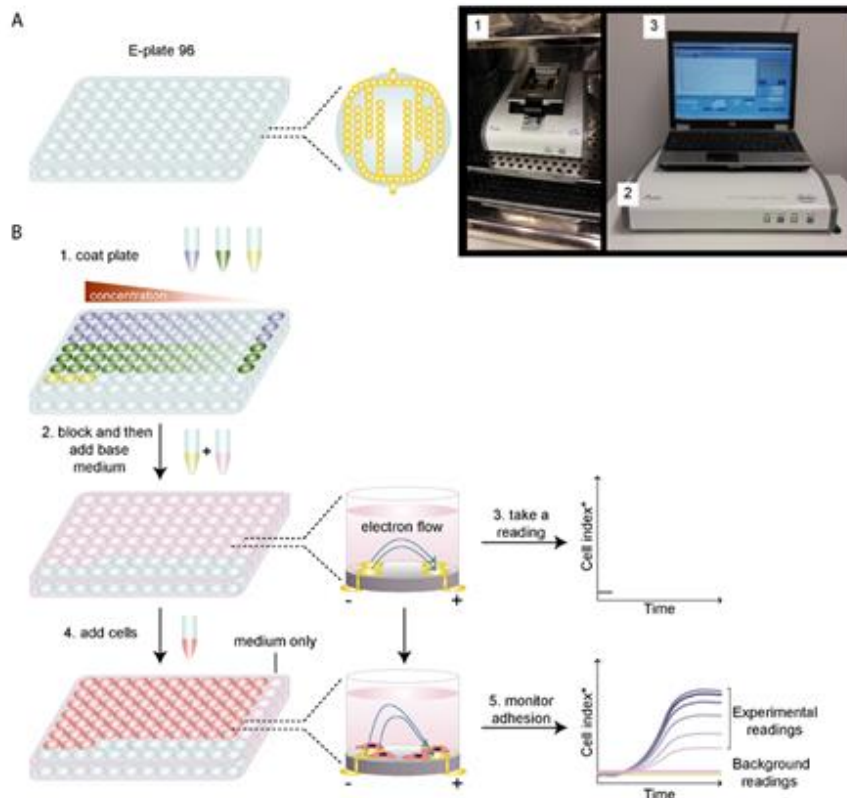


Figure 27. A. A simplified cartoon of an E-plate 96 and the gold microelectrodes embedded within each well (top view of a single well) is shown on the left. The number and size of the gold microelectrodes are not representative of the actual set-up and are for illustrative purposes only. The E-plate 96 is placed within the RTCA SP Station (1), which is kept in a humidified incubator and is connected to the RTCA Analyzer (2) and RTCA Control Unit (3). **B.** Workflow of an xCELLigence adhesion assay. Figure adapted from Hamidi et al. 2017.[5]

From Figure 27, the example assay sets out to determine the optimal concentration of two different ECM ligands (purple and green) needed to promote efficient cell adhesion and to be used for further analyses. The steps of the technique are briefly described below:

- 1) The wells in the E-plate 96 are coated with serial dilutions of the ECM ligands or with bovine serum albumin (BSA, yellow) as a negative control. All conditions are performed in triplicate.
- 2) Coating solutions are removed, wells are washed with PBS and blocked with 0.1% BSA (yellow tube) to prevent non-specific cell adhesion and then incubated with the base medium (pink) that is specific for the cell line of interest.
- 3) The plate is then placed in the RTCA SP station in the incubator and a reading is taken. A side view of a single well in the E-plate demonstrates unimpeded electron flow from the negative to the positive terminal in the presence of medium alone, which results in a low background reading.
- 4) Cells are then added to the coated wells. Some wells can be kept cell-free (medium-only wells) as another negative control that should only give background readings.
- 5) The plate is then placed back into the xCELLigence system and cell adhesion is monitored over time. A side view of a single well in the E-plate demonstrates impeded electron flow from the negative to the positive terminal in the presence of adhering cells, which results in increasing impedance over time as more cells adhere and spread on the microelectrodes.

Then, impedance in electron flow (i.e. resistance to an alternating current) is plotted as arbitrary units called cell index. The background readings are obtained from medium alone (pink line) or from BSA-coated (yellow line) wells. For sake of simplicity in the experimental readings, cell adhesion is shown for one of the ECM ligands (dark to light purple; high to low concentration of ligand) and for one technical replicate only. In Figure 27, two concentrations of the ECM ligand resulted in overlapping curves and similarly high cell index values. Therefore, the lower of these two concentrations could be used in subsequent experiments to preserve on material and reduce costs [5].

Nowadays, the main use of x-CELLigence technology relates the evaluation of multiple complex cellular behaviours and drug responses. This concerns the impact of certain drugs on proliferation, viability and migration of tumor cells [4].

B. MTT assay

MTT assay is considered one of the most common colorimetric assays to study cytotoxicity or cell viability. This assay employs 3-(4,5-dimethylthiazol-2-yl)-2,5-diphenyltetrazolium bromide (MTT). Normally, the cell viability would reflect the mitochondrial function of cells; this reagent measures the level of mitochondrial enzymes such as succinate dehydrogenase. When those enzymes are still present in the cell, MTT is reduced to purple (see Figure 28) formazan. Formazan can be quantified by light absorbance at a specific wavelength (500-600 nm).

[No copyright permission was obtained for this figure]

Figure 28. Metabolism of MTT to a formazan salt by viable cells as shown in a chemical reaction (A) and in a 96-well plate (B). Figure adapted by SIGMA-ALDRICH's protocol guide for MTT assay.

MTT assay is easy to use and with high reproducibility. Unfortunately, this technique is not very sensitive. To reduce false-positive or false-negative results brought on by background interference due to inclusion of particles, further control experiments should be realized. These interferences could cause an overestimation of the cell viability [3].

References:

- [1] Heymann, D.; Ruiz-Velasco, C.; Chesneau, J.; Ratiskol, J.; Siquin, C.; Collic-Jouault, S. Anti-Metastatic Properties of a Marine Bacterial Exopolysaccharide-Based Derivative Designed to Mimic Glycosaminoglycans. *Molecules* **2016**, *21*, 309, doi:10.3390/molecules21030309.
- [2] O'Brien, P.; Haskins, J.R. In Vitro Cytotoxicity Assessment. In *High Content Screening*; Humana Press: New Jersey, 2006; Vol. 356, pp. 415–426 ISBN 978-1-59745-217-5.
- [3] Aslantürk, O.S. In Vitro Cytotoxicity and Cell Viability Assays: Principles, Advantages, and Disadvantages. In *Genotoxicity - A Predictable Risk to Our Actual World*; 2017.
- [4] Kho, D.; MacDonald, C.; Johnson, R.; Unsworth, C.; O'Carroll, S.; Mez, E.; Angel, C.; Graham, E. Application of XCELLigence RTCA Biosensor Technology for Revealing the Profile and Window of Drug Responsiveness in Real Time. *Biosensors* **2015**, *5*, 199–222, doi:10.3390/bios5020199

[5] Hamidi, H.; Lilja, J.; Ivaska, J. Using XCELLigence RTCA Instrument to Measure Cell Adhesion. *BIO-Protoc.* **2017**, *7*, doi:10.21769/BioProtoc.2646.

III. Antiproliferative Properties of Scandium Exopolysaccharide Complexes on Several Cancer Cell Lines.

Article published in *Marine Drugs* (IF = 4.379)

Article

Antiproliferative Properties of Scandium Exopolysaccharide Complexes on Several Cancer Cell Lines

Javier Muñoz-García ^{1,†}, Mattia Mazza ^{2,3,†}, Cyrille Alliot ^{2,4}, Corinne Sinquin ⁵, Sylvia Collic-Jouault ⁵, Dominique Heymann ^{1,6} and Sandrine Huclier-Markai ^{2,3,*}

- ¹ Institut de Cancérologie de l'Ouest, Université de Nantes, Blvd Jacques Monod, F-44805 Saint-Herblain, France; javier.munoz@ico.unicancer.fr (J.M.-G.); dominique.heyman@univ-nantes.fr (D.H.)
- ² GIP ARRONAX, 1 rue Aronnax, CEDEX 3, F-44817 Nantes, France; mattia.mazza@subatech.in2p3.fr (M.M.); alliot@arronax-nantes.fr (C.A.)
- ³ Laboratoire SUBATECH, 4 rue Alfred Kastler, BP 20722, CEDEX 3, F-44307 Nantes, France
- ⁴ Centre de Recherche en Cancérologie et Immunologie Nantes Angers, INSERM, U892, 8 quai Moncoussu, CEDEX 1, F-44007 Nantes, France
- ⁵ IFREMER, Institut Français de Recherche pour l'Exploitation de la mer, rue de l'Île d'Yeu, BP21105, CEDEX 3, F-44311 Nantes, France; corinne.sinquin@ifremer.fr (C.S.); Sylvia.Collic.Jouault@ifremer.fr (S.C.-J.)
- ⁶ Department of Oncology and Metabolism, Medical School, University of Sheffield, Sheffield S10 2TN, UK
- * Correspondence: sandrine.huclier@subatech.in2p3.fr; Tel.: +33-(0)51-85-85-37 or +33-(0)28-21-25-23
- † These authors contributed equally to this work.



Citation: Muñoz-García, J.; Mazza, M.; Alliot, C.; Sinquin, C.; Collic-Jouault, S.; Heymann, D.; Huclier-Markai, S. Antiproliferative Properties of Scandium Exopolysaccharide Complexes on Several Cancer Cell Lines. *Mar. Drugs* **2021**, *19*, 174. <https://doi.org/10.3390/md19030174>

Academic Editors: Irina M. Yermak and Viktoria Davydova

Received: 27 February 2021

Accepted: 18 March 2021

Published: 23 March 2021

Publisher's Note: MDPI stays neutral with regard to jurisdictional claims in published maps and institutional affiliations.



Copyright: © 2021 by the authors. Licensee MDPI, Basel, Switzerland. This article is an open access article distributed under the terms and conditions of the Creative Commons Attribution (CC BY) license (<https://creativecommons.org/licenses/by/4.0/>).

Abstract: Antimetastatic properties on both murine and human osteosarcoma cell lines (POS-1 and KHOS) have been evidenced using exopolysaccharide (EPS) derivatives, produced by *Alteromonas infernus* bacterium. These derivatives had no significant effect on the cell cycle neither a pro-apoptotic effect on osteosarcoma cells. Based on this observation, these EPSs could be employed as new drug delivery systems for therapeutic uses. A theranostic approach, i.e., combination of a predictive biomarker with a therapeutic agent, has been developed notably by combining with true pair of theranostic radionuclides, such as scandium ⁴⁷Sc/⁴⁴Sc. However, it is crucial to ensure that, once complexation is done, the biological properties of the vector remain intact, allowing the molecular tropism of the ligand to recognize its molecular target. It is important to assess if the biological properties of EPS evidenced on osteosarcoma cell lines remain when scandium is complexed to the polymers and can be extended to other cancer cell types. Scandium-EPS complexes were thus tested in vitro on human cell lines: MNNG/HOS osteosarcoma, A375 melanoma, A549 lung adenocarcinoma, U251 glioma, MDA231 breast cancer, and Caco2 colon cancer cells. An xCELLigence Real Cell Time Analysis (RTCA) technology assay was used to monitor for 160 h, the proliferation kinetics of the different cell lines. The tested complexes exhibited an anti-proliferative effect, this effect was more effective compared to EPS alone. This increase of the antiproliferative properties was explained by a change in conformation of EPS complexes due to their polyelectrolyte nature that was induced by complexation. Alterations of both growth factor-receptor signaling, and transmembrane protein interactions could be the principal cause of the antiproliferative effect. These results are very promising and reveal that EPS can be coupled to scandium for improving its biological effects and also suggesting that no major structural modification occurs on the ligand.

Keywords: exopolysaccharides; scandium; theranostic; cancer cell lines; proliferation

1. Introduction

The key role of glycosaminoglycans (GAGs), natural polysaccharides found in mammalian tissue, has been recognized in the regulation of cell properties and functions. They are now considered as pharmacological targets to treat several diseases and notably metastatic cancers. GAGs play a central role in the organization of the extracellular matrix (ECM) through their binding to various molecules (ECM components, cell-surface receptors,

growth factors and cytokines). Nowadays, several therapeutic strategies are developed with the aim of restoring cell function due to a degradation of endogenous GAGs either in protecting endogenous GAGs or in using exogenous GAGs or GAG-mimetics [1–4].

Unfractionated heparin and its low-molecular-weight (LMW) derivatives are widely used to prevent or treat venous thromboembolism, which is a common complication in cancer patients. Clinical trials have shown that cancer patients treated with heparins have improved, with a decrease in cancer progression and a longer survival time [5,6], which may be explained by heparin's functional interference with critical biological steps of metastasis spread [7]. Despite their therapeutic potential, side-effects induced by their anticoagulant properties (e.g., hemorrhagic complications and heparin-induced thrombocytopenia) may occur, limiting thus a long-term treatment. Heparin could present also a contamination with prion proteins or oversulfated chondroitin sulfate [8]. Heparin's use in therapy is sometimes limited due to this hazard profile. As a result, the number of studies on heparin mimetic molecules has increased in recent years. Polysaccharides may be a new source of heparin-like molecules among the possible drug candidates. Traditional algal or modern bacterial polysaccharides may be used as a substitute for mammalian GAGs [9]. Furthermore, preliminary animal studies have shown that polysaccharides extracted from eukaryotes and prokaryotes living in the marine environment could reveal a better benefit/risk ratio [9]. Algal polysaccharides like fucoidans—especially low-molecular-weight fucoidan preparations—have previously been shown to have heparin-like properties with low hemorrhagic risks [10]. As soluble molecules or polymers, marine polysaccharides derived from bacteria have a lot of promise in cell therapy and tissue engineering. When compared to other polysaccharides from eukaryotes, they can be produced in bioreactors under completely regulated conditions [11].

Among these marine polysaccharides, an exopolysaccharide (EPS) of interest was isolated from the culture broth of a hydrothermal bacterium called *Alteromonas infernus*. A monosulfated nonasaccharide composed of six neutral hexoses and three hexuronic acids, including one galacturonic acid unit bearing one sulfate group, makes up the repeating unit of this EPS. It presents a high molecular weight ($>10^6$ g mol⁻¹) and a low sulfate content ($<10\%$) [12–14]. When compared to heparin, this native EPS had a very poor anticoagulant effect. To improve its biological activities and provide a GAG mimetic compound, native EPS has been modified first by radical depolymerization, then by oversulfation to create EPS derivatives [15,16]. In the following, EPS-DR denotes native EPS that has undergone radical depolymerization, whereas EPS-DRS denotes EPS that has been further over-sulfated. These two chemical modifications allow for a decrease in molecular weight while increasing sulfate content [17]. The anticoagulant efficacy of this LMW highly sulfated EPS derivative is increased over that of its native precursor, but it is still 10 and 5 times less potent than unfractionated and LMW heparin, respectively. Following the oversulfation stage, an oversulfated EPS structure (EPS-DRS) has been suggested, with three additional sulfate groups on both glucose and galactose constitutive of the repeating unit (unpublished data). It is made up of three hexose units that have been oversulfated and have been reported elsewhere [15–17].

In vitro studies on bone remodeling have displayed different levels of bone resorption regulation by EPS-DRS, most of them leading to pro-resorptive effects [15]. These results have brought to consider those compounds to be tested on osteosarcoma, characterized by high potency to induce lung metastasis [18]. EPS-DRS of different sizes have been tested against two osteosarcoma cell lines (mouse POS-1 and human HOS) revealing that an EPS derivative of 15 kDa could effectively inhibit both migration and invasiveness of osteosarcoma cells in vitro, while it could be very efficient at inhibiting the establishment of lung metastases in vivo [19].

Since their natural tropism in targeting malignant tumor and their metastasis, EPS have been recently considered as vector to be combined with theranostic radionuclide pairs. Through the possibility of doing therapy and diagnostic at the same time, theranostic compounds represent new innovative clinical tools to be employed in a perspective of “per-

sonalized/precision" medicine [20]. More precisely, a theranostic pair $^{44}\text{Sc}/^{47}\text{Sc}$ could be both employed for Positron Emission Tomography (PET) imaging to detect primary and secondary tumors, as well as for Targeted RadioTherapy in order to bombard tumor tissues with gamma radiations [21]. Complexation between EPS and scandium has already been assessed and quantified in a previous work [22]. The EPS derivatives selected for this study are a highly sulfated one, called DRS ($M_w = 27$ kDa) and a lower-sulfated one, called DR (with $M_w = 16$ kDa). The complexation properties of these two EPS with scandium were higher than the ones on glucuronic and galacturonic acids, even though Sc-EPS complexes appear to be less stable ($K_{\text{ScEPS-DR}} = 9.14$; $K_{\text{ScEPS-DRS}} = 7.69$) than scandium complexes with 1,4,7,10-Tetraazacyclododecane-1,4,7,10-tetraacetic acid (DOTA) and diethylenetriaminepentaacetic acid (DTPA), classically used in radiopharmaceutical drugs.

For further use as a therapeutic vector, it is important to ensure that EPS may keep the ability of targeting cancer cells even when complexed with scandium. For this reason, in vitro studies concerning both cell proliferation and cell viability of various tumor cell lines were realized here to evaluate if there is a synergetic effect of Sc-EPS complexes on different cancer cell lines, compared to the EPS alone and scandium alone. To this aim, the cell index of human osteosarcoma (MNNG/HOS), human melanoma (A375), human lung cancer (A549), human glioblastoma (U251), and human breast cancer (MDA231) were monitored over a week using XCELLigence[®] technology. XCELLigence measures the electric impedance of cell assessed. This impedance is directly related to the cell adhesion process and, consequently, to cell proliferation and/or cell death. Moreover, the effect of the metal-to-ligand ration of the EPS-Sc complexes was assessed and, a heparin was used as a reference system for these EPS.

2. Results

2.1. Human MNNG/HOS Osteosarcoma Cell Line

2.1.1. Effect of Scandium Alone on Cell Proliferation and Viability

Figure 1 shows the effect of scandium alone on MNNG/HOS osteosarcoma cell proliferation as well as cell viability. Concerning the cell index (CI) measured by xCELLigence RTCA, the software employed transformed the CI of all wells at all time points to the normalized cell index (NCI), which was considered the CI value of individual wells at the same time point (base-time). This transformation made the NCI more comparable between the wells [23].

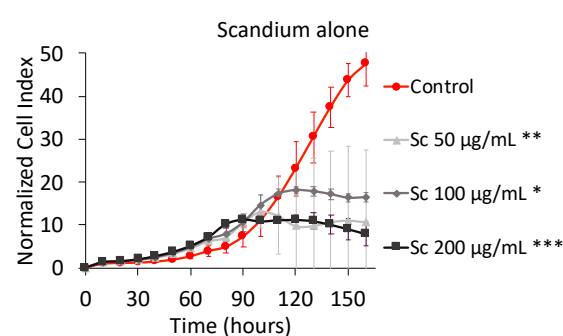


Figure 1. Normalized cell index plot of MNNG/HOS cells after 160 h of contact with Sc^{3+} at $50 \mu\text{g mL}^{-1}$ (**), $100 \mu\text{g mL}^{-1}$ (*), and $200 \mu\text{g mL}^{-1}$ (***) * = p value ≤ 0.0001 , ** = p value ≤ 0.005 , *** = p value ≤ 0.05 .

The NCI plot shown in Figure 1 depicts two different kinds of curves. The ascending bi-exponential curve of the control is due to the fact that, in its well, the space to grow up was not saturated yet. The saturation was reflected by a plateau. Normally, two scenarios can occur once the plateau is set: (1) the plateau continues until starting a definitive descending evolution characteristic of damaged cells that are not attached to the surface of the well; (2) the plateau continues until starting a momentary decrease followed by a brief rise, that is characteristic of the replacement of damaged cells by new healthy cells.

The curves for scandium concentrations at 50 and 100 $\mu\text{g mL}^{-1}$ showed a plateau that reflected no more MNNG/HOS cells proliferation but the detachment from the well was not observed yet. For the scandium concentration at 200 $\mu\text{g mL}^{-1}$, the detachment of cells slightly began at 140 h. Unfortunately, the time frame of 160 h was not sufficient to see if the decrease was definitive or kept oscillating. The MTT assay confirmed that the concentration of 200 $\mu\text{g mL}^{-1}$ displayed a reduction of cell viability of around 25% after 160 h. For lower concentrations (i.e., 50 $\mu\text{g mL}^{-1}$ and 100 $\mu\text{g mL}^{-1}$), an increase of cell viability was noticed.

2.1.2. Effect of EPS and Heparin Alone

The effect of both EPS-DR and -DRS and heparin on cell proliferation and cell viability is showed in Figure 2. It is noticed that NCI plot of EPS-DRS is very different from the ones of heparin and EPS-DR. For EPS-DRS, a second round of xCELLigence experiment was performed, leading to a higher number of MNNG/HOS cells (i.e., 5000 cells) compared to the first one (i.e., 3000 cells). This is why the control of EPS-DRS reached the peak of proliferation sooner than the two other ones, while for heparin and EPS-DR cells were still proliferating. This allowed evidencing the effect of the not modulated by the addition of heparin whatever the concentration considered. It was noticed that for 50 $\mu\text{g mL}^{-1}$ of EPS-DR, the lowest sulfated EPS of this study, 100% viability was reached compared to the control.

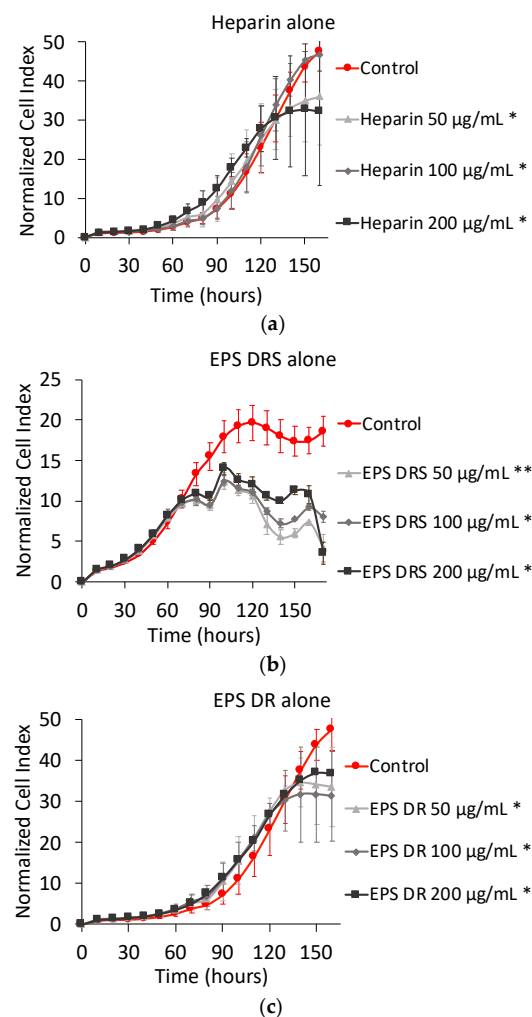


Figure 2. To the left, normalized cell index plot of MNNG/HOS cells after 160 of contact with (a) heparin alone at 50 $\mu\text{g mL}^{-1}$ (*), 100 $\mu\text{g mL}^{-1}$ (*), and 200 $\mu\text{g mL}^{-1}$ (*); (b) EPS DRS alone at 50 $\mu\text{g mL}^{-1}$ (**), 100 $\mu\text{g mL}^{-1}$ (*), and 200 $\mu\text{g mL}^{-1}$ (*); (c) EPS-DR alone at 50 $\mu\text{g mL}^{-1}$ (*), 100 $\mu\text{g mL}^{-1}$ (*), and 200 $\mu\text{g mL}^{-1}$ (*).

2.1.3. Effect of Polysaccharide:Scandium Complexes Heparin:Scandium (Hep:Sc) Complex

Figure 3 shows the NCI plot from xCELLigence RTCA of MNNG/HOS cells after 160 h of contact. The Hep:Sc complexes were prepared for four different metal-to-ligand ratios. For a metal-to-ligand ratio of 1:0.5 (Figure 3a), with a total concentration of heparin of $50 \mu\text{g mL}^{-1}$, there was no effect on cell proliferation. After 100 h of contact, for the same metal-to-ligand ratio but with higher concentrations of heparin (i.e., 100 and $200 \mu\text{g mL}^{-1}$ respectively), there was a significant decrease of the cell proliferation rates.

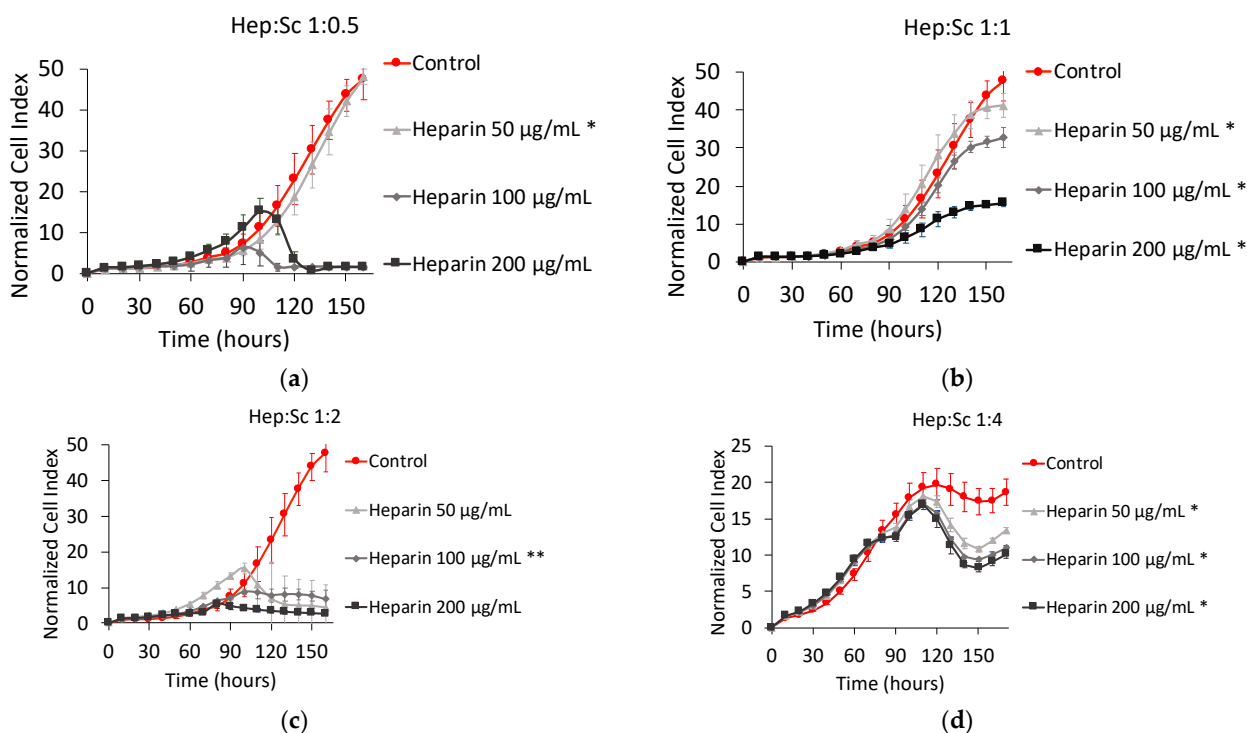


Figure 3. Normalized cell index Plot of MNNG/HOS cells after 160 h of contact with different stoichiometric ratios L:M: (a) heparin:scandium (Hep:Sc) 1:0.5 at $50 \mu\text{g mL}^{-1}$ (*), $100 \mu\text{g mL}^{-1}$, and $200 \mu\text{g mL}^{-1}$; (b) Hep:Sc 1:1 at $50 \mu\text{g mL}^{-1}$ (*), $100 \mu\text{g mL}^{-1}$ (*), and $200 \mu\text{g mL}^{-1}$ (*); (c) Hep:Sc 1:2 at $50 \mu\text{g mL}^{-1}$, $100 \mu\text{g mL}^{-1}$ (**), and $200 \mu\text{g mL}^{-1}$; (d) Hep:Sc 1:4 at $50 \mu\text{g mL}^{-1}$ (*), $100 \mu\text{g mL}^{-1}$ (*), and $200 \mu\text{g mL}^{-1}$ (*). * = p value ≤ 0.0001 , ** = p value ≤ 0.005 .

With a metal-to-ligand ratio Hep:Sc of 1:1 (Figure 3b), the decrease in cell proliferation was well displayed and dose-dependent. For metal-to-ligand ratio of Hep:Sc of 1:2 (Figure 3c), there was no further exponential growth after 90 h of contact for all the concentrations of heparin considered. Finally, for a metal-to-ligand ratio of Hep:Sc of 1:4 (Figure 3d), there were the same proliferation rates between the control and treated cells until 100 h of incubation followed by a temporary decrease of cell proliferation.

If those results are compared to the ones obtained on cell viability, the metal-to-ligand ratio ratios of 1:0.5 and 1:4 exhibited higher percentages of cell viability. In contrast, for a constant metal-to-ligand ratio of 1:1, a significant decrease of almost 40% is observed when increasing the total concentration of heparin. The only drop on cell viability is observed for a metal-to-ligand ratio of 1:2 and for a concentration of heparin of $200 \mu\text{g mL}^{-1}$; at these conditions, there is no more viable cells present in the well after 160 of contact.

EPS-DRS:Scandium (EPS-DRS:Sc) Complex

Figure 4 shows the NCI plot of MNNG/HOS cells after 160 h of contact with four metal-to-ligand ratio of EPS-DRS:Sc complex. Regarding the four metal-to-ligand ratio of the EPS-DRS:Sc complexes, the shape are very close to each other, meaning that neither the metal to ligand ratio, nor the total concentration of EPS-DRS play a key role in the cell

proliferation. Only one difference could be noticed, a slight reduction of cell proliferation, in the range 10–15 to 5–10 of NCI. For an EPS-DRS concentration of $200 \mu\text{g mL}^{-1}$, the cell proliferation decreases suddenly after 150 h, after than a plateau has been reached. This has been noticed for the four metal-to-ligand ratios considered. This seems stopping the oscillating kinetics to very low and stable NCI values, comparable to those of heparin complexes (see Figure 3). No significant changes in cell viability for the four metal-to-ligand ratios considered, was observed, even at for the concentration of $200 \mu\text{g mL}^{-1}$ in EPS-DRS.

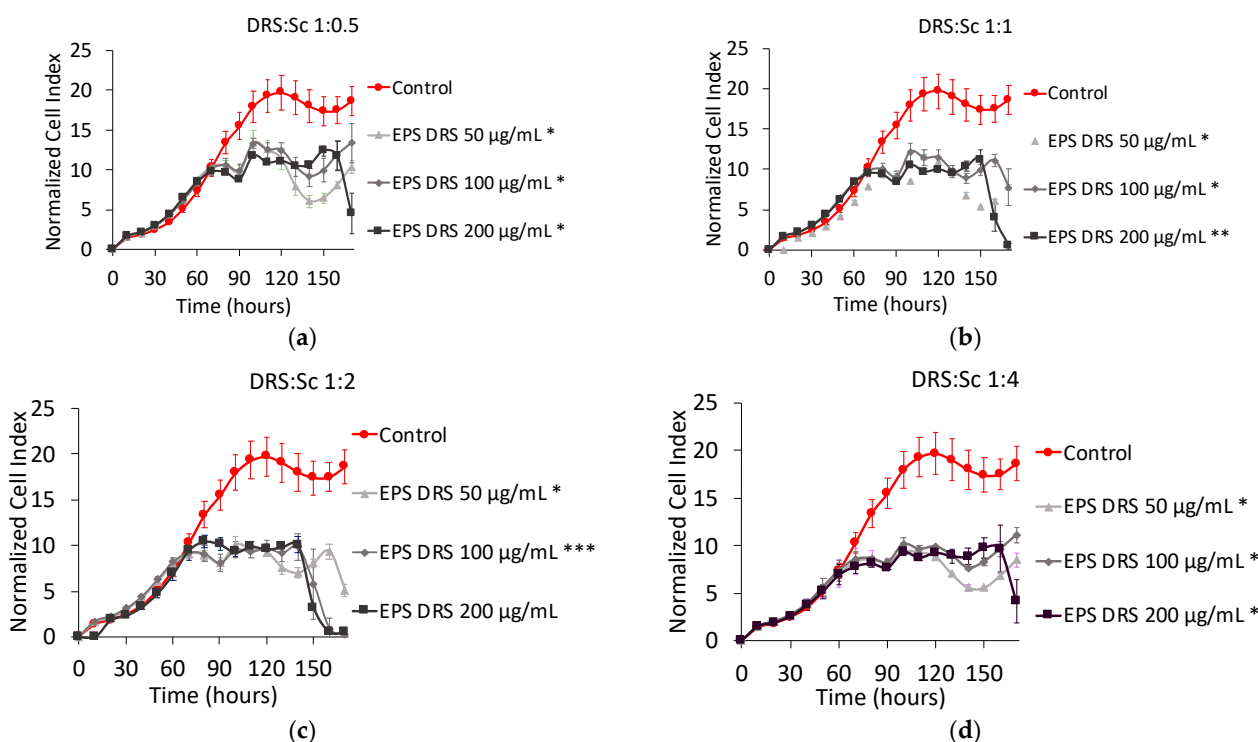


Figure 4. Normalized cell index plot of MNNG/HOS cells after 160 h of contact with different stoichiometric ratios L:M: (a) EPS-DRS:Sc 1:0.5 at $50 \mu\text{g mL}^{-1}$ (*), $100 \mu\text{g mL}^{-1}$ (*), and $200 \mu\text{g mL}^{-1}$ (*); (b) EPS-DRS:Sc 1:1 at $50 \mu\text{g mL}^{-1}$ (*), $100 \mu\text{g mL}^{-1}$ (*), and $200 \mu\text{g mL}^{-1}$ (**); (c) EPS-DRS:Sc 1:2 at $50 \mu\text{g mL}^{-1}$ (*), $100 \mu\text{g mL}^{-1}$ (***), and $200 \mu\text{g mL}^{-1}$; (d) EPS-DRS:Sc 1:4 at $50 \mu\text{g mL}^{-1}$ (*), $100 \mu\text{g mL}^{-1}$ (*), and $200 \mu\text{g mL}^{-1}$ (*). * = p value ≤ 0.0001 , ** = p value ≤ 0.005 , *** = p value ≤ 0.05 .

EPS-DR:Scandium (EPS-DR:Sc) Complex

Figure 5 shows the NCI plot on MNNG/HOS cells after 160 h of contact with four metal-to-ligand ratios of EPS-DR:Sc complex. For the ratios EPS-DR:Sc 1:1 and 1:2, the cell proliferation profiles are quite similar. For the metal-to-ligand ratio of 1:1, after 100 h of contact, a peak of proliferation was reached at very low NCI for all the EPS-DR concentrations considered. Then, there was a plateau that tended to zero NCI for the highest concentration of EPS-DR. For the ratios EPS-DR:Sc 1:1 and 1:2, the standard deviation of all the curves appeared very high. Likewise, even for metal-to-ligand ratio of 1:0.5 and 1:4, similar curves were obtained, that could be quite well superimposed with the control. For these two metal-to-ligand ratios, the cell proliferation started oscillating after 120 h.

The cell proliferation profiles were compared to the cell viability results. For metal-to-ligand ratio of 1:0.5 and 1:4, there was a high percentage of cell viability after 160 h of contact whereas for metal-to-ligand ratio of 1:1, there was a significant decrease when increasing the concentration of EPS-DR. This behavior was very similar to the one observed on Hep:Sc complexes.

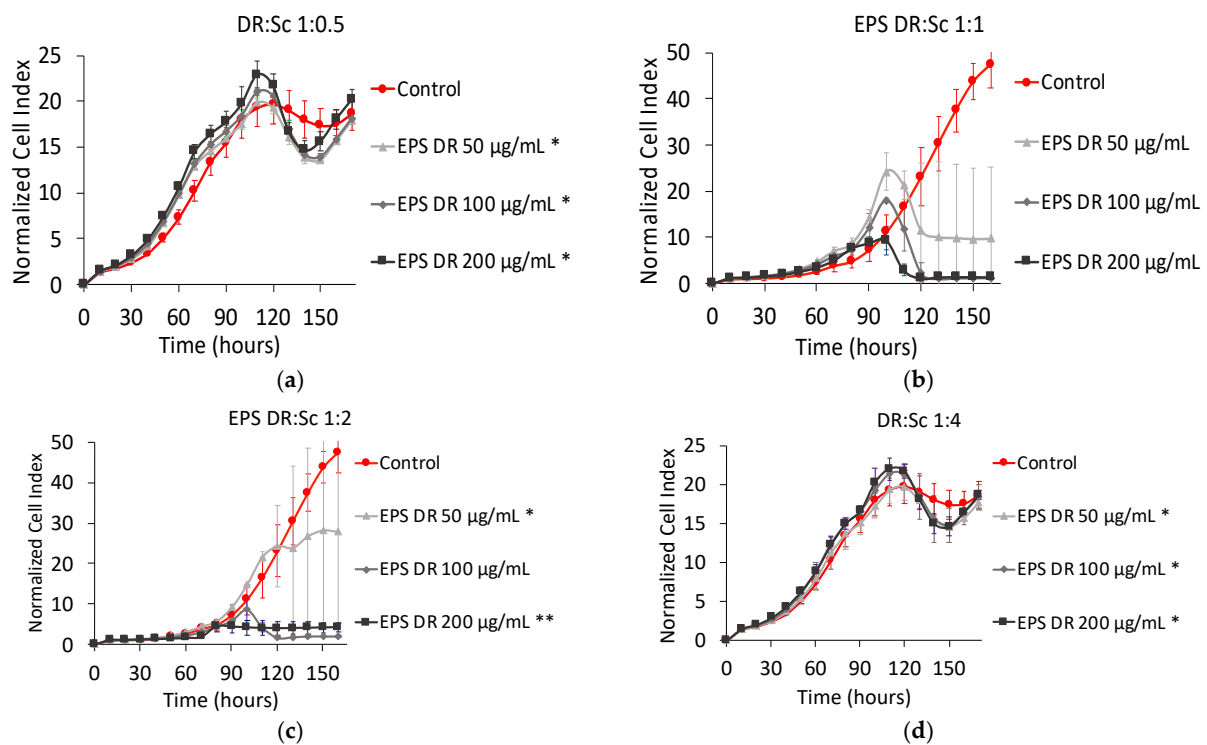


Figure 5. Normalized cell index plot of MNNG/HOS cells after 160 h of contact with different stoichiometric ratios L:M: (a) EPS-DR:Sc 1:0.5 at 50 µg mL⁻¹ (*), 100 µg mL⁻¹ (*), and 200 µg mL⁻¹ (*); (b) EPS-DR:Sc 1:1 at 50 µg mL⁻¹, 100 µg mL⁻¹, and 200 µg mL⁻¹; (c) EPS-DR:Sc 1:2 at 50 µg mL⁻¹ (*), 100 µg mL⁻¹, and 200 µg mL⁻¹ (**); (d) EPS-DR:Sc 1:4 at 50 µg mL⁻¹ (*), 100 µg mL⁻¹ (*), and 200 µg mL⁻¹ (*). * = p value ≤ 0.0001, ** = p value ≤ 0.005.

2.2. Human A375 Melanoma Cells

Effect of Scandium and Polysaccharides Alone

Figure 6 shows the effect on cell proliferation of scandium, as well as the three polysaccharides alone. All the compounds reduced the cell proliferation after 95 h of contact. The effect of scandium alone was comparable to that of heparin or EPS-DR alone. Nevertheless, the EPS-DRS alone, that had the higher sulfate content, displayed a more traditional profile of detaching cells.

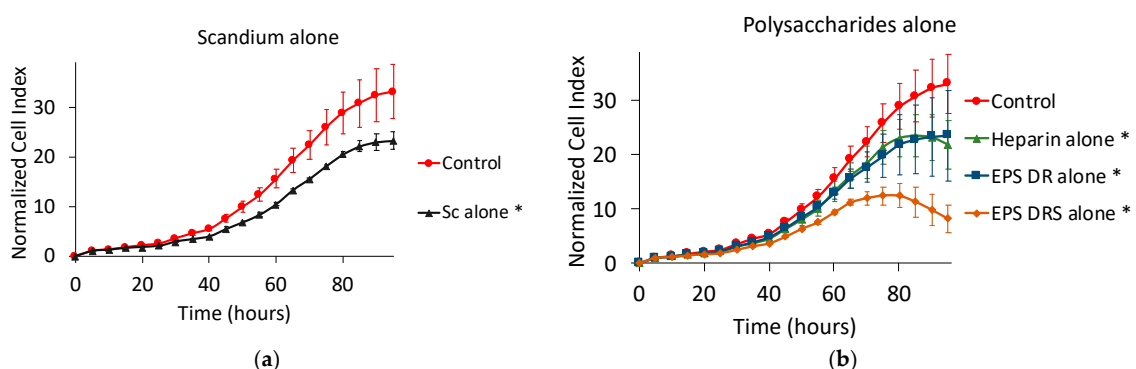


Figure 6. Normalized cell index plot of human A375 melanoma cells after 95 h of contact with (a) scandium at concentration of 100 µg mL⁻¹ (*) and (b) polysaccharides alone at concentration of 100 µg mL⁻¹: heparin (*), EPS-DRS (*), EPS-DR (*). * = p value ≤ 0.0001.

2.3. Effect of Polysaccharide:Scandium Complexes

For both EPS considered in this work, i.e., EPS-DR and -DRS, scandium-polysaccharide complexes were more efficient in reducing the cell proliferation than the EPS themselves as shown in Figure 7. For Hep:Sc (Figure 7a) and EPS-DRS:Sc (Figure 7b) complexes, at increasing metal-to-ligand ratio, a more important decrease in cell proliferation was observed. The same trend could be observed for EPS-DR:Sc complexes (Figure 7c). The best conditions for reducing the cell proliferation were reached for a metal-to-ratio of 1:2, leading to a cell proliferation reduction of approximately 55–88%.

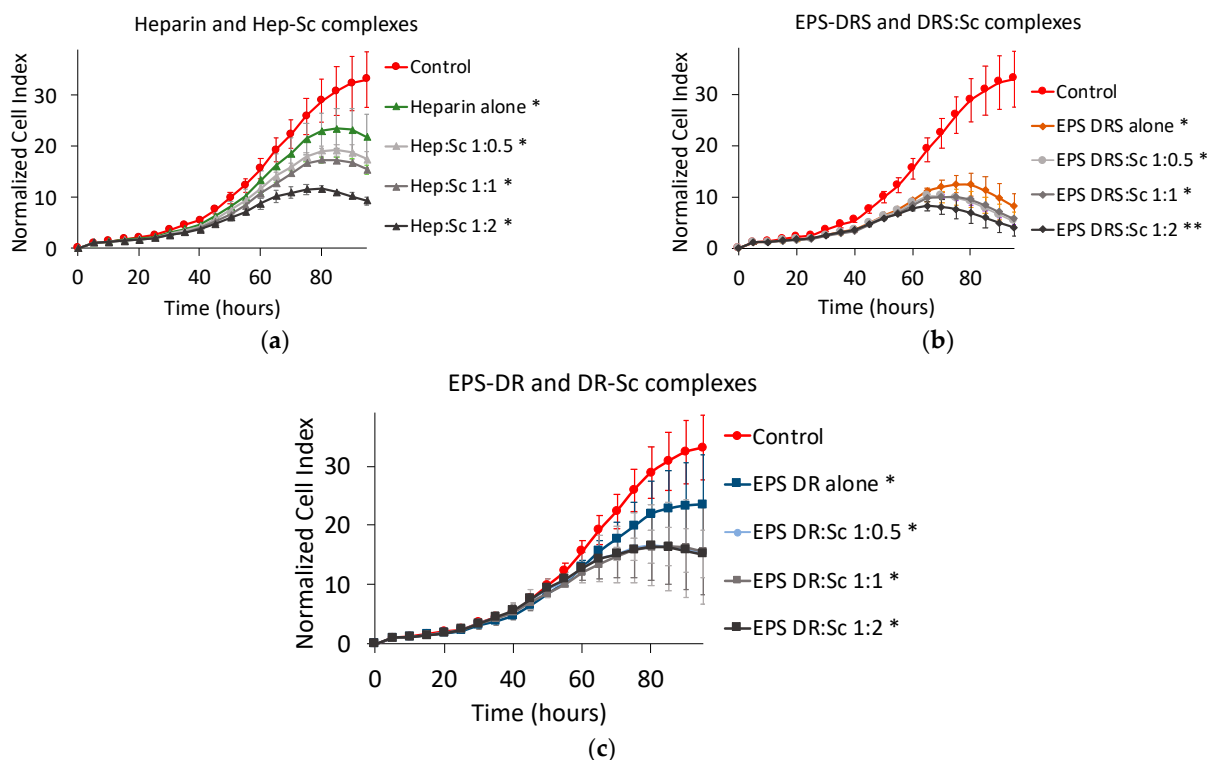


Figure 7. Normalized cell index plot of human A375 melanoma cells after 95 h of contact with different scandium-polysaccharide complexes at concentration of $100 \mu\text{g mL}^{-1}$ and various stoichiometric ratios: (a) Hep:Sc 1:0.5 (*), 1:1 (*), 1:2 (*), heparin alone (*); (b) EPS-DRS:Sc 1:0.5 (*), 1:1 (*), 1:2 (**), EPS-DRS alone (*); (c) EPS-DR:Sc 1:0.5 (*), 1:1 (*), 1:2 (*), EPS-DR alone (*). * = p value ≤ 0.0001 , ** = p value ≤ 0.005 .

2.4. Human A549 Lung Cancer Cells

2.4.1. Effect of Scandium and Polysaccharides Alone

From Figure 8a, scandium seemed having no impact on the proliferation of lung cancer cells after 95 h of contact. By contrast, among the polysaccharides considered in this work, only EPS-DRS seemed to slow down the kinetic of the cell proliferation. By comparison to EPS-DR, containing lower sulfate content, it could be assumed so far that the sulfate content of the macromolecule played a role on the cell proliferation, at least for the cell line A549.

2.4.2. Effect of Polysaccharide:Scandium Complexes

As shown in Figure 9a–c, the cell proliferation curves obtained when the cells contacted EPS-DR:Sc and Hep:Sc complexes, exhibited quite similar kinetic behaviors.

Only the metal-to-ligand ratio of 1:2 had an impact on the cell proliferation. This effect was more pronounced with EPS-DRS:Sc (Figure 9b) but for this one, there was no influence of the metal-to-ligand ratio.

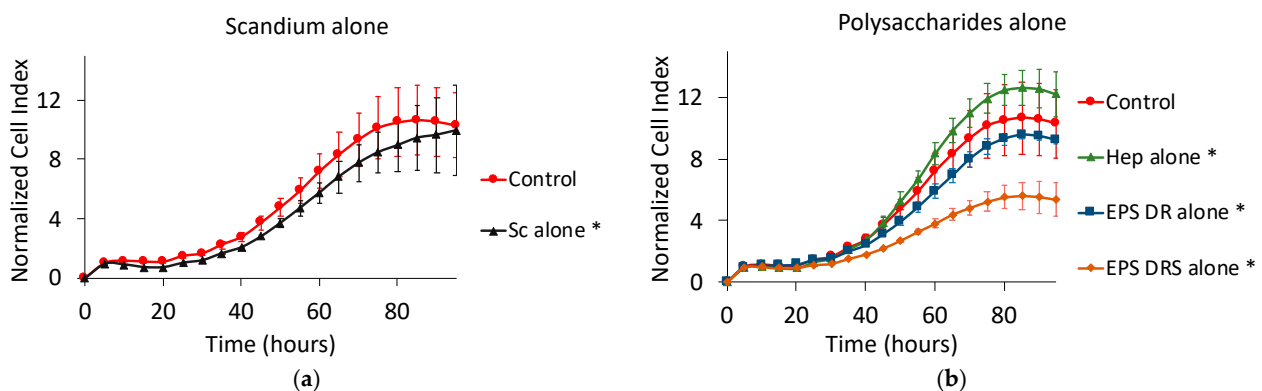


Figure 8. Normalized cell index plot of human A549 lung cancer cells after 95 h of contact with (a) scandium at concentration of $100 \mu\text{g mL}^{-1}$ (*) and (b) polysaccharides alone at concentration of $100 \mu\text{g mL}^{-1}$: heparin (*), EPS-DRS (*), EPS-DR (*). * = p value ≤ 0.0001 .

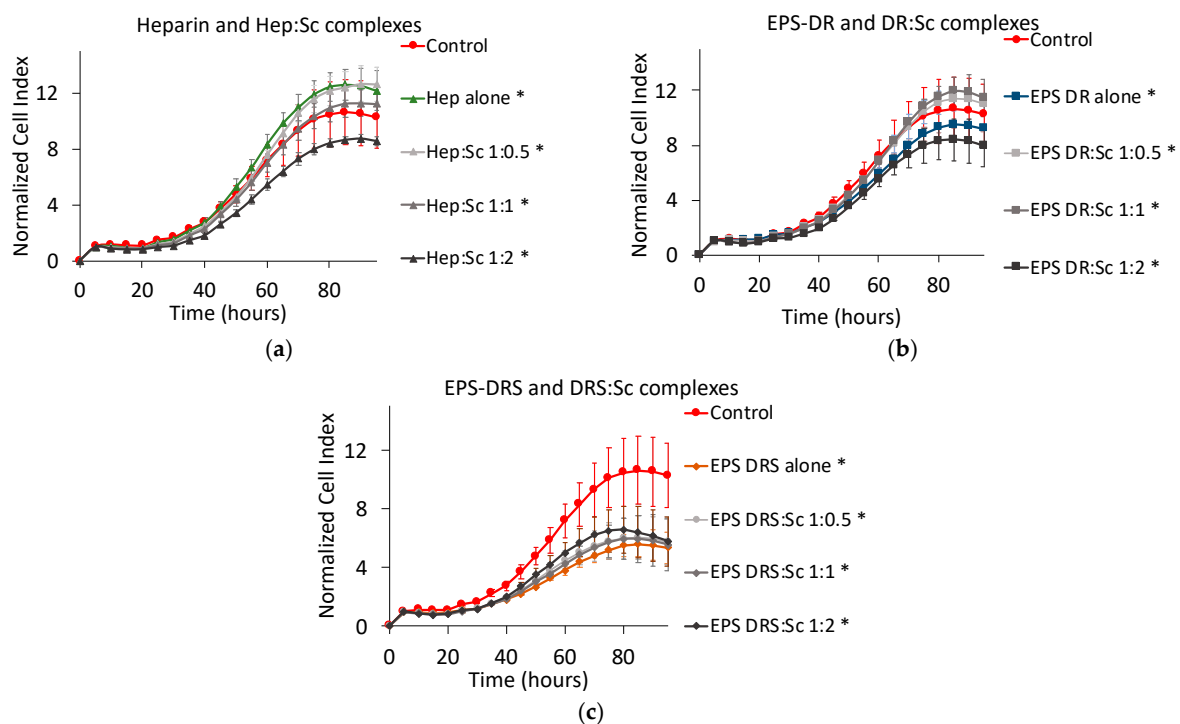


Figure 9. Normalized cell index plot of human A549 lung cancer cells after 95 h of contact with different scandium-polysaccharide complexes at concentration of $100 \mu\text{g mL}^{-1}$ and various stoichiometric ratios: (a) Hep:Sc 1:0.5 (*), 1:1 (*), 1:2 (*), heparin alone(*); (b) EPS-DR:Sc 1:0.5 (*), 1:1 (*), 1:2 (*), EPS-DRS alone (*); (c) EPS-DRS:Sc 1:0.5 (*), 1:1 (*), 1:2 (*), EPS-DR alone (*). * = p value ≤ 0.0001 .

2.5. Human U251 Glioblastoma Cells

Scandium alone induced a slight decrease of U251 cell proliferation (Figure 10a). Among the three polysaccharides, only heparin and EPS-DRS (Figure 10b), the most sulfated polysaccharides, slowed down the proliferation of approximately 45% compared to the untreated control group.

When considering the scandium complexes (Figure 10c–e), in particular, Hep:Sc and EPS-DR:Sc complexes showed a less efficient reduction in the proliferation of glioblastoma cells compared to the polysaccharide themselves. As observed for the other cell lines tested, there was an exception for the metal-to-ligand ratio 1:2 that influenced the kinetics. Additionally, EPS-DRS:Sc complexes were rather more efficient than DRS alone but this

activity was not correlated to the metal-to-ligand ratio as has been evidenced by the other cell lines tested above.

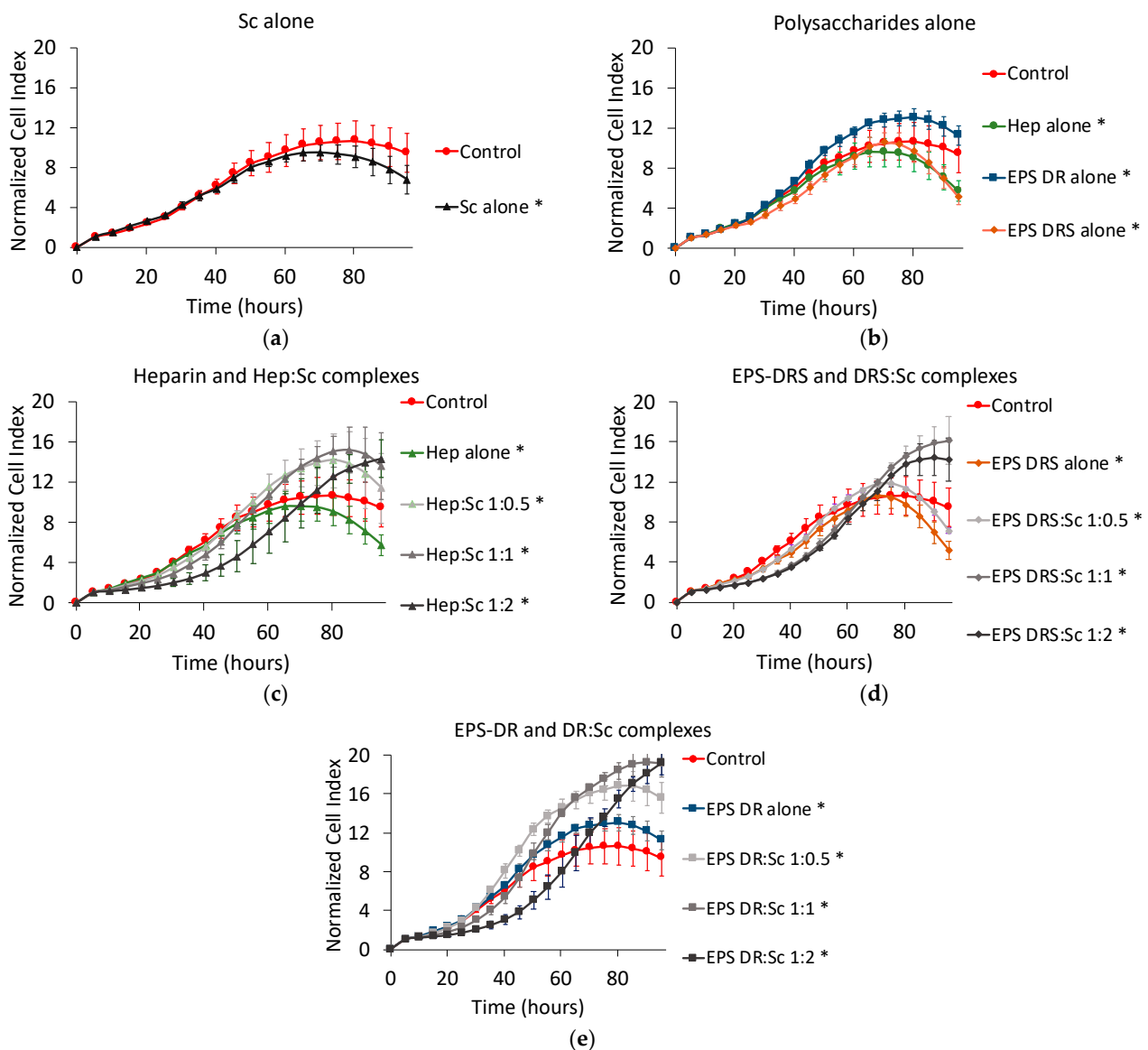


Figure 10. Normalized cell index plot of human U251 glioblastoma cells after 95 h of contact with (a) scandium at concentration of $100 \mu\text{g mL}^{-1}$ (*) and (b) polysaccharides alone at concentration of $100 \mu\text{g mL}^{-1}$: heparin (*), EPS-DRS (*), EPS-DR (*). Normalized cell index plot of U251 cells after 95 h of contact with different scandium-polysaccharide complexes at concentration of $100 \mu\text{g mL}^{-1}$ and various stoichiometric ratios: (c) Hep:Sc 1:0.5 (*), 1:1 (*), 1:2 (*), heparin alone(*); (d) EPS-DRS:Sc 1:0.5 (*), 1:1 (*), 1:2 (*), EPS-DRS alone (*); (e) EPS-DR:Sc 1:0.5 (*), 1:1 (*), 1:2 (*), EPS-DR alone (*). * = p value ≤ 0.0001 .

2.6. Human MDA231 Breast Cancer Cells

Scandium alone slightly decreased the cell proliferation of breast cancer cell, as shown in Figure 11a. Among the polysaccharides alone, only EPS-DRS demonstrated highly reducing the kinetics of proliferation (Figure 11b).

Hep:Sc and EPS-DR:Sc complexes were more efficient than the respective polysaccharides alone only at the stoichiometric ratio L:M 1:1 (Figure 11c–e), but standard deviations were very high for all the curves. EPS-DRS:Sc complexes exhibited the same effect of the polysaccharide alone (Figure 11d).

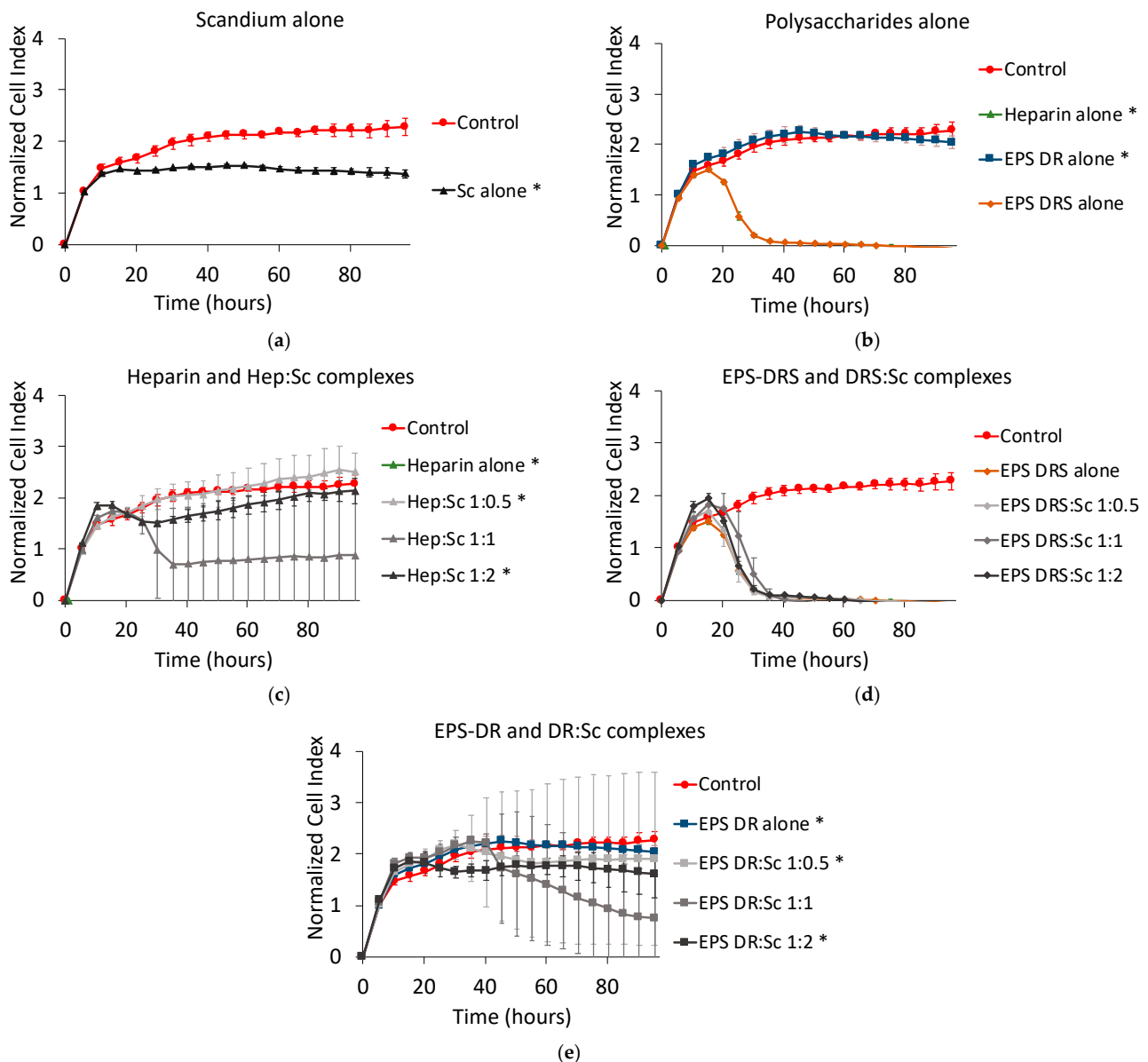


Figure 11. Normalized cell index plot of human MDA231 breast cancer cells after 95 h of contact with (a) scandium at concentration of $100 \mu\text{g mL}^{-1}$ (*) and (b) polysaccharides alone at concentration of $100 \mu\text{g mL}^{-1}$: heparin (*), EPS-DRS, EPS-DR (*). Normalized cell index plot of MDA231 cells after 95 h of contact with different scandium-polysaccharide complexes at concentration of $100 \mu\text{g mL}^{-1}$ and various stoichiometric ratios: (c) Hep:Sc 1:0.5 (*), 1:1, 1:2 (*), heparin alone (*); (d) EPS-DRS:Sc 1:0.5, 1:1, 1:2, EPS-DRS alone; (e) EPS-DR:Sc 1:0.5 (*), 1:1, 1:2 (*), EPS-DR alone (*). * = p value ≤ 0.0001 .

2.7. Human Caco2 Colon Cancer Cells

For this cell line, the contact time was prolonged to 140 h to display significant effects of compounds. Scandium alone did not have any effect on cell proliferation of colon cancer cells, as shown in Figure 12a. Once again, only EPS-DRS demonstrated significantly reducing the kinetics of proliferation (Figure 12b).

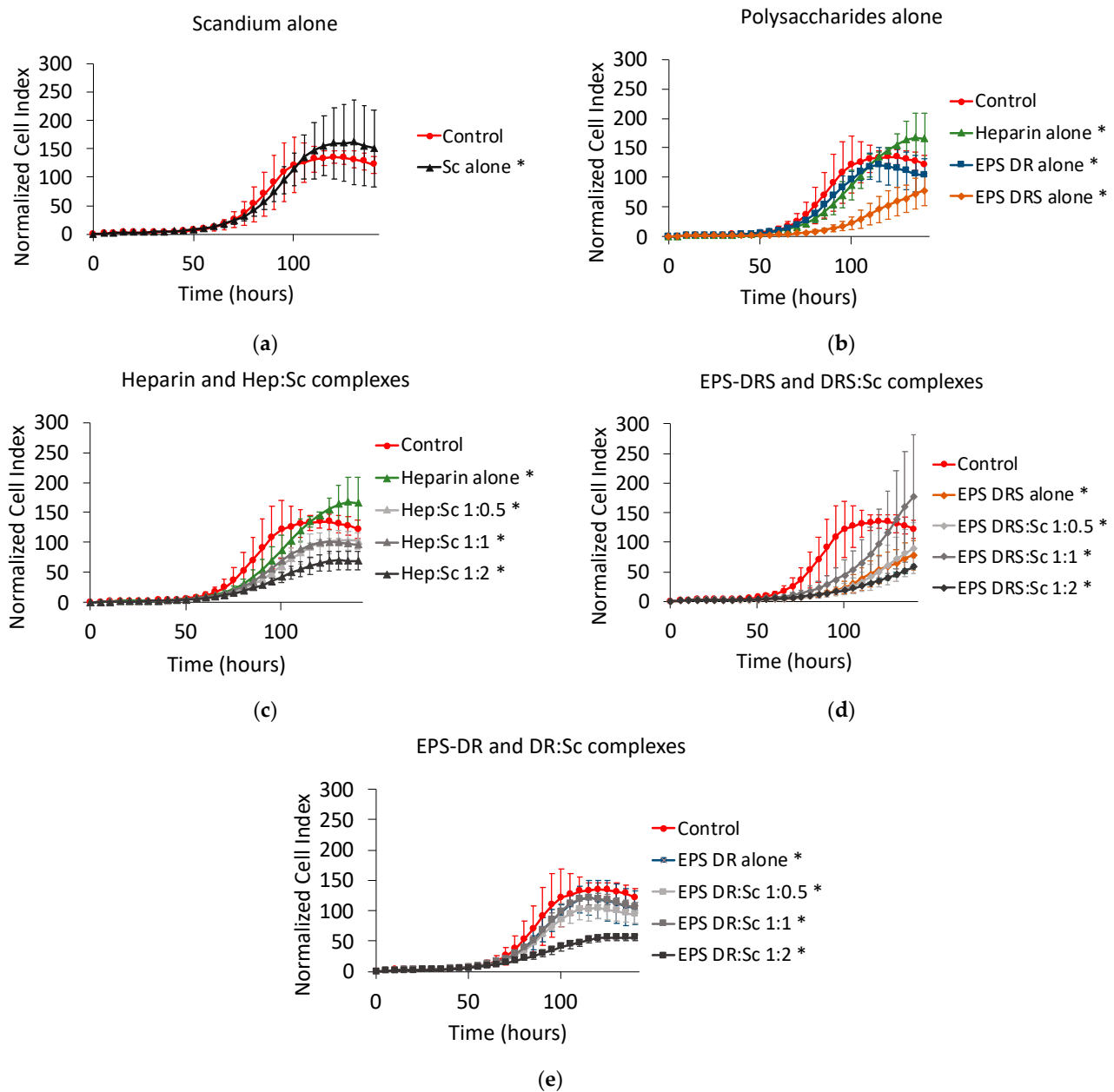


Figure 12. Normalized cell index plot of human Caco2 colon cancer cells after 140 h of contact with (a) scandium at concentration of $100 \mu\text{g mL}^{-1}$ (*) and (b) polysaccharides alone at concentration of $100 \mu\text{g mL}^{-1}$: heparin (*), EPS-DRS (*), EPS-DR (*). Normalized cell index plot of Caco2 colon cancer cells after 140 h of contact with different scandium-polysaccharide complexes at concentration of $100 \mu\text{g mL}^{-1}$ and various stoichiometric ratios: (c) Hep:Sc 1:0.5 (*), 1:1 (*), 1:2 (*), heparin alone (*); (d) EPS-DRS:Sc 1:0.5 (*), 1:1 (*), 1:2 (*), EPS-DRS alone (*); (e) EPS-DR:Sc 1:0.5 (*), 1:1 (*), 1:2 (*), EPS-DR alone (*). * = p value ≤ 0.0001 .

Hep:Sc and EPS-DR:Sc complexes were more efficient than the respective polysaccharides alone only at the stoichiometric ratio of 1:2 (Figure 12c,e). EPS-DRS:Sc complexes exhibited the same effect of the polysaccharide alone (Figure 12d), except at the ratio 1:1.

Table 1 summarizes the effect of Hep:Sc and EPS:Sc complexes for different metal-to-ligand ratio and different concentrations on human osteosarcoma, melanoma, lung cancer, glioblastoma and breast cancer cell lines.

Table 1. Summary of the effect of Hep:Sc and EPS:Sc complexes for different metal-to-ligand ratio and different concentrations on MNNG/HOS, A375, A549, U251, MDA231 and Caco3. + = low anti-proliferative effect, ++ = medium anti-proliferative effect, +++ = high anti-proliferative effect, – = low proliferative effect, – – = medium proliferative effect, – – – = high proliferative effect, NT = not tested.

Complex	Ratio	Total Conc. of GAGs	Total Conc. of Sc	Effect on Cell Proliferation					
				MNNG/HOS	A375	A549	U251	MDA231	Caco2
	M:L	$\mu\text{g mL}^{-1}$	$\mu\text{g mL}^{-1}$	Osteosarcoma	Melanoma	Lung	Glioblastoma	Breast Cancer	Colon Cancer
Hep:Sc	1:0.5	50	0.36	No effect			NT		
		100	0.71	+++	++	–	–	No effect	+
		200	1.42	+++					
	1:1	50	0.71	+				NT	
		100	1.42	++	++	No effect	– –	++	+
		200	2.83	+++					
	1:2	50	1.42	+++				NT	
		100	2.83	+++	+++	+	– –	No effect	++
		200	5.66	+++					
	1:4	50	2.83	++					
		100	5.66	++				NT	
		200	11.32	++					
EPS-DRS:Sc	1:0.5	50	0.40	++					
		100	0.79	+	+++	++	+	+++	+
		200	1.58	+					
	1:1	50	0.79	++				NT	
		100	1.58	++	+++	++	– –	+++	–
		200	3.16	+++					
	1:2	50	1.58	+++				NT	
		100	3.16	+++	+++	++	–	+++	++
		200	6.31	+++					
	1:4	50	3.16	+++					
		100	6.31	++				NT	
		200	12.62	+++					
EPS-DR:Sc	1:0.5	50	0.24	No effect					
		100	0.48	No effect	++	–	– –	No effect	+
		200	0.95	No effect					
	1:1	50	0.48	+++				NT	
		100	0.95	+++	++	–	– – –	++	+
		200	1.90	+++					
	1:2	50	0.95	++				NT	
		100	1.90	+++	++	+	– – –	+	++
		200	3.79	+++					
	1:4	50	1.90	No effect					
		100	3.79	No effect				NT	
		200	7.58	No effect					

3. Discussion

3.1. Effect of Scandium Alone

Published data are quite scarce on scandium, which seems not having a major biological role. The food chain contains trace amounts of this metal, so the average daily intake per person is less than 0.1 µg [24]. To the best of our knowledge, the toxicity of scandium has not been reported. The major risk of scandium exposure could be aerosols and gasses that can be inhaled within a working environment (for instance rare-earth mining plants). A long-term exposure by inhalations may cause lung embolism. Kawai et al. [24] have reported that low concentrations of scandium can determine an overproduction of antibiotic when added to certain *Streptomyces* cultures.

In our study, a biological effect has been highlighted on the different cancer cell lines (osteosarcoma, lung, glioblastoma, melanoma, breast). The literature found on the evaluation of scandium has described an absorption and prolonged retention of scandium in some tissues [25], especially with accumulation in the liver, spleen and bone [26] or in the bone [27]. A complete biodistribution with $^{46}\text{Sc}^{3+}$ [28] has been performed. From the best of our knowledge, there is no reported data on in vitro cytotoxicity studies of scandium with osteosarcoma cells. Only one study from Herath and Evans [29] described the effect of scandium oxide (Sc_2O_3), that is a solid compound, on a commercial human osteoblast-like cell line (TE85 HOS). Scandium oxide showed a lower cell proliferation after 3 weeks of contact compared to the control. TE85 HOS represent the parental cells from which the MNNG/HOS cells were derivated after chemical transformation with 0.01 µg mL⁻¹ MNNG (a carcinogenic nitrosamine). TE85 HOS parental cell line is not tumorigenic in mouse in contrast to MNNG/HOS. Herath and Evans [29] also demonstrated by cell viability studies, that Sc_2O_3 did not affect cell viability.

3.2. Effect of Heparin and EPS Alone

It is already known that GAG participate in the regulation of several cellular events, such as cell adhesion, proliferation and migration [4]. Actually, GAGs are heterogeneous macromolecules characterized by a high diversity of disaccharide units that forms the primary structure. Major differences include types of uronic acid and hexosamine, number and position of *O*-sulfated and *N*-sulfated groups, resulting in GAGs with different chemical and biological properties [30]. Among GAGs, heparin has already showed a significant antiproliferative effect on various cell types [31–33]. Studies have demonstrated that high contents in heparin structure of iduronic acid (IdoA) and *N*-sulfated glucosamine (GLcN) are fundamental to inhibit cell proliferation [31]. The degree of sulfation has also revealed to be a critical factor in the inhibition of cell proliferation [31]. Nikitovic et al. [34] have proved a strong inhibition of cell proliferation of both normal and transformed osteoblasts by heparin already at low concentrations. In our study, heparin reduced, the cell proliferation in a dose-dependent manner after 160 h, as shown in Figure 2a. This time, however, is not enough to observe the drop of NCI like in EPS-DRS. The higher degree of sulfation could be the cause of such drop. These results agree with the previous in vitro studies relating the effect of these EPS on cell proliferation of MNNG/HOS cells [19] and osteoblastic cells [15].

It has been shown that high concentrations of GAGs interrupted growth factor-receptor signaling in osteoblasts-like Saos-2 cells by sequestering growth factors (e.g., FGF2) and preventing their interaction with cell-surface receptors [35]. This biological effect could be realized also with EPS, explaining the slowdown in cell proliferation kinetics.

Cell viability after 160 h of contact with the polysaccharides alone has been also assessed using MTT assays (results are not showed in this paper), and it resulted high for the polysaccharide concentrations considered. Considering the fact that the cell viability measured through the MTT assays, reflects mitochondrial metabolism as biochemical marker of cell viability, it could be reasonable to think that the slowdown or drop of cell proliferation is not imputable to the blockade of this biochemical process. EPS, as GAG mimetics, interact with cell transmembrane proteins such as selectins and integrins,

responsible of cell adhesion and cell-cell interactions [36]. Since the decrease in proliferation kinetics reflects the detaching of cells from the gold biosensors in the well, it could be possible that the loss of adhesion could be derivate from the lack of normal functioning of these cell transmembrane proteins and not from an internal cell damage like the stop of metabolism.

In the literature there have been evidences on the role of heparin in lung cancer [37,38]. Low molecular weight heparins (LMWH) were found to have positive effects in decreasing the proliferation of metastasis through its anticoagulant and non-anticoagulant properties (inhibition of P- and L-selectins). The effects on cell proliferation on primary tumors are more contested since heparin and other GAGs do not seem to effectively reduce it [3,39]. By contrast, in the present study, an increase of proliferation of human lung cancer cells was clearly evidenced with heparin at the concentration of $100 \mu\text{g mL}^{-1}$ in Figure 11b, whereas EPS-DR and -DRS displayed a more moderate slowdown of the kinetics. It was evidenced also that the sulfation degree played a role on this proliferation kinetics. This increase of anti-proliferative effect with an increasing the degree of sulfation is in agreement with the results of Wright et al. [31].

LMWH have also been tested in the past on human melanoma cells displaying valid anti-proliferative effects [40]. Additional experiments on melanoma models have demonstrated a clear antimetastatic effect, attributable to the non-anticoagulant properties of heparin. The antimetastatic mechanism of that seems to reside in the inhibition of P- and L-selectins with consequent lack of cell-cell interactions [40]. In the present case, the different polysaccharides considered alone exhibited an anti-proliferative effect on the cell growth kinetics of human melanoma cells, revealing also that the degree of sulfation of these polysaccharides play a positive modulation on the proliferation by reducing it. These results agree with those showing another GAG [41], from animal environment, showing also a significant decrease in the proliferation of melanoma cells.

By contrast, the role of certain GAGs, such as chondroitin sulfate, is controversial in the pathogenesis of glioblastoma and breast cancer, since they seem enhance the tumor invasion [42,43]. The same stimulating effect on cell proliferation has been shown by heparin on colon cancer [44]. From the results presented in Figures 10b and 12b, heparin and both EPS-DR and -DRS presented a slight effect in reducing the proliferation of glioblastoma and colon cancer cells. Schnoor et al. [45] have also demonstrated in vitro that heparin can cause a decrease of glioblastoma cell growth. Concerning breast cancer cell, no significant effect on the decrease of proliferation is showed, except for EPS-DRS. Comparing the effect of these three polysaccharides of interest, EPS DRS revealed to be the most efficient in reducing the proliferation kinetics of all the four cell lines tested, especially on MNNG/HOS cells where the effect is dose dependent.

3.3. Synergic Effect of Complexes

Polysaccharide-scandium complexes (EPS-DR:Sc, EPS-DRS:Sc and Hep:Sc) are more efficient than their respective polysaccharides alone in reducing the cell proliferation. That was the case for all the cell lines tested, thus revealing that the complexation with scandium does not prevent the biological activity of these polysaccharides. There is a synergetic effect by combining these polysaccharides with scandium, since the anti-proliferative effect has risen.

3.3.1. Heparin:Sc (Hep:Sc)

On MNNG/HOS cell line, as shown in Figure 3, the complex Hep:Sc with a 1:0.5 metal-to-ligand ratio appears the most efficient complex in reducing the NCI to almost zero, followed by the metal-to-ligand ratio 1:2 of Hep:Sc. Both complexes exhibit a dose-response effect; in particular for the complex Hep:Sc with a 1:1 metal-to-ligand ratio. From a clinical point of view, the change in concentration of this complex would allow controlling its therapeutic window, revealing a good candidate for the elaboration of a new therapeutic

strategy. The effect of the other complex seems to appear, instead, as an on-off effect, more difficult to control.

For the highest concentration for all the complexes tested on MNNG/HOS cells, the profile of their proliferation kinetics was quite different. The complexation with scandium and in particular, the different ratios seem to induce different effects. This could reside in a different polymer conformation assumed by heparin at different ratios of metal. From our previous work, the effect of added counterions on polysaccharide conformation has been assessed revealing how hydrodynamic volume and gyration radius of this polyelectrolyte is influenced by the ionic strength, so by the opposite charges provided by the presence of metal ions. If the conformation of the polysaccharide changes, the way it interacts with its macromolecular targets would change as well, resulting in a different modulation of the biological effect [45].

Considering a fixed concentration of Hep:Sc complexes of $100 \mu\text{g mL}^{-1}$, the increase of the metal to ligand ratio had an important effect also on human melanoma and colon cancer cell line. After 95 h of contact for melanoma cells (140 h for colon cancer cells), the ratio 1:2 seems to exhibit the most pronounced anti-proliferative effect, whereas the decrease in cell proliferation is clearly dependent on the L:M ratio. The change in conformation mediated by the complexation would positively modulate the biological effect. By contrast, the proliferation kinetic on human lung cancer, glioblastoma and breast cancer cells did not seem to be impacted by the complex. This behavior indicates that heparin is not efficient as anti-proliferative agent on primary tumors generated from these three human cancer cell lines.

3.3.2. EPS-DRS:Sc and EPS-DR:Sc

Considering the effect of EPS-DR:Sc complexes on human osteosarcoma, melanoma cells, and colon cancer cells, the metal-to-ligand ratio of 1:1 and 1:2 revealed to have a significant impact on cell proliferation. One explanation of these two different kinetics may be related to the fact that complexation with scandium at these ratio lead into a change of conformation, this may inhibit cell proliferation for contact time superior to 90 h and at high concentrations of EPS. For metal-to-ligand ratio of 1:0.5 and 1:4, that are comparable, they show a very similar effect compared to EPS DR alone.

The same EPS-DR:Sc complexes did not display the same effect on human lung cancer, glioblastoma and breast cancer cell lines meaning that the slowdown in cell proliferation is not related to this specific kind of tumor. This seems in agreement with the fact that the biological effect normally influences only the formation of metastasis.

Glioblastoma appears to be not much sensitive to these GAG mimetics since even EPS-DRS:Sc did not show significant results in decreasing the proliferation kinetics. By the contrary, EPS-DRS:Sc revealed a great slowdown in the cell proliferation of human lung cancer, breast cancer, melanoma and colon cancer cell lines that was ratio dependent. The higher sulfate content of DRS may enhance the anticoagulant properties, resulting in a much stronger interaction with P- and L-selectins due the possibility to allow more electrostatic interactions with those proteins. Moreover, the possible change in conformation would act in a synergic way allowing a positive modulation of the anti-proliferative effect.

From cell assays, EPS-DRS:Sc with a 1:2 metal-to-ligand ratio, came out to be the best polysaccharide-scandium complex in reducing the cell proliferation of human osteosarcoma, human melanoma, human lung cancer, human breast cancer and colon cancer cells. These results confirm the importance of the degree of sulfation which positively enhances the cytostatic effect of these exopolysaccharides alone or complexed.

4. Materials and Methods

4.1. Molecules Assessed

Heparin sodium salt ($M_w = 18,320 \text{ Da}$, $S\% = 10\%$) from porcine intestinal mucosa H4784 and scandium chloride hexahydrate were purchased from Sigma-Aldrich (Saint Quentin Fallavier, France). EPS derivatives DR ($M_w = 16,440 \text{ Da}$, $S\% = 3\%$) and DRS

($M_w = 27,360$ Da, S% = 15%) were kindly provided by LEMMB laboratory of IFREMER (Nantes). Polysaccharide solutions (heparin, EPS-DR and EPS-DRS alone) were prepared at high concentration stock solutions (2×10^{-4} mol L⁻¹) in Milli-Q water; scandium alone solution was prepared at high concentration stock solution (10^{-1} mol L⁻¹) in Milli-Q water. For each of the three polysaccharides, a set of complexes with four stoichiometric metal-to-ligand ratio (1:0.5, 1:1, 1:2, 1:4) has been prepared by mixing different aliquots of the previous prepared stock solutions. Higher stoichiometric ratios have been excluded to avoid cytotoxic effects related to high ionic strengths.

Complexation between scandium and polysaccharides has been previously checked and displayed using Free-Ion Selective Radiotracer Extraction (FISRE) as described somewhere else [45]. FISRE was used to determine the stability constants of a complex L:M, at tracer level, using a cationic exchange resin Chelex 100, poured into the solutions. These solutions contained fixed 10^{-4} mol L⁻¹ Sc³⁺ and varying ligand concentration from 10^{-9} to 10^{-3} mol L⁻¹. The resulting suspensions were daily monitored and adjusted to pH = 6. The separation of the solid and liquid phases was done by sedimentation. Aliquots of the supernatant from 0.4 to 1 mL were taken for ICP-AES analysis (ICP spectrometer iCAP 6000 of Thermo Scientific, Illkirch, France).

M:L ratio has been established by preparing solutions where the concentration in mol/L of the metal was, from 0.5 to 4 times the one of ligand. After preparation, all 16 compounds (Sc alone, heparin alone and the four complexes Hep:Sc, EPS-DRS alone and the four complexes EPS-DRS:Sc, DR alone and the four complexes DR:Sc) were filtered with a 13 µm syringe filter before being frozen to prevent bacteria contamination. Fresh dilutions at 200, 100 and 50 µg/mL of each compound were obtained right before the experiments adding cell culture medium to aliquots from stock solutions.

4.2. Proliferation Assay

Human MNNG/HOS osteosarcoma cell line, A375 melanoma, A549 lung cancer, U251 glioblastoma, MDA231 breast cancer and Caco2 colon cancer cell lines were purchased from the American Tissue Cell Collection (ATCC, Molsheim, France). Human MNNG/HOS osteosarcoma cell line (ATCC) was cultured with DMEM high glucose, pyruvate, non-glutamine from Gibco (Thermo-Fisher), supplemented with glutamine (Thermo-Fisher) and 10% of fetal bovine serum (FBS, Thermo-Fisher). Human A375 melanoma cell line (ATCC) was cultured with DMEM 4.5 g/L high glucose, pyruvate, non-glutamine from Gibco (Thermo-Fisher), supplemented with glutamine (Thermo-Fisher) and 5% of fetal bovine serum (FBS, Thermo-Fisher). Human A549 lung cancer cell line (ATCC) was cultured with DEMEM/F12 (Sigma Aldrich), supplemented with glutamine (Thermo-Fisher) and 5% of fetal bovine serum (FBS, Thermo-Fisher). Human U251 glioblastoma cell line (ATCC) was cultured with DMEM 4.5 high glucose, pyruvate, non-glutamine from Gibco (Thermo-Fisher), supplemented with glutamine (Thermo-Fisher) and 5% of fetal bovine serum (FBS, Thermo-Fisher). Human MDA231 breast cancer cell line (ATCC) was cultured with L-15 media from Gibco (Thermo-Fisher), supplemented with glutamine (Thermo-Fisher) and 5% of fetal bovine serum (FBS, Thermo-Fisher). Human Caco2 colon cancer cell line (ATCC) was cultured with DMEM 4.5 g/L high glucose, pyruvate, non-glutamine from Gibco (Thermo-Fisher), supplemented with glutamine (Thermo-Fisher) and 5% of fetal bovine serum (FBS, Thermo-Fisher).

Cells were incubated at 37 °C with humidity saturated controlled atmosphere and 5% CO₂. At confluence, cells are detached using Trypsin (Thermo-Fisher) and washed to neutralize the enzyme. MNNG/HOS cells were seeded in triplicate at 5000 cells per well (50 µL) with 50 µL of culture medium (to measure the background) for 4 h, the time necessary for cell seeding, in an E-Plate view 96 (Chem Agilent, Santa Clara, CA, USA) before adding 100 µL of compound at the three concentrations (50, 100 and 200 µg mL⁻¹ for MNNG/HOS cells, 100 µg mL⁻¹ for A375, A549, U251 cells). The choice of these concentrations provided a wide range to study a possible dose dependent response. Proliferation curves are normalized respect the time point of drug incorporation. The plate was

monitored for 160 h (MNNG/HOS cells), 140 h (Caco2 cells) and 95 h (A375, A549, U251, MDA231 cells) using a RTCA instruments (Agilent and ACEA, Santa Clara, CA, USA). Experiments have been done in triplicates and repeated twice. Statistical tests have been conducted using Regression Data Analysis Tool in Excel®.

4.3. Viability Assay

MNNG/HOS cells were seeded in triplicate at 3000 cells per well (50 μ L) with 50 μ L of culture medium for 4 h in an E-Plate view 96 (Chem Agilent) before adding 100 μ L of compound at the three concentrations (50, 100 and 200 μ g mL⁻¹). The choice of these concentrations provided a wide range to study a possible dose dependent response. The plate was left 160 h: the volume of each well was reduced to 100 μ L before adding 10 μ L of 5 mg/mL MTT (Sigma-Aldrich) and incubating for at least 3 h at 37 °C and 5% CO₂. After this time, the liquid was removed and 200 μ L of DMSO was added to each well to dissolve the formed formazan crystals before proceeding to the colorimetric quantification with a multi-well spectrophotometer (Victor 3x from PerkinElmer, Villebon-sur-Yvette, France) at the wavelength of 500–600 nm.

5. Conclusions

This *in vitro* study has demonstrated the biological effects of these unconventional exopolysaccharides. EPS derivatives (-DR or -DRS). EPS derivatives can slowdown cell proliferation kinetic, confirming their anti-proliferative effect on human osteosarcoma cells without significantly influencing the cell viability. Close results have been found also on human melanoma cells, while human glioblastoma cells have not been affected by those EPS derivatives. The anti-proliferative effect on other cell lines (i.e., human osteosarcoma, melanoma, breast cancer and lung cancer) is effective with polysaccharides but even more enhanced when EPS derivatives, and heparin, are complexed to scandium, in which the impact on the NCI is dose–response. The degree of complexation is represented by the different metal-to-ligand ratio. Different behaviors in the decrease of the proliferation kinetic have been evidenced depending on the metal-to-ligand ratio, that could be related to a conformation change of the polysaccharide when complexed with scandium. EPS-DRS:Sc with a 1:2 metal-to-ligand ratio has been shown to be the most effective compound in displaying a cytostatic effect. Our group has evidenced in a previous work [45] that the rheological behavior of EPS derivatives and heparin, notably the conformation, is influenced by the ionic strength of solvent, as well as at different concentrations of scandium. Thus, it is assumed that the change in conformation could modulate positively or negatively the antiproliferative effect. Concerning the cause of the antiproliferative or cytostatic effect, a damage in the cellular metabolism does not seem to be implicated since the cells remain viable, at least in the time frame of our study. The most probable explanation would be that an inhibition of growth factor-receptor signaling, as well as an interference of cell-cell adhesion mediated by specific transmembrane proteins.

These results are very encouraging in a theranostic perspective because of the intrinsic tropism of these EPS derivatives for cancer cells is maintained, even after the complexation. Additionally, the anti-proliferative effect on certain cell lines could be modulated by the degree of complexation. In the near future, the influence of the degree of complexation will be performed to investigate which are the best metal-to-ligand ratio in terms of efficacy. Besides, xCELLigence assay with EPS derivatives could be extended to other cell lines known to be sensible to GAG properties, while testing new assays to target other cellular mechanisms involved in cellular toxicity. Moreover, the biological effects of these EPS will be tested on normal cells as well in order to guarantee no cytostatic effect on healthy cells. The efficacy of these compounds will be evaluated with the PET tracer of ^{44m/44}Sc.

Author Contributions: Conceptualization, S.H.-M., D.H., and S.C.-J.; methodology, D.H., J.M.-G., M.M. and S.C.-J.; software, J.M.-G.; validation, D.H., S.H.-M. and S.C.-J.; formal analysis, J.M.-G., M.M.; investigation, J.M.-G., M.M.; resources, C.S., S.C.-J.; data curation, M.M., J.M.-G.; writing—original draft preparation, M.M.; writing—review and editing, D.H., J.M.-G., S.C.-J., S.H.-M., C.A.;

visualization, D.H., S.H.-M.; supervision, D.H., S.H.-M.; project administration, S.H.-M.; funding acquisition, S.H.-M. All authors have read and agreed to the published version of the manuscript.

Funding: This work has been supported in part by grants from the French National Agency for Research, called “Investissements d’Avenir” IRON Labex No. ANR-11-LABX-0018-01; and Arronax-Plus Equipex No. ANR-11-EQPX-0004 and ISITE NEXt (ANR-16-IDEX-0007). We acknowledge the Institut-Mines-Telecom and the Pays de la Loire council for the financial support of M. Mazza PhD grant.

Institutional Review Board Statement: Not applicable.

Informed Consent Statement: Not applicable.

Data Availability Statement: Data available in a publicly accessible repository. The data presented in this study are openly available at [10.3390/md19030174].

Conflicts of Interest: The authors declare no conflict of interest.

Abbreviations

CI	cell index
EPS	exopolysaccharides
GAG	glycosaminoglycans
LMW	low molecular weight
LMWH	Low molecular weight heparins
NCI	normalized cell index
RTCA	Real Cell Time Analysis

References

- Borsig, L. Antimetastatic activities of heparins and modified heparins. Experimental evidence. *Thromb. Res.* **2010**, *125*, S66–S71. [[CrossRef](#)]
- Yip, G.W.; Smollich, M.; Götte, M. Therapeutic value of glycosaminoglycans in cancer. *Mol. Cancer Ther.* **2006**, *5*, 2139–2148. [[CrossRef](#)]
- Belting, M. Glycosaminoglycans in cancer treatment. *Thromb. Res.* **2014**, *133*, S95–S101. [[CrossRef](#)]
- Afratis, N.; Gialeli, C.; Nikitovic, D.; Tsegenidis, T.; Karousou, E.; Theocharis, A.D.; Pavão, M.S.; Tzanakakis, G.N.; Karamanos, N.K. Glycosaminoglycans: Key players in cancer cell biology and treatment: GAG Targeting in Cancer Cell Biology. *FEBS J.* **2012**, *279*, 1177–1197. [[CrossRef](#)] [[PubMed](#)]
- Lyman, G.H. Thromboprophylaxis with low-molecular-weight heparin in medical patients with cancer. *Cancer* **2009**, *115*, 5637–5650. [[CrossRef](#)]
- Debourdeau, P.; Elalamy, I.; De Raignac, A.; Méria, P.; Gornet, J.M.; Amah, Y.; Korte, W.; Marty, M.; Farge, D. Long-term use of daily subcutaneous low molecular weight heparin in cancer patients with venous thromboembolism: Why hesitate any longer? *Support. Care Cancer* **2008**, *16*, 1333–1341. [[CrossRef](#)] [[PubMed](#)]
- Bendas, G.; Borsig, L. Cancer Cell Adhesion and Metastasis: Selectins, Integrins, and the Inhibitory Potential of Heparins. *Int. J. Cell Biol.* **2012**, *2012*, 1–10. [[CrossRef](#)] [[PubMed](#)]
- Köwitsch, A.; Zhou, G.; Groth, T. Medical application of glycosaminoglycans: A review: Medical Application of Glycosaminoglycans. *J. Tissue Eng. Regen. Med.* **2018**, *12*, e23–e41. [[CrossRef](#)]
- Senni, K.; Pereira, J.; Gueniche, F.; Delbarre-Ladrat, C.; Siquin, C.; Ratiskol, J.; Godeau, G.; Fischer, A.-M.; Helley, D.; Collic-Jouault, S. Marine Polysaccharides: A Source of Bioactive Molecules for Cell Therapy and Tissue Engineering. *Mar. Drugs* **2011**, *9*, 1664–1681. [[CrossRef](#)]
- Jouault, S.C.; Mauray, S.; Theveniaux, J.; Sternberg, C.; Vidal, B.; Fischer, A.M.; Millet, J. Antithrombotic and Anticoagulant Activities of a Low Molecular Weight Fucoidan by the Subcutaneous Route. *Thromb. Haemost.* **1999**, *81*, 391–395. [[CrossRef](#)]
- Guezennec, J. Deep-sea hydrothermal vents: A new source of innovative bacterial exopolysaccharides of biotechnological interest? *J. Ind. Microbiol. Biotechnol.* **2002**, *29*, 204–208. [[CrossRef](#)]
- Collic-Jouault, S.; Zanchetta, P.; Helley, D.; Ratiskol, J.; Siquin, C.; Fischer, A.M.; Guezennec, J. Les polysaccharides microbiens d’origine marine et leur potentiel en thérapeutique humaine. *Pathol. Biol.* **2004**, *52*, 127–130. [[CrossRef](#)]
- Roger, O.; Kervarec, N.; Ratiskol, J.; Collic-Jouault, S.; Chevolut, L. Structural studies of the main exopolysaccharide produced by the deep-sea bacterium *Alteromonas infernus*. *Carbohydr. Res.* **2004**, *339*, 2371–2380. [[CrossRef](#)]
- Raguénès, G.H.C.; Peres, A.; Ruimy, R.; Pignet, P.; Christen, R.; Loäec, M.; Rougeaux, H.; Barbier, G.; Guezennec, J.G. *Alteromonas infernus* sp. nov., a new polysaccharide-producing bacterium isolated from a deep-sea hydrothermal vent. *J. Appl. Microbiol.* **1997**, *82*, 422–430. [[CrossRef](#)]

15. Ruiz-Velasco, C.; Baud'Huin, M.; Siquin, C.; Maillason, M.; Heymann, D.; Collic-Jouault, S.; Padrines, M. Effects of a sulfated exopolysaccharide produced by *Alteromonas infernus* on bone biology. *Glycobiology* **2011**, *21*, 781–795. [[CrossRef](#)]
16. Chopin, N.; Siquin, C.; Ratiskol, J.; Zykwincka, A.; Weiss, P.; Cérantola, S.; Le Bideau, J.; Collic-Jouault, S. A Direct Sulfation Process of a Marine Polysaccharide in Ionic Liquid. *BioMed Res. Int.* **2015**, *2015*, 50865. [[CrossRef](#)] [[PubMed](#)]
17. Jouault, S.C.; Chevotot, L.; Helley, D.; Ratiskol, J.; Bros, A.; Siquin, C.; Roger, O.; Fischer, A.-M. Characterization, chemical modifications and in vitro anticoagulant properties of an exopolysaccharide produced by *Alteromonas infernus*. *Biochim. Biophys. Acta* **2001**, *1528*, 141–151. [[CrossRef](#)]
18. Bruland, Ø.S.; Pihl, A. On the current management of osteosarcoma. A critical evaluation and a proposal for a modified treatment strategy. *Eur. J. Cancer* **1997**, *33*, 1725–1731. [[CrossRef](#)]
19. Heymann, D.; Ruiz-Velasco, C.; Chesneau, J.; Ratiskol, J.; Siquin, C.; Collic-Jouault, S. Anti-Metastatic Properties of a Marine Bacterial Exopolysaccharide-Based Derivative Designed to Mimic Glycosaminoglycans. *Molecules* **2016**, *21*, 309. [[CrossRef](#)] [[PubMed](#)]
20. Cutter, G.R.; Liu, Y. Personalized medicine: The return of the house call? *Neurol. Clin. Pract.* **2012**, *2*, 343–351. [[CrossRef](#)]
21. Huclier-Markai, S.; Alliot, C.; Sebti, J.; Brunel, B.; Aupiais, J. A comparative thermodynamic study of the formation of scandium complexes with DTPA and DOTA. *RSC Adv.* **2015**, *5*, 99606–99617. [[CrossRef](#)]
22. Mazza, M.; Alliot, C.; Siquin, C.; Collic-Jouault, S.; Reiller, P.E.; Huclier-Markai, S. Marine Exopolysaccharide Complexed With Scandium Aimed as Theranostic Agents. *Molecules* **2021**, *26*, 1143. [[CrossRef](#)]
23. Zhang, J.D. Introduction to the Data Analysis of the Roche XCELLigence—System with RTCA Package. 11. Available online: www.bioconductor.org/T1\guilsinglrightinst\T1\guilsinglrightdoc (accessed on 22 March 2021).
24. Permyakov, E. *Metalloproteomics*; Wiley: Hoboken, NJ, USA, 2009.
25. Byrd, B.L.; Watson, E.E.; Cloutier, R.J.; Hayes, R.L. Effect of Stable Scandium on the Long-term Whole Body Retention of Intravenously Administered ⁴⁶Sc Citrate in the Rat. *Health Phys.* **1975**, *29*, 375–379. [[CrossRef](#)] [[PubMed](#)]
26. Hirano, S.; Suzuki, K.T. Exposure, Metabolism, and Toxicity of Rare Earths and Related Compounds. *Environ. Health Perspect.* **1996**, *104*, 11.
27. Rosoff, B.; Siegel, E.; Williams, G.L.; Spencer, H. Distribution and excretion of radioactive rare-earth compounds in mice. *Int. J. Appl. Radiat. Isot.* **1963**, *14*, 129–135. [[CrossRef](#)]
28. Moghaddam-Banaem, L.; Jalilian, A.R.; Pourjavid, M.; Bahrami-Samani, A.; Mazidi, M.; Ghannadi-Maragheh, M. Preparation and Quality Control of Scandium-46 Bleomycin as a Possible Therapeutic Agent. *Iran. J. Nucl. Med.* **2012**, *20*, 6.
29. Herath, H.M.T.U.; Silvio, L.D.; Evans, J.R.G. Scandia—A potential biomaterial? *J. Mater. Sci. Mater. Electron.* **2005**, *16*, 1061–1065. [[CrossRef](#)]
30. Lima, M.; Rudd, T.; Yates, E. New Applications of Heparin and Other Glycosaminoglycans. *Molecules* **2017**, *22*, 749. [[CrossRef](#)]
31. Wright, T.C.; Castellet, J.J.; Petitou, M.; Lormeau, J.C.; Choay, J.; Karnovsky, M.J. Structural Determinants of Heparin's Growth Inhibitory Activity: Interdependence of oligosaccharide size and charge. *J. Biol. Chem.* **1989**, *264*, 1534–1542. [[CrossRef](#)]
32. Volpi, N.; Bolognani, L.; Conte, A.; Petrini, M. Effects of Chondroitin Sulfates with Different Structures on Leukemia Cells: U-937 Cell Proliferation and Differentiation. *Leuk. Res.* **1993**, *17*, 789–798. [[CrossRef](#)]
33. Syrokou, A.; Tzanakakis, G.; Tsegenidis, T.; Hjerpe, A.; Karamanos, N.K.; Potten, C.; Darzynkiewicz, Z.; Sasaki, K. Effects of glycosaminoglycans on proliferation of epithelial and fibroblast human malignant mesothelioma cells: A structure-function relationship. *Cell Prolif.* **1999**, *32*, 85–99. [[CrossRef](#)] [[PubMed](#)]
34. Nikitovic, D.; Zafiroopoulos, A.; Tzanakakis, G.N.; Karamanos, N.K.; Tsatsakis, A.M. Effects of glycosaminoglycans on cell proliferation of normal osteoblasts and human osteosarcoma cells depend on their type and fine chemical compositions. *Anticancer. Res.* **2005**, *25*, 2851–2856.
35. Hausser, H.-J.; Brenner, R.E. Low doses and high doses of heparin have different effects on osteoblast-like Saos-2 cells in vitro. *J. Cell. Biochem.* **2004**, *91*, 1062–1073. [[CrossRef](#)] [[PubMed](#)]
36. Stevenson, J.L.; Varki, A.; Borsig, L. Heparin attenuates metastasis mainly due to inhibition of P- and L-selectin, but non-anticoagulant heparins can have additional effects. *Thromb. Res.* **2007**, *120*, S107–S111. [[CrossRef](#)]
37. Abu Arab, W.; Kothb, R.; Sirois, M.; Rousseau, É. The Role of Heparin in Lung Cancer. *J. Neoplasms* **2017**, *1*, 14–28. [[CrossRef](#)]
38. Kucukoner, M.; Isikdogan, A.; Kaplan, M.; Inal, A.; Zincioglu, S.; Cit, M.; Cil, T.; Karadayi, B.; Dirie, A.; Yildiz, I. Can LMWH Improve the Outcome for Patients with Inoperable Stage III Non-Small Cell Lung Cancer? *Contemp. Oncol.* **2012**, *16*, 416. [[CrossRef](#)]
39. Morla, S. Glycosaminoglycans and Glycosaminoglycan Mimetics in Cancer and Inflammation. *Int. J. Mol. Sci.* **2019**, *20*, 1963. [[CrossRef](#)]
40. Bereczky, B.; Gilly, R.; Rásó, E.; Vágó, Á.; Tímár, J.; Tóvári, J. Selective antimetastatic effect of heparins in preclinical human melanoma models is based on inhibition of migration and microvascular arrest. *Clin. Exp. Metastasis* **2005**, *22*, 69–76. [[CrossRef](#)]
41. Ahn, M.Y.; Kim, B.J.; Kim, H.J.; Jin, J.M.; Yoon, H.J.; Hwang, J.S.; Park, K.-K. Anti-cancer effect of dung beetle glycosaminoglycans on melanoma. *BMC Cancer* **2019**, *19*, 1–12. [[CrossRef](#)]
42. Logun, M.T.; Wynens, K.E.; Simchick, G.; Zhao, W.; Mao, L.; Zhao, Q.; Mukherjee, S.; Brat, D.J.; Karumbaiyah, L. Surfen-mediated blockade of extratumoral chondroitin sulfate glycosaminoglycans inhibits glioblastoma invasion. *FASEB J.* **2019**, *33*, 11973–11992. [[CrossRef](#)]

-
43. Gomes, A.M.; Stelling, M.P.; Pavão, M.S.G. Heparan Sulfate and Heparanase as Modulators of Breast Cancer Progression. *BioMed Res. Int.* **2013**, *2013*, 852093. [[CrossRef](#)] [[PubMed](#)]
 44. Chatzinikolaou, G.; Nikitovic, D.; Asimakopoulou, A.; Tsatsakis, A.; Karamanos, N.K.; Tzanakakis, G.N. Heparin—A unique stimulator of human colon cancer cells' growth. *IUBMB Life* **2008**, *60*, 333–340. [[CrossRef](#)] [[PubMed](#)]
 45. Schnoor, R.; Maas, S.L.N.; Broekman, M.L.D. Heparin in malignant glioma: Review of preclinical studies and clinical results. *J. Neuro Oncol.* **2015**, *124*, 151–156. [[CrossRef](#)] [[PubMed](#)]

Conclusions and perspectives

Osteosarcoma is the most common primary malignant bone tumor in children and young adults. It is a very aggressive type of cancer with a low prognosis; but molecular mechanism of metastases have been identified for designing new therapeutic strategies in the frame of personalized medicine. Among the biomarkers considered, glycoaminoglycans (GAGs) are a hallmark related with cancer growth and spread. GAGs could be employed in new drug delivery systems to deliver active compounds for therapeutic uses. A *theranostics* approach, i.e. combination of a predictive biomarker with a therapeutic agent, has been developed in this work. The aim of this thesis is to evaluate natural exopolysaccharides as potential ligand for theranostics and to determine if they could be further coupled to scandium radionuclides.

In the first part of this manuscript, a state of the art on recent cancer approaches and the rationale of this work has been presented. Glycosaminoglycans (GAGs) such as unfractionated heparin, and its low-molecular weight (LMW) derivatives, are generally used for prevention or treatment of venous thromboembolism that frequently occurs in cancer patients. Heparin is composed of glucuronic or iduronic acid, glucosamine and has a sulfur content around 10% (from 8% to 13% according to the heparin preparation). An improved survival rate has been shown, which could be due to heparin as it is able to interfere with some of the important biological steps in the metastasis spread. Unfortunately, this kind of molecules exhibits drawbacks such as an hemorrhagic risk and could present a contamination with prion proteins or oversulfated chondroitin sulfate. This hazard profile drastically limits the use of heparin in therapy. Actually, the number of studies on exploration of heparin mimetic molecules has been raised up in recent years. Among the possible molecules, polysaccharides could be a new source of heparin-like molecules. Traditional algal or bacterial polysaccharides provide a valid alternative to mammalian GAGs. Additionally, polysaccharides extracted from eukaryotes and prokaryotes living in marine environment could potentially reveal a better benefit/risk ratio as observed in preliminary animal studies. In the past, algal polysaccharides such as fucoidans – and especially low-molecular-weight fucoidan preparation (LMWF) – have been shown to exhibit heparin-like properties with very low hemorrhagic risk. Marine polysaccharides from a bacterial source present also a high potentiality in cell therapy and tissue engineering. They can be produced under totally controlled conditions in bioreactors compared to other polysaccharides from eukaryotes.

Among these marine polysaccharides, an exopolysaccharide (EPS) of interest is extracted from the culture broth of a bacterium named *Alteromonas infernus*. The repeating unit of this EPS consists of a monosulfated nonasaccharide composed of six neutral hexoses and three hexuronic acids, among those the galacturonic acid unit bears one sulfate group. It presents a high molecular weight ($> 10^6 \text{ g mol}^{-1}$) and a low sulfate content ($< 10\%$). This native EPS demonstrated a very weak anticoagulant activity compared to heparin. In order to promote its biological activities and to provide a GAG mimetic compound, the native EPS has been modified by first a radical depolymerization (EPS DR) and then an oversulfation step (EPS DRS), these two chemical modifications allow a reduction of its molecular weight along with an increase in its sulfate content. The anticoagulant activity of this LMW highly sulfated EPS derivative is improved compared to that of its native precursor but remains lower than both unfractionated heparin and LMW heparin, 10 and 5 times less, respectively. This category of polysaccharides could pave the way for the development of new delivery systems for conventional chemotherapeutic agents, as well as new strategies in bone oncology, in the field of personalized medicine.

Nuclear medicine involves the use of radioactive isotopes in the diagnosis and treatment of diseases. Theranostics – a field of medicine that combines specific targeted therapy based on specific targeted diagnostic tests – uses specific biological pathways in the human body, to acquire diagnostic images and to deliver a therapeutic dose of radiation to the patient. Among the available radionuclides, scandium possesses two radionuclides emitting β^+ radiations, ^{44}Sc or ^{43}Sc , which makes them appropriate candidates in PET/CT (Positron Emission Tomography - Computed Tomography) diagnosis, due to their half-life of around 4 hours and decay to non-toxic Ca. ^{47}Sc , which can be used for targeted radionuclide therapy, opens the field of Sc-based vectors from diagnosis to therapy and gives a great opportunity for dosimetric calculations. The coupling of exopolysaccharide with this pair of theranostic radionuclides is thus of interest.

It is important to characterize these molecules, especially their molecular masses, by means of Asymmetrical Flow Field-Flow Fractionation (A4F) coupled to differential Refractive Index (dRI), and Multi Angle Light Scattering (MALS) detectors. Another important parameter that could influence the complexation is the polymer conformation. Therefore, the second chapter of this work has addressed the characterization of the exopolysaccharides and notably their functional properties (pKa), and their rheological properties (viscosimetry, conformation). Since these EPS have been evidenced to exhibit

heparin like properties, and since heparin is a polysaccharide, part of my work was dedicated to heparin, as a reference for GAGs. Two protonation constants were found. The first value was found to be $pK_{a1} = 3.82 \pm 0.03$, which corresponded to the carboxylic group of iduronic acid of heparin disaccharide. The second protonation constant was found at $pK_{a2} = 7.53 \pm 0.03$, that was attributed to the nitrogen atom of the sulphamino group, which is a stronger donor than the other sulphated groups.

We have confirmed that AF4 is very useful for the separation of (bio)polymers and when being coupled to MALS, it provides the determination of polymer molar masses, easily replacing SEC-MALS. EPS-DRS, the over-sulphated and radical depolymerized derivative obtained by the native EPS, exhibited a \overline{M}_w of 56.9 kDa whereas for EPS DR, the low-sulphated and radical depolymerized derivative obtained by the native EPS, \overline{M}_w was 25.6 kDa. Some discrepancies were noticed compared to SEC-MALS determination. \overline{M}_w of EPS-DR and -DRS were underestimated since SEC-MALS was used with an average $\partial n/\partial c$ values for both EPS. In this work, we have determined accurate values of $\partial n/\partial c$ for each EPS. Furthermore potential for degradation exists when analyzing long linear polymers by SEC, because of velocity gradients generated during flow. The polymer is elongated, and bonds positioned close to the middle of the chain become stretched and can break if shear rates are high enough. The end segments of a chain maintain their coiled shape; then, the maximum stress is frequently focused near the center of the polymer.

This work has examined also the viscosimetric radius ($R\eta$) and the conformation of the polymers. For the two EPS, a decrease of the hydrodynamic volume V_h was observed with increasing ionic strength. This decrease was slightly higher for EPS-DR and -DRS than for heparin, meaning that EPS-DR and -DRS are more sensitive to the ionic strength changes. This was explained by considering the overall charges surrounding EPS-DR or -DRS chains that are more important compared to the heparin ones. EPS-DR and -DRS exhibit more ionized functional groups that could be shielded by the counter-ions from the background electrolyte, leading to the folding of the polymer chain. The decrease of intrinsic viscosity with increasing ionic strength reflects a change in conformation: the expansion of the polymer chain is clearly affected by addition of ions that seem to make the ionized functional groups of the polymer inaccessible.

With our rheological approach, we have evidenced that both EPS samples exhibit nanometric sizes that correspond to one quantitative indicator of molecular conformation. This

last one controls the efficacy in drug delivery. With R_g ranging from 44 to 58 nm, these EPS are suitable with rapid *in vivo* circulation, and fast clearance then through kidneys.

For a use in theranostic approach, the scandium-exopolysaccharide complex must be thermodynamically stable and kinetically inert. The stability constants Sc-EPS was assessed through Free Ion Selective Resin Extraction (FISRE) and the influence of sulfur content on the complexation with scandium was scrutinized. The FISRE method has been used for the determination of thermodynamic stability of metallo-radiopharmaceuticals containing Y^{3+} , or for Sc^{3+} complexes with several chelating ligands, i.e, EDTA, DTPA, NOTA, and DOTA. Other techniques, such as potentiometric titrations and CE-ICP-MS were considered being less suitable to analyze Sc-EPS complexes. Potentiometric titrations could affect the integrity of the polymer chain, by exposing it to very acidic and very alkaline pH hydrolysis; whereas CE-ICP-MS could not be used because of the highly charged polysaccharides-metal complexes, leading to a difficult interpretation of the speciation. FISRE prevents from potential hydrolysis of EPS ligands. For each different ligand, only one kind of complexation site was evidenced with a stoichiometry 1:1 as regard of free Sc^{3+} ion under our experimental conditions. Complexation constants could be calculated by fitting of $\log K_{d_{norm}}$ vs. ligand concentration.

For Heparin, the monoligand complex $MHep^{2-}$ was the predominant specie in weakly acidic, neutral, and weakly basic pH ranges. With increasing pH, metal hydrolysis occurs. Water molecules are present in the inner coordination sphere of the metal that are progressively replaced by hydroxo-complexes, such as $[M(OH)Hep]^{3-}$ and $[M(OH)_2Hep]^{4-}$, with increasing pH. The following stability constants have been found for EPS: $K_{ScEPS-DR} = 9.30$ and $K_{ScEPS-DRS} = 7.85$. The stability constants found for EPS-DR and -DRS were higher than the ones from literature on glucuronic and galacturonic acids, and this could suggest the presence of hydroxo-complexes of Sc for both of them. In term of speciation, both ligands seem to quantitatively complex scandium in conditions near physiological ones. In terms of charge, EPS-DRS present three additional negative charges, related to the three sulfate groups generated by the oversulfation reaction. The presence of the sulfate groups delayed the complexation, probably due to a higher steric hindrance with DRS monomers caused by sulfates. At higher ionic strength, those groups are shielded, which makes the polymer folding into a more contracted random coil. Nonetheless, Sc-EPS complexes appear to be less stable than those between scandium and classic chelate ligands used in radiopharmaceuticals, such as DOTA and DTPA ($K_{ScDOTA} = 30.79$; $K_{ScDTPA} = 27.43$) from the values published, we calculated

the apparent complexation constant for DTPA and DOTA respectively with scandium at pH=6.1. We found 16.93 and 16.98 respectively. Even if these values are much higher than those determined for heparin, EPS-DR and –DRS (i.e. 6.38; 7.07 and 5.62), the complexation of scandium with these ligands is total.

Scandium is a metal from the first-transition series with an ionic radius of 0.75 Å (+3); it is classified as a rare-earth element and, for this reason, its chemical behaviour is pretty close to lanthanides. In aqueous solution, only the degree of oxidation (+3) is stable. Lanthanide ions are found in living organisms in trace amounts and they are considered to play a biological role. They interact with biological materials and because of their chemical analogy with actinides at their +III redox state, they may also act as substitution probes for the actinides Pu(III), Am(III), or Cm(III). Additionally, it has been clinically evidenced that polygalacturonic acids or polyuronic acids could be efficient as medication drugs in case of heavy-metal poisoning. In this work, the potential of these EPS and heparin to complex rare earth metals, especially lanthanides, has been assessed. The complexation of Eu^{3+} with these two EPS and heparin was studied by time-resolved laser-induced fluorescence spectroscopy (TRLFS). TRLFS is a very convenient tool for detecting and characterizing fluorescent lanthanide speciation – and especially europium(III) –, at trace concentrations. This method is sensitive to changes in the chemical environment of the metal through modifications of fluorescence spectra and decay-time of the excited state. The obtained spectroscopic data – i.e. spectra, peak maxima, intensities, and decay-times – give valuable information identifying the speciation of eventual Eu(III)-polysaccharides complexes. Similar works were conducted on α -D-glucose 1-phosphate, on glucose 6-phosphate, fructose 6-phosphate, lipopolysaccharides or on peptidoglycan with uranium (VI).

For EPS-DR and DRS, we observed mono-exponential luminescence decay, while for Eu-Heparin a bi-exponential was necessary. For EPS-DR and DRS, the luminescence lifetime is prolonged to $>150 \mu\text{s}$ indicating the formation of a single Eu(III) EPS species. For heparin, decay time, instead, seems to increase with Europium concentration and thus the viscosity. This could be explained by the relaxed polymer conformation (higher viscosity) that should reveal more functional groups, so less water molecules around which corresponds to a higher decay time. For Eu(II)-heparin system, two sites of complexation were necessary to model the isotherm whereas only one site was necessary to model the data for Eu(III)-EPS-DR and –DRS. The two sites observed on Eu-heparin system corresponded to the two uronic acids, in

agreement with data from Fuks and Bünzli on La(III) complexation with glucuronic acid and galacturonic acid. Compared to Scandium, Eu(III) ions are hard acceptors and form strong complexes with hard ligands containing highly electronegative donor atoms such as carbonate, phosphate, hydroxide, fluoride, and sulphate. The bonds between Eu^{3+} ions and hard ligands such as CO_3^{2-} or F^- are mainly electrostatic in character and the 4f electrons do not seem to participate to a large extent in the bonding. Another consequence of the dominantly electrostatic nature of bonding is that the coordination number and the geometry of rare earth element ions are less constrained than those of transition metal ions. From these interesting results, a possible assumption of Eu-EPS complexes can be made. Eu-DRS complexes revealed 6 water molecules in the inner sphere of coordination of Eu^{3+} (9 water molecules are considered for the aquo-ion); the remaining 3 coordination bonds could be represented by the 3 carboxylic groups. Eu-DRS complexes, instead, demonstrated 4 water molecules in the inner sphere of coordination of Eu^{3+} . These should mean that the remaining 5 coordination bonds are represented by the 3 carboxylic moieties plus 2 groups that can be only sulphate group on the main linear chain and probably an oxygen ring forming the nonasaccharide.

Finally, Exopolysaccharides (EPS) derivatives have showed antimetastatic properties on both murine and human osteosarcoma (POS-1 and HOS) cell lines. Moreover, these derivatives had no significant effect on the cell cycle and had no pro-apoptotic effect on osteosarcoma cells. To ensure the biological properties necessary to target cancer cells, scandium-EPS complexes were tested *in vitro* on HOS cell lines. An xCELLigence RTCA technology assay were used to monitor the proliferation kinetics of these cells during 160 hours of treatment first with EPS and scandium alone, and then, with scandium EPS complexes. Cell viability after 160 hours of treatment with these compounds was also assessed through MTT tests.

EPS-Sc and Heparin-Sc complexes presented an anti-proliferative effect. This effect was more effective for slowing down the proliferation kinetic than polysaccharides alone. This increase of the antiproliferative properties could be explained by a change in conformation of EPS due to their polyelectrolyte nature that is affected by complexation with scandium. The change in conformation could modulate positively or negatively the cytotoxic effect. The only cancer cell line that appeared insensible to this effect was the human glioblastoma one, which, on the contrary, showed an increase of cell proliferation. Literature provides several studies demonstrating that GAGs would act as coordinators of glioblastoma cell interactions with the

microenvironment, resulting in a major cancer proliferation and migration. Concerning the cause of the cytotoxic effect, a damage in the cellular metabolism does not seem to be implicated since the high cell viability. Cell viability was still high with almost all compounds after 160 hours of treatment, suggesting that a cytostatic effect might occur rather than a cytotoxic effect. More probably, alterations of both growth factor-receptor signalling, as well as an interference of cell-cell adhesion mediated by specific transmembrane proteins could be the principal cause of the antiproliferative effect.

These results are very encouraging in a theranostic perspective for two reasons: 1) the intrinsic tropism of these EPS for cancer cells is maintained even after the complexation and 2) the anti-proliferative effect could be modulated by the degree of complexation. Future perspective could envisage a broader campaign to investigate the influence of the degree of complexation to better see which are the best in terms of efficacy. Besides, xCELLigence assay with EPS could be extended to other cell lines known to be sensible to GAG properties, while testing new assays to target other cellular mechanisms involved in cellular toxicity.

From all these results, it would be possible to conclude that EPS clearly have the potential to be coupled to $^{44\text{m}/44}\text{Sc}$ to obtain an efficient theranostic tool. Labeling protocols should allow high labeling yields, radiochemical purity and specific activity. The production of $^{44\text{m}/44}\text{Sc}$ is already established at Arronax and allows reaching high purities batches. As a perspective of this work, the optimization of the radiolabelling of these EPS with $^{44\text{m}/44}\text{Sc}$ needs to be performed. Labelling efficiency of ligands is usually tested at different solution pH's, temperatures and ligand concentrations (or more correctly, at different radiometal-to-ligand molar ratios) and monitored as a function of time in order to optimize the radiolabeling. To test the radiolabeling yield, a radio-TLC is usually performed by spotting a solution aliquot onto a TLC Plate and eluting with a developing solution. Among the optimization parameters, the eluting solution composition is one. The resulting TLC plate is then counted on an autoradiographic system. The R_f values for unlabelled $^{44\text{m}/44}\text{Sc}^{3+}$ and $^{44\text{m}}\text{Sc}/^{44}\text{Sc}$ -conjugate are then determined. The main issue with the EPS of this work will be the eluting solution composition and monitoring the migration of the EPS alone on a TLC plate. To circumvent this problem, Asymmetrical Flow Field-Flow Fractionation (AF4) coupled with a Multi-Angle Light Scattering detector (MALS) could be used and coupled with a γ -ray detector. AF4-MALS- γ was shown to be a powerful tool for monitoring the liposome size together with the

incorporation of the high energy alpha emitter, and notably to assess the stability of ^{212}Bi -radiolabelled liposomes in serum.

Since radiolabelling would have been optimized, the serum stability of the resulting complexes will be assessed. Before any *in vivo* studies, a protocol will be developed in order to purify the radiolabelled $^{44\text{m}/44}\text{Sc}$ -EPS complexes from unchelated EPS by the mean of an HPLC process. Finally, biodistribution studies and PET imaging will be performed with $^{44\text{m}/44}\text{Sc}$ only, with the two $^{44\text{m}/44}\text{Sc}$ -EPS complexes. These studies were performed in nude mice and in osteosarcoma tumor-bearing mice at different time points.

Titre : Evaluation de glyco-saccharides dans une approche théranostique

Mots clés : Exopolysaccharides, Scandium; Théranostique ; Rhéologie; Complexation; Spectroscopie moléculaire; Evaluation Biologique

Résumé : L'ostéosarcome est la tumeur osseuse maligne primaire la plus courante chez les enfants et les jeunes adultes. C'est un type de cancer très agressif avec un pronostic faible ; mais le mécanisme moléculaire des métastases a été identifié permettant de concevoir de nouvelles stratégies thérapeutiques dans le cadre de la médecine personnalisée. Parmi les biomarqueurs considérés, les glycoaminoglycans (GAGs) sont un biomarqueur de croissance et de propagation du cancer. Les GAG pourraient être utilisés dans de nouveaux systèmes d'administration de médicaments pour fournir des composés actifs à des fins thérapeutiques. Une approche théranostique, c'est-à-dire la combinaison d'un biomarqueur prédictif avec un agent thérapeutique, a été développée dans ce travail. Tout d'abord, parce que les GAGs ont des propriétés anti-métastatiques et notamment des exopolysaccharides produits par une bactérie marine *Alteromonas infernus*. évalués sur différentes lignées de cellules cancéreuses, étant couplé ou non avec du scandium pour évaluer davantage leur efficacité en médecine nucléaire. De plus, une véritable paire théranostique de radionucléides a été envisagée, à savoir les isotopes du scandium $^{44}\text{Sc}/^{47}\text{Sc}$. Ainsi, les GAGs pourraient agir en synergie avec les radionucléides d'intérêt pour la médecine nucléaire et

l'objectif de ces travaux était d'évaluer la faisabilité du couplage EPS avec le scandium. Les caractéristiques liées à l'applicabilité de ces EPS en théranostique ont été étudiées, par exemple le comportement rhéologique des polymères. Cette stabilité dépend de la composition chimique des suspensions, mais aussi de la taille et de la distribution en taille des molécules ainsi que leur charge de surface. Ce travail présente les outils de caractérisation qui permettent d'étudier ces propriétés. La méthodologie mise au point a été utilisée pour assurer le contrôle de la composition, de la taille, de la forme et des caractéristiques de surface des EPS en vue pour de leurs injections *in vivo*. Le deuxième objectif de ce travail est de décrire et de quantifier le plus complètement possible l'interaction de ces EPS avec le scandium. Mais chaque métal est unique et est défini par son état d'oxydation, son nombre de coordination, ses caractéristiques (dures /molles), son inertie cinétique ou sa labilité, et sa stabilité redox. Par conséquent, la chimie de coordination particulière du scandium avec ces EPS a été étudiée avec précision. Enfin, le comportement biologique de ces EPS a été évalué sur différentes lignées de cellules cancéreuses, couplées ou non au scandium pour évaluer leur potentialité en médecine nucléaire.

Title: Evaluation of glyco-saccharides in a theranostic approach

Keywords: Exopolysaccharides, Scandium; Theranostic; Rheology; Complexation; Fluorescence Spectroscopy; Biological assay

Abstract: Osteosarcoma is the most common primary malignant bone tumor in children and young adults. It is a very aggressive type of cancer with a low prognosis; but molecular mechanism of metastases have been identified for designing new therapeutic strategies in the frame of personalized medicine. Among the biomarkers considered, glycoaminoglycans (GAGs) are a hallmark related with cancer growth and spread. GAGs could be employed in new drug delivery systems to deliver active compounds for therapeutic uses. A *theranostics* approach, i.e. combination of a predictive biomarker with a therapeutic agent, has been developed in this work. Firstly, because GAGs have anti-metastatic properties and especially exopolysaccharides produced by a marine bacteria *Alteromonas infernus*. Additionally, a true theranostic pair of radionuclides has been considered, namely the scandium isotopes $^{44}\text{Sc}/^{47}\text{Sc}$. Thus, GAGs could act in synergy with radionuclides of interest for Nuclear Medicine and the goal of this work was to evaluate the feasibility of coupling EPS with Sc. The characteristics related to the applicability of these EPS in theranostics have been studied, for example the rheological behavior of the polymers.

This stability depends on the chemical composition of the suspensions, but also on the size and size distribution of the molecules and their surface charge. This work presents the characterization tools that allow studying these properties. The methodology developed has been used to ensure the control of the composition, size, shape and surface characteristics of the EPS for further potential *in vivo* injections. The second objective of this work is to reach to the most comprehensive description of the interaction of these EPS with scandium. However, each metal is unique and is defined by its oxidation state, coordination number, hard-soft characteristics, kinetic inertness or lability, and redox stability. Therefore, the particular coordination chemistry of scandium to these EPS has been accurately studied. Finally, the biological behavior of these EPS has been assessed on different cancer cell lines, being coupled or not with scandium to further evaluate their potency for Nuclear Medicine.